Functional dissection of autophagy-related proteins ATG5 and ATG18 in *Plasmodium falciparum*

A thesis submitted for the degree of

DOCTOR OF PHILOSOPHY

by

Palak Agrawal

Molecular Biology and Genetics Unit

Jawaharlal Nehru Centre for Advanced Scientific Research

Bangalore - 560064 (INDIA)

October, 2019

DECLARATION

I hereby declare that the thesis entitled **"Functional dissection of autophagy-related proteins ATG5 and ATG18 in *Plasmodium falciparum*"** is an authentic record of research work carried out by me, under the guidance of **Prof. Namita Surolia** and **Prof. Ravi Manjithaya** at Molecular parasitology laboratory, Molecular Biology and Genetics Unit, Jawaharlal Nehru Centre for Advanced Scientific Research, Bangalore. In keeping with the norm of reporting scientific observations, due acknowledgement has been given wherever work based on the findings of other investigators has been cited. Any omission, owing to oversight or misjudgement is regretted.

Palak Agrawal

Place: Bangalore

Date:

CERTIFICATE

This is to certify that the work described in this thesis entitled **"Functional dissection of autophagy-related proteins ATG5 and ATG18 in *Plasmodium falciparum*"** is the result of investigations carried out by **Mrs. Palak Agrawal** in Molecular parasitology laboratory, Molecular Biology and Genetics Unit, Jawaharlal Nehru Centre for Advanced Scientific Research, Bangalore, India, under my supervision and guidance. The results presented here have previously not formed the basis for the award of any other Diploma, Degree or fellowship.

Prof. Namita Surolia
(Research Supervisor)
Bangalore, Karnataka, India.
Date:

Prof. Ravi Manjithaya
(Research Supervisor)
Bangalore, Karnataka, India.
Date:

ACKNOWLEDGEMENTS

"Synergy is what happens when one plus one equals ten or a hundred or even a thousand! It's the profound result when two or more respectful human beings determine to go beyond their preconceived ideas to meet a great challenge" - Stephen Covey. Here I take the opportunity to thank all those who have been instrumental in the successful completion of the work presented in this thesis.

First and foremost, I would like to extend my sincere gratitude to my research guide ***Prof. Namita Surolia*** *for introducing me to the exciting field of molecular parasitology and for her dedicated help, advice, inspiration, encouragement and continuous support throughout the time of research and writing of this thesis. Through innumerable discussions during the course of PhD, she has helped me to bring the best out of me. Her positive spirit has inspired me and made me believe in myself. I feel privileged to be associated with a person like her and I will always be grateful to her!*

My special words of thanks should also go to my research co-guide ***Prof. Ravi Manjithaya*** *for his continuous support, guidance, cooperation, feedback, for his insightful comments and encouragement, and also for imbibing in me the importance of analysing the data carefully. His pleasant demeanour and administrative proficiency has inspired me greatly. Thanks to him!*

I thank all the esteemed faculty of MBGU and NSU: Prof. MRS Rao, Prof. Uday Kumar Ranga, Prof. Anuranjan Anand, Prof. Maneesha Inamdar, Prof. Tapas Kumar Kundu, Prof. Hemlatha Balaram, Dr. James Chelliah, Dr. Kushagra Bansal and Dr. Sheeba Vasu for their course work and constructive feedback during annual work presentations. A special thanks to Prof. MRS Rao for reviewing the manuscript and for providing his valuable comments.

I am grateful to ***Dr. Archana Singh****, IGIB, New Delhi for permitting me in her laboratory and use the electron microscopy facility available there. I also want to thank Prof. Soumitra Das, IISc, Bangalore and Dr. James Chelliah, JNCASR, Bangalore for evaluating my PhD comprehensive exam. They have provided insightful inputs which were beneficial in the design and approach of my experiments.*

I gratefully acknowledge the intra-mural financial assistance received towards my PhD from the JNCASR. The in-house facilities at JNCASR have been very useful for my work. I thank all the instrument in-charge and the faculty in-charge for the smooth running of the facility. I also thank Suma ma'am for helping with the confocal microscopy related support.

I express my heartfelt gratitude to ***Dr. Kripa*** *and* ***Sourabh*** *for being with me as mentors throughout. Their scientific inputs, personal bits of help and friendly nature have always made me feel at ease, cheerful and motivated. They have always been there for me with their supporting hands whenever I needed it the most. From their many pep talks, I learnt that: learn from the past, act in the present and build the future…thank you for everything.*

*I am extremely thankful to my MPL lab seniors and colleagues - **Dr. Garima** for being such a wonderful person, always approachable, friendly and inspiring. Dr. Kirthana for helping me with experiments. **Dr. Shiny** for always encouraging me and sharing a great relationship as a compassionate friend. I would also like to thank Dr. Mayur, Miti, Lavanya, Ashvini, Akshaya, Satish and Ira for helping me with experiments and creating amiable lab environment. A special thanks to **Ananya** for being cooperative and sharing her reagents and culture with me, and also for many brainstorming discussions which helped me to gain scientific insights. Due regards to **Mr. Sudhakar** for excellent upkeep of the lab and seeing to it that all the reagents and equipment are available in time and within reach. I will always cherish memories spent in the lab and the warmth shown by all.*

I want to thank Autophagy lab members, especially Gaurav, Sunaina, Dr. Piyush and Dr. Suresh, for their timely help and cooperation. They always helped me out when I got any difficulties or queries regarding experiments in yeast. A special mention of thanks to my friends in JNCASR- Ananya and Sankalp for always be ready to talk about everything, helping me navigate this journey and creating lots of good memories. Chandan for always be so enthusiastic and inspiring, Disha for lending me ears and helping me with protocols and reagents, Shikha, Ekashmi, Geetika, Nikita, Harshit and many more for creating a friendly atmosphere. I will always cherish moments spent with all. Thanks for being there!

A special thanks to my elder brother Himesh Bhaiya and sister-in-law Sonakshi Bhabhi for their love and affection, and holding my hand whenever I needed support.

My heartfelt regards go to my grandmother-in-law, father-in-law and mother-in-law for believing in me and motivating me to pursue my dreams. My sister-in-law Mrs Priyanka and her family for their love and moral support.

My buddies: Beena, Chetan, Anshul, Neha Di, Nikita and Ratna we have seen it all together, the rises and falls and growing into a better person, especially Beena for the bond we share and for our sisterhood.

*I owe my deepest gratitude towards my better half and my best friend **Prashant** for his eternal support and understanding of my goals and aspirations. He has helped tremendously in shaping up this thesis. His infallible love and support have always been my strength. His patience and sacrifice will remain an inspiration throughout my life. He believed in me even when I had self-doubts. Without his help, I would not have been able to accomplish much of what I have done and become who I am.*

*To my life-coach, my **parents**: because I owe it all to them. Many Thanks!!!*

Palak Agrawal

Table of Contents

List of Figures

List of Tables

List of Abbreviations

3-MA	3-methyladenine
ACD	autophagic cell death
ACP	acyl carrier protein
ACT	artemisinin combination therapy
AIM	ATG8 interacting motif
AIR	ATG12-ATG5 interacting region
ALP	alkaline phosphatase
Ams1	α-mannosidase
Ape1	aminopeptidase 1
ART	artemisinin
ASP	apoptotic-specific protein
ATG	autophagy-related gene
ATG18	autophagy-related protein 18
ATG5	autophagy-related protein 5
CPY	carboxypeptidase Y
CRT	chloroquine resistance transporter
Cvt	cytoplasm-to-vacuole pathway
DHA	dihydroartemisinin
DIC	differential interference contrast
DPAP1	dipeptide aminopeptidase 1
DV	digestive vacuole
EEF	exoerythrocytic form
ER	endoplasmic reticulum
FADD	fas-associated death domain protein
FCP	FVYE domain-containing protein
FP1	falcipain-1
FP2	falcipain-2
FRRG	Phe-Arg-Arg-Gly
FV	food vacuole
FYVE	Fab1, YOTB, Vac1, EEA1
GFP	green fluorescent protein
GWAS	genome-wide association study
HAP	histo-aspartic protease
HcVs	hemoglobin containing vesicles
HR	helical rich domain
Hsv2	homologous with the swollen vacuole phenotype 2
IE	intraerythrocytic
IEM	immunoelectron microscopy
IFA	immunofluorescence assay
IPTG	isopropylthio-β-d-galactoside
JAS	jasplakinolide
LC3	Microtubule-associated protein 1A/1B-light chain 3
MDR1	multidrug resistant protein 1
MSP1	merozoite surface protein 1
MVB	multivesicular body
NLS	nuclear localization signal
NPP	new permeability pathways

PAS	pre-autophagosomal structure or phagophore assembly site
PE	phosphatidylethanolamine
PI	phosphatidylinositol
PI(3,5)P_2	phosphatidylinositol 3,5-bisphosphate
PI3K	phosphatidylinositol-3-kinase
PI3P	phosphatidylinositol-3-phosphate
PKA	protein kinase A
PM-I	plasmepsin I
PM-II	plasmepsin II
PM-IV	plasmepsin IV
PMN	piecemeal microautophagy of the nucleus
PMSF	phenylmethylsulphonyl fluoride
PPM	parasite plasma membrane
PROPPINs	β-propellers that bind polyphosphoinositides
PV	parasitophorous vacuole
PVM	parasitophorous vacuolar membrane
RACK1	receptor activated C-kinase 1
RBC	red blood cell
SDS	Sodium dodecyl sulfate
SEM	Standard error of the mean
SENDA	static encephalopathy of childhood with neurodegeneration in adulthood
SNP	single nucleotide polymorphism
SP	sulfadoxine-pyrimethamine
Svp1	swollen vacuole phenotype 1
TECPR1	Tectonic β-propeller repeat containing 1
TORC1	target of rapamycin complex 1
Ubl	ubiquitin-like
UPS	Ubiquitin-proteasome system
uRBC	uninfected RBC

Chapter One

Introduction

Table of Contents

1.1 Malaria: An overview

Malaria is a major cause of mortality and morbidity worldwide. It is caused by the protozoan parasite of the genus *Plasmodium* and is transmitted by the bite of a female *Anopheles* mosquito. Five species of *Plasmodium* infect humans: *P. falciparum*, *P. vivax*, *P. malariae*, *P. ovale* and *P. knowlesi*. Malaria is usually classified as asymptomatic, uncomplicated or severe. Fever, chills and muscle aches are the first typical symptoms of malaria. In the most severe cases, the disease can lead to coma or death, especially after infection with *P. falciparum* (Phillips *et al.*, 2017).

1.1.1 A brief history of the discovery of the life cycle of malaria parasite

The word malaria is derived from the Italian words “mal” and “aria”, which literally means “bad air” (Cox, 2010). In 1880, the discovery of parasites in the blood of malaria patients by Alphonse Laveran marked the beginning of the understanding of malaria parasites. In 1897, William MacCallum discovered the sexual stages of a related haematozoan, *Haemoproteus columbae* in the blood of the infected birds. Ronald Ross in 1897, elucidated the entire transmission cycle of *Plasmodium relictum*, which infects culicine mosquitoes and birds. A group of Italian malariologists, Giovanni Battista Grassi, Amico Bignami, Giuseppe Bastianelli, Angelo Celli, Camillo Golgi and Ettore Marchiafava in 1898 conclusively demonstrated that the *Anopheles* mosquitoes transmit human malaria. In 1948, Henry Shortt and Cyril Garnham discovered the liver stage infection of the malaria parasites. In 1982, the dormant stage of the parasite in the liver was demonstrated by Wojciech Krotoski (Nye, 2002; Cox, 2010).

1.1.2 Epidemiology of malaria

Malaria has been a major public health problem in terms of morbidity and mortality across the world for several years. It continues to be a threat to the world population, even in the twentieth century. In 2017, there were 219 million cases of malaria in 87 countries, which is about 2 million more than the cases reported in 2016. Malaria claims a considerable number of casualties each year; around 435,000 people died of malaria in 2017 worldwide. Children under the age of 5 years and pregnant women are at the highest risk of the disease

in malaria-endemic regions (World Health Organisation, 2018). To recognize global efforts to reduce malaria-related mortality, Malaria Day is commemorated on April 25.

Malaria is endemic in many countries, especially in the tropical and subtropical zones. Central and South America, Africa, the Middle East, Southeast Asia, the Indian subcontinent and Oceania are considered endemic regions of malaria. According to the World Malaria Report 2018, about half of the world population was at the risk of contracting the disease in 2017, of which 1.1 billion people are at higher risk of developing malaria (World Health Organisation, 2018). A high-risk area is referred to as an area with an occurrence of more than 1 malaria case per 1,000 people per year (Figure 1.1).

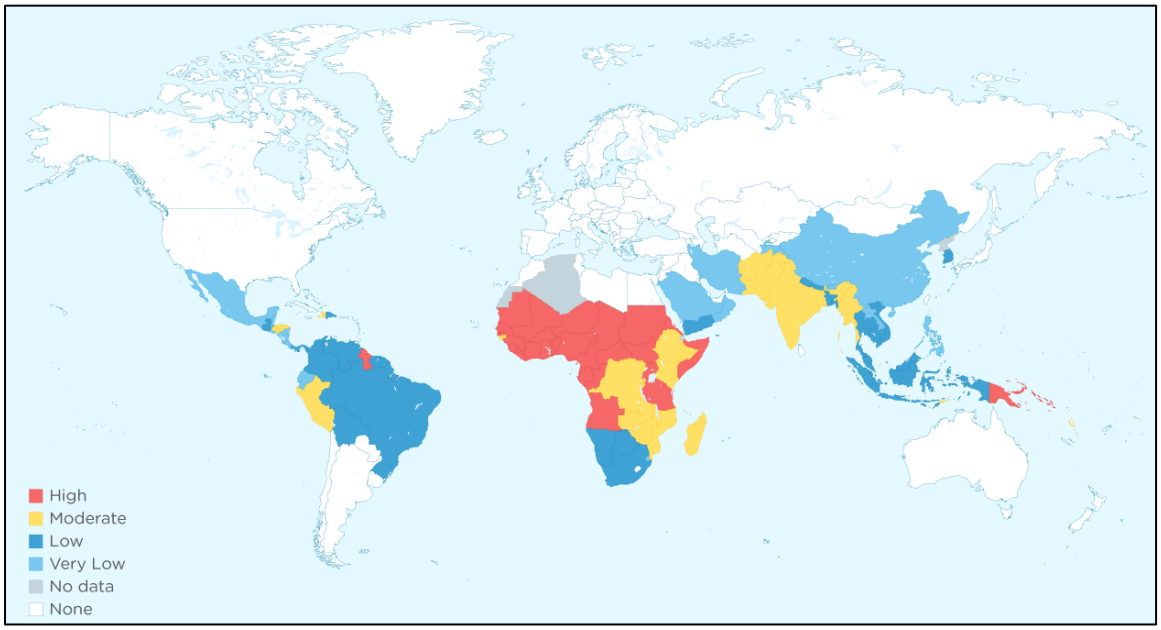

Figure 1.1: Malaria estimated risk heat map (Data sourced from CDC, 2018)

1.1.3 The burden of malaria in India

Malaria has been a challenge in India for centuries. After independence, 75 million people were affected by the disease, and the mortality was up to 0.8 million. The National Malaria Control Program (NMCP) in 1953, led to a sharp decline in the reported cases of malaria to less than 50,000 and no case of death was reported until 1961 (Dhingra *et al.*, 2010). According to the World Malaria Report 2018, more than half of the Indian population (698 million) is at the risk of malaria. It also states that India accounts for 4% of all malaria cases in the world, 4% of malaria-related deaths and 48% of the global *P. vivax* cases. According to the same report, 24% of malaria cases reduced as compared to the previous year, and the total number of malaria cases in India is estimated at 0.8 million (World Health

Organisation, 2018; Ghosh and Rahi, 2019). The Indian states Assam, Arunachal Pradesh, Manipur, Meghalaya, Nagaland, Orissa, Chhattisgarh, West Bengal, Rajasthan, Gujarat, Jharkhand, Karnataka, Madhya Pradesh, Uttar Pradesh, Haryana, Maharashtra, Tamil Nadu and Andhra Pradesh are endemic to malaria (Kakkilaya, 2019). The disease is prevalent in areas with insufficient sanitary conditions (Dayanand et al., 2017).

1.2 Biology of the human malaria parasite

1.2.1 Classification of the human malaria parasite

Plasmodium belongs to the kingdom Protista and phylum Apicomplexa, which also includes other pathogens such as *Babesia*, *Toxoplasma*, and *Cryptosporidium*. Apicomplexa is a taxonomic group of unicellular parasites that are morphologically recognized by the presence of a specialized complex of apical organelles such as micronemes, rhoptries, and dense granules. These apical organelles are required in host-cell invasion (Cowman and Crabb, 2006).

Kingdom	Protista
Subkingdom	Protozoa
Phylum	Apicomplexa
Class	Sporozoasida
Order	Eucoccidiorida
Family	Plasmodiidae
Genus	*Plasmodium*
Species	*falciparum*
	vivax
	malariae
	ovale
	knowlesi

Table 1.1: Classification of the human malaria parasite

Plasmodium lies within the order Eucoccidiorida, a group that includes apicomplexans that causes disease in humans, animals, and birds. Based on the presence of hemozoin pigment and asexual reproduction, the order is further divided into four families, of which

Plasmodium belongs to the family Plasmodiidae. There are over 200 species of *Plasmodium*, which infect a wide variety of hosts (e.g., reptiles, amphibians, birds, and mammals), of these species, only five are capable of infecting human, viz. *falciparum*, *vivax*, *malariae*, *ovale* and *knowlesi* (Table 1.1) (Pattaradilokrat *et al.*, 2013).

1.2.2 Characteristics of *Plasmodium* species infecting humans

P. falciparum is found in the tropical and subtropical areas and is predominant in Africa. *P. falciparum* infection results in severe malaria because *P. falciparum*-infected erythrocytes sequester in the blood vessels. The sequestration of erythrocytes in the blood vessel of the brain results in cerebral malaria, while in the placenta of the pregnant women leads to placental malaria (Table 1.2) (Iyer *et al.*, 2007; Autino *et al.*, 2012).

P. vivax is mainly located in Asia, Latin America, and parts of Africa. It can only infect Duffy positive blood group individuals. *P. vivax* also has a dormant liver stage called 'hypnozoite' which causes a relapse of the disease several months or years after the mosquito bite (Table 1.2) (Iyer *et al.*, 2007; Autino *et al.*, 2012).

P. ovale is dominated mainly in Africa and in the islands of the western Pacific. Biologically and morphologically, it is very similar to *P. vivax* and also has a dormant hypnozoite stage. However, *P. ovale* can infect the Duffy blood group negative individuals as well. Since the sub-Saharan African population is mostly Duffy negative, *P. ovale* infection is most prevalent in that region (Table 1.2) (Iyer *et al.*, 2007; Autino *et al.*, 2012).

P. malariae is found worldwide. The characteristic feature of *P. malariae* is that it has a quartan cycle, i.e., an intraerythrocytic (IE) cycle of three days (the previous three species have a tertian, two-day cycle). *P. malariae* can cause a long-lasting chronic infection if left untreated (Table 1.2) (Iyer *et al.*, 2007; Autino *et al.*, 2012).

P. knowlesi is originally the pathogen of long-tailed and pig-tailed macaques in Southeast Asia. This parasite species has recently been shown to infect humans in that region, particularly in Malaysia (Cox-Singh *et al.*, 2008). *P. knowlesi* has a 24 hours replication cycle and therefore multiply rapidly. Few fatal cases have been reported due to *P. knowlesi* infection (Table 1.2) (Iyer *et al.*, 2007; Autino *et al.*, 2012).

Species	Intraerythrocytic cycle periodicity	Type of RBC	Relapse (hypnozoite)	Global distribution
P. falciparum	48 hours	All	No	Tropical regions
P. vivax	48 hours	Reticulocyte	Yes	Everywhere except sub-Saharan Africa
P. ovale	48 hours	Reticulocyte	Yes	Africa
P. malariae	72 hours	Old RBC	No	Everywhere
P. knowlesi	24 hours	All	No	Southeast Asia, particularly Malaysia

Table 1.2: Characteristics of *Plasmodium* species infecting humans

1.2.3 The life cycle of *Plasmodium* species infecting humans

The malaria parasite has a complex life cycle which occurs in two hosts, the female *Anopheles* mosquito vector and the vertebrate host (Figure 1.2). Life cycles of the human malaria parasites (Table 1.2) are essentially similar with a few differences. The parasite progresses through several stages of development during its life cycle, for example, sporozoite (In Greek 'Sporos' means 'seeds'), an infectious stage, injected by mosquitoes during the bloodmeal in the bloodstream of humans; merozoite (In Greek 'Meros' means 'piece'), an infectious stage, that invades a red blood cell (RBC); trophozoite (In Greek 'Trophes' means 'nourishment'), a growing stage of parasite in RBC, which contains dark pigment called hemozoin; schizont (In Greek 'schizos' means 'to tear apart'), the multinucleate stage in RBC, containing nearly 32 merozoites that egress and infect new RBCs; gametocytes, sexual stages of the parasite. Each parasitic stage is morphologically distinct and has a unique set of proteins (Kakkilaya, 2018).

Malaria infection in humans begins when a female anopheline mosquito introduces infectious sporozoites into the host dermis while taking a blood meal (Vernick *et al.*, 2005). The sporozoites leave the site of the bite and migrate into the blood vessel and are transported to the liver. The sporozoites then invade hepatocytes forming a parasitophorous vacuole (PV) and follows a liver-stage cycle also called exoerythrocytic form (EEF). Sporozoites undergo several cycles of asexual multiplication leading to the formation of several uninucleate merozoites and release tens of thousands of first-generation merozoites. This stage is an asymptomatic stage of malaria infection (Figure 1.2) (Vaughan and Kappe, 2017).

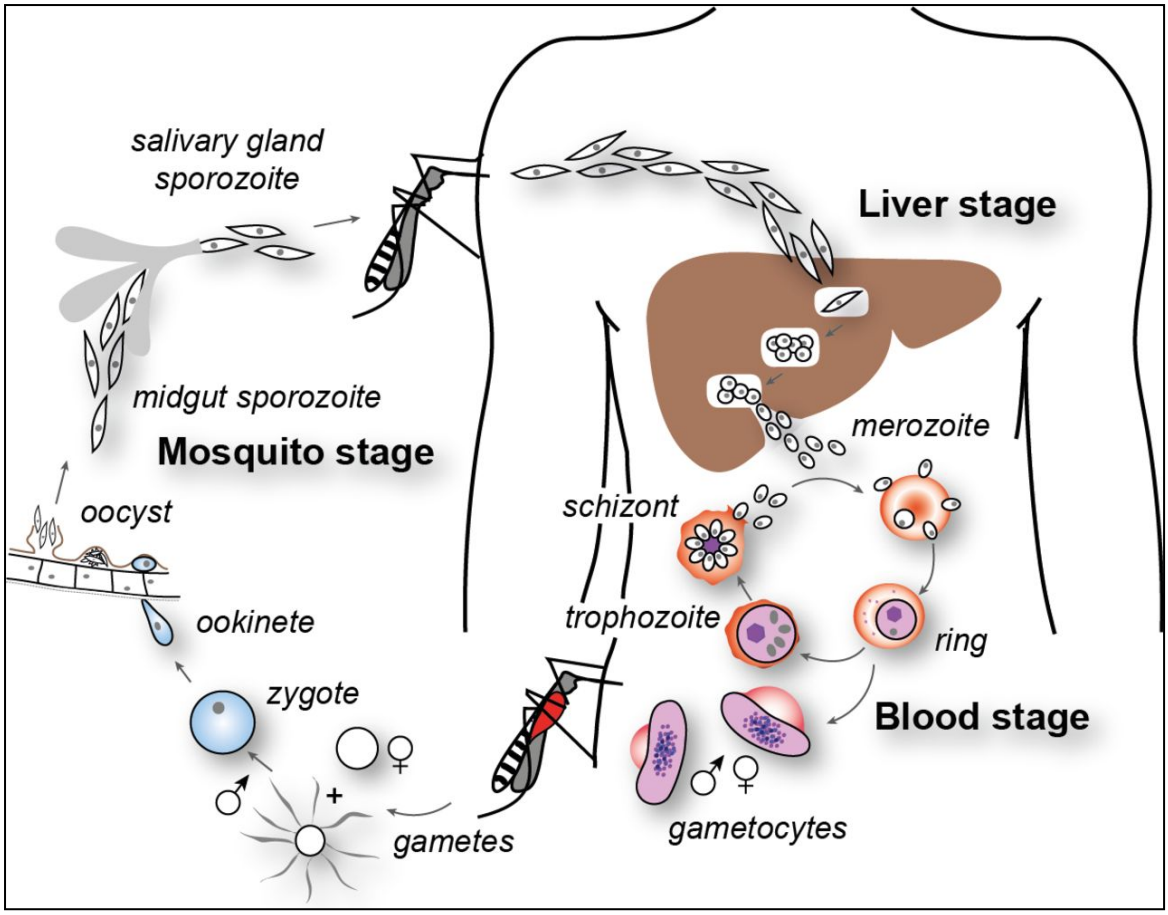

Figure 1.2: The life cycle of *Plasmodium* species infecting humans

The life cycle of *Plasmodium* involves a vertebrate host (human) and invertebrate vector (female *Anopheles* mosquito) (With permission from Cowman *et al.*, 2012, license Id 4672891266802).

Merozoites that are released from the hepatic stage of parasite enter the bloodstream to invade RBCs – thus commencing the second phase of asexual multiplication called erythrocytic schizogony (Cowman *et al.*, 2012). The erythrocytic schizogony results in the production of approximately 8-32 invasive merozoites, which are released into the circulation, where they invade uninfected RBCs (Cowman *et al.*, 2012). Each cycle of RBC invasion comprises of merozoites that progress through ring, trophozoite and schizont stages; this cycle is called the intraerythrocytic (IE) cycle or erythrocytic schizogony (Cowman *et al.*, 2012). The duration of each IE cycle depends on the *Plasmodium* species. In case of *P. falciparum*, *P. vivax*, and *P. ovale*, an IE cycle lasts 48 h (tertians); 24 h in *P. knowlesi* and 72 h in *P. malariae* (quartan) (Garcia *et al.*, 2001). The IE cycle of the parasite is responsible for the clinical manifestations of malaria. Symptoms of malaria, such as periodic fever and chills, result from the bursting of schizonts (Garcia *et al.*, 2001). During the erythrocytic schizogony, some merozoites differentiate into extracellular, non-

pathogenic male and female gametocytes. These gametocytes circulate in the peripheral blood until they are ingested by a female anopheline mosquito while drawing a blood meal from an individual infected with malaria (Figure 1.2) (Beri *et al.*, 2018; Ngotho *et al.*, 2019).

Gametocytes mature into male and female gametes within the mosquito and undergo sexual reproduction. In the lumen of the gut, fertilization of gametes forms a zygote, which develops into a motile ookinete, marking the beginning of sporogony. The ookinete enters the midgut of mosquito and develops into an oocyst. Multiplication inside the oocyst produces thousands of haploid sporozoites. After 8 to 15 days of sporogony, the oocyst ruptures to release the sporozoites into the body cavity of the mosquito, from there the sporozoites migrate to the salivary gland of the mosquito (Vernick *et al.*, 2005). During the bloodmeal, sporozoites are then injected into the blood circulation from salivary glands, causing malarial infection in the host, thus completing its life cycle (Figure 1.2) (Vaughan and Kappe, 2017).

1.2.4 Intraerythrocytic stages of *P. falciparum*

Among all *Plasmodium* species infecting humans, *P. falciparum* is considered deadliest and accounts for the highest number of cases (World Health Organisation, 2018). The clinical symptoms of malaria are due to the asexual forms of the parasite within RBCs; ranges from uncomplicated disease to fatal cerebral and placental malaria (Hanssen *et al.*, 2010). The development of asexual forms of the parasite within RBCs is called the intraerythrocytic (IE) development cycle. The parasite at this stage transforms through ring, trophozoite, and schizont, which finally bursts to release 16-32 daughter merozoites (Bannister *et al.*, 2000). Each asexual cycle is completed in ~48 h and the cell rupture stimulates periodic waves of fever in the malaria-infected patient (Hanssen *et al.*, 2010).

1.2.4.1 Merozoite stage

The invasive merozoite stage of the parasite is ovoid and flat at one end. Each merozoite is approximately 1.6 µm long and 1 µm wide. Despite its small size, the merozoite performs essential functions, such as egressing from the host RBC, attaching to the new RBC, invading it and quickly initiating the feeding process. The apex of merozoite has secretory organelles, such as rhoptry, micronemes and dense granules. As the malaria parasite

possesses these specialized apical complex, it falls under phylum apicomplexa. The secretions from rhoptry and micronemes facilitate the attachment of the merozoite to the host RBC surface and to invade it (Cowman and Crabb, 2006). The merozoite invasion forms a vacuole in the RBC, which eventually envelops the merozoite; this vacuole is called Parasitophorous Vacuole (PV). Dense granules release the contents in PV, which modifies the host RBC during the invasion. The proteins released from the apical organelles are potential vaccine candidates. Apart from apical organelles, merozoite contains a nucleus, mitochondrion, apicoplast and ribosomes (Figure 1.3A) (Bannister *et al.*, 2000; Alaganan *et al.*, 2017).

1.2.4.2 Ring stage

After the invasion, the merozoite develops into the ring within the RBCs. At the ring stage, the parasite resides inside the PV, which separates it from the RBC cytoplasm. The parasite morphology at this stage resembles a biconcave disc, thicker at the ends and thinner in the middle. The Giemsa-stained parasites appear as a signet-ring-like structure under the microscope hence named as the ring (Langreth *et al.*, 1979; Bannister and Mitchell, 2003). The nuclear shape varies from a sausage-like to a disc-shaped structure (Figure 1.3B). Ring feeds on hemoglobin and blood plasma through cytostome (Bannister and Mitchell, 2003). Hemoglobin is digested inside the food vacuole (FV) which serves as a source of amino acids for parasite growth while the by-product of hemoglobin degradation, i.e., 'heme', is polymerized into an inert, non-toxic brown crystals called hemozoin which remains within the FV throughout the IE cycle (Coronado *et al.*, 2014). As the parasite develops, the parasitophorous vacuolar membrane stretches as finger-like projections into RBCs and modifies the RBC membrane promoting its adherence to the blood vessels, including the placenta (Atkinson *et al.*, 1989).

1.2.4.3 Trophozoite stage

The ring stage is followed by the trophozoite stage, which is metabolically the most active. The ring and trophozoite stages are distinguished by the cell size and shape. At this stage, various parasite proteins are exported into the RBC cytoplasm and on the RBC surface, thus modifying its structure (Miller *et al.*, 2013). The exported proteins perform functions such as knobs formation on the RBC surface, the formation of flat membranous sacs called Maurer's cleft in the infected RBC. Parasite at trophozoite stage exports erythrocyte

membrane protein, *Pf*EMP1, to the RBC surface that promotes adherence of parasitized RBC to the endothelium of blood vessels, which prevents the removal of the parasite from the bloodstream (Miller *et al.*, 2013).

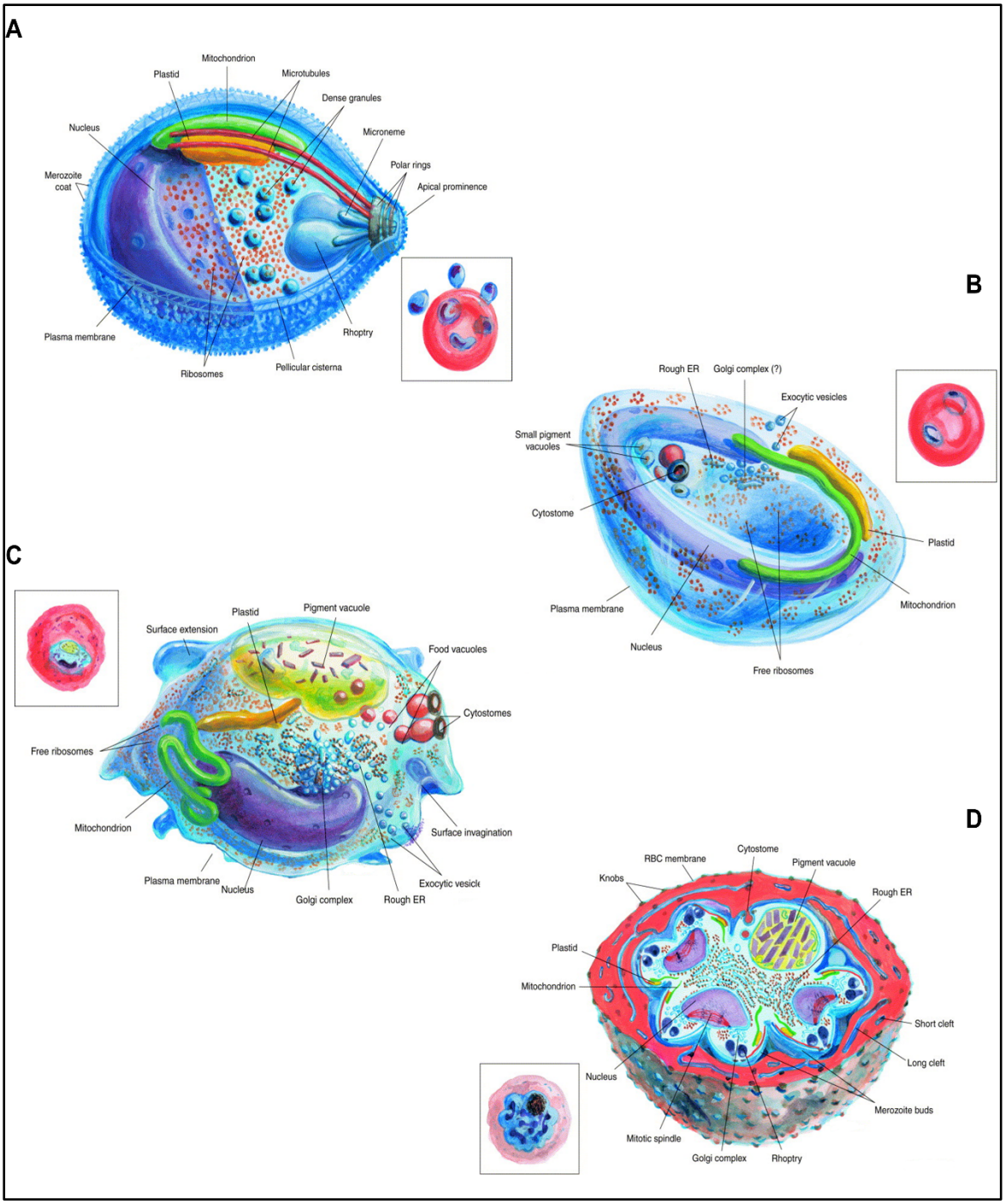

Figure 1.3: Schematic representation of intraerythrocytic stages of *P. falciparum*

Three-dimensional representation of **(A)** merozoite **(B)** ring **(C)** trophozoite and **(D)** schizont stages of *P. falciparum* (With permission from Bannister *et al.*, 2000, license Id 4672881201842)

Additionally, *Pf*EMP1 promotes the sequestration of infected RBCs to the blood vessels of the brain and placenta, leading to cerebral malaria and placental malaria, respectively

(Miller *et al.*, 2013). In the trophozoite stage, protein synthesis increases; therefore, the ER enlarges, and the numbers of free ribosomes increases. The DNA replication commences at this stage. The parasite continues to feed upon hemoglobin via cytostomes, and the hemozoin or the malaria pigment becomes prominent inside the FV, which is also visible by light microscopy (Figure 1.3C) (Bannister *et al.*, 2000; Bannister and Mitchell, 2003).

1.2.4.4 Schizont stage

At the schizont stage, the parasite undergoes multiple endomitotic nuclear divisions to produce daughter parasites or merozoites (Figure 1.3D). Until the late schizont stage, the ingestion of RBC cytosol, hemoglobin digestion and export of parasite proteins into RBC continues. The nuclear division generates about 8-32 daughter nuclei. On completion of nuclear divisions, the PV and RBC membranes are lysed by a proteolysis-dependent mechanism, thus facilitating the release of merozoites (Salmon *et al.*, 2001).

1.2.5 Amino acid metabolism in *P. falciparum*

Living organisms need a set of 20 amino acids to synthesize proteins. Biochemical pathways, involving multiple enzymes, are necessary for the synthesis of amino acids in a cell. Among eukaryotes, plants and fungi can produce all the amino acids needed for protein synthesis. While vertebrates, including humans, can *de novo* synthesize only 11 amino acids, called non-essential amino acids. Remaining 9 amino acids (Phe, Trp, Ile, Leu, Val, Lys, His, Thr, and Met), called essential amino acids, that are not synthesized by humans and must, therefore, be obtained from food. Parasites such as *P. falciparum* have lost the ability to synthesize many more amino acids, as they feed on other organisms and thrive in a nutrient-rich environment. *P. falciparum* can generate only four amino acids: asparagine, glutamine, glycine, and proline and depends upon its host for amino acid supply (Payne and Loomis, 2006).

P. falciparum majorly derives its amino acids from the hemoglobin available in RBCs (Liu *et al.*, 2006). During its asexual development in erythrocytes, parasite ingests 75% of the hemoglobin from the host RBC. Digestion of hemoglobin occurs in the FV of the parasite. It is a semi-ordered process that requires the action of a series of proteases such as plasmepsins, falcipains, aminopeptidases, and metalloproteases (Goldberg *et al.*, 1990; Francis *et al.*, 1997). The digested amino acids are then effluxed in the parasite cytoplasm

and used by the cell for protein synthesis. Excess amino acids are discharged out of the parasite (Dalal and Klemba, 2015).

Adult hemoglobin does not contain isoleucine and, therefore, is absorbed by the parasite from the blood plasma. The parasite deploys new permeability pathways (NPP) to uptake isoleucine from the extracellular environment (Martin and Kirk, 2007). It has been shown that *P. falciparum* can be cultured in a medium containing isoleucine as the sole source of the amino acid (Liu *et al.*, 2006), indicating that the parasite can obtain the remaining amino acids from the degradation of hemoglobin

1.3 Food vacuole: A site for hemoglobin digestion in *P. falciparum*

Food vacuole (FV) or digestive vacuole (DV) is a lysosome-like organelle in the parasite and is the main site for hemoglobin degradation. FV is separated from the parasite cytosol by a single lipid bilayer membrane (Figure 1.4). It has an acidic environment with pH less than 6, which is beneficial for the activity of FV proteins, for instance, plasmepsins and falcipains proteinases require pH 5-6 for their maximum activity (Bakar *et al.*, 2010). Hemoglobin uptake from the host erythrocyte during the blood-stage occurs via the endocytic pathway (Lazarus *et al.*, 2008; Milani *et al.*, 2015). Hemoglobin-containing vesicles (HcVs) delivers hemoglobin to the FV, where it is degraded by resident proteases (Goldberg, 2013). Hemoglobin degradation results in the generation of amino acids, which is used for protein synthesis by the parasite (Goldberg, 2013).

FV is also the site for heme detoxification. Heme is produced as a by-product of hemoglobin degradation and is toxic for the cell (Coronado *et al.*, 2014). Hence the toxic heme is neutralized by the parasite by crystallizing heme to form hemozoin. Hemoglobin hydrolysis and heme detoxification are two crucial processes carried out in the FV, which are essential for parasite survival. Therefore, proteins responsible for the homeostasis of FV are promising targets for developing new antimalarials (Coronado *et al.*, 2014). The most commonly used antimalarials, i.e., artemisinin, and chloroquine, targets the processes inside the FV. Artemisinin forms an adduct with heme and inhibits many enzymatic reactions in the cell, whereas chloroquine targets the polymerization of heme (Wunderlich *et al.*, 2012).

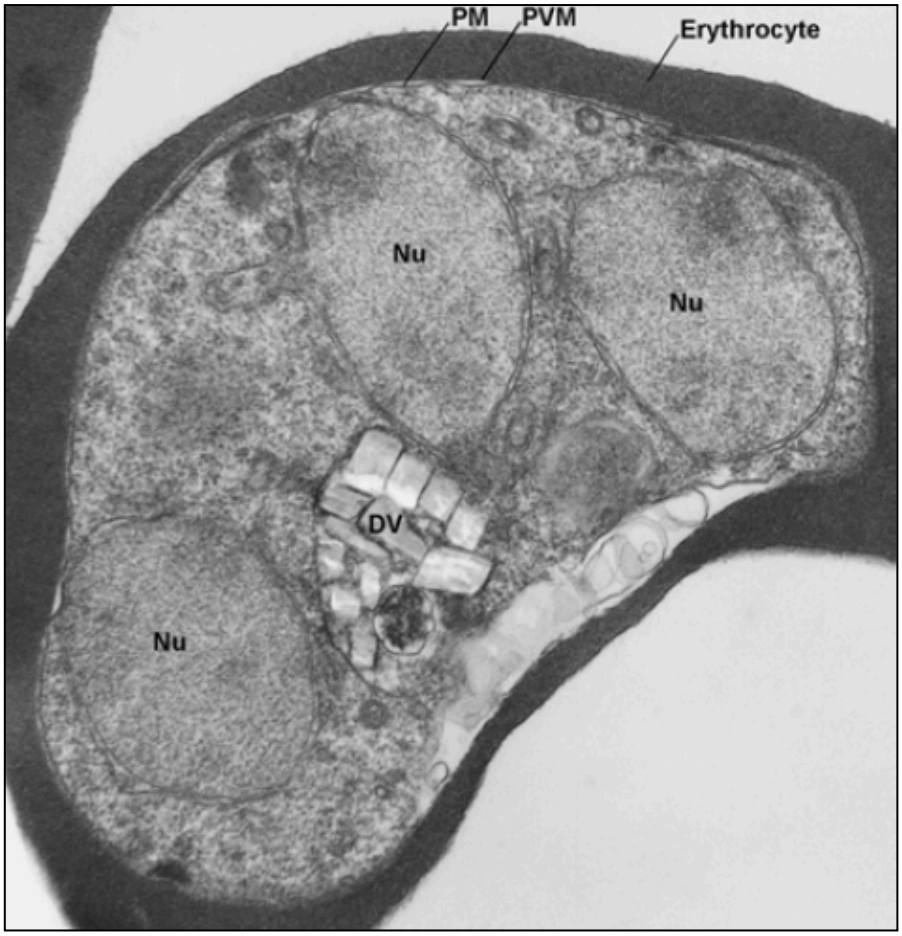

Figure 1.4: Ultrastructure of *P. falciparum* food vacuole

Ultrastructure of thin sections of a *P. falciparum*-infected erythrocyte (HB3) at the early schizont stage, DV contains ordered hemozoin crystals (With permission from Wunderlich *et al.*, 2012).

1.3.1 Formation and morphology of the food vacuole at different intraerythrocytic stages of *P. falciparum*

FV is a terminal degradative organelle essential for hemoglobin degradation in *P. falciparum*. FV is not inherited by the daughter merozoites but is developed *de novo* inside the parasite after each cycle of replication. FV exists in varied morphology, size and number in different asexual development stages of the parasite (Dluzewski *et al.*, 2008). The merozoite parasite invades the host RBC and quickly develops into ring-form inside it and initiates the uptake of hemoglobin from the host cell. This uptake pathway requires the specialized structure called cytostome, an invagination of parasitophorous vacuolar membrane (PVM) and parasite plasma membrane (PPM). The cytostome pinches off to form double membranous vesicles called hemoglobin-containing vesicles (HcVs), which contains host cytoplasm, including hemoglobin. In the ring stage, multiple dense vesicles

with 200-300 nm diameter act as lytic compartments, equivalent to FV, where hemoglobin is digested and hemozoin crystals are formed (Dluzewski *et al.*, 2008; Elliott *et al.*, 2008; Lazarus *et al.*, 2008; Bakar *et al.*, 2010; Milani *et al.*, 2015). In late ring stage, small pigment-containing vesicles coalesce to form single large FV (Dluzewski *et al.*, 2008; Wunderlich *et al.*, 2012). In trophozoite stage, the size of FV increases (2.2 μm) and occupies a significant part of the total volume of the parasite (Dluzewski *et al.*, 2008; Wunderlich *et al.*, 2012). Late trophozoites show enlarged FVs with widely dispersed hemozoin and an inward folding of the vacuolar membrane. During schizogony, the vacuole decreases in size (0.8-1.2 μm), loses membranous folds and contains large and closely packed hemozoin crystals (Dluzewski *et al.*, 2008; Wunderlich *et al.*, 2012). After the rupture of mature schizont, merozoites and membrane-bound residual bodies containing hemozoin are released outside the host RBC into the bloodstream (Dluzewski *et al.*, 2008; Wunderlich *et al.*, 2012).

FV structure and biogenesis varies across the *Plasmodium* species. In contrast to *P. falciparum*, *P. knowlesi* contains several smaller acidic compartments during its asexual cycle. While, small pre-FVs rapidly fuse to form single FV in *P. falciparum* (Wunderlich *et al.*, 2012). The feeding mechanism also differs in human and murine parasites. In murine parasite *P. chaubadi*, hemoglobin uptake involves a cytostome system comprising of a long tube connected with a tubular branching network, while in *P. falciparum,* hemoglobin uptake involves vesicles budding off from the cytostome (Wunderlich *et al.*, 2012).

1.3.2 Protein composition of the food vacuole in *P. falciparum*

FV harbours several proteins that participate in pathways that occur inside it, which include hemoglobin degradation and conversion of the toxic heme to non-toxic crystals of hemozoin (Lamarque *et al.*, 2008; Wunderlich *et al.*, 2012). These proteins are also targets of antimalarials such as chloroquine and artemisinin (Lamarque *et al.*, 2008; Wunderlich *et al.*, 2012).

FV contains four aspartic proteases: plasmepsin I (PM-I), plasmepsin II (PM-II), plasmepsin IV (PM-IV) and histo-aspartic protease (HAP) for hemoglobin degradation (Moura *et al.*, 2009). It also contains cysteine proteases falcipain-2 (FP2) and aminopeptidases (Moura *et al.*, 2009). Several transporters such as chloroquine resistance transporter (CRT) and multidrug resistance protein 1 (MDR1), responsible for providing

antimalarial resistance, are present on the FV membrane (Koenderink *et al.*, 2010; Ehlgen *et al.*, 2012). FV has an ion channel V-type H^+-ATPase, required for maintaining the acidic pH of the FV. It is also a dynamic storehouse for Ca^{2+} ions, transported across the FV by a Ca^{2+} ion channel (Biagini *et al.*, 2003). H^+-pyrophosphatases, *Pf*VP1, and *Pf*VP2 are also present on the FV membrane; they hydrolyse inorganic phosphate and establish a transmembrane proton gradient (McIntosh *et al.*, 2001).

As FV is a terminal degradation organelle, it receives several vesicles from different origins, such as host RBC, ER, Golgi and endosomal vesicles. Several proteins required for the vesicle-mediated trafficking, vesicle docking and fusion such as the ADP-Ribosylation Factor, the small GTPase Sar1, p24, and the GTPases Rab1, Rab2, Rab7, and Rab11 are found in the FV. Rab2 and Rab7 are orthologs of yeast Ypt4 and Ypt7, respectively, and are suggested to be involved in vacuole size regulation in *P. falciparum* (Quevillon *et al.*, 2003; Lamarque *et al.*, 2008).

Few parasite surface proteins are also found in FV. Proteins present on the RBC surface or PV reach to FV via HcV. Hexose transporter 2, nucleoside transporter 2 and aquaglyceroporin are PPM transporters that are shown to be localized in the FV too. Similarly, PV proteins – Exp1 and Exp2 are also found in the FV. A 19 kDa fraction of merozoite surface protein 1 (MSP1) is also detected in the FV. It is shown to be present on the FV since its formation and may be useful for FV biogenesis (Dluzewski *et al.*, 2008; Lamarque *et al.*, 2008).

Proteins involved in energy metabolism, including proteins of glycolysis such as GAPDH, are present in the cytoplasm as well as in the FV (Lamarque *et al.*, 2008). However, their function in this organelle is unknown. Chaperons such as BiP, Hsp70 are also identified in FV (Lamarque *et al.*, 2008). Chaperons may be required for protecting FV-resident proteins from oxidative damage since reactive oxygen species produced in the FV during heme oxidation may cause damage to FV-resident proteins (Lamarque *et al.*, 2008).

Many proteins whose roles are unknown also localize in FV. *Pf*ATG18 is one such protein that has been found in the FV by proteome analysis (Lamarque *et al.*, 2008). *Pf*ATG18 protein neither has signal sequence nor transmembrane domain/prodomain (found in PM-I and PM-II), required for the trafficking of proteins to the FV. In the absence of these sequences, it may follow the endosomal route to reach there (Lamarque *et al.*, 2008).

1.3.3 Protein trafficking to the food vacuole in *P. falciparum*

Resident FV proteins can be transported to the FV by multiple routes (Figure 1.5). Proteases such as falcipain 1 (FP1), FP2 and PM-II, required for the degradation of hemoglobin, utilizes parasites hemoglobin uptake pathway for trafficking to the FV. Premature proteases contain N-terminal signal peptide for entry into the ER. They also include a transmembrane prodomain that is required for subsequent transport of the protease to the FV lumen (Klemba *et al.*, 2004b; Dasaradhi *et al.*, 2007). The prodomain is cleaved in the FV, leading to the formation of mature functional protease. Another FV protease dipeptide aminopeptidase 1 (DPAP1), which cleaves hemoglobin-derived oligopeptides into dipeptide, follows a different trafficking route. Unlike PM-II or FP2, DPAP1 does not directly enter cytostome, but it first accumulates inside the PV before moving to the FV. DPAP1 contains signal sequence necessary for entry into the ER but lacks a transmembrane region. This protein is processed differently, the internal domain located in between the exclusion domain and two catalytic domains is excised. The prodomain in DPAP1 is different from that in FP2 and PM-II, which may be the reason for the difference between the trafficking of these proteins (Klemba *et al.*, 2004a).

Furthermore, it is shown that signal sequence is sufficient to traffic proteins to the FV, a reporter protein such as green fluorescent protein (GFP) fused with the FV signal peptide, can be targeted to the FV, while GFP without the targeting signal remains in the cytoplasm of the parasite (Tonkin *et al.*, 2006). *Pf*CRT traffics directly from the ER to the FV membrane (Ehlgen *et al.*, 2012) and HRPII traffics to the FV from the erythrocyte cytosol (McIntosh *et al.*, 2007). FVYE domain-containing protein (*Pf*FCP) follows a trafficking route that excludes the secretory pathway. *Pf*FCP is a PI3P-binding protein without a transmembrane domain, which is directly transported from the cytoplasm to the FV via a C-terminal 44-amino acid peptide. However, the exact trafficking pathway of this protein is unknown (McIntosh *et al.*, 2007). It is evident that FV-targeted proteins take several different routes to reach their destination and some of these pathways are still unclear (Wunderlich *et al.*, 2012).

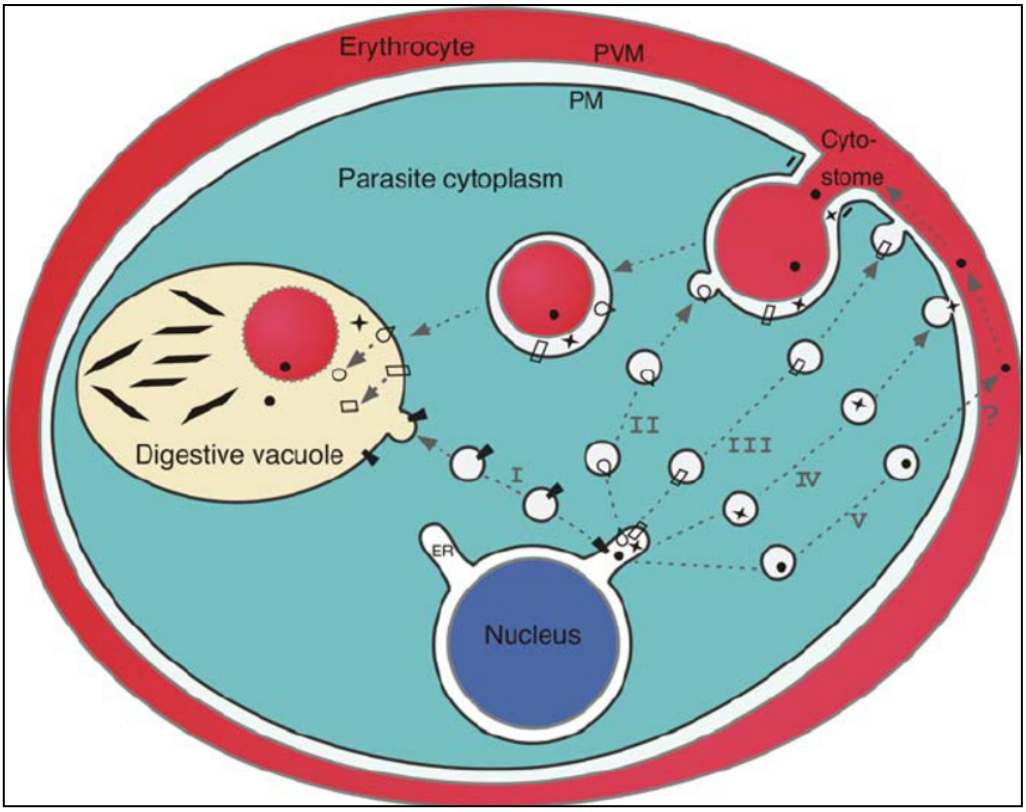

Figure 1.5: Protein trafficking to the FV in *P. falciparum*

Schematic representation of different trafficking routes taken by FV targeted proteins (With permission from Wunderlich *et al.*, 2012).

1.3.4 Hemoglobin trafficking pathway in *P. falciparum*

Parasite ingests hemoglobin from host erythrocytes, which is trafficked to the FV for degradation. The parasite degrades hemoglobin to generate amino acids and prevent premature lysis of the RBC. Hemoglobin uptake begins at the ring stage and continues until the schizont stage, but the mechanism and amount of hemoglobin uptake vary in different parasite stages (Elliott *et al.*, 2008). Parasite utilizes four independent yet overlapping pathways for hemoglobin uptake (Elliott *et al.*, 2008). Study through serial thin-section electron microscopy and three-dimensional reconstruction has shown that ingestion of hemoglobin begins in early ring stage, the parasite undergoes morphological transformation to form a cup-like structure and uptake a large amount of host RBC cytosol. This event is named “Big Gulp” (Elliott *et al.*, 2008). This uptake is independent of actin polymerization, as inhibitors of actin polymerization do not interrupt big gulp. This step is also the beginning of FV formation in the parasite. In the mature stages, hemoglobin uptake from the host cell is mediated by the cytostome (Elliott *et al.*, 2008; Smythe *et al.*, 2008; Lazarus *et al.*, 2008; Milani *et al.*, 2015).

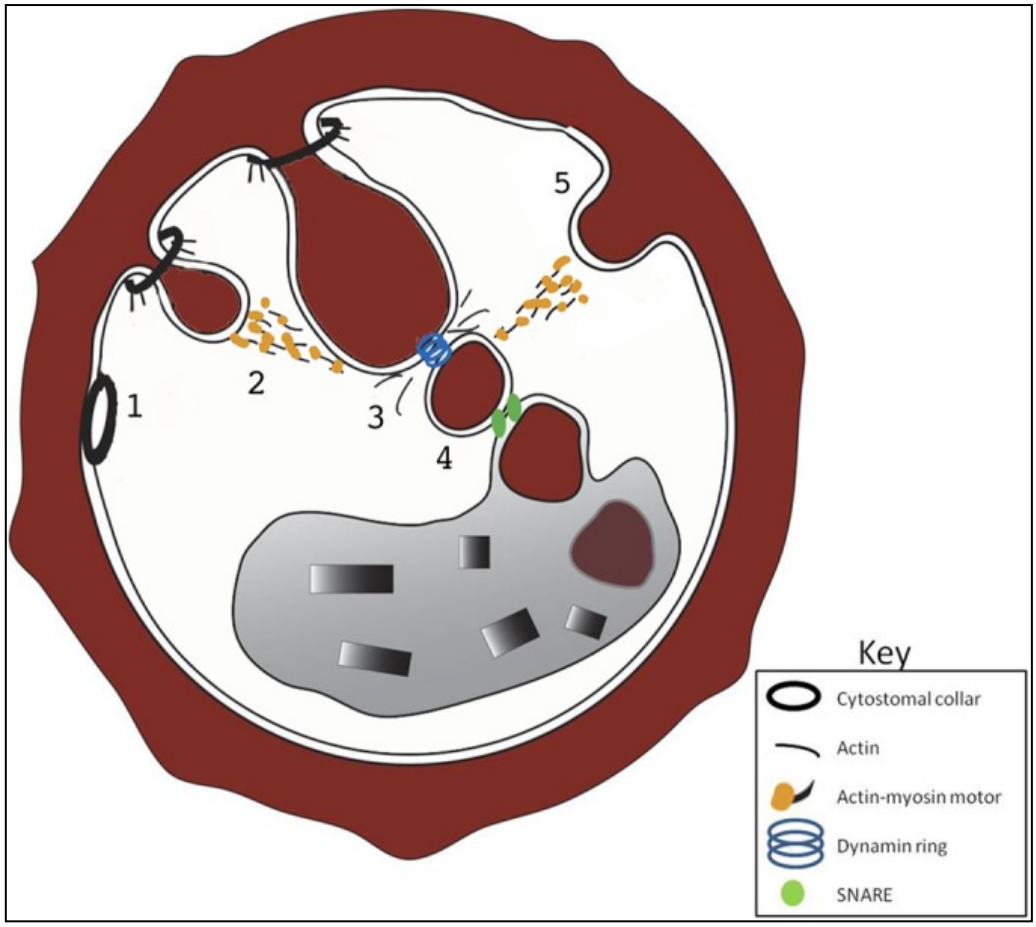

Figure 1.6: Hemoglobin trafficking pathway in *P. falciparum*

Schematic representation of hemoglobin uptake pathway in *P. falciparum* (With permission from Milani *et al.*, 2015).

Cytostomes are formed by the membrane invagination of PVM and PPM. PVM forms the inner membrane of the cytostome while PPM forms the outer membrane. The invagination is actin-dependent and the event is similar to the endocytosis pathway described in the eukaryotic cells, as the treatment of the parasite with jasplakinolide, which stabilizes actin filament, inhibits the uptake of hemoglobin (Elliott *et al.*, 2008; Smythe *et al.*, 2008; Lazarus *et al.*, 2008; Milani *et al.*, 2015). The cytostomes pinch off from the membrane to form double-membrane vesicles called HcV. This is the most characterized pathway for hemoglobin uptake in which small HcVs, resembling endocytic vesicles, are generated. The difference between HcV and endocytic vesicle is that the former is a double membrane-bound vesicle while the latter is enclosed by a single membrane. These vesicles can be distinguished by visualizing parasites under electron microscopy. The next pathway involves the formation of a long thin cytostomal tube and requires the activity of actin and dynamin (Elliott *et al.*, 2008). The last mode of hemoglobin uptake is phagotropy, which

resembles big gulp in the mature stage parasite and does not involve actin polymerization (Elliott *et al.*, 2008).

A refined model of hemoglobin uptake in *P. falciparum* has been proposed (Milani *et al.*, 2015). It states that hemoglobin transport to FV begins by the invagination of PVM and PPM forming cytostomes. The cytostomes increase in length in an actin-myosin-dependent manner. At some point, HcVs are generated from the minus end of the cytostome in a dynamin-dependent manner. The fusion of HcV with FV requires SNAREs. The outer membrane of the HcV fuses with the FV while single membrane-bound HcV is delivered inside and is degraded by FV resident lipases and proteases (Figure 1.6) (Milani *et al.*, 2015). The fusion of HcV with the FV requires actin polymerization as treatment of parasites with cytochalasin D, which depolymerizes actin, inhibits fusion of HcV and FV (Smythe *et al.*, 2008).

1.3.5 Hemoglobin degradation in *P. falciparum*

The primary function of the parasite FV is hemoglobin degradation. It is the major source of amino acids for *P. falciparum,* as the parasite lacks the biosynthesis of many amino acids. Parasite uptakes approximately 75% hemoglobin during its development in the host erythrocytes. Hemoglobin degradation also provides space for the parasite to grow in RBC and prevents the premature lysis of the host RBC (Bakar *et al.*, 2010). FV is the primary site of the hemoglobin degradation; however, the degradation initiates *en route* in the vesicles carrying hemoglobin. It has been shown that HcV contains proteases and has acidic pH, required for the degradation of hemoglobin (Bakar *et al.*, 2010). Hemoglobin lysis requires an action of a series of proteases and acidified environment (lower pH). *P. falciparum* genome encodes 10 plasmepsins out of which 4 are located in the FV, namely, PM1, PM2, HAP, and PM4. Plasmepsins and falcipains together digest globin into polypeptides (Wunderlich *et al.*, 2012). The expression of falcipains and plasmepsins are different in different developmental stages of the parasite, suggesting distinct functions during its life cycle. The maximum expression of PM1 and PM4 is in ring stage while PM2, HAP, FP2 are abundant in the trophozoite stage and FP3 is enriched in early schizont. The polypeptide fragments are digested into short peptides by metalloprotease falcilysin, which are further cleaved by DPAP1 into dipeptides (Banerjee *et al.*, 2002; Liu *et al.*, 2006; Wunderlich *et al.*, 2012).

Hemoglobin digestion can be inhibited by small-molecule inhibitors such as pepstatin and E-64. Pepstatin blocks the activity of aspartic protease plasmepsin, while E-64 inhibits cysteine protease falcipain. The combination of pepstatin and E-64 can completely block hemoglobin digestion in the FV (Moura *et al.*, 2009). Gene knockout studies have shown that individual knockout of four plasmepsin genes is insufficient for hemoglobin degradation and even when all four genes are knocked out, falcipain can compensate for the loss of plasmepsin and hemoglobin digestion continues to occur in the parasite which suggests that these enzymes are redundant in their functions. This redundancy in hemoglobin digestion may be a strategy of the parasite to survive a strong dose of protease inhibitors and ensure hemoglobin digestion (Omara-Opyene *et al.*, 2004).

1.3.6 Phosphoinositide profile of *P. falciparum*

Phosphoinositides are a family of acidic phospholipids found on cell membranes in eukaryotic cells. Phosphatidylinositol (PI) is phosphorylated at hydroxyl group of its inositol head group by specific kinases to form seven different types of phosphoinositides, namely, PI4P, PI(4,5)P_2, PI3P, PI(3,5)P_2, PI(3,4)P_2, PI(3,4,5)P_3 and I(1,4,5)P_3 (Rusten and Stenmark, 2006). These phosphoinositides are enriched on the membranes of different cellular compartments and participate in a plethora of cellular functions such as membrane trafficking, cell motility, cytoskeletal reorganization, DNA synthesis, adhesion, and signal transduction (Balla, 2013). They also provide membrane identity to the subcellular compartments, for instance, PI4P is majorly found on the Golgi apparatus, PI(4,5)P_2 at the plasma membrane, PI3P on early endosome and PI(3,5)P_2 on late endosome compartments (Rusten and Stenmark, 2006).

P. falciparum produces PI4P, PI(4,5)P2, PI3P, PI(3,4)P_2 and PI(3,4,5)P_3, but PI(3,5)P_2 is absent. Also, its genome does not encode ortholog of Fab1 kinase required for the synthesis of PI(3,5)P_2, which phosphorylates PI3P at 5′ position (Tawk *et al.*, 2010). PI(3,5)P_2 is essential for multivesicular body (MVB) formation, retrograde trafficking from late endosome to trans Golgi network, vacuole size regulation by participating in vacuole fission in yeast and mammals (Jin *et al.*, 2016; Choy *et al.*, 2018), and in the absence of this phospholipid yeast cells have abnormally large vacuole (Jin *et al.*, 2016). Since PI(3,5)P_2 is absent in *Plasmodium*, it has been suggested that endosomal trafficking in this

parasite might be different from the classical pathway known in yeast and higher eukaryotes (Tawk *et al.*, 2010).

PI3P is present in low quantity in eukaryotic cells and is vital for endosomal trafficking. It is the product of class III PI3-kinase, also called Vps34 (vacuolar protein sorting 34). Levels of PI3P is low in ring stage parasite, but it is high in the trophozoite stage due to the specific role of this lipid in later stages of the parasites. Of interest, PI3P is found on the FV membrane, apicoplast and small single membrane vesicles, which are shown by the localization of a PI3P-specific probe, i.e., GFP fused with FYVE (Fab1, YOTB, Vac1, EEA1) domain (Tawk *et al.*, 2010). Additionally, it is proposed that PI3P plays a role in targeting parasite proteins to the host cell (Bhattacharjee *et al.*, 2012) and is also involved in the endocytosis from the RBC to the parasite and hemoglobin trafficking (Vaid *et al.*, 2010).

1.4 Autophagy: An overview

Autophagy is a cellular degradation and recycling pathway, by which the cell disposes of unwanted or damaged cellular components. There are three types of autophagy in mammalian cells: microautophagy, macroautophagy, and chaperone-mediated autophagy (CMA). While each type of autophagy is morphologically distinct, they all involve the transport of the cargo to the lysosome for degradation (Figure 1.7). Microautophagy occurs directly at the lysosomal or vacuolar membrane. The limiting membrane can invaginate or protrude to engulf the cargo (Mijaljica *et al.*, 2011). CMA uses chaperon Hsc70 to identify cargo proteins comprising the pentapeptide KFERQ-like sequence; substrates are then unfolded and translocated directly across the lysosomal membrane (Massey *et al.*, 2004). In contrast, macroautophagy involves sequestration of the cytoplasmic cargo in the double-membrane vesicles called autophagosomes, which subsequently transport cargo to the lysosome (Yorimitsu and Klionsky, 2005; Parzych and Klionsky, 2014). Macroautophagy will be referred to as “autophagy” subsequently.

Autophagy is well conserved in eukaryotic cells. It occurs at a low level constitutively called the basal autophagy, which is involved in maintaining cellular homeostasis by degrading damaged or excess organelles. Also, autophagy can be induced under stress conditions, such as nutrient starvation or oxidative stress. Under stress conditions, autophagy helps to degrade cytoplasmic materials into metabolites, which can be used by

the cell for generating energy. Thus, autophagy is mainly a cell survival mechanism; however, excessive degradation of cellular components can be harmful. Accordingly, the dysfunction in the autophagic pathway is associated with a wide range of human disorders, including heart disease, neurodegeneration, cancer and aging (Mizushima, 2007; Parzych and Klionsky, 2014).

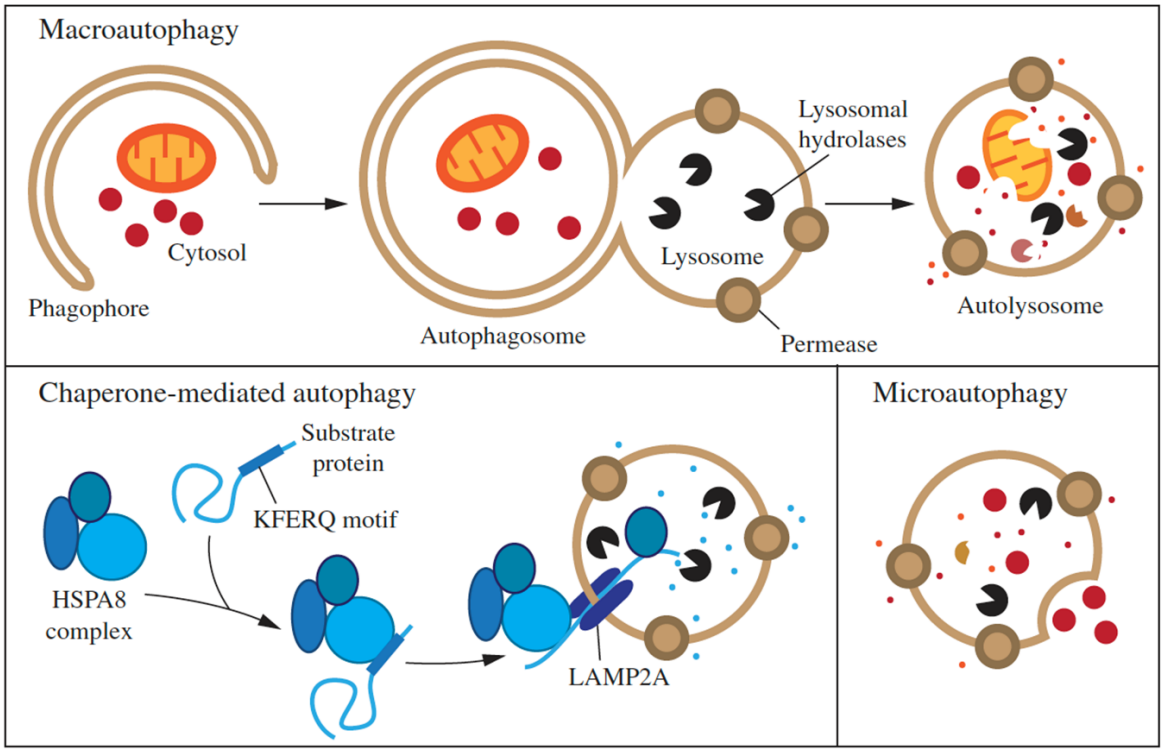

Figure 1.7: Schematic representation of types of autophagy

Types of autophagy: macroautophagy, chaperone-mediated autophagy and microautophagy (With permission from Parzych and Klionsky, 2014).

1.4.1 A brief history of autophagy

The term 'autophagy' was coined by Christian de Duve in 1963. In 1955, de Duve had identified an organelle containing lytic enzymes by cell fractionation of the rat liver cell and termed it as the lysosome. In 1956, Novikoff and colleagues showed the morphology of lysosome by electron microscopy (EM) in rat liver cells (Yang and Klionsky, 2010; Ohsumi, 2014; Mizushima, 2018).

During 1956-1957, Novikoff and S Clark found irregularly shaped vesicles containing mitochondria and cytoplasmic contents in kidney tubules cells; now known as autophagosomes. In 1968, Astila and Trump showed that in the beginning, the double-membrane autophagosomes are formed that contains cytoplasmic materials but lacks lytic

enzymes while single membrane-bound organelles called autophagolysosomes are formed subsequently, which degrades the contents of autophagosomes (Yang and Klionsky, 2010; Ohsumi, 2014; Mizushima, 2018).

Insights into the molecular mechanism of autophagy commenced in the late 1990s. Y Ohsumi *et al.* have been instrumental in identifying autophagy proteins and assigning their functions. They executed the first genetic screen for yeast mutants that affected protein degradation and identified genes involved in nonspecific macroautophagy. Similar genetic screens were carried out that affected peroxisome degradation (pexophagy), transport of vacuolar hydrolases [Cytoplasm to vacuole targeting (Cvt) pathway] and selective degradation of mitochondria. ATG1 was the first autophagy-related (*ATG*) gene to be identified. Currently, about 42 ATG proteins are known to be involved in autophagy in yeast. Significant milestones were achieved when the role of autophagy was identified in human health and diseases such as cancer, neurodegenerative diseases, aging and longevity, innate and adaptive response to pathogens (Yang and Klionsky, 2010; Ohsumi, 2014; Mizushima, 2018).

1.4.2 Functions of autophagy

Recent studies have implicated that autophagy has a great variety of physiological and pathological roles such as adaptation during starvation, protein aggregates and organelle clearance, differentiation and development, anti-aging, innate and adaptive immunity, cell death, tumor suppression. The diverse roles of autophagy may be attributed to the "induced autophagy" or "basal autophagy". The former is benefitted to produce metabolites following nutrient stress, while the latter is used for eliminating cytosolic components constitutively. Functions of autophagy can be further categorized into two groups: Physiological and pathological (Mizushima, 2007).

1.4.2.1 Physiological functions of autophagy

1.4.2.1.1 Cell survival

During normal conditions and a very brief period of starvation, amino acid pools are maintained in the cell by Ubiquitin-proteasome system (UPS). However, in the case of persistent starvation, necessary amino acids are provided by autophagy. These amino acids are used by the cell to generate energy via gluconeogenesis, the TCA cycle, or can be used

for protein synthesis. Autophagy is also known to play a crucial role in hypoxia and other metabolic stress conditions. The production of amino acids by autophagy can support cell viability during stress (Mizushima, 2007).

1.4.2.1.2 Clearance of macromolecules and organelles

The cell removes damaged proteins and organelles via autophagy. It is, therefore, a method of quality control of the cell. Autophagy-deficient mutants in various cell types have been shown to contain a higher number of abnormal proteins and damaged organelles. Autophagy is also useful for removing unwanted organelles. For example, excess peroxisomes are eliminated by selective autophagy called pexophagy, and damaged mitochondria are cleared by mitophagy (Mizushima, 2007).

1.4.2.1.3 Transportation of proteins from the cytoplasm to vacuole

Autophagy also plays a role in the trafficking of vacuole proteins, such as aminopeptidase 1 (Ape1), α-mannosidase (Ams1), and aminopeptidase 4 (Ape4) from the cytoplasm to the lysosome or vacuole by Cvt pathway (Mizushima, 2007).

1.4.2.1.4 Cell death

Although autophagy is a mechanism of cell survival (as described above), it is also one of the three types of cell death which includes apoptosis (type I cell death), autophagic cell death (ACD) (type II cell death), and necrosis (type III cell death). It is called apoptotic cell death when there are characteristic cell changes such as nuclear fragmentation, chromatin condensation, DNA fragmentation, cell shrinkage (Das *et al.*, 2012). Whereas necrosis is morphologically characterized by translucent cytoplasm, organelle swelling, increased cell volume, resulting in the disruption of the plasma membrane (Golstein and Kroemer, 2007). While it is called ACD when autophagic vacuoles are increased during cell death but are not accompanied by the chromatin condensation (Das *et al.*, 2012).

1.4.2.2 Pathological functions of Autophagy

1.4.2.2.1 Autophagy and cancer

The role of autophagy in cancer is correlated with the stage of the disease. In the early stage of cancer, autophagy acts as a tumor suppressor by eliminating damaged proteins and organelles, mainly mitochondria. However, at later stages of tumor progression, autophagy

acts as a tumor protectant, because it provides cancer cells with nutrients that promote cell survival under conditions of metabolic stress and hypoxic conditions (Mizushima, 2007; Klionsky and Codogno, 2013).

1.4.2.2.2 Autophagy in diseases

An essential function of autophagy is to eliminate unwanted and damaged proteins and organelles. Therefore, defect in autophagy leads to the accumulation of aggregated proteins in neurons causing neurodegenerative diseases such as Alzheimer's, Huntington's, Parkinson's disease. Autophagy is also essential for the health of the heart and pancreas (Mizushima, 2007; Klionsky and Codogno, 2013).

1.4.2.2.3 Autophagy in aging and longevity

Autophagy significantly reduces upon aging. In the screening for aging factors in short-lived *S. cerevisiae* mutants, ATG null mutants including ATG1, ATG7, ATG18, and Beclin1 have been identified. Reports in mice have shown that ATG knockouts are not viable during the postnatal period. In *C. elegans*, the mutation of essential *ATG* genes has been shown to prevent longevity (Rubinsztein *et al.*, 2011).

1.4.2.2.4 Innate and adaptive response

Autophagy facilitates not only the degradation of cellular self-components but also intracellular pathogens. Pathogenic bacteria, such as *Streptococcus pyogenes* and *Shigella flexneri*, are sequestered by large autophagosomes and are degraded after fusion with lysosomes. *Mycobacterium tuberculosis* inhibits the maturation of phagosomes and continues to grow inside it. However, when autophagy is stimulated by starvation or rapamycin, autophagosome formation completes and these bacteria can then be eliminated by degradation in the lysosome (Deretic, 2005; Xu and Eissa, 2010).

1.4.3 Mechanism of autophagy

The sequestration of the cargo is the most critical and complex part of autophagy. It involves a double-membrane structure, the autophagosome. The formation of the autophagosome is a transient and dynamic event involving several protein complexes that participate at various stages of autophagy. Autophagosome formation or biogenesis can be divided into five main events: induction, nucleation, expansion, fusion, and degradation

(Figure 1.8). About 20 ATG proteins are involved in autophagosome formation in yeast, orthologs of many of these proteins are also found in higher eukaryotes (Feng *et al.*, 2014; Yin *et al.*, 2016; Suzuki *et al.*, 2017). The details of the various events of the autophagy and its machinery are described subsequently.

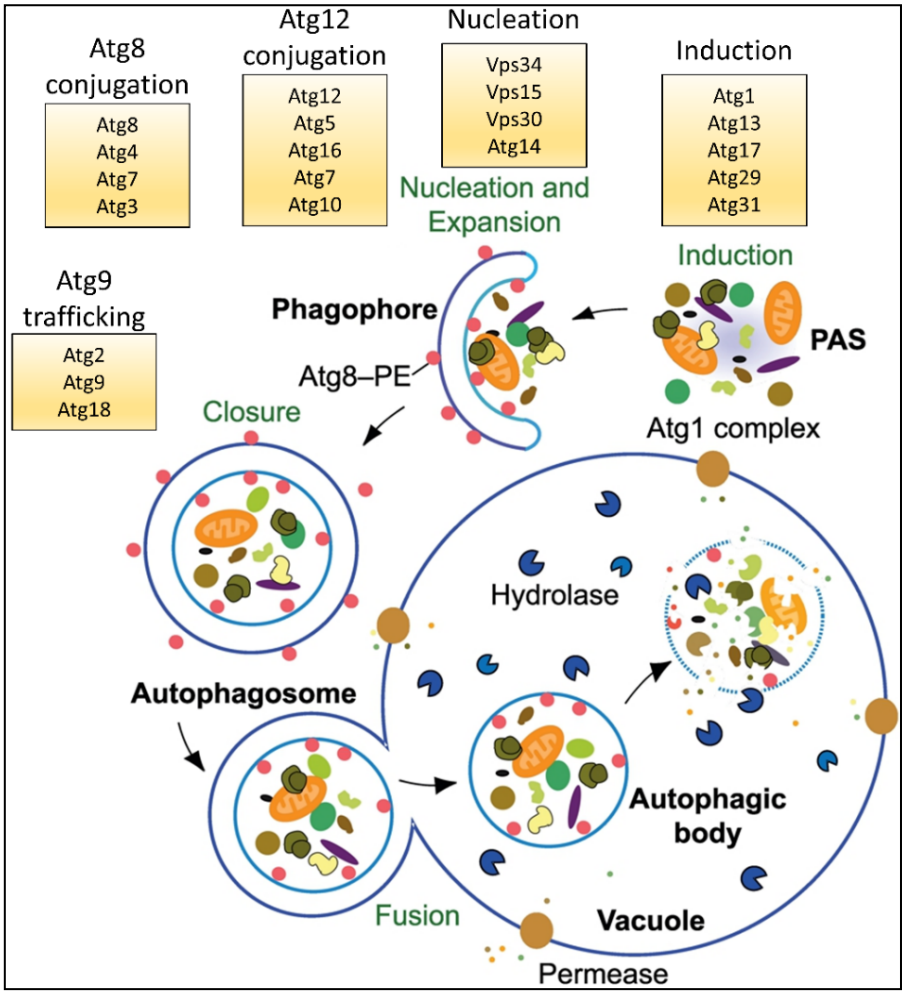

Figure 1.8: Mechanism of autophagy

The mechanical features of autophagy and its protein machinery (Modified with permission from Yin *et al.*, 2016).

1.4.3.1 Induction

Autophagy is induced in response to extracellular environment stress. Target of rapamycin complex 1 (TORC1) is one of the key players by which the cell senses the shift in nutrient availability. Nutrient starvation initiates an intracellular signaling cascade, which results in the inactivation of TORC1, causing activation of the ATG1 kinase complex. The ATG1 kinase complex consists of ATG1, regulatory protein ATG13, and a scaffold subcomplex that includes ATG17, ATG31, and ATG29 (Figure 1.8). This complex recruits other ATG proteins to the PAS, and therefore, it is crucial for autophagy. The ATG1 complex takes

input signal from protein kinase A (PKA), Gcn2 and Snf1/AMPK pathways as well (Feng *et al.*, 2014; Yin *et al.*, 2016; Suzuki *et al.*, 2017).

1.4.3.2 Nucleation

Nucleation is the event that results in the recruitment of ATG proteins to PAS that is required for the phagophore expansion. The class III PI3K complex I is an autophagy-specific PI3K complex that is recruited on the PAS after autophagy induction. The complex is comprised of the lipid kinase Vps34, the regulatory kinase Vps15, Vps30/ATG6, ATG14 and ATG38 (Figure 1.8). Vps34 produces phosphatidylinositol-3-phosphate (PI3P) from PI at the PAS which is crucial for the precise localization of the ATG18-ATG2 complex, which in turn recruits ATG8, ATG9 and ATG12 on the PAS (Feng *et al.*, 2014; Yin *et al.*, 2016; Suzuki *et al.*, 2017).

1.4.3.3 Expansion

The expansion or elongation of the autophagosome membrane involves two ubiquitin-like (Ubl) conjugation systems: ATG12 and ATG8 conjugation system and ATG9 trafficking system. ATG12 is a Ubl protein that forms a Ubl conjugation with ATG5 by the action of E1 and E2-like enzymes ATG7 and ATG10, respectively. There is no typical E3 enzyme involved in ATG12-ATG5 conjugation. ATG12-ATG5 conjugate then interacts with a small coiled-coil protein, ATG16, leading to the formation of ATG12-ATG5-ATG16 multimeric complex (Figure 1.8). The conjugation of ATG12-ATG5 occurs constitutively and irreversibly, which is conserved in yeast and higher eukaryotes (Geng and Klionsky, 2008). ATG8 is another Ubl protein implicated in autophagy, which forms a Ubl conjugation with a lipid phosphatidylethanolamine (PE) with the help of ATG4, which exposes C-terminal glycine of ATG8 and recycles it, ATG7, an E1-like enzyme, and ATG3, an E2-like enzyme. ATG8-PE is closely associated with the autophagosome membrane. ATG12-ATG5 accelerates the transfer of ATG8 from ATG3 to PE, so this complex is considered as an E3-like enzyme for ATG8 conjugation (Figure 1.8) (Geng and Klionsky, 2008).

Autophagosomes are double membranous vesicles, and unlike vesicles involved in endocytosis, autophagosomes do not bud off from an existing organelle membrane. Instead, the membrane is generated *de novo* inside the cell. ATG9 is the only transmembrane protein that might function as a membrane transporter for the phagophore expansion. It shuttles

between the PAS and membrane sources such as ER and Golgi. ATG9 localizes to the PAS from peripheral sites with the help of ATG11, ATG23, and ATG27. The retrieval of ATG9 from PAS to peripheral sites involve ATG1-ATG13 and ATG2-ATG18 complexes (Figure 1.8) (Feng *et al.*, 2014; Yin *et al.*, 2016; Suzuki *et al.*, 2017).

1.4.3.4 Fusion

After autophagosome formation is completed, it targets to, tethers/docks and then fuses with the vacuole. The outer membrane of the autophagosome fuses with the vacuole, while the inner membrane containing cytoplasmic materials is released into the vacuole lumen. The docking and fusion machinery include SNAREs and homotypic fusion and vacuole protein sorting (HOPS) proteins, which are common in other types of vesicle fusion with the vacuole (Feng *et al.*, 2014; Yin *et al.*, 2016; Suzuki *et al.*, 2017).

1.4.3.5 Degradation

Once the autophagosome is delivered inside the vacuole, its membrane is degraded by a lipase, ATG15, which is followed by the degradation of cargo by resident hydrolases. The macromolecules generated after the degradation are released into the cytosol through various permeases, including ATG22 (Feng *et al.*, 2014; Yin *et al.*, 2016; Suzuki *et al.*, 2017).

1.4.4 Modulators of autophagic flux

The autophagy pathway involves the formation of autophagosomes as an intermediate structure. The number of autophagosomes observed at any point in time is an equilibrium between its rate of generation and degradation in the vacuole, called the autophagic flux. The autophagic flux is induced by inducers such as amino acid deprivation, ER stress inducers such as Brefeldin A, Thapsigargin, Tunicamycin and mTOR inhibitor rapamycin (Figures 1.9 and 1.10). Whereas it is decreased upon the inhibition of autophagy at the upstream of the autophagosome formation by using PI3K inhibitors such as 3-methyladenine (3-MA), wortmannin and LY294002 (Figures 1.9 and 1.10). The inhibition of autophagy after the completion of autophagosome formation by vacuolar-type H^+-ATPase inhibitor Bafilomycin A1 causes a reduction in autophagic flux but results in accumulation of autophagosomes in the cytosol leading to increase in the autophagosome number (Figures 1.9 and 1.10). Similar to Bafilomycin A1 treatment, chloroquine and

hydroxychloroquine, lysosomal lumen alkalizer, impair lysosomal activity, leading to a reduction in autophagic flux but increase in the autophagosome number (Figures 1.9 and 1.10). Leupeptin, E64d, Pepstatin A are acid protease inhibitors that inhibit the degradation of autophagosome components (Mizushima *et al.*, 2010; Yang *et al.*, 2013; Klionsky *et al.*, 2016; Torggler *et al.*, 2017) (Figure 1.9).

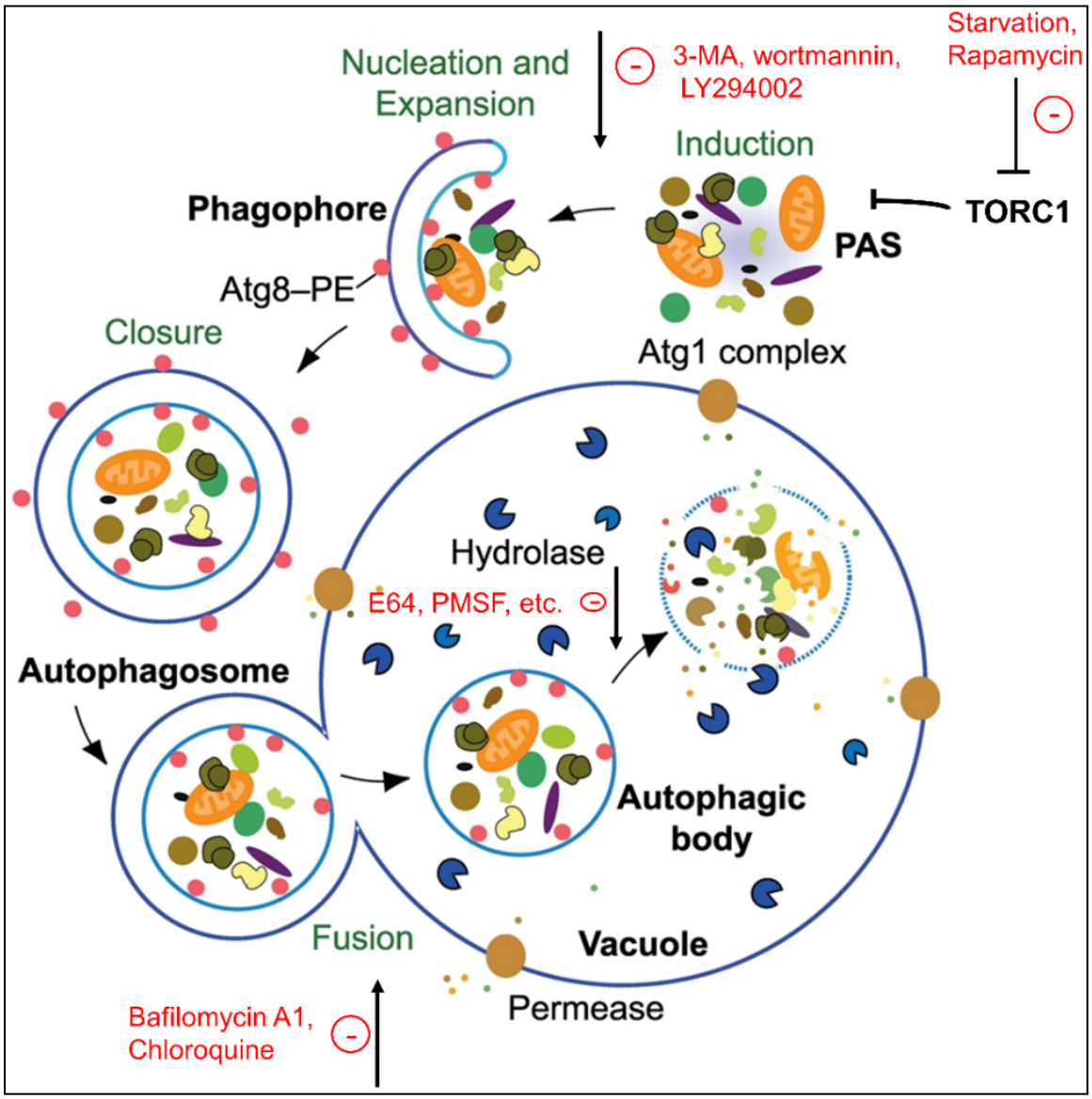

Figure 1.9: Modulators of autophagy

Activators and inhibitors of autophagy and the steps of autophagy affected by these modulators are indicated. The target of rapamycin complex I, TORC1, pre-autophagosomal structure (PAS) (Modified with permission from Yin *et al.*, 2016).

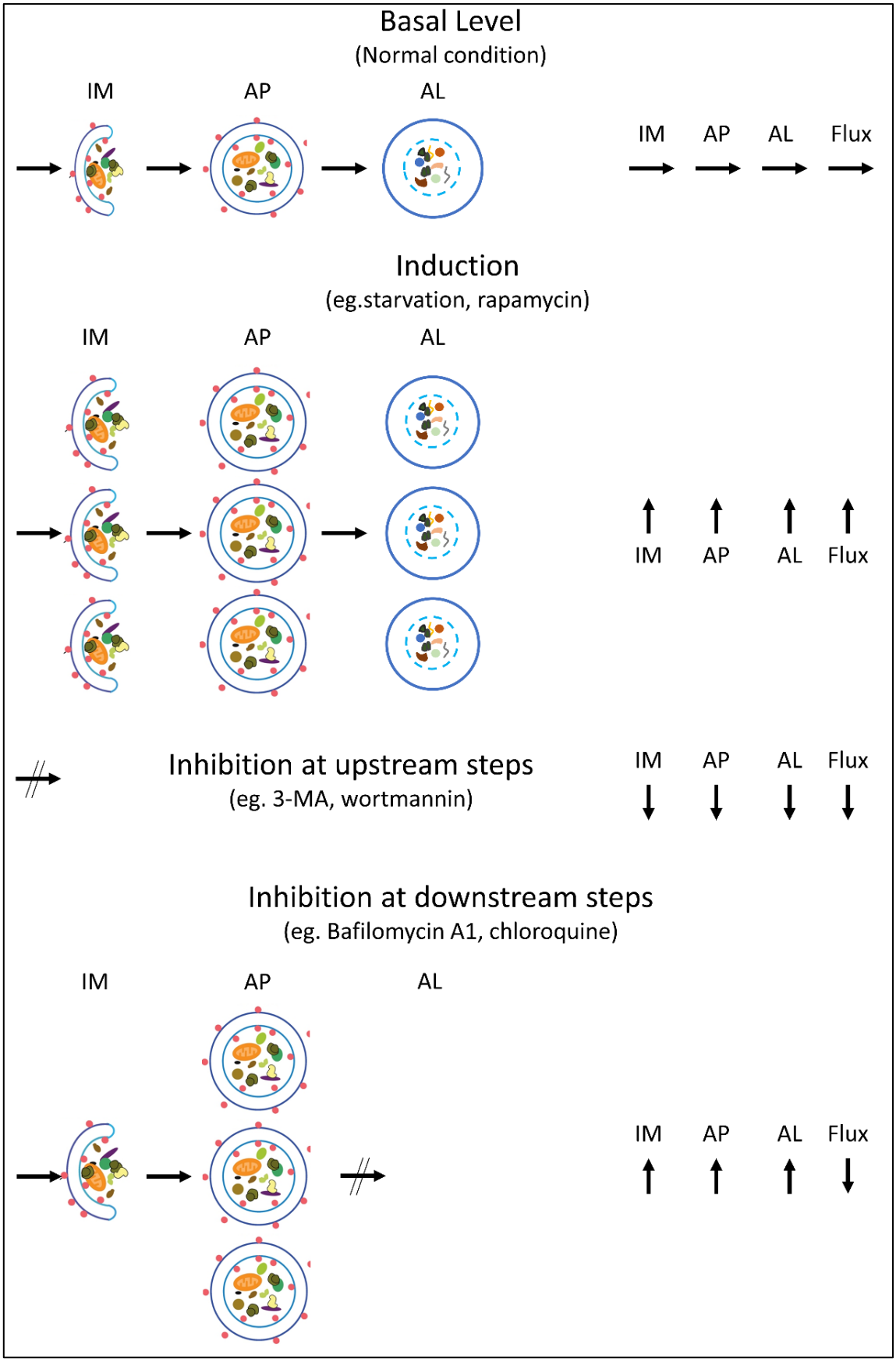

Figure 1.10: Effect of autophagy modulators on autophagic flux

Effect on autophagic flux in different conditions. IM: Isolation membrane, AP: Autophagosome, AL: Autolysosome (Modified with permission from Mizushima *et al.*, 2010, license Id 4672961125932).

1.5 Autophagy-related protein 5 (ATG5)

ATG5 is a core autophagy-related protein and is essential for autophagosome expansion and, therefore, has a conserved role in non-selective as well as selective autophagy. It is a part of the ATG12-ATG5.ATG16 complex, which catalyses ATG8-PE conjugation process. The *ATG5* mutant is defective in the autophagy and the Cvt pathway, and the null mutant exhibits decreased viability during starvation and have reduced overall lifespan. The *ATG5* mutant yeast cells show a decrease in ATG8 processing and recruitment to the PAS (Table 1.3).

	Yeast	Mammals	Features	Function
ATG12 conjugation system	ATG12	ATG12	Ubiquitin-like	The ATG12-ATG5-ATG16(L) dimer acts as an E3-like enzyme for ATG8/LC3-PE conjugation. This complex is present on the outer side of the isolation membrane and is essential for the proper elongation of the isolation membrane.
			Conjugates to ATG5	
			Interacts with ATG3	
	ATG7	ATG7	E1-like enzyme	
	ATG10	ATG10	E2-like enzyme	
	ATG5	ATG5	Conjugated by ATG12	
	ATG16	ATG16L	Homodimer	
			Interacts with ATG5	

Table 1.3: Members of ATG12 conjugation system and their role in autophagosome formation

1.5.1 A brief history of ATG5

ATG5, previously called as Apg5, has been identified as an autophagy-related protein in the genetic screening of yeast mutants that are deficient in autophagy in yeast. In the *ATG5* mutant yeast strain, autophagic bodies are not found inside the vacuoles during autophagy-inducing conditions; thus, the involvement of ATG5 in autophagy has been confirmed. It is also found that, in yeast, ATG5 is not essential for normal growth but is required during the starvation condition, as the viability of the mutant cell decreases considerably after three days of starvation (Tsukada and Ohsumi, 1993).

In mammals, ATG5 was previously called apoptotic-specific protein (ASP) because its expression was found only under apoptotic conditions, but not during normal conditions. Since ASP is found near non-muscle actin, it was thought to be a cytoskeleton-associated protein (Grand *et al.*, 1995). Later, it was found that ASP was very similar to *Sc*Atg5 (Hammond *et al.*, 1998) and further research has shown that ATG12 conjugates to ATG5 in mammalian system (Mizushima *et al.*, 1998b) similar to that in yeast (Mizushima *et al.*, 1998a), indicating that conjugation process is conserved in eukaryotes.

1.5.2 Domain architecture of ATG5

ATG5 comprises a helical rich domain (HR) flanked by two ubiquitin-like domains, UblA and UblB, located respectively at the N-terminus and the C-terminus. The linker regions L1 and L2 connect HR with UblA and UblB, respectively. ATG5 also has an N-terminal α-helix, in addition to the ubiquitin domains, HR and linkers (Figure 1.11A). UblA and UblB contain five β-sheets and two α-helices, this is a conserved structure in the ubiquitin superfamily proteins, including the autophagy-related proteins ATG12 and ATG8. Lys149 in *Sc*Atg5, which binds to ATG12, is located on α4 of the HR (Figure 1.11B). ATG5 domain architecture includes UblA, UblB, and HR regions, which is conserved in its orthologs present in different species. Loop1 and N-terminal α-helix are also conserved, but loop2 varies from one species to another (Matsushita *et al.*, 2007).

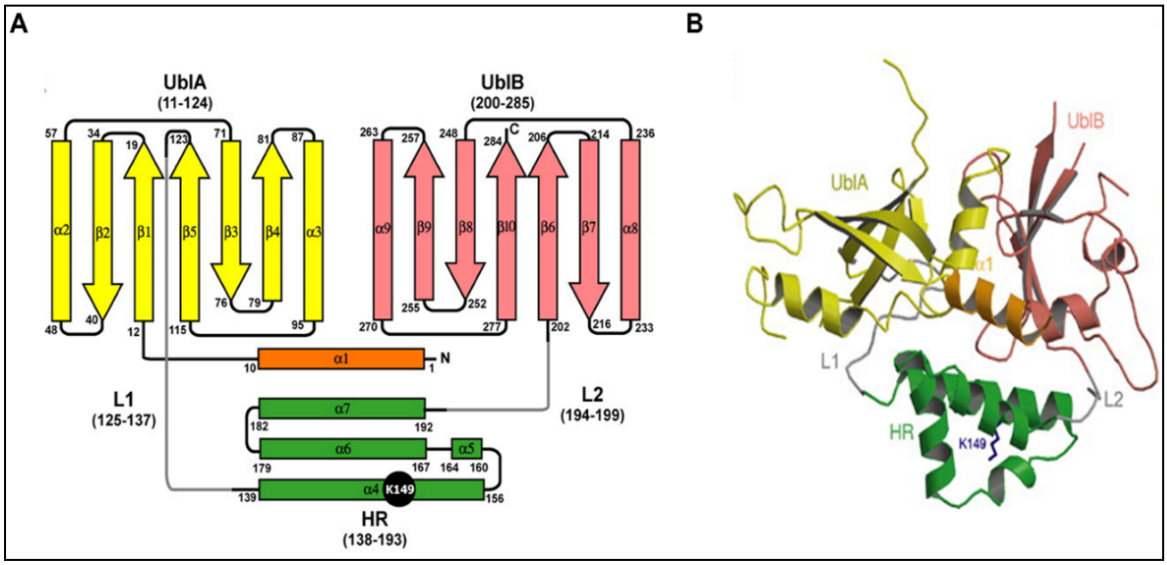

Figure 1.11: Domain architecture and crystal structure of ATG5

(A) Domain architecture of ATG5. **(B)** 3-D structure of ATG5 (With permission from Matsushita *et al.*, 2007, license Id 467297094824).

1.5.3 ATG12-ATG5.ATG16 complex formation

ATG5 exists in conjugation with ATG12. ATG12 is a Ubl protein that is activated by the E1-like activating enzyme ATG7. Activated ATG12 is then transferred to the E2-like conjugating enzyme ATG10, which helps to conjugate ATG12 with its only target, ATG5. The terminal glycine of ATG12 forms an isopeptide bond with the lysine side chain of ATG5 (Lys149 in case of *S. cerevisiae* and Lys130 in mammals) (Figure 1.12) (Mizushima *et al.*, 1998a; Mizushima *et al.*, 1998b). This interaction is similar to the ubiquitin conjugation. The ATG12-ATG5 complex exists in the cell cytoplasm under normal growing conditions (Geng and Klionsky, 2008).

ATG16 has been identified as an interacting partner of ATG12 by two-hybrid screening in yeast, using ATG12 as a bait. ATG16 is a small 17 kDa protein with a coiled-coil domain towards its C-terminus in yeast. ATG16 binds to the ATG12-ATG5 conjugate via ATG5 during autophagy. ATG16 interacts with ATG5 through the N-terminus, which stimulates self-multimerization of ATG16 through its coiled-coil domain, leading to the formation of a multimeric complex of about 350 kDa with the ATG12-ATG5 conjugate in yeast (Mizushima *et al.*, 1999). ATG16 is critical for the localization of the ATG12-ATG5 complex to the PAS and is, therefore, indispensable for both the autophagy and the Cvt pathway (Kuma *et al.*, 2002). In mammals, a protein similar to ATG16 is called ATG16-like protein or ATG16L. It contains seven WD repeats towards its C-terminus in addition to the coiled-coil domain. The interaction of ATG16L with the ATG12-ATG5 conjugate is also via ATG5. Like yeast, ATG12-ATG5.ATG16L complex exists in the multimeric form in mammals, mediated by the homo-oligomerization of ATG16L, forming a complex of approximately 800 kDa. ATG12-ATG5.ATG16 complex formation is necessary for autophagosome elongation, an essential step in autophagosome biogenesis (Figure 1.12) (Mizushima *et al.*, 2003).

ATG5 is a membrane-bound protein, but its interaction with ATG12 makes it cytosolic. ATG5 conjugated to ATG12 is present in the cytosol under normal nutrient conditions. However, under starvation conditions, ATG16 interacts with ATG12-ATG5 conjugate, which helps in the recruitment of the complex to the isolation membrane in yeast as well as in mammals (Mizushima *et al.*, 2001). ATG5 is involved in autophagosome elongation and can be found on the outer membrane of the isolation membrane or phagophore. It leaves the autophagosome upon the completion of autophagosome formation (George *et al.*,

2000). Additionally, it has been proposed that the positively charged residues in yeast ATG5, i.e., lysine160, and arginine171, interacts with the negatively charged membrane and facilitate the recruitment of ATG12-ATG5 complex on the membrane (Romanov *et al.*, 2012).

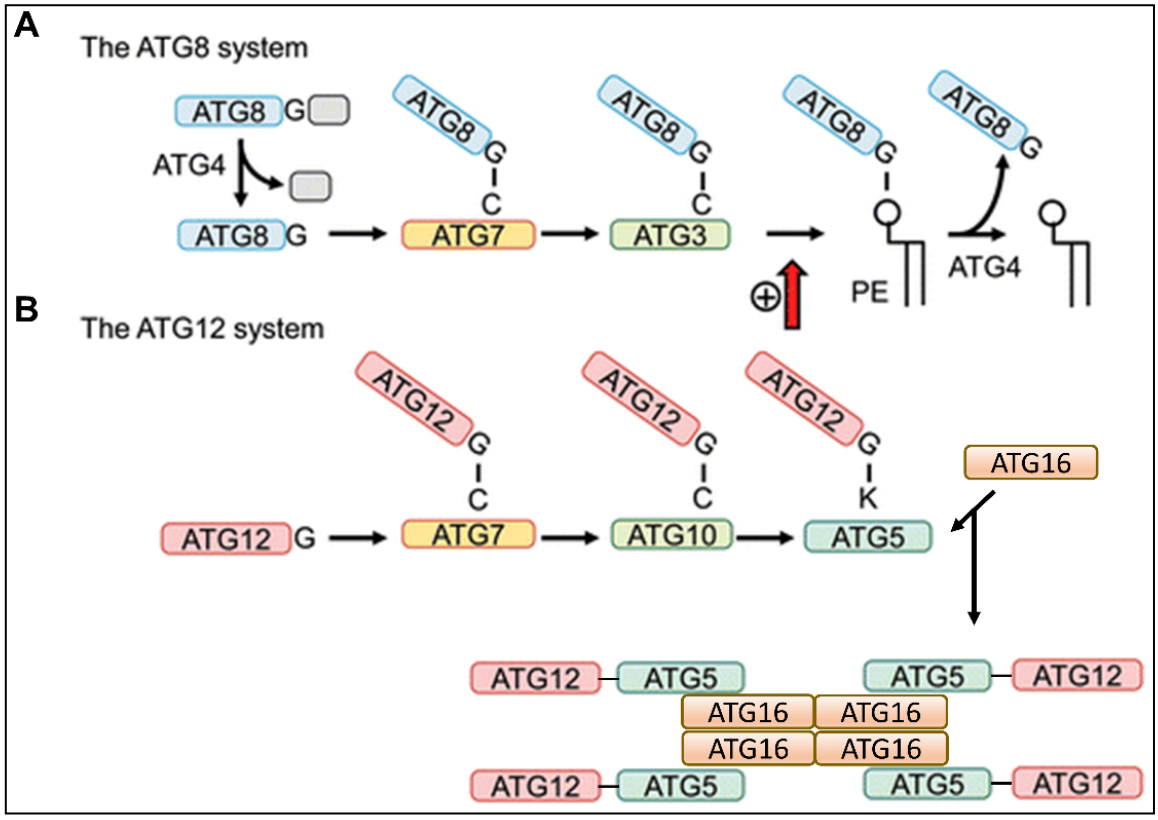

Figure 1.12: Ubiquitin-like conjugation systems involved in autophagy

Model of the ATG8 and ATG12 conjugation system. **(A)** The ATG8 conjugation system. **(B)** The ATG12 conjugation system (Modified with permission from Mizushima and Sahani, 2014).

The localization of ATG5 on the PAS is dependent on the PI3K activity in yeast and mammals (Suzuki *et al.*, 2007; Koyama-Honda *et al.*, 2013). In yeast, ATG5 localizes to the PAS after the recruitment of ATG1 (Suzuki *et al.*, 2007), while, in mammalian cells, ATG5 is recruited to phagophore synchronously with ULK1 (mammalian counterpart of ATG1) (Koyama-Honda *et al.*, 2013). In *Arabidopsis thaliana*, ATG5 is located on the phagophore site from the onset of autophagosome formation and defines a torus-shaped structure on an early phagophore. ATG5 decorates the high curvature domain of the phagophore and leaves it as soon as the aperture is sealed (Le Bars *et al.*, 2014).

1.5.4 Role of ATG5 in autophagy

ATG5 is essential for autophagic vesicle formation, and therefore, it is indispensable for canonical and non-canonical autophagy (Geng and Klionsky, 2008). Downregulation or knockout of ATG5 results in inhibition of autophagy, indicating that ATG5 plays a central role in autophagy. Thus, ATG5 is often targeted in autophagy gene editing assays. ATG5 is also involved in other functions in mammals, which includes quality control of mitochondria upon oxidative stress, regulating innate antiviral immune response, lymphocyte development, antigen presentation by MHC II; adipocyte development; and apoptotic cell death (Pierdominici *et al.*, 2012). Genome-wide association study (GWAS) shows the direct association between ATG5 and autoimmunity, such as systemic lupus erythematosus, systemic sclerosis, rheumatoid arthritis, and multiple myeloma (Pierdominici *et al.*, 2012; Mitchell *et al.*, 2016).

ATG5 levels are also critical for autophagy modulation in mammals. It is cleaved by a calcium-dependent cysteine protease Calpain I. When the intracellular Ca^{2+} levels are low, the cleavage activity of Calpain I is downregulated, leading to the accumulation of ATG5 and in turn ATG5-ATG12 complex, and thereby upregulating autophagy (Xia *et al.*, 2010). Similarly, ATG5 levels are also regulated by microRNA miR181a. ATG5 mRNA and protein levels decrease significantly when this miRNA binds to the miRNA response element present in the 3′ UTR of ATG5, thus causes autophagy inhibition (Tekirdag *et al.*, 2013). ATG5 in the mammalian system can modulate autophagy during nutrient deprivation or rapamycin blockage by forming a complex with receptor-activated C-kinase 1 (RACK1), to initiate autophagosome biogenesis. Knockdown of RACK1 inhibits autophagy, due to the lack of RACK1-ATG5 complex formation (Erbil *et al.*, 2016).

ATG12-ATG5.ATG16 participates in autophagosome membrane elongation by involving in ATG8-PE conjugation and by directly binding with the autophagosomal membrane. This complex acts as an E3-like enzyme in the ATG8/LC3-PE conjugation system (Eskelinen, 2008). The precursor ATG8 is first cleaved by cysteine protease ATG4, which excises the C-terminal arginine residue to expose a glycine residue. This glycine is conjugated to PE by the action of E1 protein ATG7 and ATG8-specific E2 conjugating protein ATG3. Although ATG3 can induce lipidation of ATG8, this process is accelerated *in vitro* by the ATG12-ATG5 conjugate and requires ATG16 *in vivo* (Suzuki *et al.*, 2007). This complex facilitates the efficient production of ATG8-PE conjugate on the isolation membrane and

thus contributes to the autophagosome formation (Hanada *et al.*, 2007). E3 ligases required for ubiquitin conjugation are HECT-type or RING-type ligases. Both ATG12 and ATG5 lack determining features of ubiquitin E3 ligases. ATG12 contains a ubiquitin-like fold, while ATG5 contains two ubiquitin-like fold and an HR domain. Altogether, ATG12-ATG5 conjugate includes three ubiquitin-like folds, which is structurally different from the canonical E3 ligase. ATG12 instead serves as a binding module for ATG3 so that ATG5 can interact with ATG3 and facilitate ATG8 lipidation (Hanada *et al.*, 2007; Mizushima *et al.*, 2011; Tamura *et al.*, 2013).

Additionally, the direct binding of this complex with autophagosome is necessary for membrane elongation. ATG5 has the ability to bind with the membrane, while ATG12 inhibits membrane interaction. Binding with ATG16 regains its membrane binding, and the complex is able to form giant unilamellar vesicles (Romanov *et al.*, 2012).

ATG5 also plays a role in the fusion of the autophagosome with a lysosome in mammals. ATG5 interacts with Tectonic β-propeller repeat containing 1 (TECPR1), present on the lysosomal membrane, and regulate fusion. During autophagy conditions, ATG12-ATG5 interacting region (AIR) domain of TECPR1 binds with ATG5-ATG12, and its PH domain binds with PI3P of the autophagosomal membrane, thus mediating autophagosome-lysosome fusion (Chen and Zhong, 2012).

1.5.5 Role of ATG5 in cell death

Besides promoting autophagy, ATG5 is also involved in the pro-apoptotic pathway. ATG5 initially participates in autophagy and promotes cell survival, then engages in apoptosis and induces cell death. Upon stimulation of mammalian cell death, by triggers such as anticancer drugs, a cysteine protease calpain cleaves ATG5 at Thr193, generating a 24 kDa fragment. The cleaved product of ATG5 translocates to the mitochondria and induces the release of cytochrome c, which in turn induces apoptosis. Thus, ATG5 represents a molecular switch between autophagy and apoptosis (Yousefi *et al.*, 2006). There is additional evidence suggesting that ATG5 plays a role in cell death regulation. For instance, ATG5 has been described to associate with Fas-associated death domain protein (FADD) and IFN-induced cell death (Pyo *et al.*, 2005). Reports suggest that ATG5 mediates apoptotic cell death but not autophagic cell death, as it has been shown that ATG5 mutant that cannot interact with ATG12 can trigger apoptosis but fails to participate in autophagy

and calpain-mediated truncated ATG5 is unable to promote autophagy, but induces apoptosis (Codogno and Meijer, 2006; Yousefi *et al.*, 2006).

ATG5 can also induce cell death during DNA damage. ATG5 is commonly localized inside the cytoplasm, but, in case of DNA damage, the expression of ATG5 is increased and it is translocated to the nucleus via a leucine-rich nuclear export signal (Maskey *et al.*, 2013). ATG5 binds to survivin inside the nucleus resulting in the mitotic catastrophe and G2/M cell cycle arrest and eventually leading to cell death (Maskey *et al.*, 2013).

1.6 Autophagy-related protein 18 (ATG18)

ATG18 belongs to β-propellers that bind polyphosphoinositides (PROPPINs) family of proteins. It is conserved from yeast to human and interacts with phospholipids, PI3P and phosphatidylinositol 3,5-bisphosphate [PI(3,5)P_2]. ATG18 participates in at least two distinct molecular pathways in yeast: autophagy and vacuole fission. ATG18 deficient yeast strain is viable in normal growing conditions but demonstrates plethora of phenotypic and functional abnormalities, such as it has enlarged vacuoles, elevated levels of PI(3,5)P_2, defective autophagy pathway, membrane trafficking defect, abnormal hyperosmotic stress response, sporulation defect, and blockages in Cvt and pexophagy (Barth *et al.*, 2001; Kim *et al.*, 2001; Guan *et al.*, 2001).

Proteins present in the PROPPINs family, including ATG18, have a conserved motif comprising of four amino acid residues Phe-Arg-Arg-Gly (FRRG), required for lipid binding. *S. cerevisiae* contains three PROPPINs: ATG18, ATG21 and homologous with the swollen vacuole phenotype 2 (Hsv2). ATG18 is a core autophagy-related protein required for macroautophagy, Cvt and piecemeal microautophagy of the nucleus (PMN) (Barth *et al.*, 2001; Guan *et al.*, 2001). ATG18 localizes to the PAS in a PI3P-dependent manner, and along with ATG2, helps in ATG9 recycling from the PAS to peripheral sites (Reggiori *et al.*, 2004). It localizes on the vacuole and performs non-autophagic functions, such as the regulation of the PI3P 5-kinase Fab1, vacuole morphology maintenance, vacuole fission, and the vesicular transport from the vacuole to the Golgi (Dove *et al.*, 2004; Efe *et al.*, 2007). ATG21 is specific to the Cvt pathway (Strømhaug *et al.*, 2004), while Hsv2 has a molecular role in microautophagy (Table 1.4).Mammals contain four PROPPINs WIPI1-WIPI4 (WD-40 repeat-containing protein that interacts with

phosphatidylinositides), WIPI1 and WIPI2 are orthologs of ATG18 and participates in autophagy (Table 1.4).

Organism	Name	Function
S. cerevisiae	ATG18	Fab1/PI(3,5)P_2 pathway
		Autophagy
		Pexophagy
		Cvt pathway
		Vacuole -to-Golgi membrane recycling
	ATG21	Cvt pathway
		Peroxisome degradation
	Hsv2	Microautophagy
Mammalian Cells	WIPI1	Apoptosis
		Autophagy
		MP6R recycling
	WIPI2	Apoptosis
		Autophagy
	WIPI3	Membrane recycling
	WIPI4	Chromatin assembly
		Apoptosis
		Cell cycle
		RNA processing
		Vesicular trafficking

Table 1.4: PROPPINs and their functions in yeast and mammals

1.6.1 A brief history of ATG18

ATG18 was previously named as Aut10p, Cvt18 and Gsa12 and shown to participate in autophagy, Cvt pathway and pexophagy (Barth *et al.*, 2001; Guan *et al.*, 2001). Unlike other ATG proteins, ATG18 is found to localize on the vacuolar membrane (Barth *et al.*, 2001; Guan *et al.*, 2001). Later, ATG18 was also identified in the screen of yeast mutants that has abnormally large vacuole morphology. Therefore, ATG18 was also named as Swollen Vacuole Phenotype 1 (Svp1) (Dove *et al.*, 2004).

In mammals, WIPI1 also called as WIPI49 was previously shown to be required for endosomal organization and this function also requires its phosphoinositide binding motif for membrane interaction (Jeffries *et al.*, 2004). Later, it has been shown that WIPI is localized on the autophagosomal structures in human melanoma cells, and the localization is dependent on its interaction with phospholipid PI3P (Proikas-Cezanne *et al.*, 2004).

1.6.2 Domain architecture of ATG18

ATG18 is a multi-WD-containing protein that is postulated to fold into seven-bladed β-propeller. Sequence alignment shows that the predicted β-strands of the propeller blades are well conserved between ATG18 and its homologs, but the intervening loops are highly variable. The C-terminal domain is also divergent among ATG18 from different species (Dove *et al.*, 2004).

Structural analysis of ATG18 shows that the protein acquires β-propeller structure that resembles a donut ring. It possesses two PI3P binding sites FRRG, located in neighbouring blades 5 and 6, and each blade harbours a PI3P binding site (Baskaran *et al.*, 2012; Krick *et al.*, 2012; Watanabe *et al.*, 2012; Scacioc *et al.*, 2017). The arginine residues in the FRRG motif represent separate phosphoinositide-binding site and are believed to interact with phosphoinositide PI(3)P and PI(3,5)P2. Substitutions of arginine-to-threonine in the FRRG motif results in the loss of phosphoinositide binding leading to the defect in autophagy (Krick *et al.*, 2006). Additionally, the unstructured long β3-β4 loop called CD loop in blade 6 of ATG18 is significant for docking the protein to the membrane. When ATG18 contacts membrane containing PI(3,5)P2 and/or PI(3)P, the CD loop reorganizes into an amphipathic helix, which assists in penetrating the lipid bilayer (Gopaldass *et al.*, 2017). When hydrophobic residues in this region of ATG18 are mutated, the binding of the protein to the membrane is abolished (Baskaran *et al.*, 2012; Watanabe *et al.*, 2012; Busse *et al.*, 2015). It is proposed that ATG18 adopts a perpendicular orientation towards the membrane which enables the membrane binding sites to interact with PI3P on the membrane surface directly, and then the hydrophobic loop penetrates the membrane to stabilize the interaction (Figure 1.13B) (Baskaran *et al.*, 2012; Krick *et al.*, 2012; Watanabe *et al.*, 2012; Scacioc *et al.*, 2017).

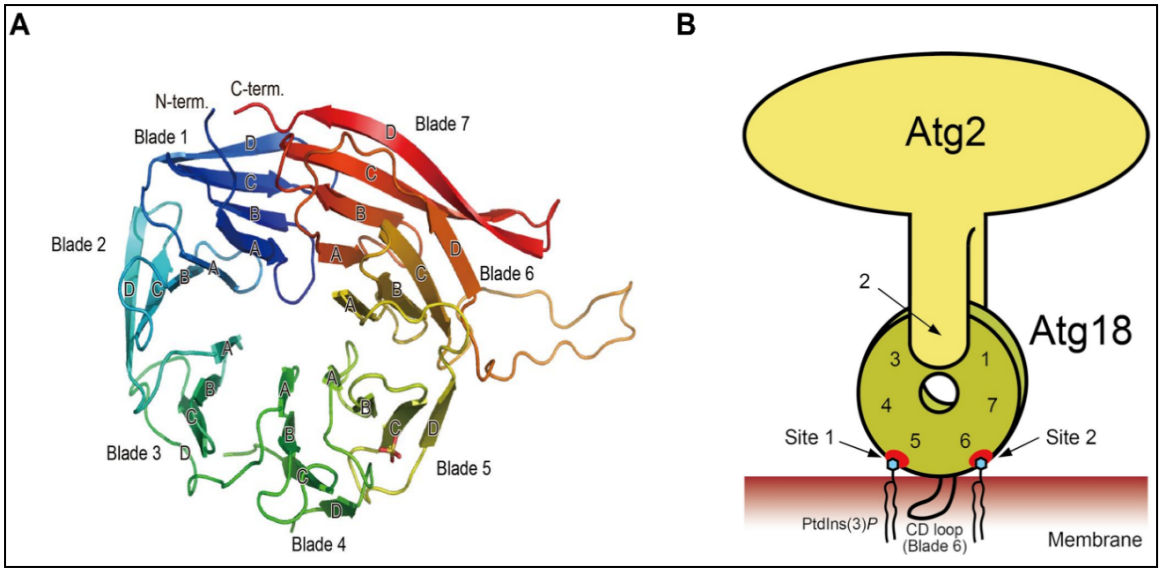

Figure 1.13: Structure of ATG18 and model for its interaction with phosphoinositides

(A) Structure of ATG18 represented in ribbon diagram. The seven blades are labelled and colored differently. Each blade consists of four β-strands, which are labelled alphabetically. **(B)** Schematic representation of the ATG2-ATG18 complex on the membrane. ATG2 (yellow) holds the ring-like structure of ATG18 (green) at blade 2, while ATG18 interacts with the membrane (dark red) via blades 5 and 6 (With permission from Watanabe *et al.*, 2012, license Id 4673011201579).

1.6.3 Role of ATG18 in autophagy

ATG18 is an essential component of autophagosome formation in autophagy (Barth *et al.*, 2001; Guan *et al.*, 2001). It forms a complex with ATG2, which is crucial for autophagy (Suzuki *et al.*, 2007). This complex is formed in the cytoplasm upon induction of autophagy. The immunoprecipitation experiment shows that ATG18 directly interacts with ATG2. ATG18 interacts with ATG2 through loop region in blade2, whereas the basic pockets in blade 5 and blade 6 are essential for phosphoinositide binding (Watanabe *et al.*, 2012). ATG18-ATG2 interaction is independent of the membrane docking (Watanabe *et al.*, 2012). ATG18 binds to phosphoinositide and ATG2 simultaneously, and act as a scaffold for the assembly of protein-lipid complexes (Watanabe *et al.*, 2012). Yeast two-hybrid assay shows that ATG18 interacts with ATG2 by loop2, which connects blade 2 and blade 3 (Rieter *et al.*, 2013).

It has also been shown that PI3P is not required for ATG18-ATG2 complex formation and that this complex can be formed in the PI3P-binding mutant of ATG18 ($ATG18^{FTTG}$) or PI3K-deficient yeast strain (Suzuki *et al.*, 2007; Obara *et al.*, 2008). The interaction of ATG18 with PI3P is critical for targeting the complex to the PAS. It has been shown that

when the PI3P-binding mutant ATG18^{FTTG} is artificially targeted to the PAS, the autophagy pathway is restored in the ATG18 mutant yeast strain (Obara *et al.*, 2008). Another report shows that if ATG2 is directed to the PAS by tagging with FYVE, autophagy function can be restored in the ATG18 mutant strain, suggesting that the prominent function of ATG18 is to target ATG2 to the PAS (Kobayashi *et al.*, 2012). Both ATG2 and PI3P are needed for the localization of ATG18 to the PAS (Rieter *et al.*, 2013).

The ATG18-ATG2 complex, together with ATG1-ATG13 complex, is required for the retrieval of ATG9 from PAS. ATG9 is a multispanning transmembrane protein and is essential for autophagy in yeast and mammals. It is highly conserved across species and ubiquitously expressed in multicellular organisms. This protein is believed to be involved in the supply of lipid bilayers required for the formation of the autophagosome and, therefore, is essential for both the Cvt pathway and autophagy. ATG9 is distributed in several subcellular organelles and cycles between the PAS and other peripheral sites. ATG9 requires retrieval mechanism to dissociate it from the lipid bilayer. The retrieval of ATG9 from the PAS involves the ATG1-ATG13 complex that localizes on the PAS during the early stage of the autophagosome biogenesis. ATG1-ATG13 complex stimulates the interaction of ATG9 with ATG18 and ATG2 at PAS, where ATG2 interacts with ATG9 directly. The depletion of any of these proteins restricts ATG9 on the PAS. In the absence of ATG9 retrograde trafficking, autophagy is stalled due to the exhaustion of lipid bilayer (Reggiori *et al.*, 2004). Recently, it has been shown that ATG18-ATG2 complex tethers ER to isolation membrane (Kotani *et al.*, 2018) and ATG2 transfers lipid from ER for autophagosome biogenesis (Valverde *et al.*, 2019).

ATG18, along with ATG21, prevents the premature cleavage of ATG8-PE. ATG8 is a Ubl protein that conjugates with lipid during autophagy. ATG4, a cysteine protease, exposes glycine at the C-terminus of ATG8, thus, helps in the conjugation of ATG8 with PE, involving the action of ATG7 and ATG3. Lipidated ATG8 associates with the inner and outer membrane of the expanding phagophore and labels autophagosome until its fusion with the vacuole. After fusion, ATG8 is deconjugated from the outer membrane of the autophagosome by the second ATG4-dependent cleavage event, whereas the ATG8-PE-labelled inner membrane is degraded in the vacuole. ATG4 is present in the cytosol and if it gets access, can cleave ATG8-PE prematurely. This premature cleavage of ATG8-PE is prevented by ATG18 and ATG21. They do so by limiting the access to ATG4 from ATG8-

PE. This action of ATG18 and ATG21 is required for the efficiency of the Cvt and autophagy pathways, respectively and are PI3P-dependent. ATG18, and ATG21 along with the ATG12-ATG5.ATG16 complex and the PI3K complex protects the premature cleavage of ATG8-PE. These proteins dissociate from the autophagosome following the completion of the autophagosome formation; thus, ATG4 can access ATG8-PE and cleave it from the outer membrane of the autophagosome. ATG8 liberated from the autophagosome by ATG4 is reused again in the autophagy pathway (Nair *et al.*, 2010).

WIPI family proteins are homologs of ATG18 in mammals. WIPI genes were identified by the BLAST search of the human genome database. Four WIPI proteins are divided into two paralogous groups; WIPI1 and WIPI2 belong to one group and WIPI3 and WIPI4 belong to the other. Homology modelling predicts that these proteins fold into seven-bladed beta-propellers. WIPI1, WIPI2 and WIPI4 can bind to phosphoinositides PI3P and PI(3,5)P_2. The interaction of WIPI3 with phospholipids is not known yet. WIPI1 functions in autophagy similar to ATG18 and localizes to the phagophore. The localization of WIPI1 on the phagophore depends upon binding with PI3P, as treatment with class III PI3K inhibitors such as wortmannin or LY249002 leads to the inhibition of WIPI1 puncta formation (Proikas-Cezanne *et al.*, 2007). WIPI1 also has physiological importance in cancer. It is found to be expressed aberrantly in many tumour tissues, for instance, kidney, pancreatic and skin cancers (Proikas-Cezanne *et al.*, 2004; Proikas-Cezanne *et al.*, 2007). WIPI2 binds with ATG16L1, recruits the ATG12-ATG5-ATG16L1 complex to phagophore and promotes autophagosomal biogenesis (Dooley *et al.*, 2014).

The induction of autophagy can be examined by assessing the mRNA level of WIPI1. The transcription of WIPI1 significantly increases by inducers of autophagy, correlating with the induction of autophagosome formation (Tsuyuki *et al.*, 2014). Similarly, the localization pattern of WIPI1 can be used to determine the status of autophagy. In general, WIPI1 is diffused in the cytosol under nutrient-rich condition, but it demonstrates punctate localization on the autophagosome upon autophagy induction, which colocalizes with Microtubule-associated protein 1A/1B-light chain 3 (LC3), a mammalian homolog of ATG8 (Proikas-Cezanne *et al.*, 2004; Proikas-Cezanne *et al.*, 2007). The number of WIPI1 puncta in normal condition represents basal autophagosomes, which increase upon induction of autophagy by starvation or treating the mammalian cells with mTOR inhibitor rapamycin and ER stress inhibitors such as thapsigargin. Therefore, the quantification of

WIPI1 puncta gives the estimation of total autophagosomes formed. Levels of WIPI1 puncta are comparable with that of LC3-II (LC3 conjugated to PE) puncta (Proikas-Cezanne *et al.*, 2004; Proikas-Cezanne *et al.*, 2007).

1.6.4 Role of ATG18 in vacuole fission

Vacuoles are the most acidic compartment of the cell and host a wide range of biological processes such as degradation and turnover of cellular components, storage of ions and metabolites, cellular homeostasis, nutrient transport and the regulation of growth via the cell cycle. They share similar features with mammalian lysosomes and plant vacuoles (Li and Kane, 2009).

Yeast propagates in a variety of extracellular conditions and frequently experiences nutrient deficiency and osmotic stress. In response to external stress conditions, vacuole changes its shape, size and copy number via a balance of fission and fusion. Changing the vacuolar morphology, by vacuole fission or fusion, is a rapid method adopted by the cell to maintain homeostasis upon a change in the ion and water content inside the cell. During the exponential phase, actively metabolizing cells have vacuoles that are comprised of 1-5 medium-sized vacuoles. They tend to fuse in response to nutrient deprivation. The fusion allows vacuole to store more hydrolases and generate amino acids via autophagy during nutrient deprivation. Vacuole fusion also occurs during hypoosmotic conditions. The process of vacuole fusion is well studied in yeast. It involves four main steps: priming, tethering, docking, and fusion (Mijaljica *et al.*, 2007).

On the contrary, vacuole fragments during hyperosmotic stress, ER stress and cell cycle progression (Figure 1.14A) (Richards *et al.*, 2010). Unlike fusion, fission of a vacuole is a rapid process that can happen within minutes of hyperosmotic shock. Fission of vacuoles is necessary for proper vacuolar transmission during mitotic cell division and in response to hyperosmotic shock. The hyperosmotic condition causes vacuole to shrink immediately to compensate for the water loss from the cell. Thus, the vacuole fragments to establish the surface-to-volume ratio (Figure 1.14B). The understanding of fission of vacuoles is limited and factors causing the vacuole fission are also largely unexplored (Zieger and Mayer, 2012).

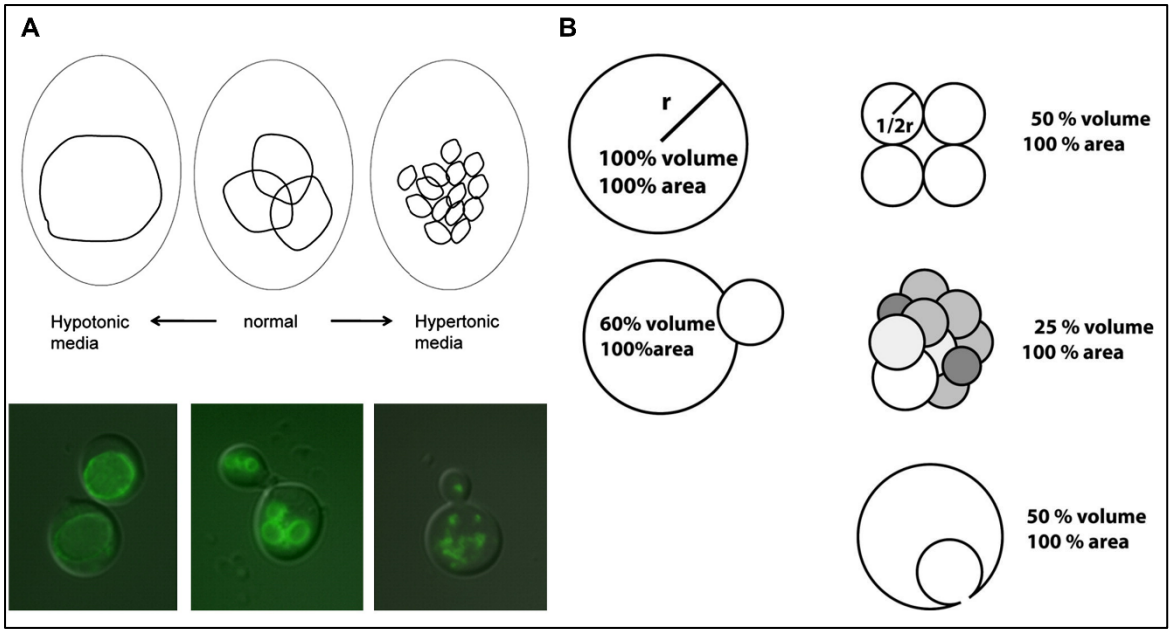

Figure 1.14: Schematic representation of vacuolar morphology

(A) Vacuolar morphology in different growth conditions. Top: Illustration of vacuole phenotype under normal, hypoosmotic and hyperosmotic conditions. Bottom: Fluorescent images of yeast vacuoles grown in respective medium (With permission from Li and Kane, 2009, license Id 4672990626219). **(B)** Schematic representation of the relationship between the vacuole fission with surface area, volume and diameter (With permission from Zieger and Mayer, 2012, license Id 4673000984679).

ATG18 has a regulatory role in maintaining vacuolar homeostasis. ATG18-deficient yeast strain has abnormally large vacuole. Binding of ATG18 with $PI(3,5)P_2$ facilitates its localization to the vacuole and is part of the Fab1 complex (Dove *et al.*, 2004; Efe *et al.*, 2007). Vacuole fission in yeast involves the action of Fab1, a PI3P-kinase, which produces $PI(3,5)P_2$. Fab1 forms a complex with Vac14 and Vac7, positive regulators of Fab1 activity, at the vacuolar membrane. The mutants which do not produce $PI(3,5)P_2$ such as *fab1*Δ, *vac14*Δ, and *vac7*Δ, exhibit vacuole fission defect, whereas ATG18 is the only protein whose absence results in elevated levels of $PI(3,5)P_2$ and demonstrate a vacuole fission defect. It is shown that ATG18 is a scission-specific Fab1 effector protein, which brings about vacuole fission and it also negatively regulates $PI(3,5)P_2$ by participating in membrane recycling (Efe *et al.*, 2007; Michaillat and Mayer, 2013).

Vacuole fission occurs in two steps in yeast. Each stage of vacuole fission requires specific protein and lipid composition. In the first step, the vacuole shrinks to develop deep invaginations and tubular structures. This step requires the dynamin Vps1 and proton gradient induced by V-ATPase, and PI3P is enriched at the vacuolar membrane by the

action of PI3K complex II (Vps34, Vps 34, Vps15, and Vps30). The presence of PI3P helps in generating membrane invaginations and in stabilizing them. After the vacuolar invagination, PI3P is replaced by PI(3,5)P_2 by the activity of Fab1 complex (Fab1, Vac14, and Vac7), resulting in the separation of vesicles from the tip of the tubular structures generating the fragmented vacuoles of desired sizes. ATG18 interacts with both PI3P and PI(3,5)P_2 and accelerates the entire fission process. (Figure 1.15) (Zieger and Mayer, 2012).

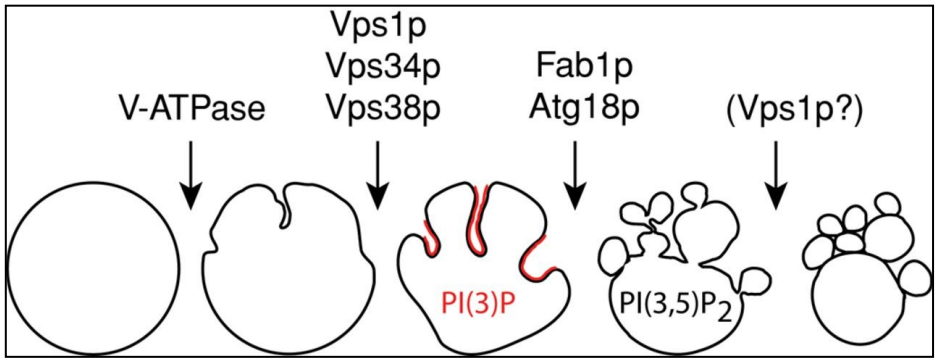

Figure 1.15: Critical steps involved in vacuole fragmentation

Schematic representation of two distinct steps involved in the vacuole fragmentation (With permission from Zieger and Mayer, 2012, license Id 4673000984679).

Further, it is suggested that PROPPINs proteins, including ATG18, have membrane scission property (Gopaldass *et al.*, 2017). They contain an unstructured hydrophobic loop (CD-loop) in the blade 6 of the β-propeller between the two lipid binding sites. This CD-loop has the potential to fold into an amphipathic α-helix. It has been proposed that when ATG18 contacts with the membrane, the CD-loop changes its conformation and transforms into an amphipathic α-helix, which is then inserted in the lipid bilayer and allows ATG18 to anchor itself to the membrane. This insertion promotes curvature and scission of the membrane (Gopaldass *et al.*, 2017). ATG18 also has an oligomerization property (Scacioc *et al.*, 2017) and therefore, multiple ATG18 molecules may be recruited at the vacuolar membrane, which results in the membrane scission by the crowding effect. The CD-loop is conserved in other PROPPINs, but its sequence is variable in ATG18 from different species (Gopaldass *et al.*, 2017).

The phosphorylation state of ATG18 also influences its localization to the vacuolar membrane and thus, regulates the fission process in *Pichia pastoris*. *Pp*ATG18 is phosphorylated at serine and threonine residues of blade 6 and blade 7. *In vitro* analysis has shown that dephosphorylated ATG18 has more affinity for phospholipids and therefore, it

binds to the membrane. The cell biology assays show that ATG18 is dephosphorylated during vacuole fission conditions such as hyperosmotic or high nutrient conditions, resulting in its association to the vacuole via $PI(3,5)P_2$ and causes vacuole septation. On the other hand, when ATG18 is phosphorylated under hypoosmotic or nutrient starvation conditions, it dissociates from the membrane and as a result, vacuole coalesces (Tamura *et al.*, 2013).

The evidence suggests that vacuole inheritance involves ATG18 (Efe *et al.*, 2007). The vacuole is inherited from the mother yeast to the daughter bud during mitotic cell division, which is spatially and temporally controlled. It starts early in the cell cycle before nuclear migration begins. Tubular structure originates from the vacuole in the mother cell and moves along to the daughter cell. The mother-daughter vacuole transport is an actin-myosin motor dependent process involving the Myo2p and Vac17p and Vac8p molecular motors. Vac17 interaction with Myo2 is crucial for the vacuole inheritance, and ATG18 physically binds to Vac17, and thus assist the vacuole inheritance from mother to daughter cell during mitosis (Efe *et al.*, 2007; Li and Kane, 2009).

1.7 Autophagy in protozoan parasites

Protozoan parasites are unicellular eukaryotic pathogens, members of this group include *Leishmania* spp., *Trypanosoma cruzi, Trypanosoma brucei*, *Toxoplasma gondii*, *Plasmodium* spp., which cause diseases namely, malaria, toxoplasmosis, sleeping sickness, Chagas disease and leishmaniasis, respectively, in a large population of humans worldwide. Autophagy in these eukaryotic pathogens plays a critical role in their biology, for instance, in cell differentiation and survival under stress (Kiel, 2010). Autophagy has been shown to be involved in a wide range of diseases in humans, for instance, cancer, neurodegeneration, myopathies, eliminating certain bacteria and pathogens. Therefore, targeting ATG proteins by pharmacological inhibitors is an attractive strategy for treating cancers and immune disorders, where autophagy is either excessively active or impaired. Accordingly, it is possible that if autophagy-mediated differentiation interferes in protozoa, it may stall their development and proliferation in hosts. Our focus is to understand the autophagy pathway in the human malaria parasite *P. falciparum*. There is relatively little information on the autophagy-like pathway in this parasite, whereas it is significantly explored in other closely related species *Leishmania*, *Trypanosoma,* and *Toxoplasma*. Molecular details of the autophagy pathway in these parasites are described below.

1.7.1 Autophagy in *Leishmania*

Leishmania infects mainly humans and dogs. The parasite exists in different developmental forms in sandflies (vector) and mammals. In the insect vector, *Leishmania* exists in two forms known as promastigotes: the non-infective, multiplicative procyclic and the infective, non-multiplicative metacyclic. Upon entering the vertebrate host, promastigotes reside inside macrophages, where promastigote differentiate into amastigotes (Bates and Rogers, 2004).

Genome studies have revealed that proteins involved in two ubiquitin conjugation systems are present in *L. major*. *Lm*ATG8 has a high similarity with yeast and mammalian ATG8. It is a true ortholog of ATG8 as it has been shown to complement *Sc*Atg8 in *S. cerevisiae* and appear to localize on the autophagosome in the parasite (Williams *et al.*, 2009). *L. major* expresses the orthologs of ATG3 and ATG7 and two variants of ATG4 peptidases (*Lm*ATG4.1 and *Lm*ATG4.2). *Lm*ATG4.1 exposes the terminal glycine of *Lm*ATG8 and facilitates *Lm*ATG8 conjugation with PE while *Lm*ATG4.2 assists in the deconjugation of *Lm*ATG8-PE and releases *Lm*ATG8 from the autophagosome membrane and aids in its recycling (Williams *et al.*, 2009). ATG5 and ATG10 homologs in *L. major* could replace their yeast counterparts despite their low similarity with the yeast and mammalian proteins. *Lm*ATG12 has a few amino acids extension after the C-terminal glycine residue, responsible for the isopeptide bond formation with ATG5, while in other eukaryotes glycine is at the C-terminal end. When the C-terminal glycine of *Lm*ATG12 is exposed, it can successfully complement *Sc*Atg12 (Williams *et al.*, 2009; Rigden *et al.*, 2009; Kiel, 2010; Brennand *et al.*, 2011).

Evidence has shown that autophagy is necessary for the differentiation of procyclic into metacyclic form and of metacyclic promastigotes into amastigotes. An increase in the level of autophagosomes and protein turnover is observed during cell differentiation (Besteiro *et al.*, 2006). Accordingly, *L. major* mutant lacking ATG5 has abnormalities in differentiation and has decreased virulence (Williams *et al.*, 2012).

1.7.2 Autophagy in *Trypanosoma cruzi*

During the life cycle of *T. cruzi*, a non-infective epimastigote transforms into an infective metacyclic trypomastigote in the insect, which is transmitted by insect bite and enters the

mammalian host. The metacyclic trypomastigote differentiates into an amastigote, which is then transformed into trypomastigote in mammals and causes Chagas disease.

Genome analysis of *T. cruzi* has revealed that many autophagy-related genes are present in this parasite. It expresses the orthologs of ATG3, ATG7, two variants of ATG8 (*Tc*ATG8.1 and *Tc*ATG8.2) and two candidates of ATG4 (*Tc*ATG4.1 and *Tc*ATG4.2). *Tc*ATG8.1 complements the function of *Sc*Atg8 and is the true ortholog of ATG8. Both *Tc*ATG4s can complement *Sc*Atg4 mutant, but only *Tc*ATG4.1 can perform *Tc*ATG8.1 and *Tc*ATG8.2 processing (Rigden *et al.*, 2009; Kiel, 2010; Brennand *et al.*, 2011). *T. cruzi* has conserved ATG8 conjugation system, but BLAST analysis shows that components of ATG12 conjugation system, i.e., ATG5, ATG12, ATG7, and ATG10 are not found in the genome of this parasite. Thus, suggesting that ATG12-ATG5 conjugation system is most likely absent in *T. cruzi* or their protein sequence has significantly diverged from that of yeast and hence might not be detected by bioinformatic analysis (Alvarez *et al.*, 2008). There are no experimental studies on the ATG12-ATG5 complex in this parasite.

Autophagy is involved in cell differentiation in *T. cruzi*, as it is shown that nutritional stress can trigger the differentiation of epimastigote. It is further supported by the observation that the expression of autophagy marker protein *Tc*ATG8 increases in differentiating epimastigote and localizes on the reservosome, a lysosome-like organelle (Kiel, 2010; Brennand *et al.*, 2011). Recently, autophagy has been shown to regulate the differentiation of epimastigote into metacyclic trypomastigote during metacyclogenesis (Vanrell *et al.*, 2017).

1.7.3 Autophagy in *Trypanosoma brucei*

T. brucei is transmitted by the tsetse fly to humans and injects the metacyclic form of the parasite into the bloodstream of the human during the blood meal. The parasite then develops into slender form, then to short-stumpy form in humans, which causes sleeping sickness. The latter form of the parasite is ingested by the fly during the bloodmeal and transforms in a procyclic form in the midgut of the insect (Kiel, 2010; Brennand *et al.*, 2011).

The ATG8 Ubl conjugation system (ATG8, ATG3, and ATG7) is conserved in *T. brucei* and contains three orthologs of ATG8 (*Tb*ATG8.1, *Tb*ATG8.2, and *Tb*ATG8.3).

*Tb*ATG8.1 and *Tb*ATG8.2 share high sequence similarity. The peptide sequence of *Tb*ATG8.1 ends atypically with a glycine residue, which is also the case in some plants and apicomplexans *Toxoplasma* and *Plasmodium*, and therefore may not require ATG4-mediated processing for its activity. *Tb*ATG5 has low sequence similarity with yeast and mammalian ATG5. However, the knockdown of *Tb*ATG5 reduces the autophagosome formation, suggesting that it is a true ortholog of ATG5 (Proto *et al.*, 2014). Studies indicate that *Tb*ATG8.2-labelled autophagosome-like structures are formed during starvation in a procyclic stage that leads to autophagy-related cell death in *T. brucei*, which can be reversed by inhibiting the expression of autophagy-related proteins *Tb*ATG8.1, *Tb*ATG8.2, *Tb*ATG3 and *Tb*ATG7 by RNAi (Li *et al.*, 2012).

1.7.4 Autophagy in *Toxoplasma gondii*

Toxoplasma gondii is an obligate intracellular parasite that belongs to apicomplexa. This parasite causes toxoplasmosis. Cats are the primary host of the parasite where sexual reproduction takes place. The asexual reproduction can occur in any warm-blooded animals called the intermediate host.

Many protein components of the core autophagy machinery are found in *T. gondii* but lack proteins involved in the selective autophagy such as Cvt targeting and pexophagy. *T. gondii* genome analysis reveals that it has conserved proteins involved in the ATG8 conjugation system (ATG8, ATG3, and ATG7), but the proteins involved in ATG12 conjugation system show low sequence similarity. ATG1, a component of the autophagosome induction complex, is present in *T. gondii*. ATG8 in this parasite also ends with a glycine residue at its C-terminus. *Tg*ATG4, a protease for ATG8 processing, is found in *T. gondii*, but is shown to be required only for the recycling of the *Tg*ATG8 but not for its processing (Besteiro *et al.*, 2011; Ghosh *et al.*, 2012; Besteiro, 2012; Nguyen *et al.*, 2017).

Studies have shown that autophagy is involved in cell survival as *Tg*ATG8-decorated autophagosomes have been observed in the egressed parasite until the nutrient supply in the new cell is established. Also, knockdown of ATG3 in *T. gondii* leads to severe growth arrest and loss of mitochondrial integrity. Therefore, it has also been proposed that autophagy might be responsible for organelle maintenance and homeostasis in *T. gondii* (Besteiro *et al.*, 2011; Besteiro, 2012). Autophagy also aids in the survival of the parasite during ER stress (Nguyen *et al.*, 2017). During amino acid starvation, the parasite

undergoes autophagy-mediated mitochondrial fragmentation resulting in the parasite cell death (Ghosh *et al.*, 2012). ATG9, an autophagy-related protein required for the membrane cycling, is identified in the *Toxoplasma* genome and is essential for the cell survival, as the absence of ATG9 reduces parasite survival during extracellular stress and leads to reduced virulence in mice (Nguyen *et al.*, 2017). Apart from the role in autophagy, *Tg*ATG8 is also shown to participate in the apicoplast inheritance in the parasite. The apicoplast is a non-photosynthetic plastid enclosed by four membranes found in the apicomplexans. The depletion of *Tg*ATG8 results in the loss of apicoplast in this parasite (Lévêque *et al.*, 2015).

A protein similar to ATG5 is found by BLAST analysis, but the protein is considerably large and shows a weak similarity of about 22% with its yeast counterpart (Ghosh *et al.*, 2012). Recently, it is reported that in *T. gondii*, ATG5 and ATG12 interact non-covalently to form a complex, and does not involve E1-like and E2-like enzymes ATG7 and ATG10. This complex could positively regulate autophagy in the parasite (Pang *et al.*, 2019).

Two PROPPINs are identified in *Toxoplasma gondii* genome database, *Tg*PROP1, and *Tg*PROP2. Knockout study shows that *Tg*PROP1 is dispensable for the normal growth of the parasite, but might be required for the survival of parasite under stress inside the host. However, *Tg*PROP2 (*Tg*ATG18) is indispensable for the growth of the parasite. Both proteins associate with early autophagic structures and display punctate localization under starvation conditions and partially colocalize with autophagosome marker *Tg*ATG8 and completely colocalize with membrane recycling protein *Tg*ATG9 (Nguyen *et al.*, 2018).

*Tg*PROP2 or *Tg*ATG18 is predicted to fold as seven-bladed β-propellers and shares a 41% sequence identity with *Pf*ATG18. It localizes on the punctate structures in the parasite cytosol by binding with phospholipids PI3P and PI(3,5)P_2. Conditional knockout study reveals that parasites without *Tg*ATG18 experience delayed death. *Tg*ATG18 is shown to be essential for the apicoplast biogenesis and regulates the lipidation of *Tg*ATG8, thereby affecting apicoplast biogenesis (Bansal *et al.*, 2017), which too participate in apicoplast biogenesis in *Toxoplasma* (Lévêque *et al.*, 2015).

1.8 Autophagy in *P. falciparum*

The protozoan parasite *Plasmodium falciparum* infects millions of people worldwide each year and resulted in thousands of deaths in 2017 (World Health Organisation, 2018). The

parasite experiences heat, nutritional, oxidative and other stresses during its intraerythrocytic life-cycle (Babbitt *et al.*, 2012; Percário *et al.*, 2012; Engelbrecht and Coetzer, 2013) and also undergoes differentiation from one form to another, therefore requires degradation of stage-specific organelles and proteins (Cervantes *et al.*, 2014). The dissection of the autophagy-like pathway and its role in *Plasmodium* would provide critical insights to understand processes aiding survival and homeostasis for developing novel antimalarial therapeutics.

1.8.1 Autophagy machinery in *P. falciparum*

Homologs of many autophagy-related genes are identified in *P. falciparum* genome by bioinformatics analysis (Table 1.5 and Figure 1.16). ATG1 and ATG17 together with ATG13 form an autophagy induction complex, homologs of yeast ATG1 and ATG17 are present in *P. falciparum*, but ATG13 seems to be missing. Moreover, the ATG13 binding motif is absent in *Pf*ATG1. Thus, functional studies are needed to confirm the true homolog of ATG1 in *P. falciparum*. VPS34 and VPS15, part of PI3K complex in yeast (VPS34, VPS15, ATG6 and ATG14) seem to be present in the parasite. ATG9, a transmembrane protein required for membrane recycling is not conserved in *P. falciparum*. *Pf*ATG18 contains WD40 domain and is predicted to fold in a conserved seven-bladed β-propeller structure. It has a conserved PI3P-binding motif (FRRG) and is identified as an effector of PI3P in this parasite (Hain and Bosch, 2013; Navale *et al.*, 2014; Bansal *et al.*, 2017). ATG2, a constituent of ATG18-ATG2 complex in yeast, seems to have a little homology in parasite and is shown to function as Golgi Protein 1 in *P. falciparum* (Hallée *et al.*, 2018).

Proteins necessary for ATG8 conjugation system (ATG8, ATG3, ATG4, and ATG7) are conserved in the parasite. Like *Toxoplasma* and *Trypanosoma*, *Pf*ATG8 also ends with a C-terminal glycine residue (Hain and Bosch, 2013). *Pf*ATG7, an E1-like enzyme, is present in the parasite and is essential for its survival (Walker *et al.*, 2013). Pull-down of *Pf*ATG8 shows that *Pf*ATG8 interacts with *Pf*ATG7 (Cervantes *et al.*, 2014). ATG3, an E2-like protein, is identified in *P. falciparum* genome and contains an ATG8 interacting motif (AIM). The structure of the ATG8-ATG3 complex is characterized in this parasite, which reveals that an additional loop is present in *Pf*ATG3, but is absent in human ATG3, and therefore *Pf*ATG3 is proposed as a therapeutic target against *P. falciparum* (Hain *et al.*, 2012; Hain *et al.*, 2014; Hain *et al.*, 2016).

Stage of autophagy	*S. cerevisiae* homolog	*P. falciparum* homolog	Identity with *S. cerevisiae* homolog
Induction	ATG1	PF3D7_1450000	2.40e-22
	ATG13		
	ATG17	PF3D7_1120000	1.4e-10
	ATG29		
	ATG31		
Nucleation	Vps34	PF3D7_0515300	8.50e-75
	Vps15	PF3D7_0823000	2.2e-14
	Vps30/ATG6		
	ATG14		
IM Assembly/ATG9 cycling	ATG2	PF3D7_1320000	0.0034
	ATG18	PF3D7_1012900	5.1e-31
	ATG9		
Vesicle expansion and completion	ATG4	PF3D7_1417300	4.5e-09
	ATG8	PF3D7_1019900	3.10e-24
	ATG3	PF3D7_0905700.1	3.30e-40
	ATG7	PF3D7_1126100	4.0e-09
	ATG10		
	ATG12	PF3D7_1470000	3.4e-09
	ATG16		
	ATG5	PF3D7_1430400	3.3e-05

Table 1.5: Conservation of autophagy machinery in *P. falciparum* (With permission from Navale *et al.*, 2014)

P. falciparum genome contains homologs of ATG5, ATG12 and ATG7. Protein, ATG10, similar to E2-like enzyme, required for ATG12 conjugation, is not found in the genome of the parasite. Similar to *Toxoplasma*, *Pf*ATG5 is relatively larger than its yeast and mammalian counterpart and shows weak identity by BLAST analysis (Rigden *et al.*, 2009; Duszenko *et al.*, 2011; Brennand *et al.*, 2011; Hain and Bosch, 2013). Recently, it has been shown that a transition from covalent to non-covalent interaction between ATG5 and ATG12 has occurred during evolution in apicomplexans like *Toxoplasma* and *Plasmodium*, and some yeast species such as *Komagataella phaffii* (or *Pichia pastoris*). These species lack the C-terminal glycine residue of ATG12 and E2-like enzyme ATG10, which are essential for covalent interaction. This non-covalent complex of ATG12-ATG5 can still facilitate ATG8-PE conjugation, suggesting that ubiquitin-like covalent conjugation has evolved into a simpler non-covalent interaction (Pang *et al.*, 2019). *P. falciparum* expresses Rab7 and SNAREs such as VAMP8 and Vtilb, required for fusion of the autophagosome with the lysosome. Proteases are necessary for the degradation of autophagosomes inside the vacuole or lysosomes. *P. falciparum* FV contains several cysteine and aspartate

proteases that might degrade autophagosomal contents (Rigden *et al.*, 2009; Duszenko *et al.*, 2011; Brennand *et al.*, 2011; Hain and Bosch, 2013).

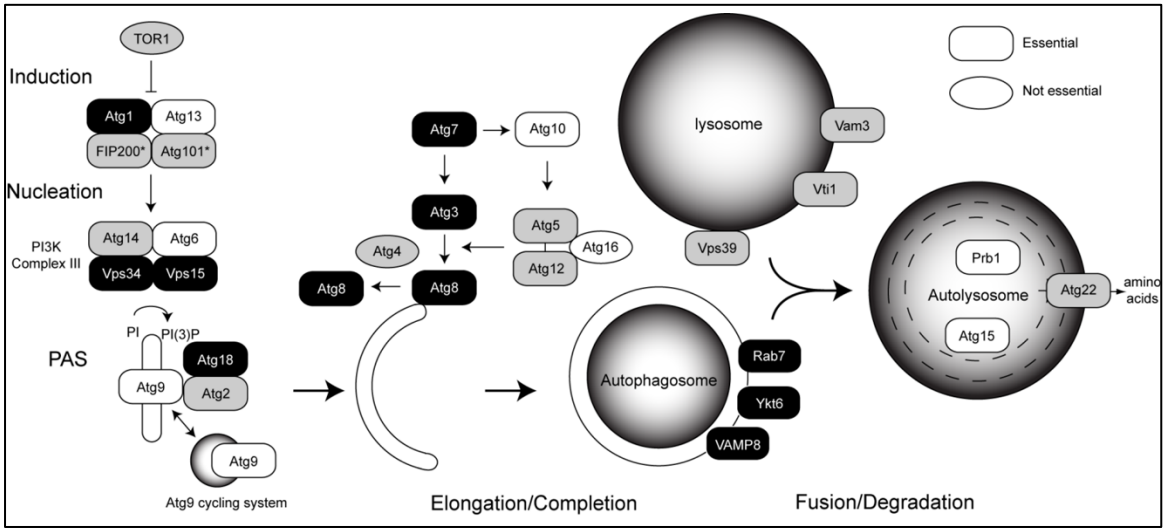

Figure 1.16: Conservation of the autophagy machinery in *P. falciparum*

Black indicates strong evidence for homology; grey indicates less clear homology while white indicates no ortholog was identified in *P. falciparum* by BLAST (With permission from Hain and Bosch, 2013).

1.8.2 Role of autophagy in *P. falciparum*

Malaria parasites, during its entire life cycle, undergo many morphological and functional changes, involving 15 functionally distinct stages. Autophagy has been suggested to play a crucial role in the parasite development, for example, it is involved in the clearance of micronemes during differentiation of sporozoites to merozoites in liver stage parasite (Jayabalasingham *et al.*, 2010; Coppens, 2011). ATG8 is widely used as a marker for autophagosome (Kitamura *et al.*, 2012). Concomitantly, it has been shown that *Pb*ATG8 colocalizes with the microneme before its expulsion, thus, helps in remodeling the parasite and mediates its differentiation. A slight increase in *Pb*ATG8 expression results in the development of immature merozoites that are incapable of inflicting a blood infection (Voss *et al.*, 2016). Similarly, differentiation of blood stage parasite to gametocytes may also involve autophagy, as a change in the number of *Pf*ATG8-labelled structures is observed in gametocytes (Cervantes *et al.*, 2014). Also, when the basal level of autophagy is inhibited by 3-MA, the viability of the parasite, as well as the invasion of merozoites decreases, indicating that basal autophagy is needed for the development of *P. falciparum* (Joy *et al.*, 2018).

The autophagy pathway culminates in the lytic compartment, which involves degradation of autophagosomes and recycling its contents. The blood stage of *P. falciparum* contains a lysosome-like compartment food vacuole (FV), where hemoglobin from the host RBC is degraded to provide amino acids (Wunderlich *et al.*, 2012). During starvation, *Pf*ATG8 is observed on the double-membrane vesicles near FV, which indicate that autophagy-like pathway is functional in the parasite during stress conditions (Tomlins *et al.*, 2013). It is also reported that during starvation, *Pf*ATG8 is present in the host cytosol and has a pro-survival role (Gaviria *et al.*, 2013). In the same report, it was suggested that ATG8-mediated autophagy protects parasites against chloroquine (Gaviria *et al.*, 2013). Findings from our group show that the protein expression of *Pf*ATG8 is upregulated under stress conditions such as starvation and when the autophagy is inhibited during stress, the viability of the parasite is reduced, indicating that autophagy has a role in the survival of the parasite during stress (Joy *et al.*, 2018). The proteomic analysis of *Pf*ATG8 pull-down has identified several ATG proteins. The components associated with ribophagy and piecemeal microautophagy of the nucleus have been detected, indicating that selective autophagy might be functional in *P. falciparum* (Cervantes *et al.*, 2014). In the liver stage of the parasite, autophagy-like cell death has been observed (Eickel *et al.*, 2013). However, the marker of autophagosome *Pb*ATG8 localizes on apicoplast and does not relocalize to the vacuoles in the dying parasite (Eickel *et al.*, 2013).

Autophagy is considered as a mechanism for artemisinin resistance in *P. falciparum* (Suresh and Haldar, 2018). Recently, it has been shown that *Pf*ATG18 is one of the targets of artemisinin (Wang *et al.*, 2015). Artemisinin is an antimalarial lactone endoperoxide derived from *Artemisia annua,* also called qinghao or sweet wormwood. Tu Youyou discovered artemisinin in 1972 as a treatment against *P. falciparum* malaria. Currently, an artemisinin derivative dihydroartemisinin (DHA) is used in the ACT, to treat *P. falciparum* malaria as it has high parasite clearance rate. It removes young ring-stage parasite and prevents parasite maturation and sequestration, which were the drawbacks of earlier chloroquine-based treatment. Recently, a detailed analysis of artemisinin targets in malaria parasite has been carried out using an alkyne-tagged artemisinin analog coupled with biotin. Proteins that are targeted by artemisinin were biotinylated, pulled down by passing through streptavidin beads and were detected by mass spectrometry. 124 parasite proteins, including *Pf*ATG18, have been detected as direct targets of artemisinin (Wang *et al.*, 2015).

Although artemisinin is the most effective treatment, parasites resistant to this drug have emerged (Noedl *et al.*, 2008; Dondorp *et al.*, 2009). The artemisinin-resistant parasites have been detected in different parts of the world, including Thailand, Myanmar, India and Vietnam (Fairhurst and Dondorp, 2016; Rosenthal, 2018). Resistant parasites show delayed clearance time following artemisinin treatment (Hott *et al.*, 2015). There are various mechanisms proposed for artemisinin resistance, such as dormancy (Cheng *et al.*, 2012) and upregulation of phospholipid PI3P due to mutations in Kelch13-propeller protein (Mbengue *et al.*, 2015).

Recently, the autophagy-like pathway is associated with artemisinin resistance in parasite. Genome-wide association study (GWAS) from the Southeast Asia and China-Myanmar border regions have been carried out to identify genes polymorphism causing resistance against artemisinin in *P. falciparum* field isolates. This study notably associated a non-synonymous SNP in *Pf*ATG18, which substitutes a single amino acid at the 38th position, threonine with isoleucine (T38I) or asparagine (T38N). This SNP results in the slow parasite clearance rate in patients treated with an artemisinin derivative (Miotto *et al.*, 2015; Wang *et al.*, 2016b).

A study underwent to understand the contribution of T38I polymorphism in conferring artemisinin resistance in *P. falciparum*. The *ATG18* gene was edited using CRISPR/Cas9 to introduce a T38I mutation into a *k13*-edited Dd2 parasite. *Pf*ATG18^{T38I} parasites have shown greater resistance against artemisinin compared to the wild-type parasites. *Pf*ATG18^{T38I} could confer the resistance even in the absence of *k13* mutation. Interestingly, this mutation could increase the survival of *P. falciparum* in glucose deprivation. At 50% decrease in the nutrient concentration, *Pf*ATG18^{T38I} parasite strain shows better viability as compared to the wild-type parasites or the parasites with *k13* mutation R539T. For these reasons, it is believed that autophagy may provide a fitness advantage to artemisinin-resistant parasites and can be explored as a therapeutic target.

1.8.3 Role of autophagy-related proteins in apicoplast biogenesis in *P. falciparum*

The apicoplast is a non-photosynthetic plastid found in the apicomplexans. The apicoplast contains enzymes involved in the synthesis of type II fatty acid required for isoprenoid biosynthesis and in heme-biosynthetic pathways (Surolia and Surolia, 2001; Wilson, 2005).

It has been shown that inhibition of apicoplast protein translation by tetracyclines results in the loss of apicoplast and causes cell death of the parasite in the second replication cycle, which is referred to as delayed death (Dahl *et al.*, 2006).

Many reports suggest a non-canonical role of *Pf*ATG8 in the apicoplast biogenesis. Studies show that *Pf*ATG8 partially localizes with the apicoplast under normal growth condition in *P. bergeii* and *P. falciparum* and is essential for branching and segregation of the apicoplast in asexual developmental stages (Kitamura *et al.*, 2012; Tomlins *et al.*, 2013; Mizushima and Sahani, 2014; Cervantes *et al.*, 2014; Jayabalasingham *et al.*, 2014). Accordingly, *Pf*ATG8 knockdown results in the growth inhibition in the second cycle of the parasite replication, which is associated with delayed cell death due to the loss of apicoplast (Walczak *et al.*, 2018). It has also been reported that an OTU-like cysteine protease plays an essential role in apicoplast maintenance and regulates *Pf*ATG8 deconjugation from the apicoplast membrane (Datta *et al.*, 2017).

Additionally, it has been shown that ATG18 is involved in the apicoplast biogenesis in *P. falciparum* and its depletion results in the loss of apicoplast, which leads to parasite growth attenuation in the second cycle of the parasite infection (Bansal *et al.*, 2017). It has been suggested that *Pf*ATG18 might regulate apicoplast biogenesis by affecting the association of *Pf*ATG8 to the apicoplast membrane (Bansal *et al.*, 2017). Although *Pf*ATG18 is not shown to localize at the apicoplast, albeit is present as punctate vesicular structures in the parasite cytoplasm and near FV (Bansal *et al.*, 2017).

Thus, the current knowledge indicates that autophagy machinery in *P. falciparum* has a specialized role in apicoplast biogenesis. As most ATG genes are essential for parasite viability, it is, therefore, implicated that the role of ATG proteins in apicoplast biogenesis is crucial for the parasite. However, this function seems to be independent of canonical autophagy, as ATG proteins are shown to participate in the parasite survival during stress conditions, for instance, brief periods of starvation and providing resistance against drugs as well as during the development of the parasite, although, the exact molecular mechanism is currently unknown.

1.9 Thesis objectives

During autophagy, the cell degrades its cytosolic contents in the lytic organelle and recycles nutrients to promote cell survival during stress conditions. About 42 autophagy-related proteins are required for the functioning of autophagy in yeast. Protozoans parasites such as *Leishmania*, *Trypanosoma* and *Toxoplasma* have conserved only a limited set of ATG proteins. However, autophagy is shown to be essential for the survival of protozoan during environmental stress conditions, for instance, nutrient, temperature and oxidative stress in the host cell. Autophagy is also required for cellular differentiation during the life cycle of protozoan parasites (Kiel, 2010). Thus, autophagy is proposed as a promising target to combat parasitic diseases.

P. falciparum, a causative agent of malaria, is an obligatory parasite, causing thousands of malaria-related deaths every year. It has a complex life cycle involving the sexual and asexual cycle occurring in the mosquito vector and human host, respectively. Since the parasite develops in two hosts, it changes its morphology and needs to adapt to different environmental conditions. Autophagy might play an essential role in cellular differentiation and survival during various stress in this organism. During its intraerythrocytic cycle too, the parasite experiences heat, nutritional, oxidative and other stresses (Babbitt *et al.*, 2012; Percário *et al.*, 2012; Engelbrecht and Coetzer, 2013). In order to target the autophagy pathway, it is prerequisite to understand this pathway in *P. falciparum*. As *P. falciparum* has conserved only a limited set of ATG proteins, its involvement in autophagy is debatable. The functional role of many ATG proteins is not yet explored in *P. falciparum*. To understand the involvement of ATG proteins in the autophagy-like pathway in *P. falciparum*, it is inevitable to elucidate the functions of individual ATG proteins in the malaria parasite. Most of the studies regarding autophagy in *P. falciparum* are centered around studies with the autophagy marker protein ATG8 (Kitamura *et al.*, 2012; Tomlins *et al.*, 2013; Gaviria *et al.*, 2013; Cervantes *et al.*, 2014; Walczak *et al.*, 2018) which is shown to perform multiple functions in the malaria parasite such as autophagy, apicoplast biogenesis, protein turnover and cellular differentiation (Tomlins *et al.*, 2013; Cervantes *et al.*, 2014; Voss *et al.*, 2016; Joy *et al.*, 2018).

Autophagy-related proteins, ATG5 and ATG18 are indispensable for autophagosome formation. ATG5 aids in the elongation of the phagophore, while ATG18 recruits other autophagy-related proteins necessary for autophagosome biogenesis. Functional

characterization of *Pf*ATG5 and *Pf*ATG18 will provide mechanistic insights into some of the most pertaining questions regarding autophagy in the intraerythrocytic stage of *P. falciparum*.

The aim of this work described in the thesis is to understand if *P. falciparum ATG* genes are involved in the autophagy-like pathway and to functionally decipher the role of essential autophagy-related proteins, ATG5 and ATG18 in *P. falciparum*. The following objectives were defined to achieve the aim of the study.

1. Analysing the involvement of putative *ATG* genes in the autophagy-like pathway in *P. falciparum*.
2. Deciphering the role of putative *Pf*ATG5 in the autophagy-like pathway in *P. falciparum*.
3. Performing a detailed characterization of autophagy-related protein *Pf*ATG18 in *P. falciparum*.
4. Deciphering canonical function of *Pf*ATG18 in the autophagy-like pathway and non-canonical function in the regulation of vacuolar dynamics in *P. falciparum.*

Chapter Two

Materials and Methods

Table of Contents

2.1 *Plasmodium falciparum* culture, isolation and transfection

2.1.1 *In vitro P. falciparum* culture and viability assay

P. falciparum 3D7 strain was cultured in O^+ erythrocytes and RPMI 1640 (Sigma-Aldrich), which was supplemented with 0.2% $NaHCO_3$, 25 mM HEPES, 20 μg ml^{-1} gentamycin and 10% (v/v) heat-inactivated O^+ human serum (complete RPMI 1640 medium). *P. falciparum* 3D7 strain was also cultured in a starvation medium, i.e., RPMI 1640 without amino acids and serum (HyClone Laboratories Inc.) for different time periods as indicated in the respective experiments. Parasite cultures were maintained by a standard candle jar method (5% CO_2/5% O_2/90% N_2) at 37°C (Trager and Jensen, 1976). Giemsa-stained thin blood smears were made after each time point for visualizing parasite morphology by microscopic analysis.

For viability assay, parasites were incubated with a starvation medium for the indicated time period and then parasites were washed twice with incomplete RPMI and incubated into complete medium containing amino acids for 48 h. Giemsa-stained thin blood smears were made after 48 h. Parasitemia was calculated by counting the numbers of ring stage parasites per 10,000 RBCs, which represents viable parasites. Live parasites were also determined by labelling parasite nucleus and mitochondrion with Hoechst33258 (Sigma-Aldrich) and 100 nM MitoTracker Red CMXRos (Invitrogen) respectively (Jogdand *et al.*, 2012).

2.1.2 *P. falciparum* synchronization and isolation

The intraerythrocytic stages of the parasites were synchronized by treating with 5% D-sorbitol for 5 min (Lambros and Vanderberg, 1979). Immediately after the sorbitol treatment, the parasite culture was enriched at the ring stage. The culture was then harvested at the ring (0-18 h), early trophozoite (24-26 h), late trophozoite (28-30 h) and schizont (36-45 h) stages.

For parasite isolation, the harvested cultures were washed with ice-cold phosphate-buffered saline pH7.4 (PBS). The parasites were released from RBCs by lysing erythrocytes

membrane by 0.15% (w/v) saponin (Sigma-Aldrich) for 15 min at 37°C, followed by washing the parasite pellet several times with PBS.

2.1.3 Episomal transfection of *Plasmodium falciparum*

The malaria parasites were transfected as previously described (Fidock and Wellems, 1997). Briefly, ring-stage parasites (12 hpi) at ~5% parasitemia were mixed with 400 µl CytoMix (120 mM KCl, 2 mM EGTA, 0.15 mM $CaCl_2$, 5 mM $MgCl_2$, 10 mM K_2HPO_4/KH_2PO_4, 25 mM HEPES, pH 7.6) containing 100 µg of plasmid (pARL1-a-*Pf*ATG18-GFP or pARL1-a-*Pf*ATG18^{FTTG}-GFP). The suspension was electroporated by GenePulser II (BioRad) (0.31 kV, 960 µF) and electroporated parasites were immediately resuspended in fresh complete medium and red blood cells. The culture was subsequently maintained in 2.5 nM WR99210 (Jacobus Pharmaceutical Co.).

2.1.4 Treatment of *P. falciparum* with small molecule inhibitors

Trophozoite-stage parasites (24 hpi) at 5% parasitemia were treated with small molecule inhibitors: 5 mM 3-Methyladenine (Sigma-Aldrich), 5 µM Wortmannin (Sigma-Aldrich), 75 nM Artemisinin (Sigma-Aldrich), 7 µM Jasplakinolide (ApexBio), 200 µM Dynasore (MilliporeSigma), 400 nM MG132 (ApexBio), 10 µM E64d (ApexBio), 10 µM ALLN (Calbiochem) for 4 h each, or 25 mM BDM (Sigma-Aldrich) for 1 h. The treated parasites were then harvested for protein expression analysis and localization studies.

2.1.5 *In vitro* removal of apicoplast from *P. falciparum*

Apicoplast was removed from parasites as described earlier (Dahl *et al.*, 2006). Briefly, late-ring stage parasites at 0.1% parasitemia were treated with 1 µM doxycycline for 48 hours. The medium was changed every 24 h. Parasites were allowed to grow without the drug and supplemented with 200 µM isopentenyl pyrophosphate (IPP) for another 24 h. Samples were then fixed and immunofluorescence assay (IFA) protocol was followed.

2.1.6 *Pf*ATG8 knockdown *P. falciparum*

Conditional knockdown *Pf*ATG8 cell line, a kind gift from Dr. Yeh, Stanford Medical School, San Francisco, was maintained in the presence of 0.5 µM anhydrotetracycline (aTC) (Walczak *et al.*, 2018). For *Pf*ATG8 knockdown, aTC was removed from the ring-stage parasites by washing them twice in incomplete RPMI. Parasites were cultured for two IE cycles in the absence of aTC and the medium was supplemented with 200 µM IPP to ensure parasite survival in the absence of *Pf*ATG8. After each cycle, the parasite culture was diluted 5-fold with fresh medium and RBCs. Experiments were performed in the second cycle after the removal of aTC (Walczak *et al.*, 2018).

2.2 Yeast strains, media and growth conditions

Yeast strains wild-type (WT) and knockout mutant strains *atg18*Δ, *fab1*Δ and *vps34*Δ, were derived from BY4741. Genotypes of various strains used in this study are listed in Table 2.1. Yeast cells were grown in YPD (1%Yeast extract, 2% Peptone, 2% Dextrose) at 30°C. Synthetic defined medium without nitrogen source (0.17% yeast nitrogen base lacking amino acids and ammonium sulfate plus 2% dextrose) was used to induce autophagy. Cultures were withdrawn at different time points as specified in the experiments, for western blot analysis or microscopic studies. Yeast cells were treated with phenylmethylsulfonyl fluoride (PMSF) to prevent the degradation of autophagic bodies inside the vacuole at the final concentration of 1 mM for 4 h.

2.2.1 Yeast transformation

LiAc/SS carrier DNA/PEG method was used for transformation in yeast (Gietz and Schiestl, 2007). A single colony of the yeast strain from YPD agar plate was inoculated into 5 ml liquid medium (YPD broth) and incubated overnight on a rotator shaker at 200 rpm at 30°C. The primary culture was diluted to OD_{600} = 0.2 (2×10^6 cells ml^{-1}) and allowed to grow for 3-4 h until the OD_{600} reaches 1 (1×10^7 cells ml^{-1}). The cells were then harvested by centrifugation at 3,000×g, followed by washing the cell pellet twice with autoclaved water. The cell pellet was resuspended in 1.0 ml of sterile water and 100 µl of the cell suspension was used for each transformation. Cells were then resuspended in 360 µl of transformation mix containing 5 µg plasmid DNA (Table 2.2) and incubated at 42°C for 40 min. The positive transformants were selected by allowing the transformed cells to

grow on synthetic defined medium devoid of leucine and uracil (0.17% yeast nitrogen base, 0.5% ammonium sulfate, 2% dextrose, 2% agar, 0.002% histidine, 0.002% methionine).

Strain	Genotype	Source
BY4741	MATa his3Δ leu2Δ ura3Δ met15Δ	Brachmann *et al.*, 1998
sPA1	BY4741 GFP::LEU2 2xmCherry-*Sc*Atg8::URA3	This Study
sPA2	BY4741 *Pf*ATG18-GFP::LEU2 2xmCherry-*Sc*Atg8::URA3	This Study
sPA3	BY4741 GFP::LEU2 2xmCherry-*Sc*Atg8::URA3 atg18Δ::KanMX4	This Study
sPA4	BY4741 *Pf*ATG18-GFP::LEU2 2xmCherry-*Sc*Atg8::URA3 atg18Δ::KanMX4	This Study
sPA5	BY4741 *Pf*ATG18(FTTG)-GFP::LEU2 2xmCherry-*Sc*Atg8::URA3 atg18Δ::KanMX4	This Study
sPA7	BY4741 *Pf*ATG18-GFP(TFPTS)::LEU2 2xmCherry-*Sc*Atg8::URA3 atg18Δ::KanMX4	This Study
sPA8	BY4741 *Sc*Atg18-GFP::LEU2 2xmCherry-*Sc*Atg8::URA3 atg18Δ::KanMX4	This Study
sPA9	BY4741 *Pf*ATG18-GFP::LEU2 fab1Δ::KanMX4	This Study
sPA10	BY4741 *Pf*ATG18-GFP::LEU2 vps34Δ::KanMX4	This Study

Table 2.1: Genotype of various yeast strains used in this study

Transformation Mix components	Vol (µl)
PEG 3350 (50% (w/v))	240
LiAc 1.0 M	36
Single stranded DNA carrier (2 mg ml^{-1})	50
Plasmid DNA plus sterile water	34
Total volume	360

Table 2.2: Yeast transformation mix

The list of components required for the preparation of the transformation mix to carry out yeast transformation (Adapted from Gietz and Schiestl, 2007).

2.2.2 Spot assay for yeast

Spot assay was performed as described previously (Tong, 2012). Single yeast colony from the freshly grown plate was inoculated overnight in selection media at 30°C. 3 µl culture from exponentially growing yeast strain was ten-fold serially diluted, spotted onto the

selection plate and incubated at 30°C for 2 days (labelled as Day 0). The same culture was used to induce autophagy by resuspending the cells in synthetic medium devoid of nitrogen source followed by ten-fold serial dilution and spotting on a selection plate (devoid of nitrogen source). The experiment was carried out for up to 5 days of nitrogen starvation. The plates were grown for 2 days at 30°C and then imaged using GelDoc XR (Bio-Rad).

2.2.3 mCherry-*Sc*Atg8 processing assay

S. cerevisiae strains containing the 2xmCherry-*Sc*Atg8 (pRS316 vector) plasmid were grown in synthetic defined medium lacking leucine and uracil at 30°C. A secondary culture was inoculated at OD_{600} = 0.2 and grown until OD600 reached ~0.7. The cultures were transferred to nitrogen deprived medium (SD-N) and samples were collected after 4 h. Collected cells were used for fluorescence microscopy to visualize the mCherry signal.

2.3 Expression of *Pf*ATG5 domain in BL21(DE3) codon-plus bacteria

The recombinant protein was expressed in *Escherichia coli* as described previously (Rosano and Ceccarelli, 2014). *Pf*ATG5 (116-266 amino acids) domain, which includes peptide region used for generating anti-*Pf*ATG5 antibodies, was cloned into the *Nco*I and *Xho*I restriction sites of the pET-28a (+) plasmid (Novagen). The expression vector pET28a-*Pf*ATG5$^{116\text{-}266}$ with a C-terminal His_6 tag was transformed into *Escherichia coli* BL21(DE3) codon-plus (Stratagene) strain. The positive transformant was grown in terrific broth at 37°C. After OD_{600} reached 0.8, protein expression was induced with 1 mM isopropylthio-β-d-galactoside (IPTG). About 10 mg cell pellet was suspended in 200 µl lysis buffer (50 mM NaH_2PO_4, 300 mM NaCl, 10 mM imidazole, 30% Glycerol, 20 mM β-mercaptoethanol) containing protease inhibitor PMSF. It was then lysed on ice by sonication, giving ten 40 second pulse at 300 W with intermittent cooling. After lysis, the cell debris was removed by centrifugation for 45 minutes at 10,000×g at 4°C. The proteins present in supernatant were separated using 15% SDS-PAGE gel and the specificity of anti-*Pf*ATG5 antibodies was determined by western blotting.

2.4 Cloning and site-directed mutagenesis

2.4.1 Agarose gel electrophoresis

DNA and RNA samples were isolated and resolved on agarose gel (0.8-1.5%) containing ethidium bromide. Samples were mixed with bromophenol blue dye to a final concentration of 1× and loaded on gel followed by electrophoresis at 100V in 1×TAE. Nucleic acid samples were visualized under long wavelength UV using GelDoc XR (BioRad).

2.4.2 Plasmids and strains

A yeast expression shuttle vector, p415-ADH was used for the expression of *Plasmodium* proteins in the budding yeast *S. cerevisiae*. p415-ADH (7747bp) is a CEN/ARS low copy number plasmid comprises of alcohol dehydrogenase (ADH) promoter, a selectable leucine marker, multiple cloning array and a CYC1 terminator sequence (Figure 2.1B). 2xmCherry-*Sc*Atg8 is present in a pRS316 yeast expression vector, which contains a selectable uracil marker (Figure 2.1C). This construct was a kind gift from Prof. Yoshinori Ohsumi, Tokyo Institute of Technology, Tokyo and received from Prof. Ravi Manjithaya, JNCASR, Bangalore. pET28a (+) (Novagen) was used for the expression of *Pf*ATG5 domain with a C-terminal His_6 tag (Figure 2.1A). For episomal expression of proteins in *P. falciparum*, pARL-1a vector was used. pARL1-a contains human dihydrofolate reductase gene (*h*DHFR) as a selectable marker that is constitutively expressed under calmodulin (CAM) promoter. The gene of interest was fused with a C-terminal GFP tag and expressed under chloroquine resistance transporter (CRT) promoter (Figure 2.1D) (Crabb *et al.*, 2004). *Escherichia coli* DH5α or XL10-Gold competent cells were used for cloning.

2.4.3 *P. falciparum* genomic DNA isolation

The parasite pellet was resuspended in the lysis buffer (0.01M Tris pH8.0, 2% SDS, 0.01M NaCl, 0.01M EDTA pH8.0 and Pronase 200 μg ml^{-1}) and incubated overnight at 37°C. The DNA was extracted with 1 volume of water-saturated phenol and 1 volume of 3% isoamyl alcohol in chloroform. The upper aqueous phase was extracted and $1/10^{th}$ volume of 1M NaCl and 2 volumes of ice-cold ethanol was added, followed by keeping the solution at -

20°C overnight. The DNA threads were spooled out and reconstituted in nuclease-free water (Moll *et al.*, 2013).

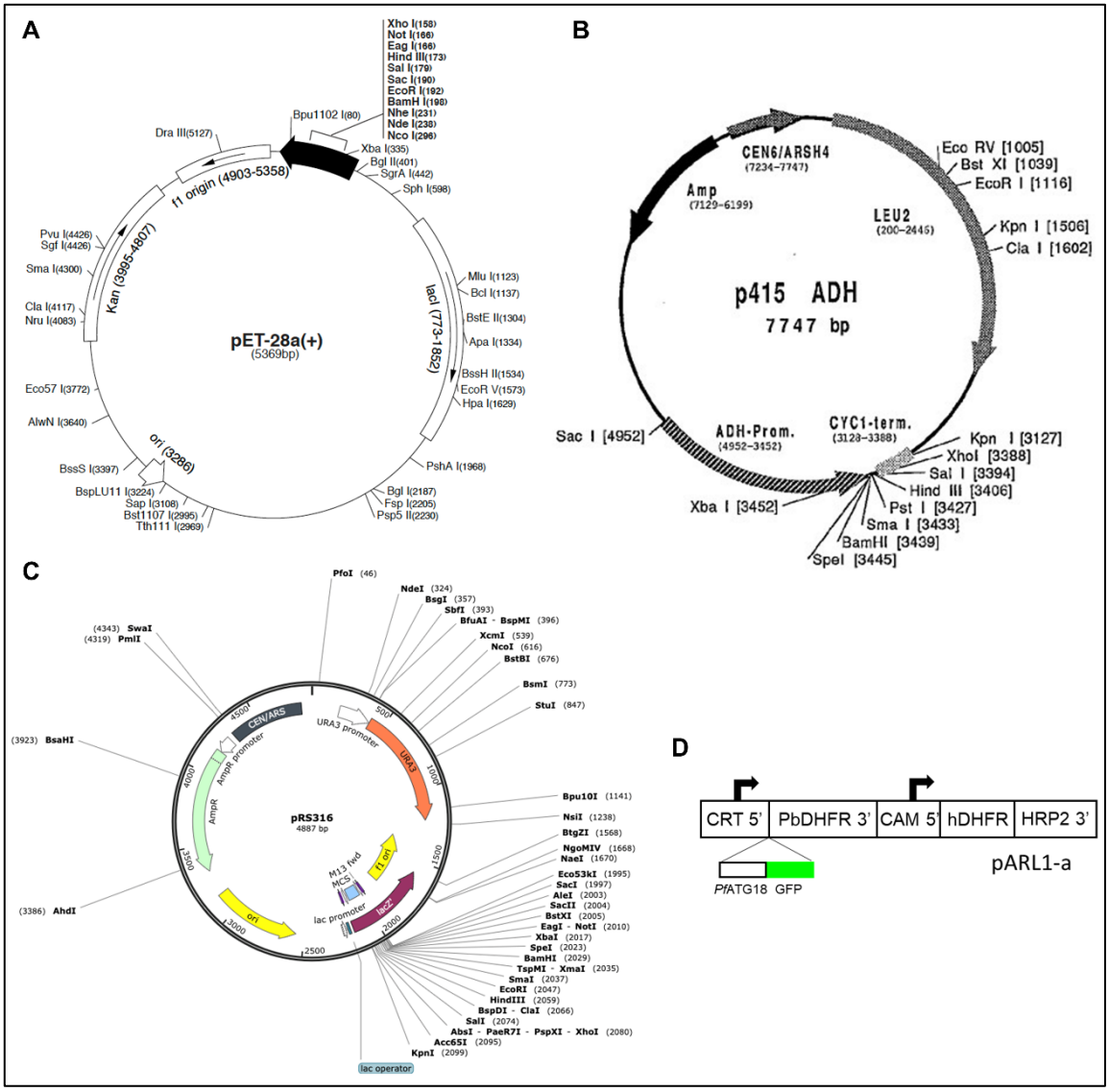

Figure 2.1: Vector maps of the plasmids

Vector maps of the plasmids used for the construction of various expression cassettes used in the study.

2.4.4 *P. falciparum* RNA isolation and cDNA preparation

For cloning *Plasmodium* genes mentioned in this study, *in vitro P. falciparum* culture was used for RNA isolation. Total RNA was extracted from the samples using TRI Reagent (Sigma-Aldrich), according to the instruction by the manufacturer. RNA was then reconstituted in Diethyl pyrocarbonate (DEPC) treated water. The samples were then treated with RNase free DNaseI (QIAGEN, Germany) to remove contaminating genomic DNA according to instruction by the manufacturer. The first strand cDNA was synthesized

from 1 µg of RNA using M-MulV Reverse Transcriptase (New England Biolabs) and Oligo-dT primers (New England BioLabs) in a 20 µl reaction. As a negative control, the second set of cDNA without reverse transcriptase (-RT) was generated.

2.4.5 Cloning

The genomic DNA or cDNA obtained was used for the amplification of respective genes using gene-specific primers as listed in Table.2.3. The amplicons were purified by agarose gel extraction. The purified insert DNA (1 µg) and the vector (1 µg) were subjected to digestion at 37°C overnight with respective restriction enzymes (New England Biolabs), mentioned with each clone, in their recommended digestion buffers.

Primer name	Plasmid	Restriction site	Primer	5'-3' primer sequence	Tm
ATG18-kpnI	pARL1a	KpnI	FP	CCGGGGTACCATGGTATCATTAAGATTAGATAATAATAG	55
ATG18-AvrII		AvrII	RP	CCGGCCTAGGATCAAAACTGTGTGATGATATTTTAAAC	55
ATG-co	p415	XbaI	FP	GCTTGGTACCTCTAGAATGG	55
ATG18-co		BamHI	RP	TAGGGGATCCATCAAATGAATGTG	55
*Sc*Atg18	p415	XbaI	FP	CCGGTCTAGAATGTCTGATTCATCACCTACTATCAAC	55
*Sc*Atg18		SpeI	RP	CCGGACTAGTTCAATCCATCAAGATGGAATACTGTGAC	55
ATG5-115	pET28a	NcoI	FP	CATGCCATGGGTCTA GATTGGAGGCTACCAATTGGTG	55
ATG5-266		XhoI	RP	CCGGCTCGAGGTTACCCTTATATAAAATATCGTCACC	55

Table 2.3: Details of primers used for cloning

The table enlists the name of the primers, cloning plasmid vector, a restriction site, the nucleotide sequence of the primer with restriction site highlighted in red and Tm of the primers.

The digested products were gel extracted and purified. Ligation reactions were carried out at 1:5 molar ratio of vector to insert using T4 DNA ligase (New England Biolabs) at 16°C overnight. The ligation reactions were transformed into *E. coli* (DH5α) competent cells and plated on to LB agar containing appropriate antibiotics (ampicillin or kanamycin), depending on the selectable marker gene in the vector. The colonies were screened for the presence of cloned insert by colony PCR. The colonies positive for the clone were inoculated in LB broth containing the selectable antibiotic followed by isolation of the plasmid. The clones were verified for the insert by gene amplification using gene-specific primers, restriction digestion, and sequencing (Figure 2.2 A-E).

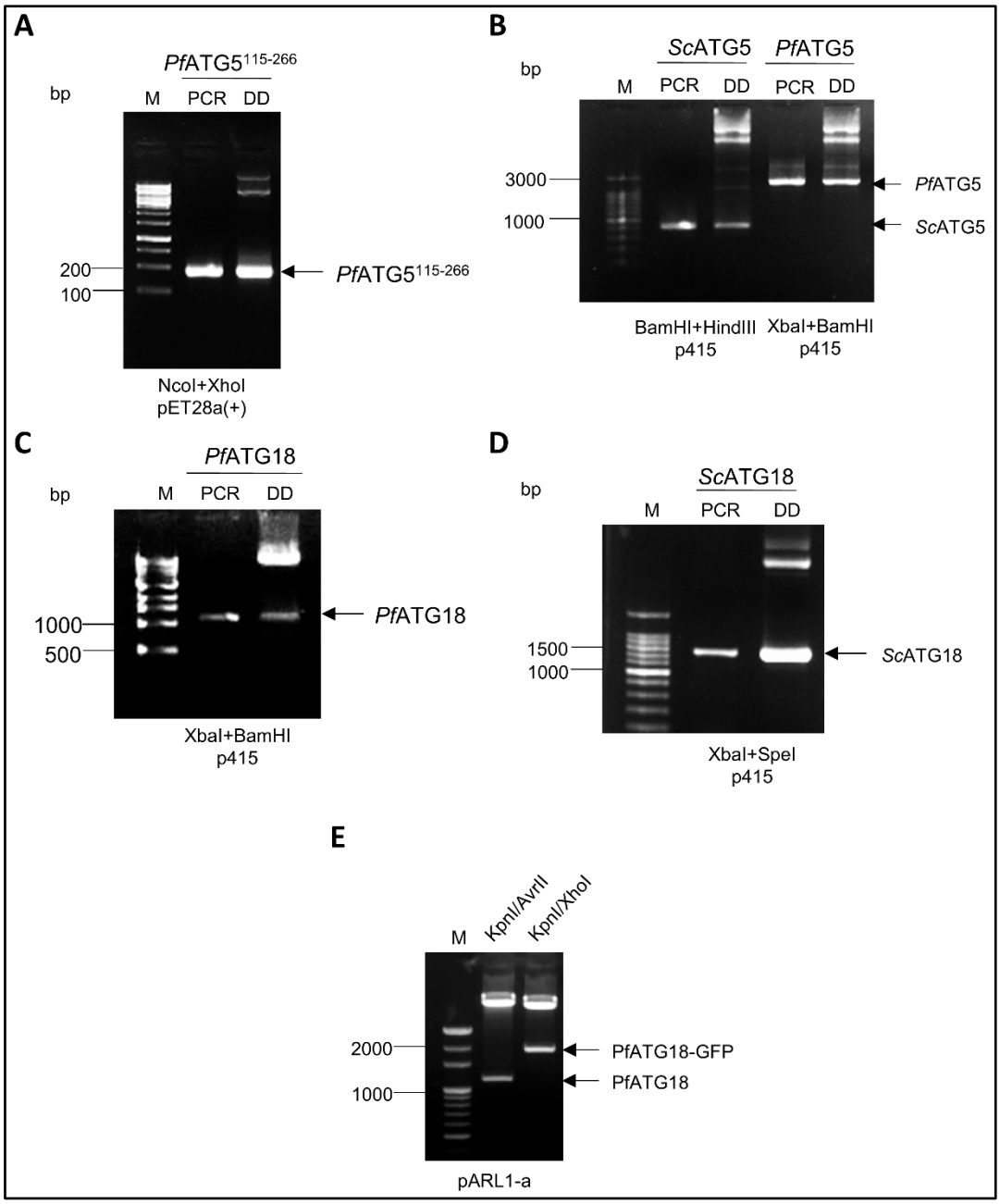

Figure 2.2: Confirmation of clones with various constructs

Confirmation of clones with various constructs is shown by PCR amplification and restriction digestion of the clones for the insert-release of the expected size. For each construct, the restriction sites and the vector used for cloning are mentioned below their respective agarose gel picture. M - DNA ladder, PCR - PCR amplicon, DD - double digested DNA, EV - Empty vector. **(A)** *Pf*ATG5$^{116-266}$ in pET28a (+) vector, **(B)** *Sc*Atg5 and *Pf*ATG5 in p415 vector, **(C)** *Pf*ATG18 in p415 vector, **(D)** *Sc*Atg18 in p415 vector, **(E)** *Pf*ATG18 in pARL1-a vector.

2.4.6 Site-directed mutagenesis

*Pf*ATG18^{FTTG} was generated from *Pf*ATG18 by introducing point mutations at nucleotides corresponding to arg238 and arg239 and changed to thr238 and thr239 by using Quik

Change II XL Site-Directed Mutagenesis Kit (Agilent Technologies, USA), as per instruction by the manufacturer. A similar strategy was used to generate *Pf*ATG18^{TFPTS} from *Pf*ATG18 by introducing point mutations at nucleotides corresponding to ser100, ser101 and asn102 and changed to pro100, thr101 and ser102. The clones were verified by gene amplification using gene-specific primers and expected size insert-release upon restriction digestion (Figure 2.3 A-F). All clones carrying the mutations were verified by sequencing (Figure 2.3 A-F). The set of primers used for site-directed mutagenesis are summarized in Table 2.4.

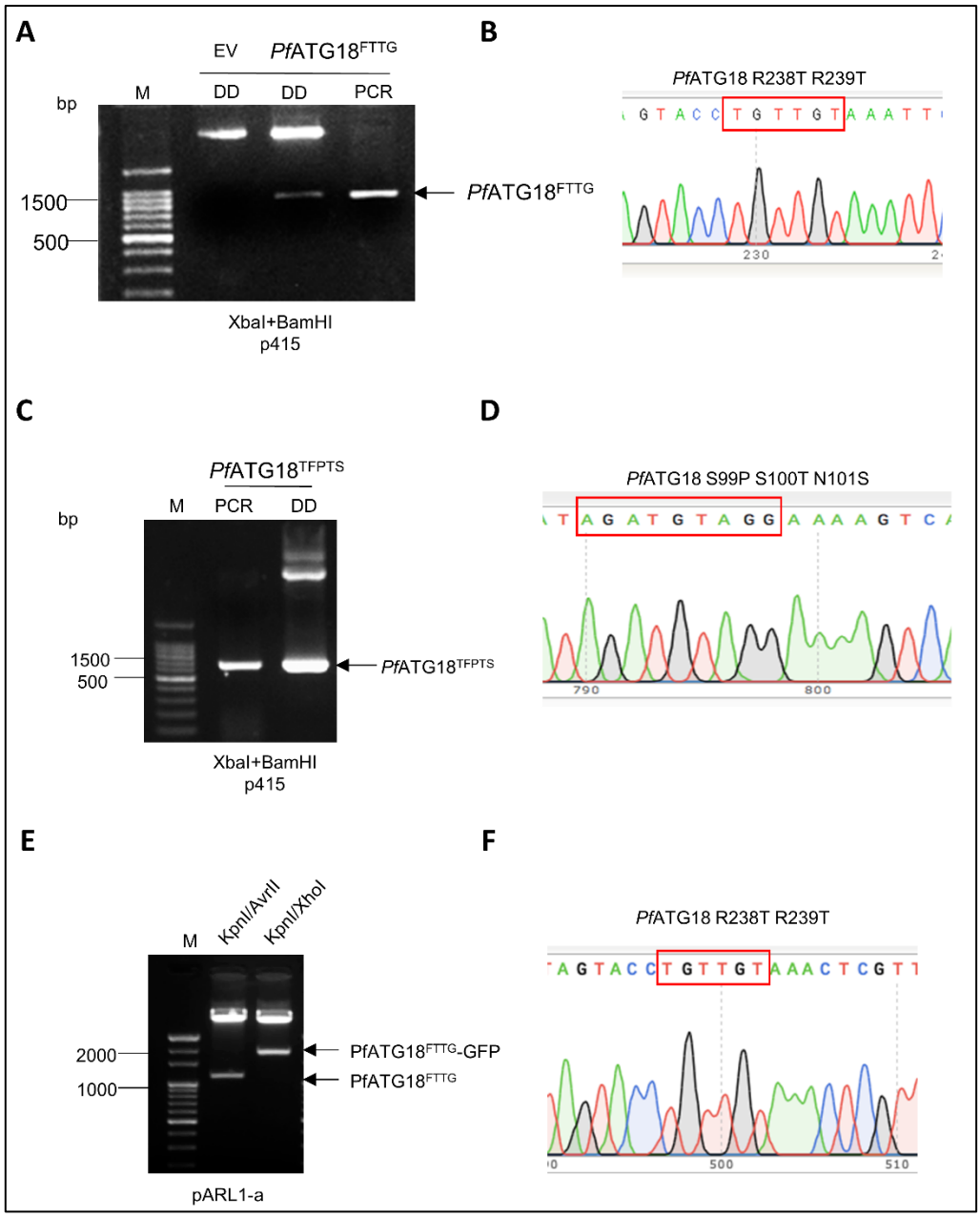

Figure 2.3: Confirmation of clones carrying site-directed mutagenesis constructs

Confirmation of clones with various constructs is shown by PCR amplification and restriction digestion of the clones for the insert-release of the expected size. For each construct, the restriction sites and the vector

used for cloning are mentioned below their respective agarose gel picture. M - DNA ladder, PCR - PCR amplicon, DD - double digested DNA. **(A)** *Pf*ATG18^{FTTG} in p415 vector, **(B)** Electropherogram highlighting the mutated nucleotides (red box) and the corresponding amino acid change. **(C)** *Pf*ATG18^{TFPTS} in p415 vector, **(D)** Electropherogram highlighting the mutated nucleotides (red box) and the corresponding amino acid change. **(E)** *Pf*ATG18^{FTTG} in pARL1-a vector, **(F)** Electropherogram highlighting the mutated nucleotides (red box) and the corresponding amino acid change.

Primer name	Plasmid	Primer	5'-3' primer sequence	Tm
ATG18-CO-FTTG	p415	FP	GTTGAACGAGTTTACAACAGGTACTAAAAATGC	55
		RP	GCATTTTTAGTACCTGTTGTAAACTCGTTCAAC	55
ATG18-PTS	p415	FP	GAGAGAAATCGCAAAATTGACTTTTCCTACATCTATTATTGGTGTTAG	55
		RP	CTAACACCAATAATAGATGTAGGAAAAGTCAATTTTGCGATTTCTCTC	55
ATG18-FTTG	pARL1a	FP	TAAATGAATTTACAACAGGTACTAAAAATGC	55
		RP	GCATTTTTAGTACCTGTTGTAAATTCATTTA	55

Table 2.4: Details of primers used for site-directed mutagenesis

The table enlists the nucleotide sequences of the primers used to create site-directed mutations in the various constructs.

2.5 Antibodies

2.5.1 Generation of polyclonal antibodies

Anti-*Pf*ATG5 polyclonal antibodies were custom synthesized against peptide sequence HINIVKLKGTDKNYDKKSNER corresponding to amino acids 170-190, in the rabbit (Genemed Synthesis). While, anti-*Pf*ATG18 polyclonal antibodies were custom synthesized against peptide sequence TGNKNDKKGKWAKN (67-81), in the rabbit (GenScript, USA). KLH was used as a carrier protein to immunize the rabbits. Affinity-purified antibodies were confirmed for specificity and used for western blotting and immunofluorescence assay.

2.5.2 Other antibodies

Commercially available antibodies – mouse anti-GFP (Roche), rabbit anti-Rab7 (Genex), rabbit anti-β-Actin (Sigma-Aldrich), rabbit anti-GAPDH (Sigma-Aldrich), mouse anti-KDEL (Abcam), and mouse anti-PI3P (Echelon Biosciences) were used in this study. Rabbit anti-ApeI was a kind gift from Prof. Klionsky, University of Michigan, Ann Arbor.

Mouse anti-Rab7and mouse anti-falcipain2 were received from Dr. Asif Mohammed, ICGEB, New Delhi. Anti-Plasmepsin-II antibodies were provided by Prof. Daniel Goldberg, Washington University School of Medicine, St. Louis. anti-*Pf*SSB was a kind gift from Dr. Deepak Gaur, Jawaharlal Nehru University, New Delhi. Previously generated antibodies in the lab, mouse anti-*Pf*ACP and rabbit anti-*Pf*ATG8, were also used.

2.5.3 Antibodies dilutions

The primary antibodies for indirect immunofluorescence assay were used with the following dilutions – 1:200 for mouse anti-GFP, rabbit anti-Rab7, mouse anti-KDEL, mouse anti-PI3P and mouse anti-*Pf*SSB; 1:400 for mouse anti-falcipain2, rabbit anti-*Pf*ATG5 and rabbit anti-*Pf*ATG18; 1:100, 1:300 and 1:600 for rabbit anti-Plasmepsin-II, mouse anti-*Pf*ACP and rabbit anti- *Pf*ATG8 respectively.

For western blot analysis, the primary antibodies were used at the following dilutions – 1:3000 for rabbit anti-β-Actin, rabbit anti-GFP, rabbit anti-ApeI and rabbit anti-*Pf*ATG8; 1:1000 for rabbit anti-*Pf*ATG5 and rabbit anti-*Pf*ATG18.

2.6 Real-time PCR analysis (relative quantification method)

The tightly synchronized parasites were harvested at different stages of IE cycle for stage-specific gene expression analysis. For relative gene expression under nutrient deprivation conditions, parasites were grown in a complete culture medium and then shifted to the starvation medium at the trophozoite stage, for the indicated period. Total RNA was extracted from samples and cDNA was synthesized, as described earlier. Primers used to amplify the gene products are listed in Table 2.5. Ten ng of each cDNA was used to amplify gene transcripts. The abundance of the transcript was determined by the threshold cycle (Ct) using SYBR Green-based fluorescent labelling of DNA in CFX96 Touch™ Real-Time PCR Detection System (Bio-Rad). Gene expression was normalized with the housekeeping gene β-Actin and fold difference during starvation was calibrated with 0 h sample, quantified using $2^{-\Delta\Delta Ct}$ method (Livak and Schmittgen, 2001).

Target	Amplicon size	Primer	5'-3' sequence	Tm
VPS34	146	FP	TAAAGAAATGATTGAAGCTATGGG	50
		RP	TTTAATCCTGCATCACACATTGC	50
ATG1	135	FP	GATCAAAGATTTAGTTGTGCTGA	50
		RP	AACTAGCTTTTTTCTTGTCCAATC	50
VAMP8	127	FP	ATTGCTTCTTGAAATAATACCACC	50
		RP	TACAGGTTTAAATTCTTCATCCAG	50
YKT6.2	113	FP	CGGCACTAGATTTATCTTCATTTC	50
		RP	AACTTCACGTGTACCTTTTTGTG	50
ATG2	108	FP	GTCTTTTATGTTTCATGGGTCAC	50
		RP	ATTTGTATTATTTTCATTGTAACTTGG	50
ATG18	127	FP	ATATGTAAAGGAAAAAATGTATCCCC	55
		RP	GCAAAACTCCATTCACTATTTAAATAC	55
ATG5	122	FP	TGGATTAGTATTATGTGTTTCTC	50
		RP	CAAGACATTTAGGTATGATATTGGATA	50
ATG8	116	FP	CATCAACATATTAATCAAAGTGCATATGG	55
		RP	AAATCTTGCATTAACAATCCTGTTTTAGG	55
Cyclophilin A	131	FP	GGACCAAATACCAACTCATCAC	50
		RP	GCTCCTTCCTTTTCCATTTCTC	50
GAPDH	136	FP	CAACATTATTCCAGCTTCCACTGGTG	55
		RP	GTA ATC TGC AAA CTA AAT CAA CAA CTG	55
Actin	131	FP	CCATGAAAATTAAAGTTGTTGCACCAC	55
		RP	TTGGTCCTGATTCATCGTATTCCTC	55

Table 2.5: Details of primers used for real-time PCR

The primer used for Real-time PCR analyses. All the primers were designed by Oligo 6.0 software.

2.7 Protein lysate preparation and detection

2.7.1 Parasite lysate preparation

The parasite lysate was prepared by resuspending the isolated parasite pellet in Laemmli sample buffer (60 mM Tris-Cl pH6.8, 2% SDS, 10% Glycerol, 100 mM DTT and protease inhibitor cocktail) or RIPA buffer (150 mM NaCl, 50 mM Tris pH 7.4, 1 mM EDTA, 0.25% sodium deoxycholate w/v, 1% NP-40, 1 mM sodium orthovanadate and protease inhibitor cocktail). The resuspended parasites were lysed by sonication giving three 2 second pulse with intermittent cooling. The standard Bradford method was used to estimate protein concentration (Kruger, 2009).

2.7.2 Subcellular localization of proteins in the parasite

Localization of proteins in RBC, PVM or the parasite was determined by sequential lysis of iRBCs, as described before (Heiber and Spielmann, 2014). Parasitized RBCs were separated by Percoll gradient. iRBCs were selectively permeabilized by incubating with 1 µg ml^{-1} Tetanolysin O (Sigma-Aldrich) for 30 min at 37°C; the supernatant thus obtained corresponds to proteins present in iRBC cytosol. The pellet obtained was then lysed with 0.03% saponin (w/v) for 5 min on ice. The supernatant acquired after the saponin lysis corresponds to proteins present in the parasitophorous vacuole. The resulting parasite pellet was resuspended in Laemmli sample buffer to get the parasite proteins. Each subcellular fraction was separated by SDS-PAGE and detected by western blotting.

2.7.3 Yeast lysate preparation

Whole cell yeast extracts were prepared from exponentially growing yeast cell cultures via trichloroacetic acid (12.5% TCA w/v) precipitation, followed by ice-cold (80%) acetone washes (twice) and air-drying of the pellets. Finally, the air-dried pellets were resuspended in 1% SDS-0.1 N NaOH solution (Mishra *et al.*, 2017).

2.7.4 SDS-polyacrylamide gel electrophoresis (SDS-PAGE)

Parasite and yeast lysates were separated on varying percentages of SDS-PAGE gels, depending upon the molecular weights of proteins to be analyzed. *Pf*ATG18 and *Pf*ATG5 were separated using 12% and 10% SDS-PAGE gels, respectively. The stacking gel was composed of 5% acrylamide. Prior to loading, the protein samples were mixed with 5× Laemmli sample buffer and boiled for 10 min. The samples were then electrophoresed in Tris-glycine SDS buffer. Gels were proceeded for western blotting.

2.7.5 Western blot analysis

The parasite lysate was resolved on SDS-PAGE (MiniProtean Tetrad apparatus, BioRad) and equilibrated in the transfer buffer (192 mM Glycine, 25 mM Tris, 20% MeOH and 0.038% SDS) for 10 min and blotted on to methanol activated PVDF membrane (Millipore). The semidry transfer apparatus (BioRad) was used for the protein transfer at 15V for 30-50 min depending on the molecular weight of the protein. The PVDF membrane

was blocked with 5% skimmed milk in PBS for an hour at room temperature. The blot was then probed with primary antibodies diluted in blocking buffer for 12 h at 4°C. Horseradish peroxidase-conjugated secondary antibodies diluted in blocking buffer (1:3000) were incubated with blot for 12 h at 4°C to bind the primary antibodies. The signals in the western blot were detected by ECL advance system (BioRad) by chemiluminescence using VersaDoc (BioRad).

2.8 Fluorescence-based assays

2.8.1 Immunofluorescence assay (IFA) in *P. falciparum*

Immunofluorescence assay was performed as described previously (Tonkin *et al.*, 2004). Parasites were washed twice with PBS and fixed using 0.0075% glutaraldehyde (ProSciTech, EMgrade) and 4% paraformaldehyde in PBS (ProSciTech, EMgrade) at room temperature for 30 min. Fixed cells were then washed twice and permeabilized using 0.1% Triton X-100 in PBS at room temperature for 10 min, followed by blocking with 3% BSA in PBS at 4°C for 1 h. Primary antibodies were diluted in blocking solution and incubated with the parasite for 1 h at room temperature. Secondary antibodies used were Alexa Fluor 488 and 568 conjugated to goat anti-rabbit and goat anti-mouse antibodies (1:200) diluted in 3% BSA in PBS and incubated with the parasite for 1 h at room temperature (Invitrogen). Nucleus was stained with Hoechst33258 (Sigma-Aldrich) and then mounted over the glass slides using VECTASHIELD (Vector Laboratories).

2.8.2 MitoTracker and LysoTracker staining

Parasites were incubated with pre-warmed 100 nM MitoTracker Red CMXRos (Invitrogen) for 15 minutes at 37°C to stain mitochondrion. Cells were then washed twice with pre-warm PBS and was either observed directly under a confocal microscope or fixed to perform IFA (Jogdand *et al.*, 2012). Similarly, parasites were incubated with pre-warmed 75 nM LysoTracker Red DND-99 (Invitrogen) for 1 h at 37°C to stain acidic organelle FV, followed by washing cells with PBS (Howe *et al.*, 2013). Images were immediately acquired using a confocal microscope.

2.8.3 Zenon labelling

Zenon labelling was used for co-immunolocalization of antibodies belonging to the same species. The first primary antibody was labelled by above mentioned IFA protocol. The second primary antibody was conjugated with Zenon Rabbit IgG 488 (Zenon Alexa Fluor 488 Rabbit IgG Labeling Kit, ThermoFisher Scientific). Zenon complex IgG 488 was made at a molar ratio of 6:1, as recommended by the supplier. This complex was then incubated with parasite pellet for 1 h. Parasites were imaged within 30 min to avoid dissociation of the complex (Joy *et al.*, 2018).

2.8.4 FM4-64 staining

FM4-64 (ThermoFisher Scientific) was used to label vacuole in yeast, as shown previously (Tong, 2011). Briefly, 8 µM FM4-64 was used to label 1 ml of exponentially growing yeast culture for 30 min in YPD medium. Cells were then washed twice with sterile water and re-suspended in fresh YPD medium and allowed to grow for another 90 min, followed by visualizing them under a confocal microscope using laser 568.

2.8.5 Confocal microscopy and image processing

Transgenic parasites and yeast transformants expressing *Pf*ATG18-GFP were observed under a ZEISS LSM 700 confocal microscope (Carl Zeiss) using 488 nm laser and 63×/1.4 NA oil objective. Hoechst 33342 (Sigma-Aldrich) was used for labelling nucleus and observed under LSM 700 using laser 405 nm. LysoTracker Red DND-99 (ThermoFisher Scientific, USA) and MitoTracker Red CMXRos (Invitrogen) labelled parasites were imaged using laser 555 nm. For time-lapse imaging, the *z*-sections were acquired at 0.2 µm step size after indicated time intervals. At each time interval, the *z*-stacks projection was obtained. Image processing was performed with Zen (blue edition) and colocalization events were quantified using line profile option in Zen (blue edition) software.

Yeast cells were grown in their respective media, centrifuged (20000×g, 2min) and were mounted on agarose pads (2% w/v) for microscopy. Images were acquired using a ZEISS LSM 700 confocal microscope or Delta Vision microscope (GE Healthcare, USA) fitted with 100×/1.4 NA objective and Cool-SNAP HQ2 camera. Images were acquired using FITC and TRITC filters. Image processing was performed with SoftWorx and Fiji (NIH)

softwares. Images were de-convolved before representation. Colocalization events were quantified using the line profile option in Zen (blue edition) software.

2.9 Immunoelectron microscopy

For immunodetection of *Pf*ATG5 and *Pf*ATG18-GFP in infected RBCs, a previously described pre-embedding silver enhancement immunogold method (Melo *et al.*, 2014) was used with slight modifications.

The parasitized erythrocytes were fixed in 2% paraformaldehyde and 0.05% glutaraldehyde dissolved in 0.1 M sodium phosphate buffer (PB) (pH 7.4) for 2 h and then washed three times with PBS. Cells were then resuspended in 2% agar and pelleted again. Cell pellets were immersed in 30% sucrose (w/v) overnight at 4 °C. Immunolabeling was performed on 10 µm thick cryostat sections after blocking with 0.1% gelatin (w/v)/1% BSA (w/v) in 0.02M PBS for 30 min (blocking buffer 1) followed by another blocking in 1% NGS in PBS-gelatin-BSA buffer (blocking buffer 2).

Sections were incubated for 2 hours at room temperature with 1:10 dilution of rabbit anti-*Pf*ATG5 in blocking buffer 2. After washing, sections were incubated with ultra-small gold particles (1:50 dilution, Electron Microscopy Sciences) for 4 h at room temperature and followed by washing and post-fixation with 2% glutaraldehyde for 20 min. Silver enhancement (R-GENT SE-EM, Electron Microscopy Sciences) was performed en-bloc for 10 minutes, followed by dehydration in graded series of ethanol. Finally, the sections were embedded in Epon 812 resin and allowed to polymerize overnight at 60°C. Ultrathin sections (70 nm thick) were cut on RMC ultramicrotome, stained with 1% Uranyl acetate and imaged in Tecnai G2 20 twin (FEI) transmission electron microscope.

2.10 Graphical representation and statistical analysis

All graphs were generated by GraphPad Prism. The mean±SEM is shown in all graphs. Student's *t* test and one-way analysis of variance were used to calculate statistical significance, *** refers to $P<0.0005$, ** indicates $P<0.005$, while * depicts $P<0.05$, values higher than $P>0.05$ are non-significant (ns).

Results

Table of Contents

3.1 Analysing the relative gene expression of putative *ATG* genes upon brief starvation in *P. falciparum*

Autophagy is an intracellular degradation system in eukaryotes. This process requires the formation of double-membrane sequestering vesicles called autophagosomes. Autophagy gets triggered due to a variety of cellular stresses and promotes cell survival in adverse conditions. Upon autophagy induction, a small portion of cytoplasmic materials is enclosed by a phagophore or isolation membrane, which matures to form autophagosome. Autophagosome then fuses with the lytic organelle lysosome, and the contents inside the autophagosome are degraded by lysosomal hydrolases and recycled. Autophagy is essential for various physiological and pathological processes: for example, development, and differentiation, generation of amino acids during starvation, eliminating damaged and excess organelles and degradation of intracellular bacteria (Mizushima, 2007).

Autophagosome biogenesis in yeast requires the synchronized action of about 20 ATG proteins (Feng *et al.*, 2014). The initiation step involves ATG1-ATG13-ATG17-ATG31-ATG29 complex and ATG9-containing vesicles. Next, the PI3K complex I (Vps30/ATG6-ATG14-Vps15-Vps34) produces PI3P on PAS, which recruits the ATG2-ATG18 complex. Finally, the ATG12-ATG5.ATG16 complex and the ATG8-PE conjugate are needed for phagophore elongation and completion of the autophagosome (Feng *et al.*, 2014; Yin *et al.*, 2016). These proteins were initially discovered in *S. cerevisiae* through screening assays, and are essentially conserved in mammals, while they are only partially conserved in parasitic protists such as *Plasmodium* (Duszenko *et al.*, 2011). Many reports indicate the presence of autophagy-like pathway in the malaria parasite (Coppens, 2011; Tomlins *et al.*, 2013; Cervantes *et al.*, 2014; Voss *et al.*, 2016; Joy *et al.*, 2018). However, in the putative ATG repertoire in *Plasmodium*, it is evident that a few vital proteins are not found, for example, ATG9 – a transmembrane protein supposedly required for providing membrane for autophagosome biogenesis. On the contrary, proteins involved in ATG8 conjugation system are well conserved (Hain and Bosch, 2013; Mizushima and Sahani, 2014). As there is a limited set of ATG proteins in *Plasmodium*, the main question in the field is whether the parasite can generate autophagosomes and has a functional autophagy pathway (Hain and Bosch, 2013; Mizushima and Sahani, 2014).

To answer this, we studied the effect of amino acid starvation on the viability of *P. falciparum* and its effect on the autophagy machinery of the parasite. It is found that the growth of the parasite was stalled after 4 h of amino acid deprivation. However, the parasites remain viable for about 24 h of starvation, and the growth of parasites resume when the culture medium is supplemented with amino acids. Since morphologically, 4 h starved parasites appear to be the same as fed parasites, the effect of amino acid starvation on the expression levels of *ATG* genes in *P. falciparum* is analysed at this time point. We find that expression of *P. falciparum ATG* genes is significantly upregulated upon 4 h of starvation. This observation indicates that putative *ATG* genes may be involved in autophagy-like pathway upon nutrient-limitation in the parasite.

3.1.1 *P. falciparum* remains viable upon brief starvation

The autophagy pathway is regulated by the nutritional state of the cell and is induced when the cell senses nutrient deprivation (Feng *et al.*, 2014). To study the autophagy pathway in *P. falciparum*, we assessed the effect of amino acid starvation on the asexual blood stages of *P. falciparum*. Synchronized parasites at early trophozoite stage (24 hpi) were cultured in medium devoid of amino acids and serum (-aa) for 4, 6, 12, 18, and 24 hours. In amino acid-rich medium, parasites developed normally and continued to grow from trophozoite to schizont (Figure 3.1A). In the absence of amino acids, the morphology of the parasites was similar to that of control parasites for up to 4 h (Figure 3.1A). However, when the parasites were starved for a longer period (up to 24 h), developmental abnormalities were detected (Figure 3.1A). Parasite growth was stalled and subsequently, the cytosol became condensed and the cells appeared densely stained. These parasites remained in a shrunken form in the culture and were unable to develop into schizonts (Figure 3.1A). This finding is consistent with the previous report, which shows that isoleucine starvation results in the hibernation of the parasite (Babbitt *et al.*, 2012).

To determine whether amino acid-starved parasites maintain viability, we incubated synchronized early trophozoite-stage parasites in the amino acids and serum deprived medium (-aa) for varying periods (4, 8, 12 and 24 hours). After the indicated time period, starved culture was supplemented with complete medium (CM) containing amino acids and parasites were allowed to grow for an additional 48 h. Parasitemia after recovery was measured by counting the iRBCs in Giemsa-stained blood smear. When the parasites were

starved for amino acids for 4 h, followed by supplementation with complete media, almost the entire parasite population (92.15±4.27%) was able to recover (Figs 3.1B and C). Parasites starved for longer periods (up to 24 h) followed by supplementation with nutrient-rich medium, showed lesser recovery (up to 64.81±4.55%) (Figs 3.1B and C). The recovery of growth by parasites following starvation suggests their viability under nutrient limitation.

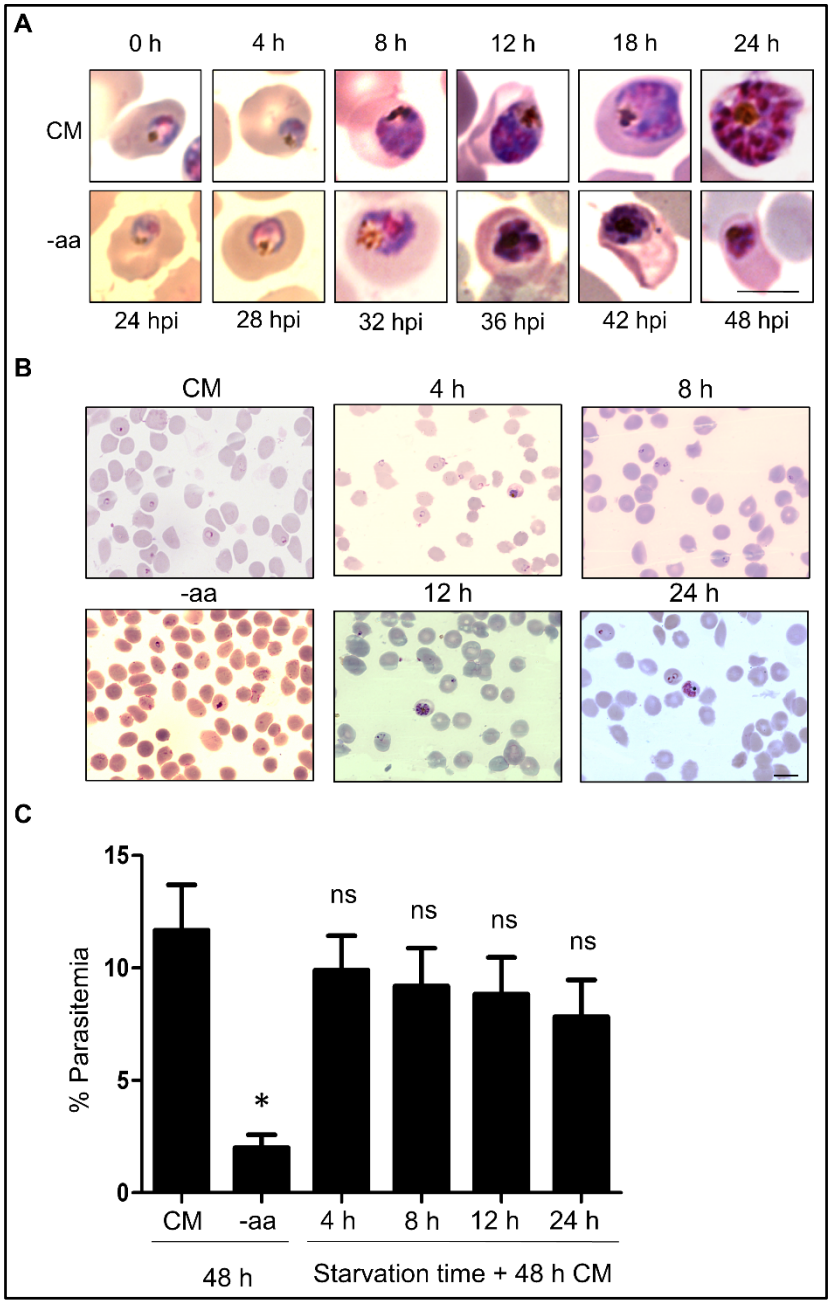

Figure 3.1: *P. falciparum* recovers upon amino acid starvation followed by supplementation

(A) Representative images of Giemsa-stained thin blood smears prepared from *P. falciparum* at 0, 4, 8, 12, 18 and 24 hours of incubation in complete medium (CM) or amino acids and serum-free medium (-aa). N=100 parasites, n=3 experiments, Scale bar=5 µm. **(B)** Growth recovery following amino acid supplementation of

parasites that were starved for the indicated time. Two control sets of parasites were respectively fed or starved for 48 h. Parasitemia of all cultures was measured by counting the number of ring stage parasites per 10,000 RBCs in the Giemsa stained thin blood smear after 48 h of recovery. Representative images of Giemsa-stained thin blood smears after each time point is shown. n=3 experiments, Scale bar=5 µm. **(C)** Graph represents the mean parasitemia ± SEM; n=3 experiments. * represents P<0.05, values higher than P>0.05 are non-significant (ns), analysed by unpaired Student's *t* test.

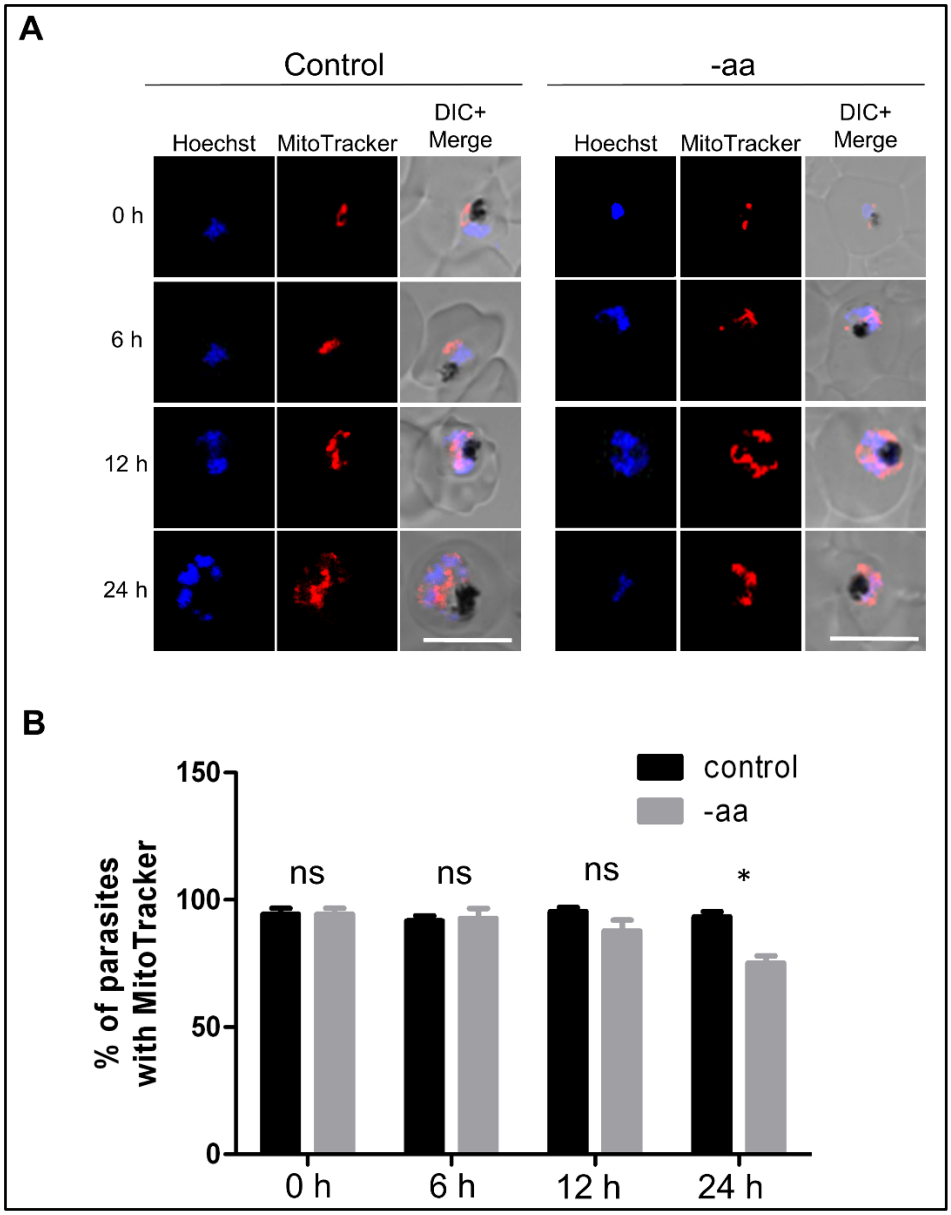

Figure 3.2: *P. falciparum* remains viable upon brief amino acid starvation

(A) Parasites were separately incubated in complete medium (control) or amino acids and serum-free medium (-aa) for indicated time periods. All parasites were labelled with MitoTracker Red CMXRos to detect live cell. Samples were analysed by confocal microscopy; N=100 parasites, n=3 experiments, Scale bar=5 µm. **(B)** Graph represents the percentage of live parasites upon amino acid starvation for indicated time periods. Data show the mean parasitemia ± SEM; n=3. * represents P<0.05, values higher than P>0.05 were non-significant (ns), analysed by unpaired Student's *t* test.

The viability of parasites upon amino acid starvation was further assessed by staining the *P. falciparum*-infected erythrocytes with MitoTracker Red CMXRos dye, which labels only live cells with viable mitochondria (Jogdand *et al.*, 2012). *P. falciparum* cultures were separately incubated with complete medium (control) or amino acids and serum-free medium (-aa) for 6, 12, and 24 hours. The fluorescence of CMXRos dye, representing live parasite populations, was detected in control as well as in starved parasites (Figure 3.2), which indicated that parasites could survive nutrient starvation for at least 24 h.

3.1.2 *P. falciparum ATG* genes expression is upregulated upon brief starvation

About 20 core ATG proteins are directly involved in autophagosome formation in yeast (Feng *et al.*, 2014). Previous studies have identified a limited set of autophagy-related genes in *P. falciparum* (Hain and Bosch, 2013; Navale *et al.*, 2014). Homologs of a few *ATG* genes are present in *P. falciparum,* which were identified by analysing the parasite genome database using the yeast and human autophagy-related proteins as queries (Hain and Bosch, 2013; Navale *et al.*, 2014). The predicted *Plasmodium* autophagy repertoire includes proteins involved in induction – ATG1 (PF3D7_1450000) and ATG17 (PF3D7_1120000), nucleation of phagophore – VPS34/PI3K (PF3D7_0515300), VPS15 (PF3D7_0823000), ATG18 (PF3D7_1012900) and ATG2 (PF3D7_1320000), expansion and completion of autophagosome – ATG12 (PF3D7_1470000, ATG5 (PF3D7_1430400), ATG7 (PF3D7_1126100), ATG8 (PF3D7_1019900, ATG4 (PF3D7_1417300) and ATG3 (PF3D7_1450000).

We examined the transcriptional expression of a few putative *Plasmodium* autophagy-related genes (*ATG1*, *VPS34*, *ATG18*, *ATG2*, *ATG5*, *ATG8*), representing different steps of the autophagy pathway, and SNAREs (*VAMP8* and *YKT6.2*) required for autophagosome and lysosome fusion (Pryor *et al.*, 2004; Tai *et al.*, 2004), during asexual blood stages of *P. falciparum* by semi-quantitative RT-PCR. The transcripts of the analysed genes were detected in the ring, trophozoite and schizont stage parasites (Figure 3.3), indicating that these genes are co-transcribed in blood stages.

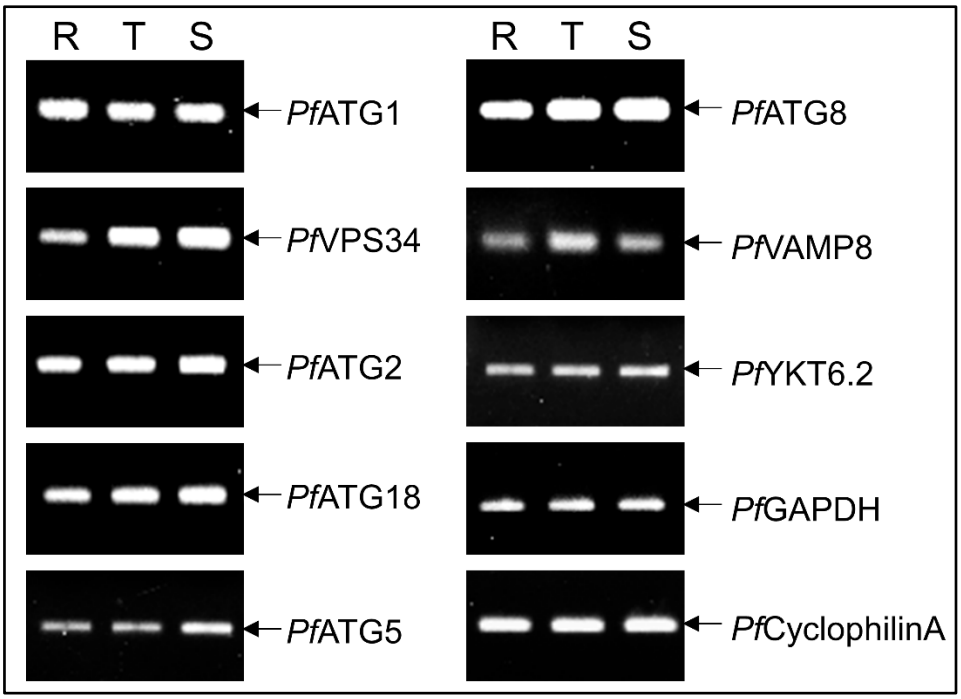

Figure 3.3: Transcription of *ATG* genes in asexual blood stages of *P. falciparum*

The expression of *PfATG1*, *PfVPS34*, *PfATG2*, *PfATG18*, *PfATG5*, *PfATG8*, *PfVAMP8*, *PfYKT6.2*, *PfGAPDH* and *PfCyclophilinA* genes was determined by semi-quantitative RT-PCR using specific primers. Agarose gel electrophoresis images showing the expression levels in ring (R), trophozoite (T) and schizont (S) of *P. falciparum*. *PfGAPDH* and *PfCyclophilinA* were used as housekeeping genes; n=3 experiments.

Continuous supply of nutrients during starvation is probably the best-known role of autophagy (Klionsky *et al.*, 2012). Hence, amino acid starvation is routinely used as an inducer of autophagy, which results in an increase in the expression of autophagy-related genes (Zhao *et al.*, 2007; Settembre *et al.*, 2011; Fiorentino *et al.*, 2013; Tsuyuki *et al.*, 2014). We, therefore, analyzed the mRNA levels of the aforementioned *ATG* genes upon starvation. The synchronized culture at trophozoite stage was deprived of amino acids and serum for 4 h, since no change was detected in the morphology of the parasite until this time point (Figure 3.1A). Relative gene expression of *ATG* genes in control and starved parasites was determined by quantitative RT-PCR using gene-specific primers. The relative gene expression of *PfATG1*, *PfVPS34*, *PfATG18*, *PfATG5* and *PfATG8* were significantly upregulated upon starvation (Figure 3.4). While mRNA levels of SNAREs *PfVAMP8* and *PfYKT6.2*, and housekeeping genes, *PfCyclophilinA* and *PfGAPDH* were not affected by starvation (Figure 3.4). These results demonstrate that putative *ATG* genes expression is upregulated upon brief starvation, suggesting that these genes may have a potential role in the autophagy-like pathway in the parasite. Therefore, in subsequent studies, we characterized the roles of two ATG proteins, *Pf*ATG5 and *Pf*ATG18, in detail.

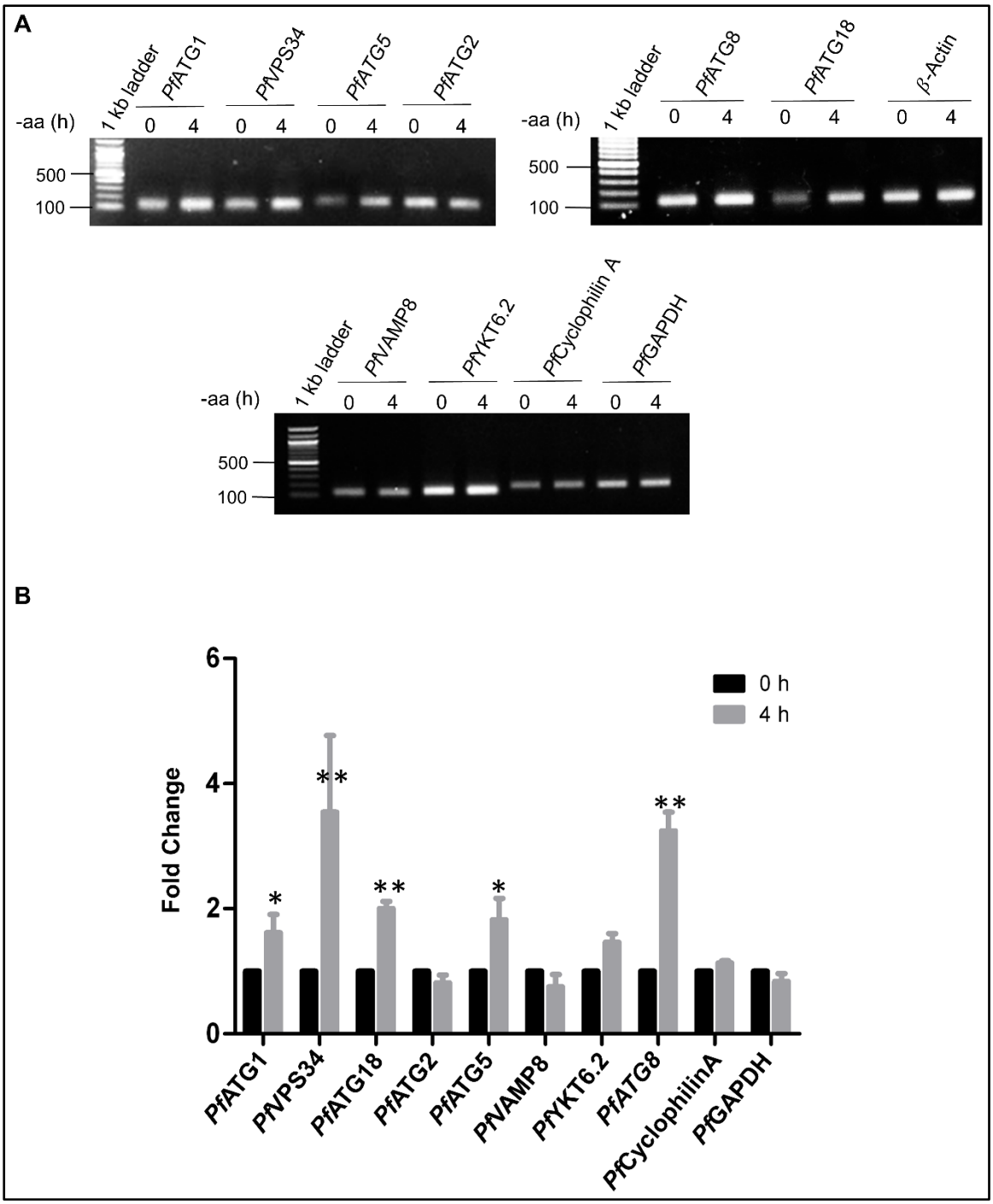

Figure 3.4: Expression of *ATG* genes is upregulated upon brief starvation in *P. falciparum*

(A) Parasite culture was synchronized, and RNA was isolated from control (0 h) and starved (4 h) parasites. The expression levels of the putative *P. falciparum* autophagy-related genes *PfATG1*, *PfVPS34*, *PfATG18*, *PfATG2*, *PfATG5*, *PfVAMP8*, *PfYKT6.2* and *PfATG8* were determined in control and amino acid-starved conditions (4 h) by RT-PCR. Agarose gel electrophoresis images showing amplicons obtained from RT-PCR; n=3 experiments **(B)** Graph represents the fold change in the autophagy-related gene expression upon starvation. β-Actin was used as the reference gene. $2^{-\Delta\Delta Ct}$ method was used to determine relative gene expression; n=3 experiments. Error bar represents ± SEM, ** represents P<0.005; * represents P<0.05, data analyzed by Student's *t* test.

3.2 Investigating the role of the putative *Pf*ATG5 in the autophagy-like pathway in *P. falciparum*

The core autophagy machinery involves proteins for autophagosome formation, delivery to the lysosome, degradation and recycling of the cellular components. Autophagy is conserved in eukaryotes and involves two ubiquitin-like conjugation systems, the ATG8 conjugation system (ATG7, ATG3 and ATG8) and the ATG12 conjugation system (ATG7, ATG10, ATG5, ATG12 and ATG16). These conjugation systems are required for autophagosome formation during autophagy (Geng and Klionsky, 2008). ATG12-ATG5 conjugate binds to the isolation membrane during the early stage of autophagosome formation and dissociates from the membrane as soon as its formation is complete. Lipidated ATG8 binds to the autophagosomal membrane at a later stage, which is facilitated by the ATG12-ATG5 complex (Fujita *et al.*, 2008; Noda *et al.*, 2012). Therefore, ATG5 is important for autophagosome formation.

ATG12 is a ubiquitin-like protein and is activated by ATG7 (E1-like enzyme). After activation, it is transferred to ATG10 (E2-like enzyme) and eventually conjugates with its sole substrate ATG5 through isopeptide bond which is formed between the terminal glycine residue of ATG12 and the internal lysine residue of ATG5 (Lys 149 in yeast), forming ATG12-ATG5 conjugate (Geng and Klionsky, 2008). Upon autophagy induction, ATG5 in ATG12-ATG5 complex binds with coiled-coil protein ATG16, which assists the association of this complex to the autophagosome. This complex then binds to the isolation membrane and promotes ATG8 lipidation, which in turn is required for autophagosome membrane expansion (Fujita *et al.*, 2008).

Bioinformatics analysis has identified ATG5 and ATG12 in *P. falciparum* genome with low homology with its yeast and mammalian counterparts, whereas other proteins such as ATG10 and ATG16, constituents of ATG12 conjugation system, are not found in the parasite. The putative ATG12 protein in *P. falciparum* does not have C-terminal glycine residue, while lysine residue in *Pf*ATG5 appears to be conserved (Hain and Bosch, 2013). Recently, it has been shown that ATG5 interacts with ATG12 non-covalently in parasites such as *Toxoplasma* and *Plasmodium* (Pang *et al.*, 2019). The homologs of ATG5 found in other protozoans participates in autophagy, for instance, in *Leishmania major*, *Lm*ATG5 is indispensable for autophagosome formation (Williams *et al.*, 2012), and *Tg*ATG5 has a

conserved role in ATG8 lipidation (Pang *et al.*, 2019). However, the function of ATG5 in *P. falciparum* is not known.

In this study, we have characterized the putative *Pf*ATG5 and deciphered its functional role in the autophagy-like pathway in *P. falciparum*. We demonstrate that *Pf*ATG5 is expressed during all the blood stages of *P. falciparum* and is present as distinct cytoplasmic puncta, which colocalize with the autophagy marker protein *Pf*ATG8. The localization of *Pf*ATG5 on double-membrane vesicles is also shown, which is reminiscent of the autophagosome-like structures. The number of *Pf*ATG5-labelled vesicles increases when parasites are subjected to autophagy inducing condition such as starvation; whereas their number decreases upon treatment of parasites with PI3-kinase inhibitor 3-methyladenine, corroborating with the reported change in ATG5-labelled vesicles in mammals during these conditions (Mizushima *et al.*, 2001; Suzuki *et al.*, 2007). Thus, this study provides insights into the molecular and functional details of ATG5 in the autophagy-like pathway in *P. falciparum* (Joy *et al.*, 2018).

This work has been published in the journal *Cell Death Discovery* in 2018. The complete reference is as follows:

Joy, S., Thirunavukkarasu, L., Agrawal, P., Singh, A., Sagar, B.K.C., Manjithaya, R., and Surolia, N. (2018) Basal and starvation-induced autophagy mediates parasite survival during intraerythrocytic stages of Plasmodium falciparum. *Cell Death Discovery* **5**(1), 43–55.

3.2.1 Bioinformatic analysis of ATG5 homolog in *P. falciparum*

A homolog of ATG5 is identified in *P. falciparum* genome (PF3D7_1430400), which shares 44% identity with 19% query coverage with *Hs*ATG5, while it shares 41% identity with 18% query coverage with *Sc*Atg5. Although the identity is low, the putative *Pf*ATG5 contains a conserved lysine residue (Lys479) (Navale *et al.*, 2014) (Figure 3.5A and Appendix1). This residue of ATG5 in other eukaryotes has been shown to conjugate with the C-terminus glycine of ATG12 (Mizushima *et al.*, 1998a; Mizushima *et al.*, 1998b).

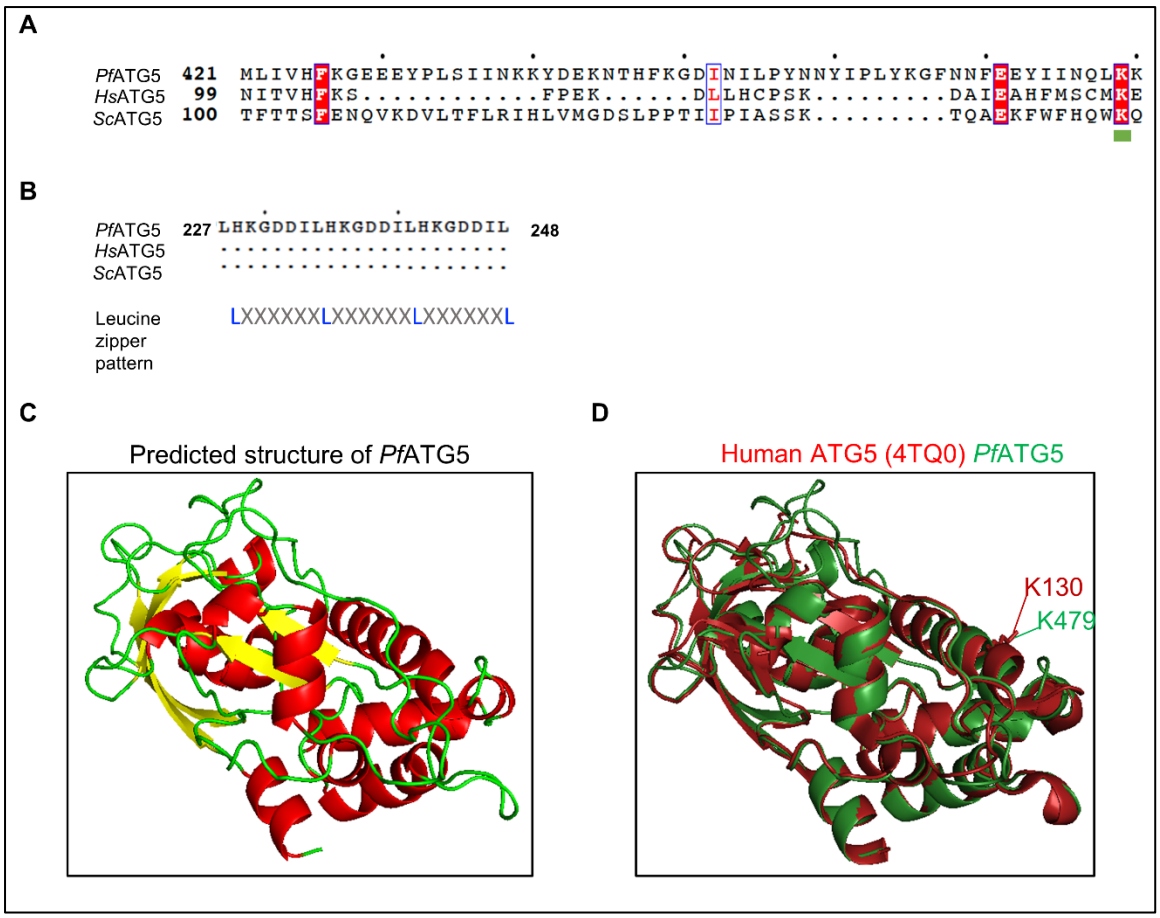

Figure 3.5: Sequence and structure-based comparison of *Pf*ATG5

(A) Sequence comparison of *Pf*ATG5, *Hs*ATG5, and *Sc*Atg5 was performed by Clustal Omega and visualized by ESPript 3.0. The green bar indicates conserved lysine residue; K130 in *Hs*ATG5, K149 in *Sc*Atg5, and corresponding K479 in *Pf*ATG5. **(B)** Leucine zipper pattern in *Pf*ATG5 predicted by MotifScan. **(C)** Structure of *Pf*ATG5 is predicted by Phyre2 and visualized by PyMOL. Ribbon diagram of the predicted structure showing sheets (yellow), helix (red) and loop (green). **(D)** Structure-based alignment of *Hs*ATG5 (PDB: 4TQ0) (red) and *Pf*ATG5 (green) was performed by PyMOL. Lysine 130 of *Hs*ATG5 and Lysine 479 of *Pf*ATG5 are highlighted.

The PlasmoDB database shows that the putative *ATG5* gene is located on chromosome 14 of *P. falciparum*. The predicted ORF is 2,592 bp long, intron-free and codes for 863 amino acid long protein, while human and yeast ATG5 comprises 275 and 294 amino acid residues respectively. The calculated molecular mass of *Pf*ATG5 is 102 kDa, and the isoelectric point is 6.18. *Pf*ATG5 is rich in asparagine (16%), isoleucine (11%) and lysine (10.4%) analyzed by ProtParam. *Pf*ATG5 has no predicted N-terminal signal sequence and does not contain a transmembrane domain. Therefore, it is predicted to be present in the cytosol of the parasite. A DNA-binding leucine zipper pattern was identified in *Pf*ATG5 by

MotifScan, which is not conserved in yeast or human homologs (Figure 3.5B). Lysine and arginine-rich nuclear localization signal (NLS) was also predicted in *Pf*ATG5.

*Hs*ATG5 has a conserved three-dimensional structure comprising of a helix-rich (HR) domain flanked by N- and C-terminus ubiquitin-like domains, UblA and UblB, connected by the linker regions L1 and L2 (Matsushita *et al.*, 2007). The three-dimensional structure of *Pf*ATG5 was predicted using the bioinformatics tool Phyre2 (Protein Homology/analogy Recognition Engine V 2.0) and visualized by PyMOL (Figure 3.5C). The structure-based comparison of *Pf*ATG5 and *Hs*ATG5 (PDB: 4TQ0) was performed by PyMOL, which shows significant overlap (Figure 3.5D), indicating that *Pf*ATG5 might have conserved domain architecture of ATG5.

3.2.2 Specificity of the anti-*Pf*ATG5 antibodies against *Pf*ATG5

To investigate the role of *Pf*ATG5 in *P. falciparum* autophagy, anti-*Pf*ATG5 antibodies were custom generated against the *Pf*ATG5 peptide, IPVVCERANRSNLPIIEKKK (28-47), by Genemed Synthesis Inc, USA. The specificity of antibodies was validated by probing them against recombinant *Pf*ATG5 protein and also by peptide blocking assay in *P. falciparum*.

Recombinant *Pf*ATG5 (116-266 amino acids) with His-tag was expressed in *E. coli* expression system. This fragment includes the peptide region used for antibodies generation (Figure 3.6A). *Pf*ATG5$^{116\text{-}266}$ was cloned in the bacterial expression vector, pET28a. The vector contains inducible T7 lac promoter and C-terminal His tag. pET28a vector alone and the vector containing *Pf*ATG5$^{116\text{-}266}$ were transformed in *E. coli* BL21 strain. The protein expression was induced by 1 mM IPTG at 37°C. Bacterial lysates were probed with anti-*Pf*ATG5 and anti-His antibodies. A band of the expected size of the recombinant *Pf*ATG5$^{116\text{-}266}$ protein (~22 kDa) was detected in the bacterial lysate with both antibodies, while no band was seen in the bacterial strain containing empty vector (Figure 3.6B), indicating the specificity of the *Pf*ATG5 antibodies.

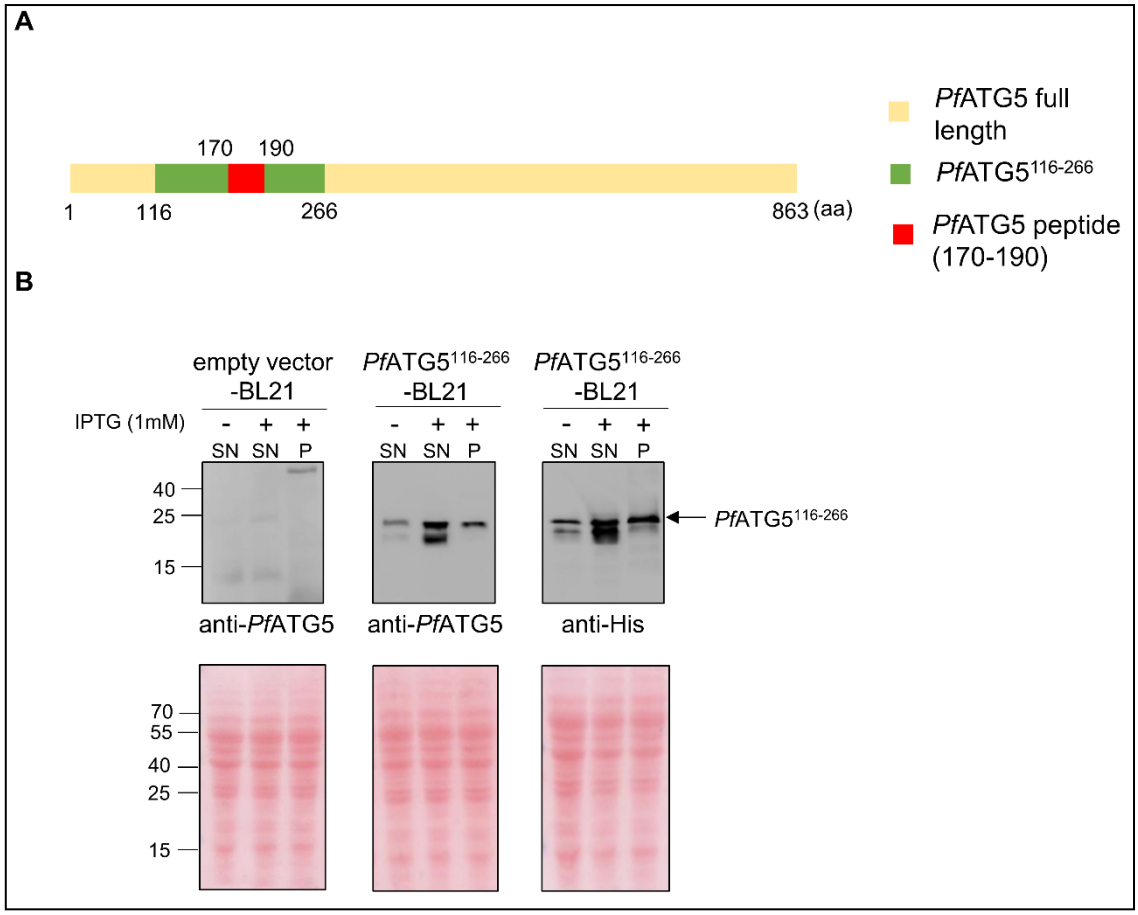

Figure 3.6: Anti-*Pf*ATG5 antibodies recognize *Pf*ATG5$^{116\text{-}266}$ in *E. coli* BL21

(A) Schematic representation of *Pf*ATG5 protein; highlighting the fragment 116-266 amino acid cloned in *E. coli* BL21, *Pf*ATG5$^{116\text{-}266}$ (green) and *Pf*ATG5 antigenic peptide (red). **(B)** Detection of *Pf*ATG5$^{116\text{-}266}$ using anti-*Pf*ATG5 antibodies in bacterial lysate by western blotting. *E. coli* BL21 containing empty vector pET28a or *Pf*ATG5$^{116\text{-}266}$ were grown to mid-log phase and the protein expression was induced by 1 mM IPTG. Bacterial cultures were lysed and the protein lysates were analyzed by western blotting using anti-*Pf*ATG5 and anti-His antibodies. Ponceau-stained transferred blot shows that the same amount of proteins from each fraction was resolved by SDS-PAGE; n=3 experiments. SN-supernatant, P-pellet.

The specificity of the anti-*Pf*ATG5 antibodies against *Pf*ATG5 during intraerythrocytic development of parasite was detected by western blot. When the parasite lysate was probed with anti-*Pf*ATG5 antibodies, a band was observed at ~102 kDa corresponding to the predicted molecular weight of *Pf*ATG5 (Figure 3.7). Apart from ~102 kDa band, multiple lower molecular weight bands were also seen using these antibodies, which might be the fragmented product of this protein. Whereas, when the parasite lysates were probed with anti-*Pf*ATG5 antibodies blocked with *Pf*ATG5 antigenic peptide, no bands were detected (Figure 3.7), indicating that the synthesized antibodies can recognize *Pf*ATG5 in parasite lysate.

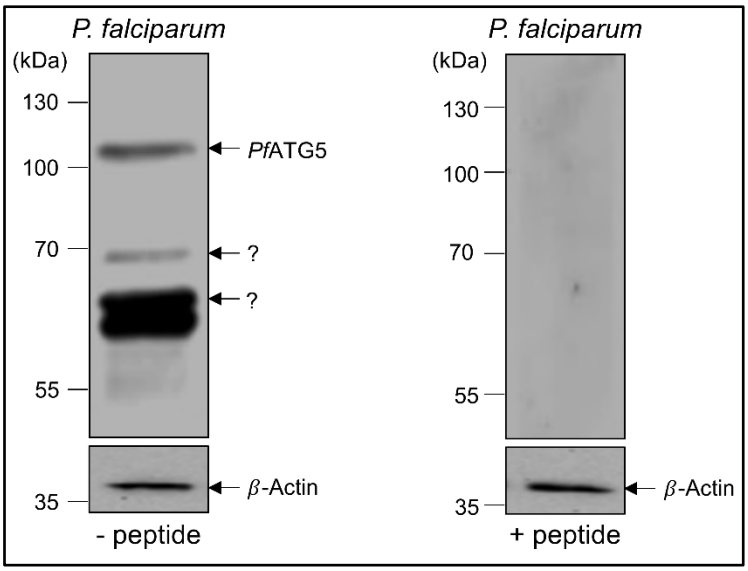

Figure 3.7: Anti-*Pf*ATG5 antibodies recognize *Pf*ATG5 during IE development of *P. falciparum*

Parasite lysate was probed with anti-*Pf*ATG5 antibodies incubated with (+peptide) or without (-peptide) *Pf*ATG5 peptide and analyzed by western blotting. β-Actin was used as loading control; n=3 experiments.

3.2.3 *Pf*ATG5 localizes within the parasite in infected RBC

P. falciparum resides inside the parasitophorous vacuole (PV), which is enclosed by the parasitophorous vacuole membrane (PVM) in the host RBC. Parasite transports proteins to RBC surface and PV to modify the host RBC, gain nutrients from the host and protect itself from the host immune system (Spielmann and Gilberger, 2015). Parasite proteins can, therefore, be found in RBC cytoplasm, PV, or inside the parasite. To investigate the subcellular localization of *Pf*ATG5 in the infected RBC (iRBC), iRBCs were sequentially permeabilized to selectively release contents from the RBC cytosol, PV and resident parasite respectively. The localization of *Pf*ATG5 was determined in these subcellular fractions by western blotting.

First, iRBCs were separated from uninfected RBCs (uRBCs) by Percoll gradient centrifugation. The iRBCs were then treated with Tetanolysin O, which permeabilizes the RBC membrane but leaves the Maurer's clefts and PVM intact (Figure 3.8A). This fraction corresponds to proteins present in RBC cytosol (Grüring *et al.*, 2012). Next, the resultant parasite fraction was treated with saponin which permeabilizes RBC, Maurer's clefts and PV membranes but does not lyse parasite plasma membrane (Ansorge *et al.*, 1996) (Figure 3.8A). This fraction represents the proteins present in Maurer's clefts and PV. Finally, the resultant parasite fraction was lysed by sodium dodecyl sulfate (SDS), which solubilizes membranes and releases proteins from all compartments of the parasite (Figure 3.8A). The

RBC, PV and parasite fractions, obtained after the sequential lysis, were analyzed by western blot using anti-*Pf*ATG5 antibodies. *Pf*ATG5 band was detected only in the parasite fraction (Figure 3.8B), suggesting that this protein resides within the parasite boundary.

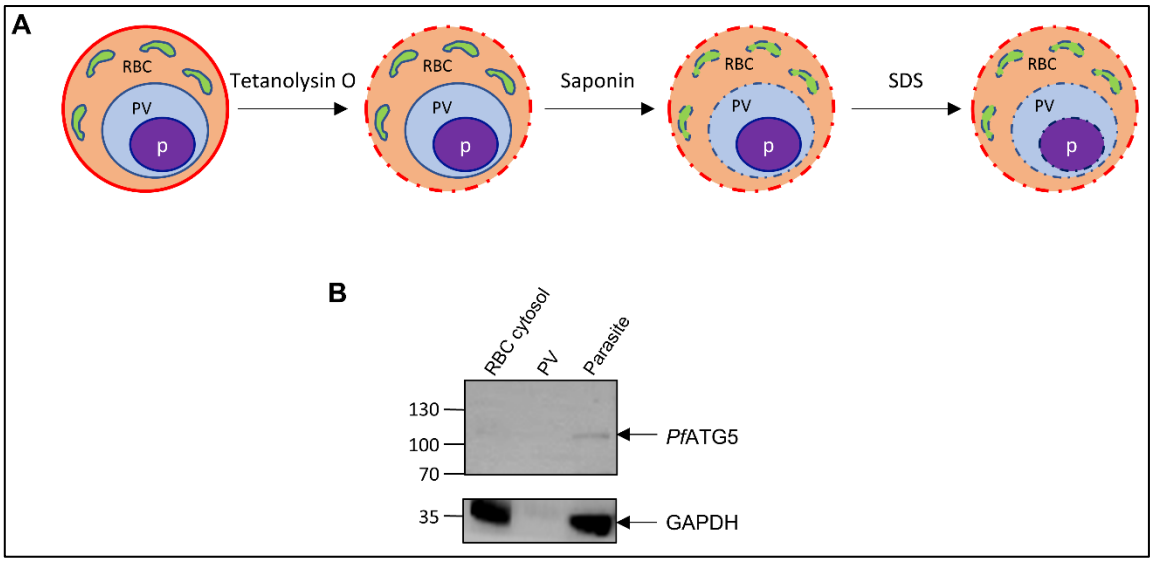

Figure 3.8: *Pf*ATG5 localizes within the parasite boundary in iRBC

(A) Schematic representation of infected RBC. Parasite-infected RBCs were lysed with either Tetanolysin O, saponin or SDS (2%). **(B)** RBC cytosol (upon Tetanolysin O lysis), PV (upon saponin lysis) and parasite fractions (upon SDS lysis) were analyzed by western blotting using anti-*Pf*ATG5 antibodies. GAPDH was used as a positive control for RBC and parasite fractions, which was detected by the anti-GAPDH antibodies; n=3 experiments.

3.2.4 *Pf*ATG5 is expressed during all the intraerythrocytic stages of *P. falciparum*

Expression and the relative abundance of *PfATG5* transcript at different asexual blood stages, i.e., ring, trophozoite and schizont, was evaluated by quantitative real-time PCR (RT-PCR). Parasites were synchronized and harvested at each stage. RT-PCR was performed using gene-specific primers. β-Actin was used as a reference gene. Relative gene expression of normalized *PfATG5* in rings was compared with expression in other blood stages. The RT-PCR analysis showed that *PfATG5* gets transcribed in all three asexual blood stages. The expression levels increased by ~2.6 and 2.4 folds in trophozoite and schizont stages, respectively, as compared to the expression in the ring stage (Figure 3.9A and B).

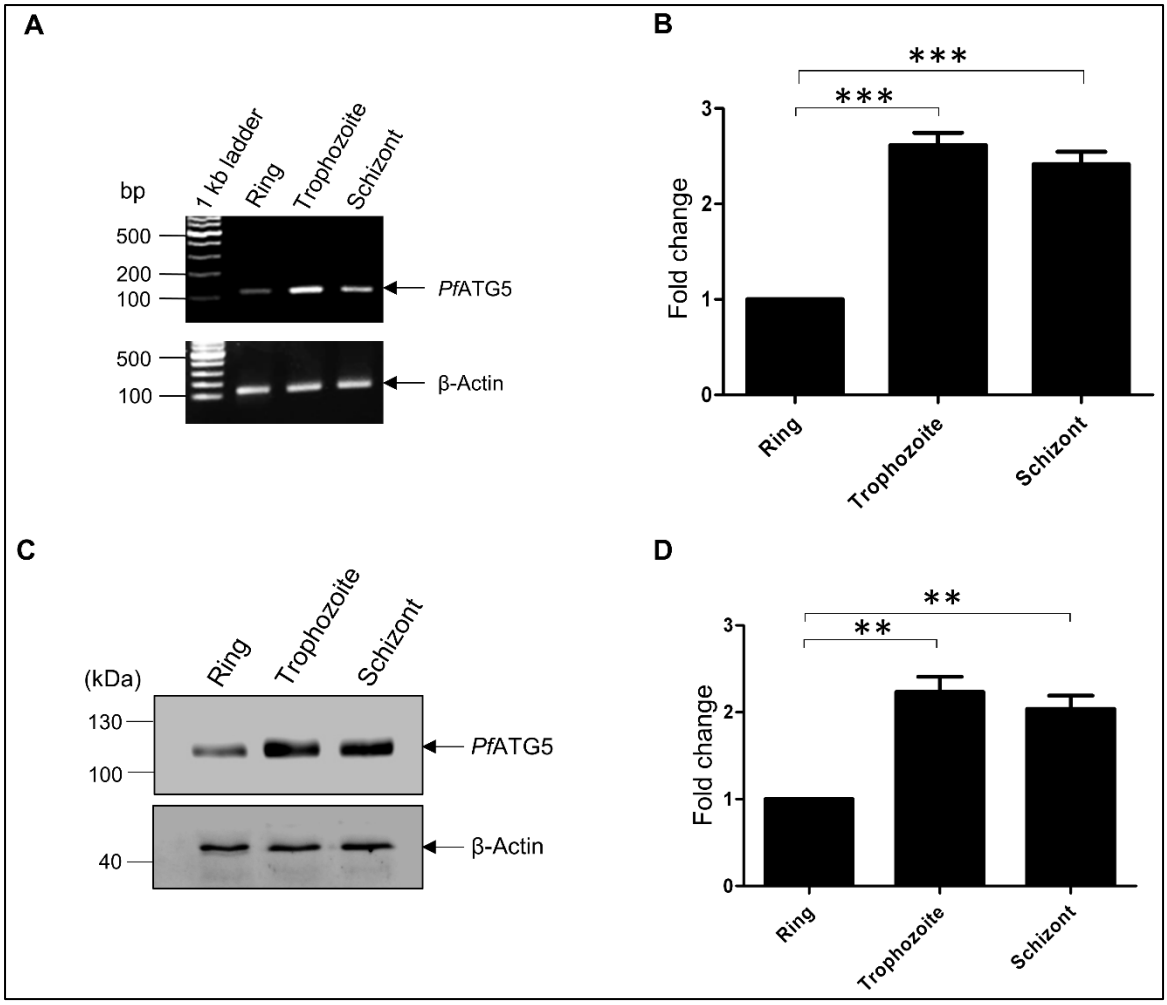

Figure 3.9: *Pf*ATG5 is expressed during all asexual blood stages of *P. falciparum*

(A) Parasite culture was synchronized, and RNA was isolated from rings, trophozoites and schizonts. Relative gene expression of *Pf*ATG5 was determined by quantitative RT-PCR using *Pf*ATG5 specific primers. β-Actin was used as the reference gene. Agarose gel electrophoresis images showing *Pf*ATG5 and β-Actin amplicons obtained from RT-PCR; n=3 experiments. **(B)** Bar graph represents the fold change in the relative gene expression of *Pf*ATG5 in trophozoites and schizonts as compared to rings, analyzed by $2^{-\Delta\Delta Ct}$ method; n=3 experiments. Error bar represents ± SEM; *** represents P<0.0005, data analyzed by paired Student's *t* test. **(C)** Parasite culture was synchronized, and parasite protein was isolated from rings, trophozoites and schizonts. *Pf*ATG5 protein expression was determined by western blotting using anti-*Pf*ATG5 antibodies (1:1000). β-Actin was used as a loading control; n=3 experiments. **(D)** Graph represents the fold change in *Pf*ATG5 protein expression as compared to rings. β-Actin was used for normalization; n=3 experiments. Error bar represents ±SEM; ** represents P<0.005, analyzed by unpaired Student's *t* test.

To further understand *Pf*ATG5 protein expression profiles in asexual stages, western blot analysis was performed with parasite lysates, prepared from synchronized rings, trophozoites and schizonts using anti-*Pf*ATG5 antibodies. *Pf*ATG5 protein was found to be present in all three asexual blood stages of the parasite (Figure 3.9C). As compared to

rings, the expression of *Pf*ATG5 increased ~2.5 and 2.3 folds in the trophozoite and schizont stages, respectively (Figs 3.9C and D). β-Actin was used as a loading control to confirm equal protein loading (Figure 3.9C). Thus, the gene and protein expression results reveal that *Pf*ATG5 is expressed in all the IE developmental stages with the expression of *Pf*ATG5 slightly higher in the later IE developmental stages of the parasite.

3.2.5 *Pf*ATG5 localizes on the autophagosome-like vesicles in *P. falciparum*

To determine the intracellular localization of *Pf*ATG5, asexual stages of *P. falciparum* were analyzed by immunofluorescence assay (IFA). The parasites were fixed at ring (12 hpi), early trophozoite (20 hpi), late trophozoite (32 hpi) and schizont (40 hpi) stages. Using anti-*Pf*ATG5 antibodies, the presence of *Pf*ATG5 was observed during all asexual stages inside the parasite (Figure 3.10A), consistent with our findings that *Pf*ATG5 is expressed in all the intraerythrocytic stages and is present in the parasite cytosol. Additionally, *Pf*ATG5 was associated with punctate structures of approximately 200-350 nm diameter (Figure 3.10A), which is similar to that of reported *Pf*ATG8 vesicle size (Navale *et al.*, 2014; Cervantes *et al.*, 2014). The number of *Pf*ATG5-decorated vesicles in rings, early trophozoites, late trophozoites, and schizonts was quantified and found to be nearly 5, 12, 15 and 18, respectively (Figure 3.10B). This result is consistent with our earlier observation that *Pf*ATG5 expression increases in the later stages of IE development of the parasite.

In eukaryotes, autophagosomes are dynamic structures. ATG5 is recruited on the isolation membrane at an early stage of autophagosome formation and present on it till its complete formation while ATG8 is recruited on the autophagosome at a later stage of its biogenesis and remains associated with the autophagosome till its fusion with the vacuole (Suzuki *et al.*, 2007). As *Pf*ATG5-decorated vesicles appeared similar to *Pf*ATG8 vesicles, resembling autophagosomes, we validated the localization of *Pf*ATG5 on autophagosomes by studying its colocalization with the autophagosome-marker *Pf*ATG8 (Tomlins *et al.*, 2013). In trophozoites, a few *Pf*ATG5-positive puncta partially colocalized with *Pf*ATG8, suggesting the presence of *Pf*ATG5 on autophagosome-like structures (Figure 3.11A).

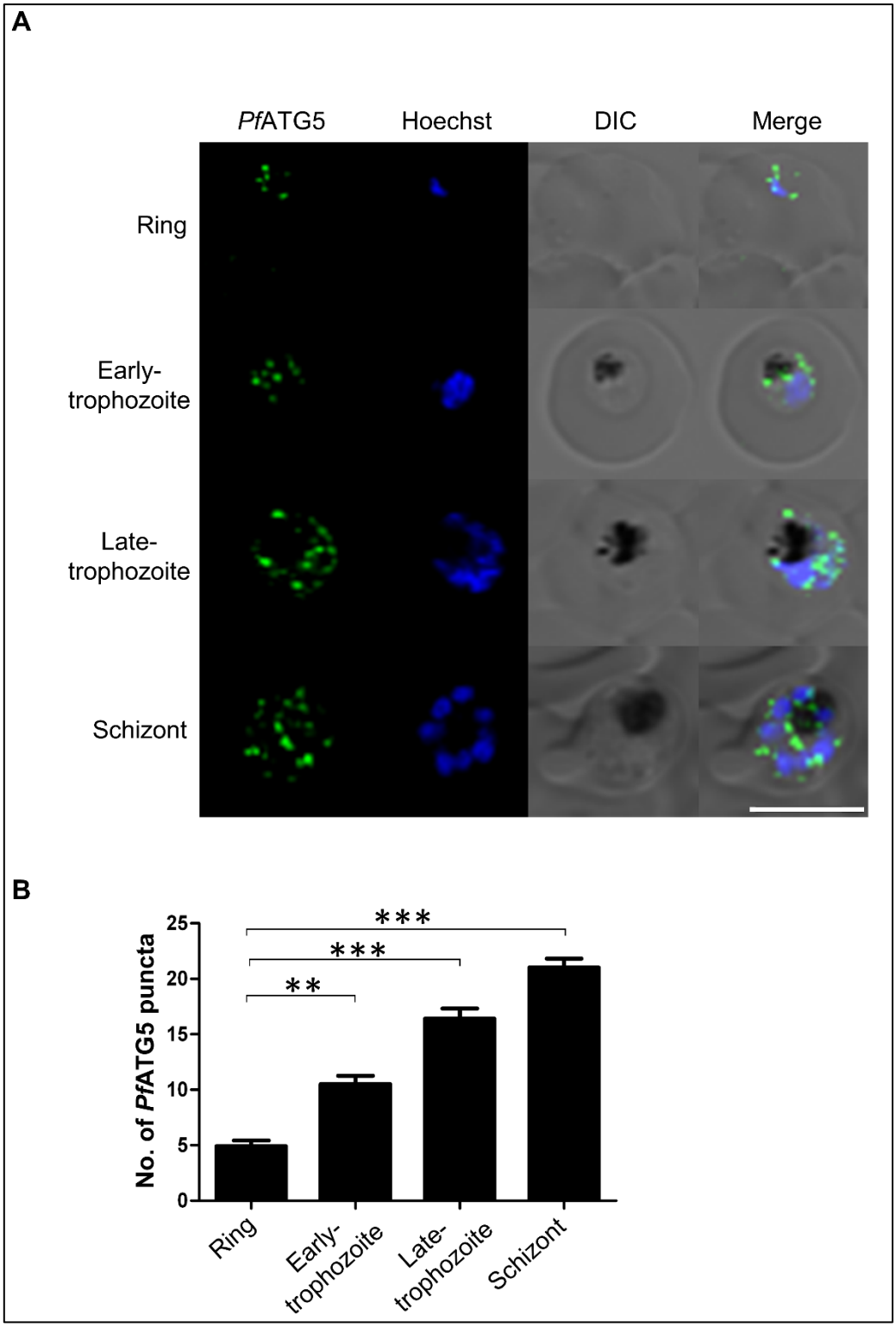

Figure 3.10: *Pf*ATG5 is present as punctate structures in IE stages of *P. falciparum*

(A) Ring, early trophozoite, late trophozoite and schizont stages of *P. falciparum* were probed for the localization of *Pf*ATG5 by IFA using anti-*Pf*ATG5 antibodies (1:400). Nucleus was stained with Hoechst. *Pf*ATG5 signal is present throughout the parasite in all blood-stages and appears to be associated with vesicular structures; N=25 parasites, n=3 experiments, Scale bar=5 µm. **(B)** Graph represents the number of *Pf*ATG5-labelled vesicles in indicated parasite stages; N=25 parasites, n=3 experiments. Error bar represents ± SEM; *** represents P<0.0005, ** represents P<0.005, analyzed by unpaired Student's *t* test.

Autophagosomes are double-membrane vesicles, which sequester cytoplasmic cargo for autophagic degradation (Mizushima *et al.*, 2010). To validate if *Pf*ATG5 localizes on autophagosome-like structures, the ultrastructure of *Pf*ATG5-labelled vesicles was acquired by immunoelectron microscopy using anti-*Pf*ATG5 antibodies. Interestingly, *Pf*ATG5 was found on double-membrane vesicles in trophozoites (Figure 3.11B), confirming the presence of *Pf*ATG5 on autophagosome-like structures in the parasite.

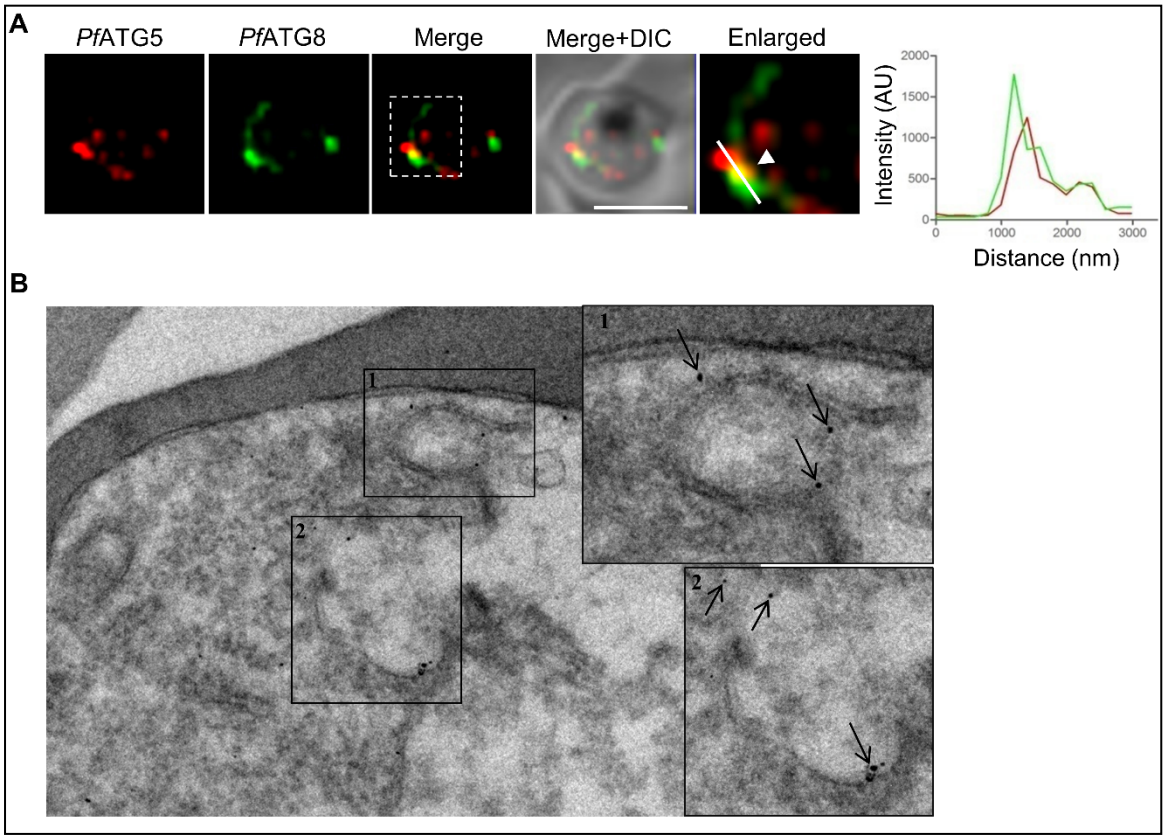

Figure 3.11: *Pf*ATG5 localizes on autophagosome-like vesicles in *P. falciparum*

(A) Synchronized trophozoites were immunolabelled with anti-*Pf*ATG5 (1:200) and anti-*Pf*ATG8 (1:200) antibodies using the Zenon antibody labelling system. Enlarged panel: magnified view of the dotted region. Graph represents the line profile of *Pf*ATG5 (red) and *Pf*ATG8 (green) quantified along the white line shown in the enlarged panel. Arrowhead indicates the puncta where the *Pf*ATG5 signal overlaps the *Pf*ATG8 signal; N=10 parasites, n=3 experiments, scale bar=5 µm. **(B)** RBCs infected with *P. falciparum* were analyzed by immunoelectron microscopy using anti-*Pf*ATG5 antibodies. Insets 1 and 2 show enlarged images of *Pf*ATG5-decorated double-membrane structures. Arrows indicate *Pf*ATG5 signal on double-membrane vesicles; n=3 experiments, Scale bar=0.2 µm.

In higher eukaryotes, autophagosome biogenesis takes place next to ER. However, membranes are also contributed by mitochondria, plasma membrane and Golgi (Mizushima *et al.*, 2001; Suzuki *et al.*, 2007; Shibutani and Yoshimori, 2014). We, therefore,

investigated the colocalization of *Pf*ATG5 with ER, mitochondria and apicoplast organelle markers. ER was labelled with anti-KDEL peptide antibodies, which recognizes ER-resident proteins. *Pf*ATG5 and KDEL labelled trophozoite samples were analyzed by confocal microscopy. *Pf*ATG5-decorated vesicles partially colocalized with the ER marker (Figure 3.12). Similarly, the parasite mitochondrion was stained with MitoTracker Red CMXRos. Partial colocalization of *Pf*ATG5 with mitochondrion too was observed (Figure 3.12). The localization of *Pf*ATG5 with apicoplast marker *Pf*SSB was analysed (Prusty et al., 2010). *Pf*ATG5 and *Pf*SSB labelled sample showed partial colocalization between them (Figure 3.12). The partial colocalization of *Pf*ATG5 with ER, mitochondria and apicoplast organelle markers indicate that *Pf*ATG5 is present on these organelles and may exert an essential function at these sites for autophagosome formation.

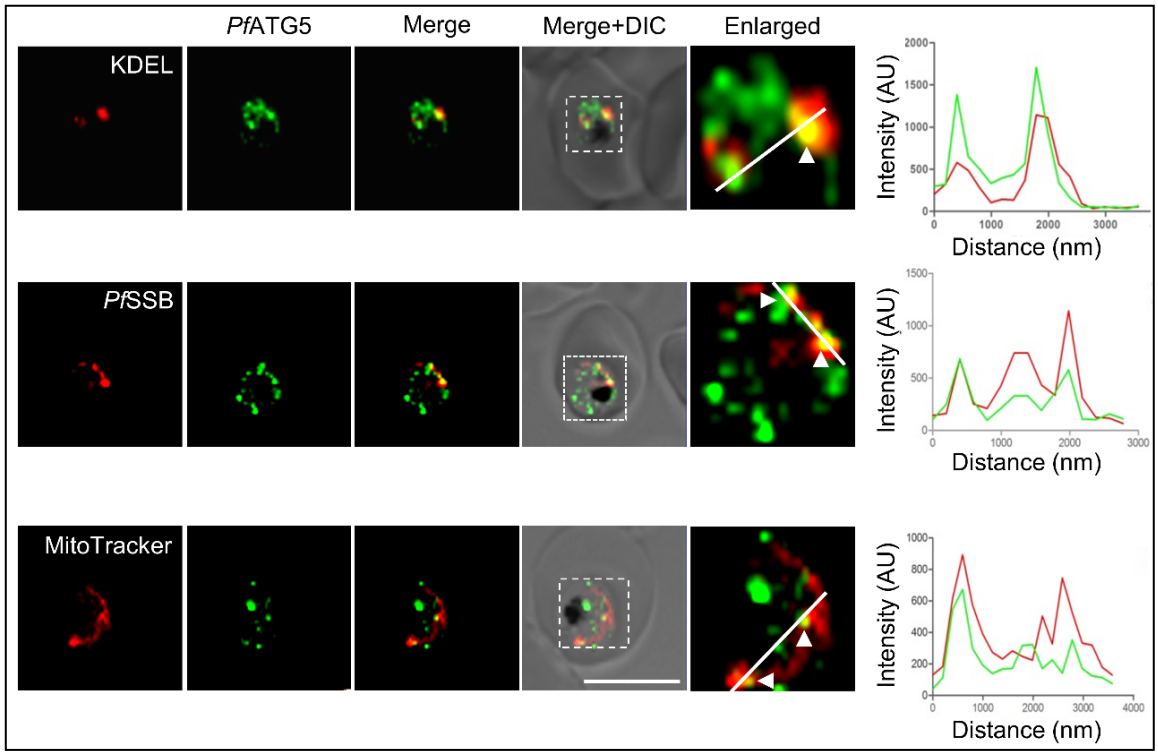

Figure 3.12: *Pf*ATG5 partially localizes on ER, mitochondria and apicoplast in *P. falciparum*

Synchronized parasites at trophozoite stage were immunolabelled with anti-*Pf*ATG5 antibodies (1:400) along with organelle markers: anti-KDEL antibodies (1:200), which recognize ER resident proteins, MitoTracker Red CMXRos (100 nM) which labels mitochondrion and anti-*Pf*SSB antibodies (1:200) which labels apicoplast protein *Pf*SSB. Nucleus was labelled by Hoechst. Enlarged panel: magnified view of the dotted region. Graphs represent the line profile of *Pf*ATG5 (green) and organelle marker (red) quantified along the white line shown in the enlarged panels. Arrowhead indicates puncta where the *Pf*ATG5 signal overlaps with the organelle markers; N=25 parasites, n=3 experiments. Scale bar=5 µm.

3.2.6 Autophagy induction and inhibition modulates *Pf*ATG5 puncta in *P. falciparum*

In yeast and mammalian cells, ATG5 localizes with the autophagosomal membrane. The expression of ATG5 as well as ATG5-decorated autophagosomes increases during autophagy-inducing conditions such as nutrient deprivation or inhibition of mTOR (Mizushima *et al.*, 2001; Williams *et al.*, 2012). To understand the participation of *Pf*ATG5 in the autophagy-like pathway in the parasite, the expression of *Pf*ATG5 and *Pf*ATG5-positive puncta was observed upon induction of autophagy by amino-acid deprivation. Trophozoites were cultured in the medium devoid of amino acids and serum for 4 h and the parasite samples were evaluated for *Pf*ATG5 expression and puncta number. Protein level of *Pf*ATG5 upon starvation was determined by western blotting. The expression of *Pf*ATG5 increased 2 folds in the starved parasites as compared to the control parasites, which were cultured in nutrient-rich conditions (Figure 3.13C). Similarly, the number of *Pf*ATG5-positive puncta was quantified in control and starved parasites by immunocytochemical analysis of *Pf*ATG5 using anti-*Pf*ATG5 antibodies. *Pf*ATG5-positive puncta increased by 2.3 folds upon starvation (Figure 3.13A and B). An increase in expression and puncta number of *Pf*ATG5 upon starvation corroborates with the previous studies, which show that in mammals, ATG5 puncta formation is induced upon amino acid starvation (Mizushima *et al.*, 2001), indicating that *Pf*ATG5 participates in autophagy in *P. falciparum*.

The nucleation of autophagosome requires class III PI3-kinase activity and has a role in the recruitment of the ATG12-ATG5.ATG16 and ATG2-ATG18 complexes to the PAS (Suzuki *et al.*, 2007). The most commonly used pharmacological inhibitors of autophagy involves the use of PI3-kinase inhibitors such as wortmannin, LY294002 or 3-MA, which inhibit early steps of autophagosome formation (Mizushima *et al.*, 2010). To understand the effect of autophagy inhibition on the expression and localization of *Pf*ATG5 in *P. falciparum*, trophozoite stage parasites were deprived of amino acids and treated with 3-MA for 4 h and then assessed for *Pf*ATG5 expression levels and localization. The number of *Pf*ATG5-decorated vesicles reduced to half in the starved parasites treated with 3-MA (Figure 3.13A and B) as evaluated by the immunocytochemical study. Consistent with the IFA data, the protein expression of *Pf*ATG5 also reduced as compared to both control and starved parasites (Figure 3.13C). This result is in line with the previous study, which

showed that ATG5 puncta formation is repressed upon inhibition of autophagosome formation (Mizushima *et al.*, 2001), indicating that *Pf*ATG5 is involved in the autophagy-like pathway in the human malaria parasite.

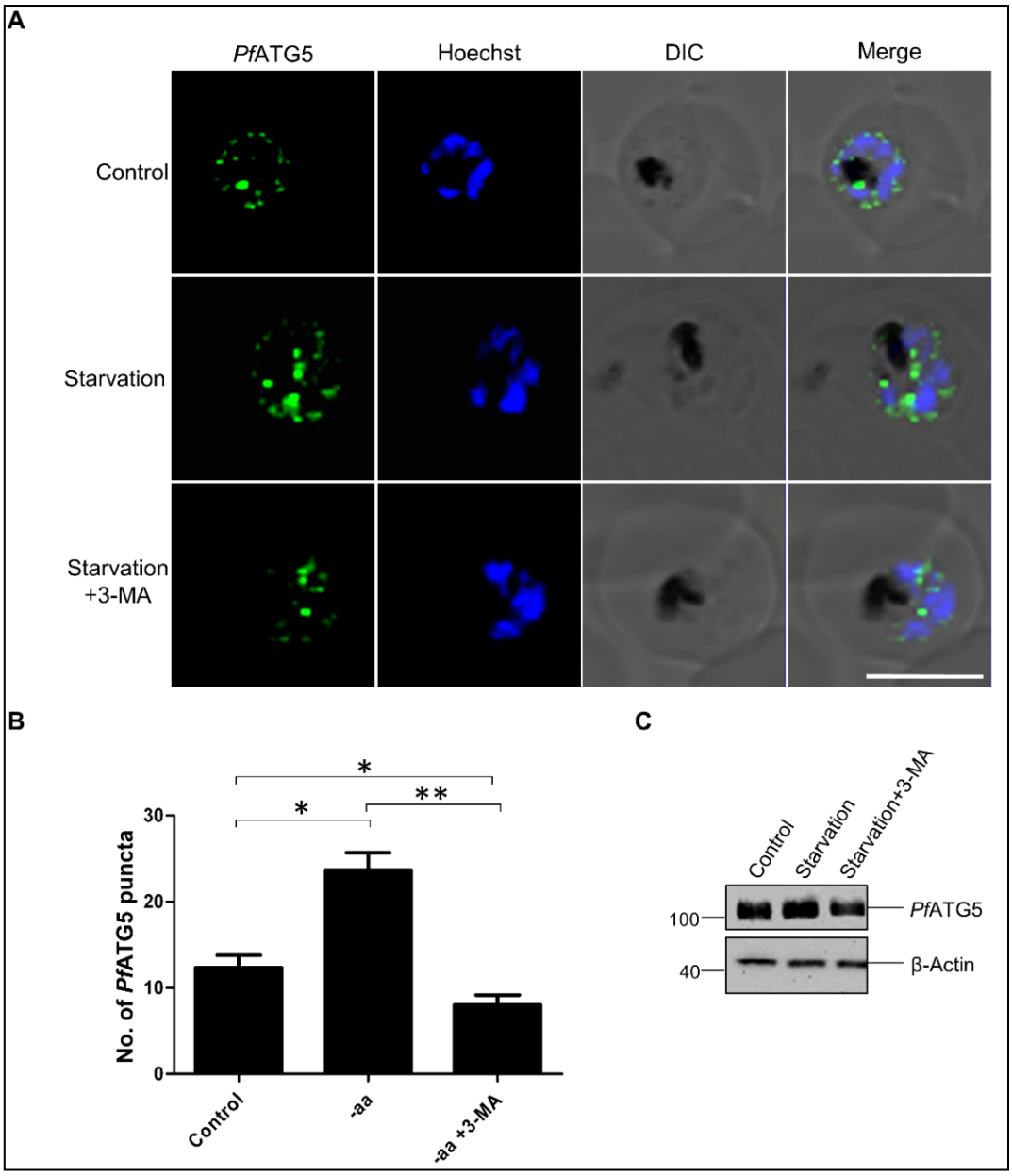

Figure 3.13: Autophagy induction and inhibition modulates *Pf*ATG5 puncta-formation in *P. falciparum*

(A) Synchronized parasites at trophozoite stage were incubated with amino acid and serum-free medium with or without 3-MA for 4 h and the parasites were fixed and immunolabelled with anti-*Pf*ATG5 antibodies (1:400). Nucleus was labelled by Hoechst; N=25 parasites, n=3 experiments, Scale bar=5 µm. **(B)** Graph represents the number of *Pf*ATG5-decorated vesicles in control, starved and 3-MA treated parasites; N=25 parasites, n=3 experiments. Error bar represents ± SEM. ** represents P<0.005, * represents P<0.05, analyzed by unpaired Student's *t* test. **(C)** Protein expression of *Pf*ATG5 upon starvation and 3-MA treatment was determined by western blotting using anti-*Pf*ATG5 antibodies (1:1000). β-Actin was used as loading control; n=3 experiments.

3.3 Investigating the role of *Pf*ATG18 in food vacuole fission and the autophagy-like pathway in *P. falciparum*

ATG18 is a member of the PROPPIN family, which folds into seven-bladed β-propeller and binds with phospholipids PI(3,5)P_2 and PI3P (Efe *et al.*, 2007). In yeast, ATG18 has two main physiological functions, namely, autophagy and vacuole morphology regulation (Efe *et al.*, 2007; Obara *et al.*, 2008; Rieter *et al.*, 2013). Under autophagic conditions, ATG18 forms a complex with ATG2 in an interdependent manner, which in turn localizes on the PAS via the interaction between ATG18 and PI3P (Obara *et al.*, 2008). ATG18 is one of the proteins involved in retrograde trafficking of ATG9 and assists in redistribution of ATG9 from PAS to the peripheral pools during autophagy (Reggiori *et al.*, 2004). ATG18 and ATG21 protect lipidated ATG8 from premature cleavage by ATG4 (Nair *et al.*, 2010). Recently, it has been found that ATG18-ATG2 complex is crucial for tethering PAS to ER and facilitates autophagosome formation (Kotani *et al.*, 2018). Further, ATG18 localizes on the vacuolar membrane via its interaction with PI(3,5)P_2 and mediates vacuole fission, thus regulating vacuole morphology (Efe *et al.*, 2007). Vacuole fission process occurs at a slow rate in nutrient-rich conditions but gets enhanced during hyperosmotic stress (Li and Kane, 2009). The localization of ATG18 changes dramatically upon changes in external nutrient and osmotic conditions. During nutrient-limitation, ATG18 localizes on PAS and exerts an essential role in autophagy, whereas in hyperosmotic conditions it is recruited on the vacuolar membrane and accelerates membrane fission process (Dove *et al.*, 2004; Efe *et al.*, 2007; Krick *et al.*, 2008; Obara *et al.*, 2008; Zieger and Mayer, 2012).

The *P. falciparum* genome encodes a homolog of ATG18. For autophagy, ATG18 forms a complex with ATG2 in yeast (Obara *et al.*, 2008). A putative homolog of ATG2 has been identified in the malaria parasite, although, it has low sequence identity with its yeast and human counterparts (Hain and Bosch, 2013; Navale *et al.*, 2014). The recruitment of ATG18 to the PAS and vacuolar membrane requires phospholipids PI3P and PI(3,5)P_2, respectively, in yeast. PI3P is found in *P. falciparum,* which is produced by *Pf*VPS34/ *Pf*PI3K, however, PI(3,5)P_2 is not synthesized by the malaria parasite (Tawk *et al.*, 2010).

A recent study reported that *Pf*ATG18 is essential for apicoplast biogenesis and targets *Pf*ATG8 to the apicoplast membrane (Bansal *et al.*, 2017). Its ortholog in *Toxoplasma gondii* also performs a similar function (Bansal *et al.*, 2017). In another study, it is reported that *Pf*ATG18 is one of the targets of artemisinin (Wang *et al.*, 2015). Additionally, it is

shown that a mutation in *Pf*ATG18 is associated with artemisinin resistance in *P. falciparum* clinical isolates (Wang *et al.*, 2016b). This mutation in *Pf*ATG18 provides a fitness advantage to the parasite during starvation (Breglio *et al.*, 2018). However, molecular details pertaining to the role of *Pf*ATG18 in autophagy and vacuole fission is largely unexplored in this parasite.

This study aims to understand the role of *Pf*ATG18 in food vacuole (FV) fission and the autophagy-like pathway in *P. falciparum*. The localization of endogenous and the fluorescently tagged *Pf*ATG18 (*Pf*ATG18-GFP) is followed in the parasite. *Pf*ATG18 is found to be localized on the parasite FV and cytoplasmic vesicular structures. Through site-directed mutagenesis approach, the interaction between *Pf*ATG18 and phospholipid PI3P is found to be critical for the precise subcellular localization of *Pf*ATG18. Further, functional complementation in *S. cerevisiae* has been carried out. The study demonstrates that *Pf*ATG18 is transported to the FV via the hemoglobin uptake pathway. We find that *Pf*ATG18 is present on hemoglobin containing vesicles (HcVs) and is carried along with them to the FV. The participation of *Pf*ATG18 in an autophagy-like pathway in the parasite is demonstrated by the increased expression of *Pf*ATG18 transcript and protein under autophagy inducing condition. *Pf*ATG18 is found on autophagosome-like structures colocalizing with autophagosome markers *Pf*ATG8 and *Pf*ATG5 during nutrient-rich as well as starved conditions. *Pf*ATG18 also colocalizes with *Pf*ATG8 in apicoplast-minus parasites as well, demonstrating that *Pf*ATG18 has additional functions that are independent of apicoplast biogenesis as described earlier (Bansal *et al.*, 2017). We find that *Pf*ATG18 localization on autophagosome is unaffected by the knockdown of *Pf*ATG8, suggesting that autophagosomes might have formed in the knockdown cells. Overall, this study demonstrates the role of *Pf*ATG18 in food vacuole fission and the autophagy-like pathway in *P. falciparum*.

This work is under revision in the journal *Molecular Microbiology*. The complete reference is as follows:

Agrawal, P., Manjithaya, R., & Surolia, N. *Plasmodium falciparum* autophagy-related protein *Pf*ATG18 participates in food vacuole fission dynamics and autophagy-like pathway. (Manuscript under revision).

3.3.1 Bioinformatics analysis of ATG18 homolog in *P. falciparum*

The characteristic feature of ATG18/WIPI is its seven WD40 repeats, which are stretches of nearly 40 amino acids that end with tryptophan (W) and aspartate (D) residues providing it a seven-bladed β-propeller structure. It contains phosphoinositides binding motif FRRG that facilitates the binding of ATG18/WIPI to phosphoinositides PI3P and PI(3,5)P_2 in yeast and mammals (Dove *et al.*, 2004; Proikas-Cezanne *et al.*, 2004). A homolog of ATG18 annotated as PF3D7_1012900 has been identified in *P. falciparum* genome database by the BLAST search using yeast and human ATG18/WIPI sequences (Hain and Bosch, 2013; Navale *et al.*, 2014). PlasmoDB database shows that *PfATG18* gene is located on chromosome 10. It contains two exons, its transcript length is 1143 bp and translates into 380 amino acids long protein. The predicted molecular weight of *Pf*ATG18 protein is 43.5 kDa, and since it contains many positively charged amino acids, its isoelectric point is 9.61. *Pf*ATG18 does not contain a signal peptide or possesses any transmembrane domain.

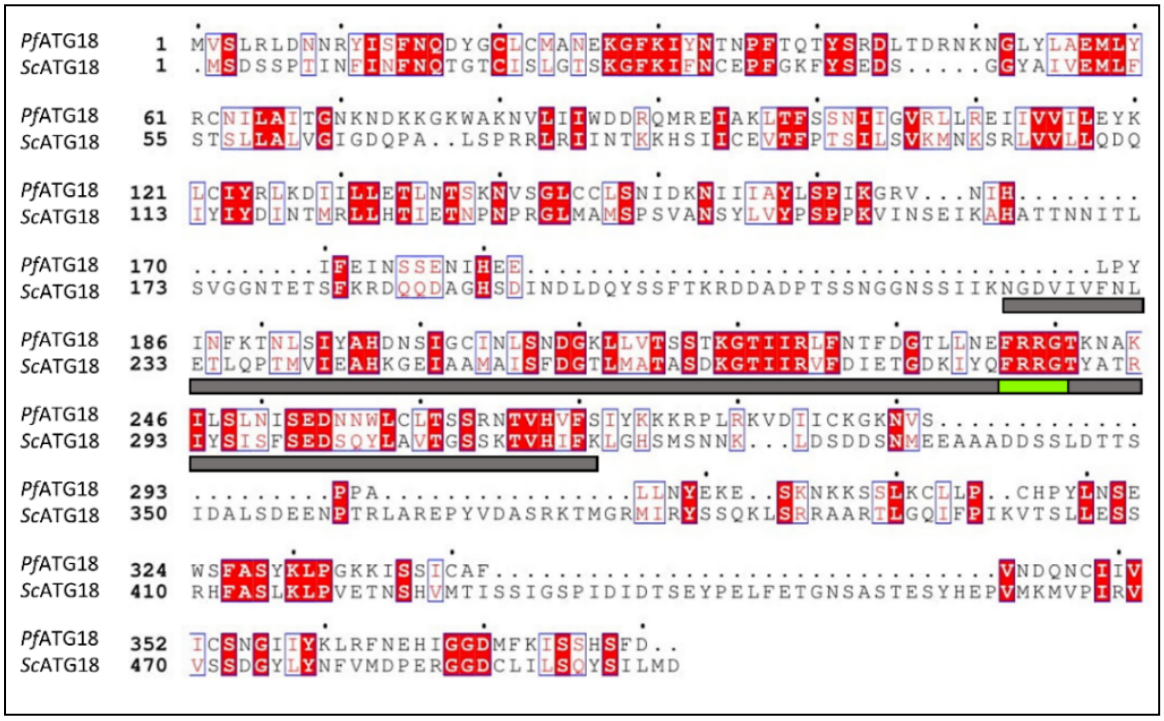

Figure 3.14: Sequence-based comparison of *Pf*ATG18 with *Sc*Atg18

The alignment was performed using the Clustal Omega program and is represented using ESPRIPT 3. The conserved residues are in the red box, WD40 repeat domains are indicated by grey bar. Both the proteins contain the FRRG motif (green bar) that is essential for binding of ATG18 to PI3P and PI(3,5)P_2.

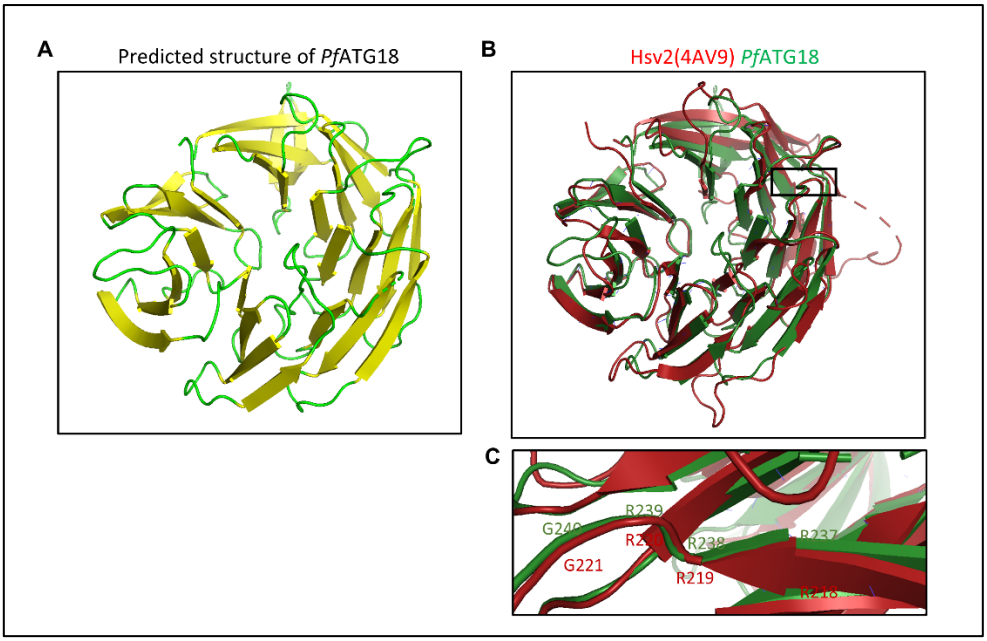

Figure 3.15: Structure-based comparison of *Pf*ATG18 with Hsv2

(A) Structure of *Pf*ATG18 was predicted by Phyre2.0, secondary structures sheet and loop are shown in yellow and green respectively. **(B)** Structural alignment of Hsv2 (ATG18 paralog in yeast, red) and *Pf*ATG18 (green) was achieved by PyMol. **(C)** Magnified view of the box shows ^{218}FRRG^{221} of Hsv2 and ^{237}FRRG^{240} of *Pf*ATG18.

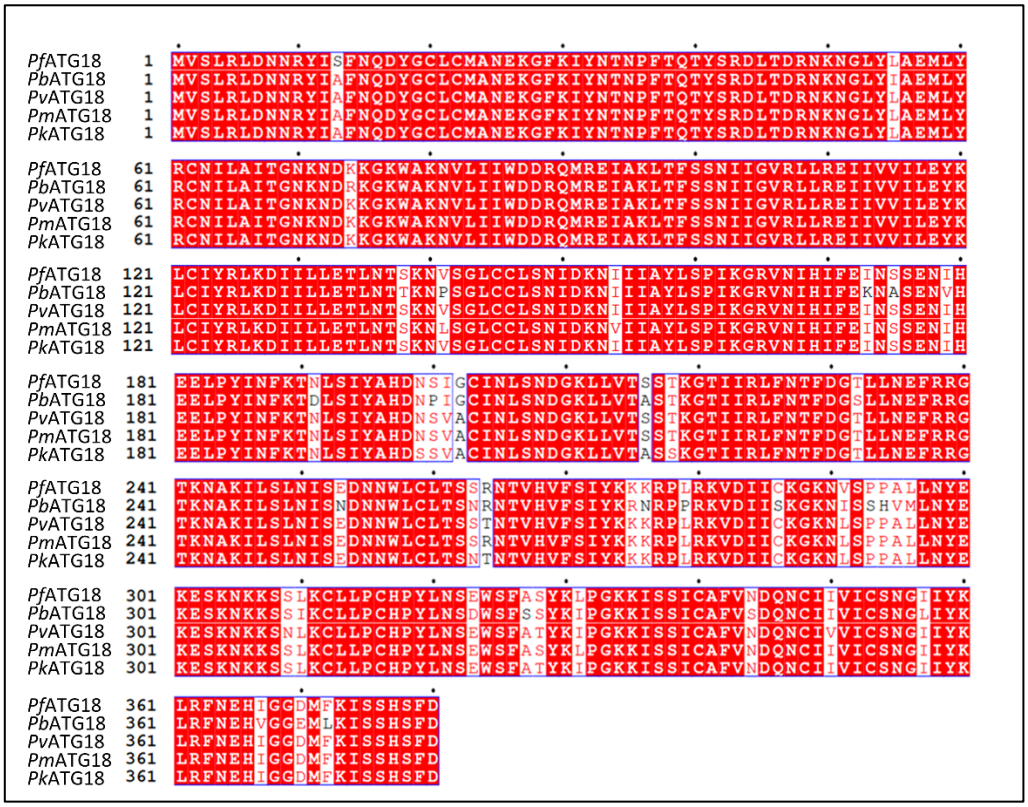

Figure 3.16: Sequence-based comparison of ATG18 homologs from *Plasmodium* species

Alignment of ATG18 homologs from *P. falciparum, P. berghei, P. vivax, P. malariae, P. knowlesii* species, performed using the Clustal Omega program and represented using ESPRIPT 3. The conserved residues are indicated in the red box.

The pairwise alignment shows that *Pf*ATG18 and *Sc*Atg18 share 28% protein sequence identity. The Clustal Omega-based multiple sequence alignment of *Pf*ATG18 with *Sc*Atg18 indicates that *Pf*ATG18 contains a WD40 repeat domain and a conserved FRRG motif (Figure 3.14). A model for *Pf*ATG18 structure was generated using Phyre2.0 (Figure 3.15A). By aligning the predicted *Pf*ATG18 structure with the crystal structure of Hsv2, a paralog of ATG18 in yeast revealed that all seven blades of the ATG18 β-propeller are conserved (Figure 3.15B). BLAST search identified ATG18 homologs in other *Plasmodium* species also. Multiple sequence alignment of ATG18 from different *Plasmodium* species exhibits that this protein is highly conserved in malaria parasites (Figure 3.16).

3.3.2 *Pf*ATG18 is expressed in all intraerythrocytic stages of *P. falciparum*

To investigate the role of *Pf*ATG18 in *P. falciparum* autophagy and FV fission, anti-*Pf*ATG18 antibodies were custom generated against the *Pf*ATG18 peptide, TGNKNDKKGKWAKN (67-81), by GenScript, USA. The specificity of antibodies was validated by probing them against uninfected RBC and mixed culture blood-stage *P. falciparum* lysates. Anti-*Pf*ATG18 antibodies detected a single band at the expected size (~40 kDa) corresponding to *Pf*ATG18 in the parasite lysate by western blot analysis, but did not react with the uninfected RBC lysate (Figure 3.17A), indicating that the antibodies are specific for *Pf*ATG18.

To determine the intracellular localization of *Pf*ATG18, immunofluorescence assay (IFA) of IE stages of *P. falciparum* was carried out. Parasites were fixed at ring (12 hpi), trophozoite (28 hpi) and schizont (40 hpi) stages. Using anti-*Pf*ATG18 antibodies, *Pf*ATG18 signals were observed during all asexual blood stages inside the parasite and appeared to localize near FV in trophozoites and schizonts (Figure 3.17B). Additional *Pf*ATG18-decorated vesicles were also observed near the parasite boundary (Figure 3.17B).

To corroborate our localization results, we generated transiently transfected cell line which expresses *Pf*ATG18-GFP. *Pf*ATG18 was tagged with GFP at its C-terminus, cloned into the *P. falciparum* transient expression vector pARL1-a (Crabb *et al.*, 2004) and transfected in *P. falciparum* 3D7 cells (Figure 3.18A). Expression of *Pf*ATG18-GFP in the transiently transfected parasites was verified by western blotting using anti- *Pf*ATG18 and anti-GFP

antibodies. A band corresponding to *Pf*ATG18-GFP was detected in the parasite lysate by both anti-*Pf*ATG18 and anti-GFP antibodies at the expected size (~70 kDa), further confirming the specificity of anti-*Pf*ATG18 antibodies (Figure 3.18B).

The localization of *Pf*ATG18-GFP was followed in the IE stages of recombinant parasites by live cell confocal microscopy. *Pf*ATG18-GFP displayed a similar localization pattern in transfected cell line as observed for endogenous *Pf*ATG18. *Pf*ATG18-GFP appeared to localize on the food vacuole-limiting membrane in trophozoite and schizont stages (Figure 3.18C). The only difference was that *Pf*ATG18-GFP completely enveloped FV while *Pf*ATG18 was present as punctate structures surrounding FV (Figure 3.18C). Furthermore, the signals with anti-*Pf*ATG18 and the anti-GFP antibodies showed significant colocalization in asexual stages of transfected parasites (Figure 3.18D), suggesting that both these antibodies recognize the same structures, further verifying that anti-*Pf*ATG18 antibodies are specific.

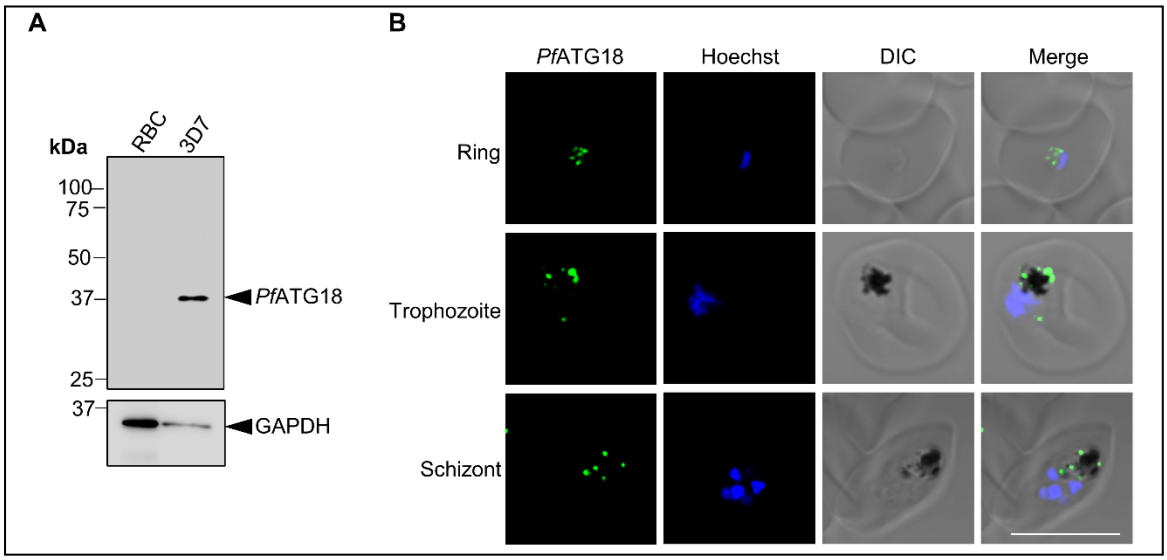

Figure 3.17: *Pf*ATG18 expression and localization in intraerythrocytic stages of *P. falciparum*

(A) Western blot analysis of RBC and *P. falciparum* 3D7 lysates showing the presence of *Pf*ATG18 in the parasite lysate at the expected molecular weight using anti-*Pf*ATG18 antibodies. GAPDH was used as loading control; n=3 experiments. **(B)** Localization of *Pf*ATG18 during the intraerythrocytic cycle was verified by IFA. Synchronized parasites were immunolabelled with anti-*Pf*ATG18 (1:400) antibodies. *Pf*ATG18 appears to surround FV in trophozoite and schizont stages. Additional *Pf*ATG18-decorated vesicles were observed near parasite boundary; N=25 parasites, n=3 experiments, Scale bar=5 µm.

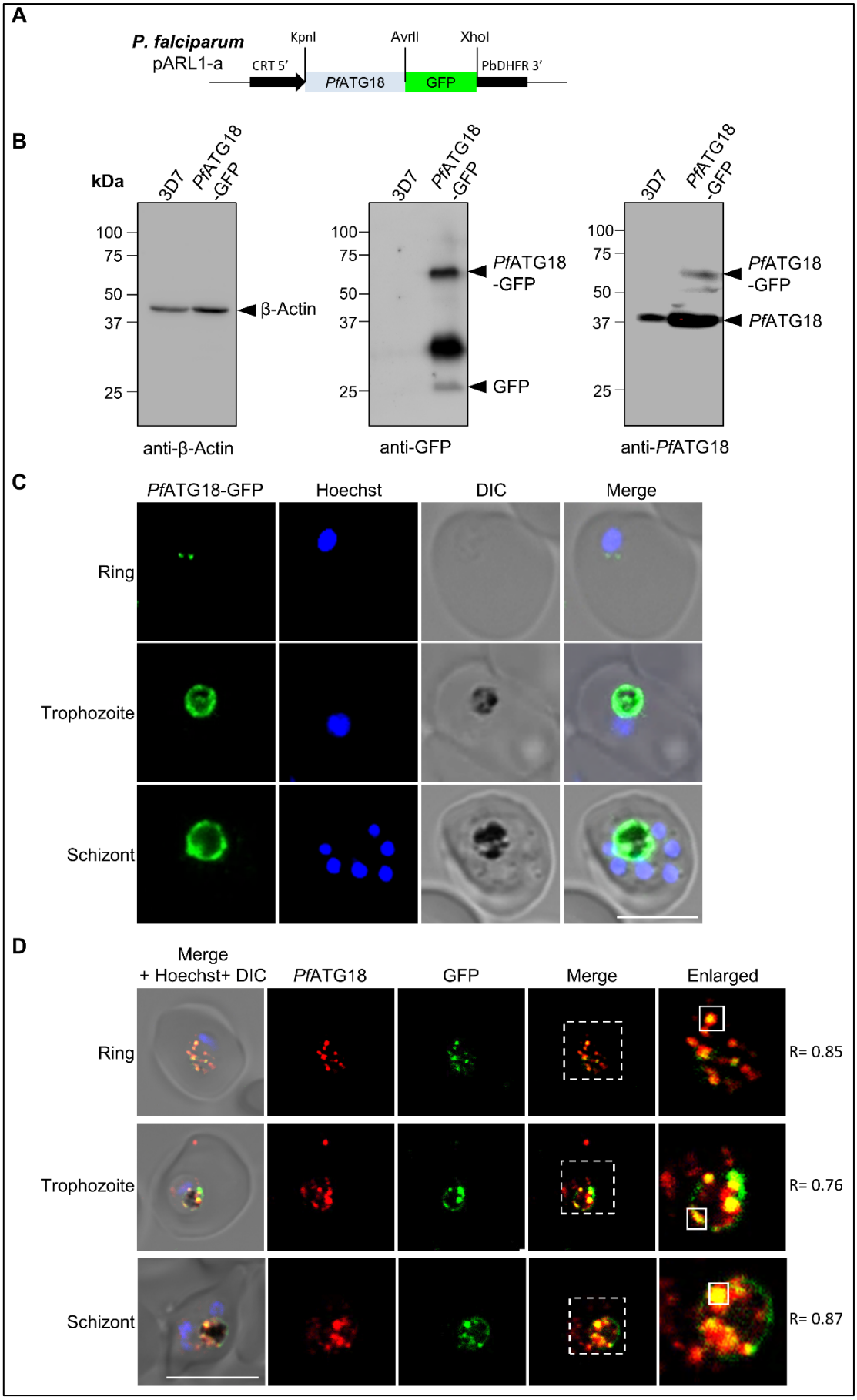

Figure 3.18: *Pf*ATG18-GFP expression and localization in intraerythrocytic stages of *P. falciparum*

(A) Schematic representation of recombinant vector constructs for episomal expression of *Pf*ATG18-GFP in *P. falciparum* using expression vector pARL1-a. The complete coding sequence of *Pf*ATG18 without stop codon was cloned in frame with GFP (green) using unique restriction sites as indicated. The fusion protein is expressed under constitutively active promoter CRT; n=3 experiments **(B)** Western blot analysis of parasite lysate overexpressing *Pf*ATG18-GFP. Endogenous *Pf*ATG18 was detected using anti-*Pf*ATG18 antibodies, whereas fusion protein was detected by both anti-*Pf*ATG18 and anti-GFP antibodies at the expected molecular weight. β-Actin was used as loading control; N=25 parasites, n=3 experiments, Scale bar=5 µm. **(C)** Live cell confocal microscopy of *Pf*ATG18-GFP parasites depicting localization of *Pf*ATG18-GFP on punctate structures in rings, on FV membrane in trophozoites and schizonts. C. Recombinant *P. falciparum* parasites were assessed for colocalization of *Pf*ATG18-GFP and *Pf*ATG18 using anti-GFP and anti-*Pf*ATG18 antibodies. Enlarged panel: magnified view of the dotted region shown in the merged image. The Pearson's coefficient (R) represents the degree of colocalization between *Pf*ATG18-GFP and *Pf*ATG18, evaluated from the signal within the square region shown in the enlarged image. *Pf*ATG18-GFP and *Pf*ATG18 signals overlapped in parasites. Nucleus was stained by Hoechst; N=25 parasites, n=3 experiments, Scale bar=5 µm.

3.3.3 *Pf*ATG18 localizes on food vacuole membrane in *P. falciparum*

IFA studies using anti-*Pf*ATG18 antibodies indicated that *Pf*ATG18 localizes on FV in parasites. To confirm the localization of *Pf*ATG18 on FV, colocalization studies using FV lumen protein falcipain-2 (FP-2); a cysteine protease involved in hemoglobin degradation, was performed (Dasaradhi *et al.*, 2007). *Pf*ATG18 signal was found adjacent to FV lumen marker FP2 (Figure 3.19A). To further validate these observations, FV of transfected parasites were labelled with FP-2 and LysoTracker Red DND99, a dye that stains the FV (Howe *et al.*, 2013). *Pf*ATG18-GFP signal was found to encircle FP-2 and LysoTracker Red DND99 signals (Figure 3.19B), indicating that *Pf*ATG18-GFP localizes on the food vacuole limiting membrane, thus, corroborating our previous observations.

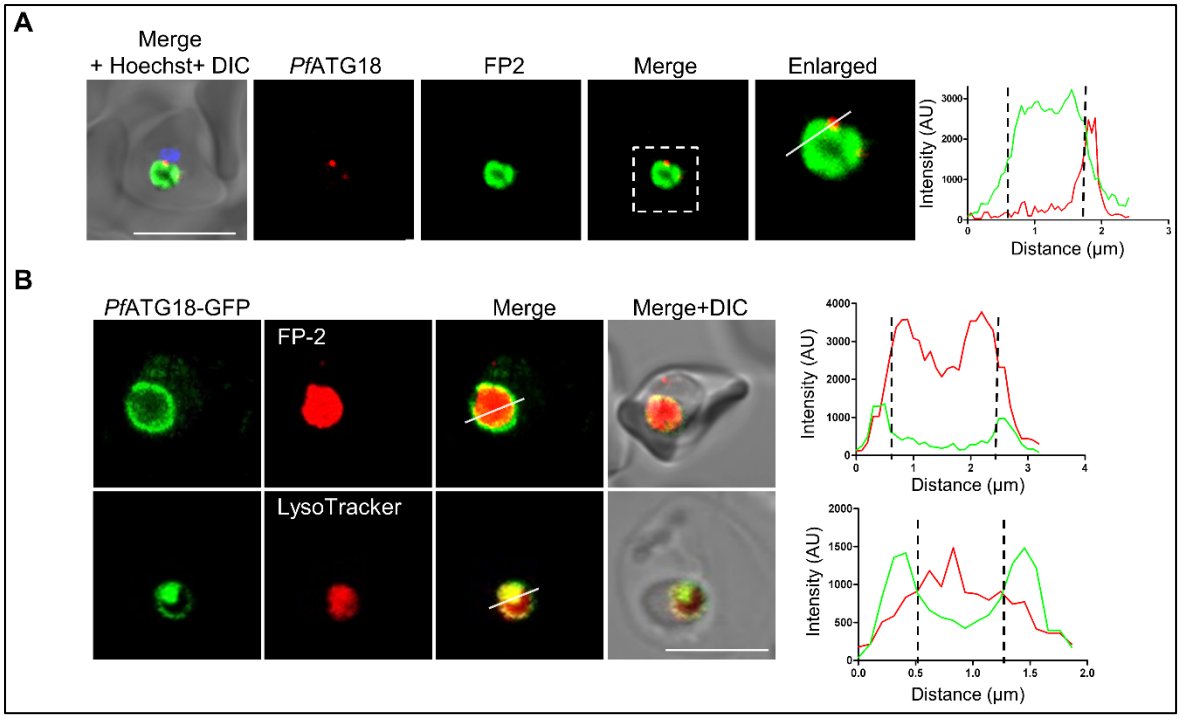

Figure 3.19: *Pf*ATG18 localizes on FV membrane in *P. falciparum*

(A) Immunofluorescence staining using anti-*Pf*ATG18 (1:400) and anti-falcipain-2 (1:200) antibodies imunolabelled using Zenon antibody labelling system detecting the localization of *Pf*ATG18 on FV membrane of *P. falciparum*. Nucleus was stained by Hoechst; N=25 parasites, n=3 experiments, Scale bar=5 µm. Enlarged panel: magnified view of the dotted region shown in the merged image. Line scan analysis of fluorescence intensities along the white line shown in the enlarged image. Red: *Pf*ATG18, Green: FP2. *Pf*ATG18 was found to be located adjacent to the FV lumen protein FP2. **(B)** Localization of fusion protein *Pf*ATG18-GFP on FV was assessed by analysing the colocalization between *Pf*ATG18-GFP with falcipain-2 (FP2) (top) using anti-GFP and anti-falcipain-2 antibodies, and by colocalization between *Pf*ATG18-GFP and LysoTracker Red DND99 (bottom) in transgenic parasite 3D7, observed by live cell confocal microscopy. N=25 parasites, n=3 experiments, Scale bar=5 µm. Line scan analysis of fluorescence intensities along the white lines shown in the merge panel. Red: FP2 or LysoTracker Red DND99, Green: *Pf*ATG18-GFP. The region within the dotted line in the line graph shows the lumen of the FV. *Pf*ATG18-GFP encircled FV lumen markers FP2 and LysoTracker Red DND99.

3.3.4 *Pf*ATG18 is not found on localizes on apicoplast and mitochondrion in *P. falciparum*

ATG18 in *T. gondii* and *P. falciparum* is reported to be involved in apicoplast biogenesis (Bansal *et al.*, 2017). Though the authors of the study did not find the localization of *Pf*ATG18 on apicoplast. We, therefore, analyzed the colocalization of *Pf*ATG18 and *Pf*ATG18-GFP with the apicoplast marker protein acyl carrier protein (ACP) in various IE stages of parasites using anti-*Pf*ATG18 or anti-GFP and anti-*Pf*ACP antibodies. Apicoplast

appeared as a small, discrete organelle in early stages of the parasite development and as a highly branched structure in the later stages of the parasite (Figure 3.20), consistent with the reports published in the literature (van Dooren *et al.*, 2005). *Pf*ATG18 (Figure 3.20A) and *Pf*ATG18-GFP (Figure 3.20B) did not exhibit colocalisation, however, some puncta are found close to the apicoplast (Figure 3.20A and B), consistent with the previous report (Bansal *et al.*, 2017).

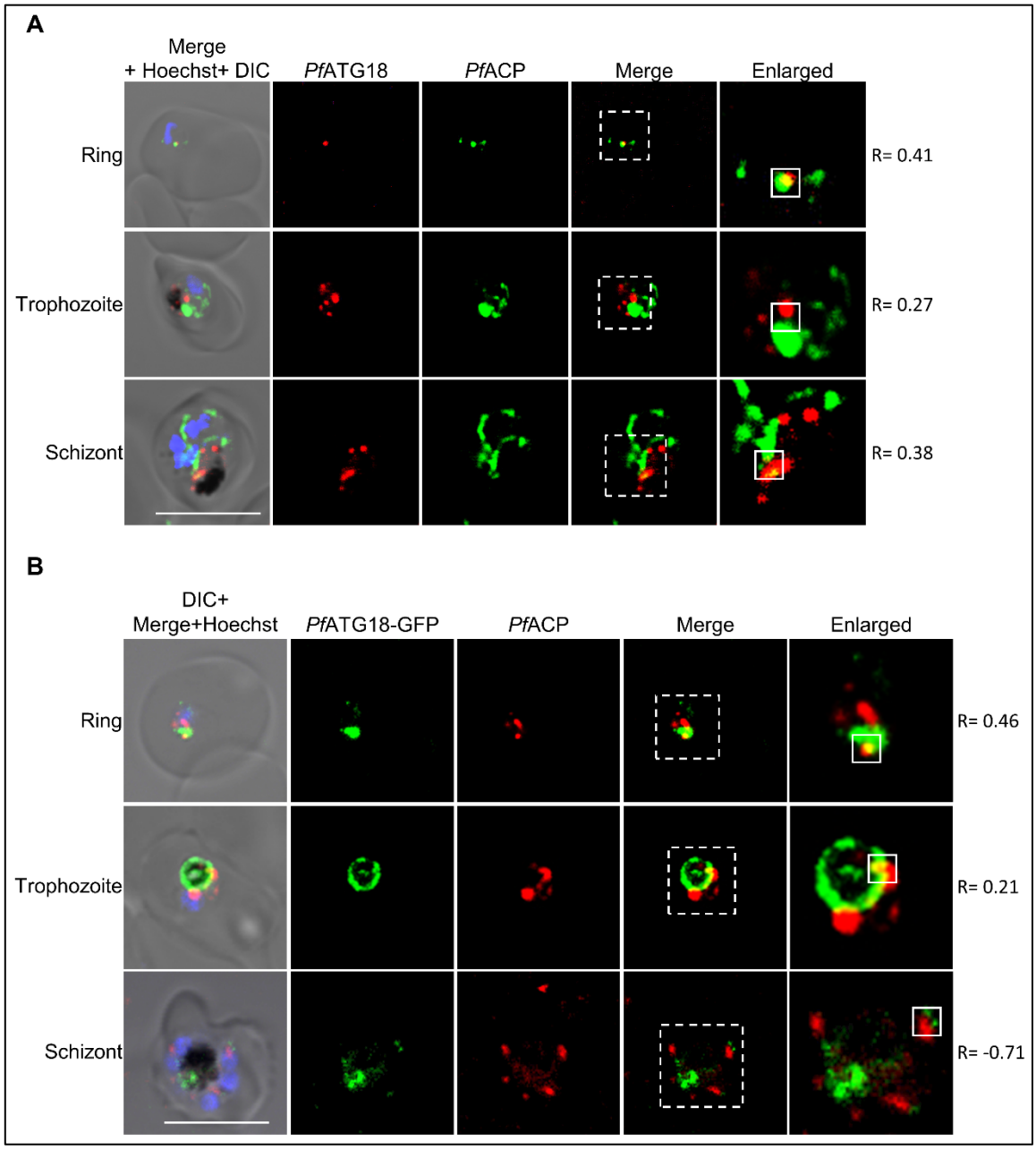

Figure 3.20: Localization of *Pf*ATG18 on apicoplast in *P. falciparum*

(A) Intraerythrocytic stages of parasites were evaluated for the localization of *Pf*ATG18 on apicoplast immunolabelled with anti-*Pf*ATG18 (1:400) and anti-*Pf*ACP (1:200) antibodies using the Zenon antibody labelling system; N=25 parasites, n=3 experiments, Scale bar=5 µm. **(B)** Recombinant *P. falciparum* parasites were assessed for localization of *Pf*ATG18-GFP on apicoplast using anti-GFP (1:200) and anti- *Pf*ACP

(1:200) by immunofluorescence staining. Enlarged panel: magnified view of the dotted region shown in the merged image. Nucleus was stained by Hoechst. N=25 parasites, n=3 experiments, Scale bar=5 µm. The Pearson's coefficient (R) represents the degree of colocalization between *Pf*ATG18 (A) or *Pf*ATG18-GFP (B) with *Pf*ACP in the square region shown in the enlarged image.

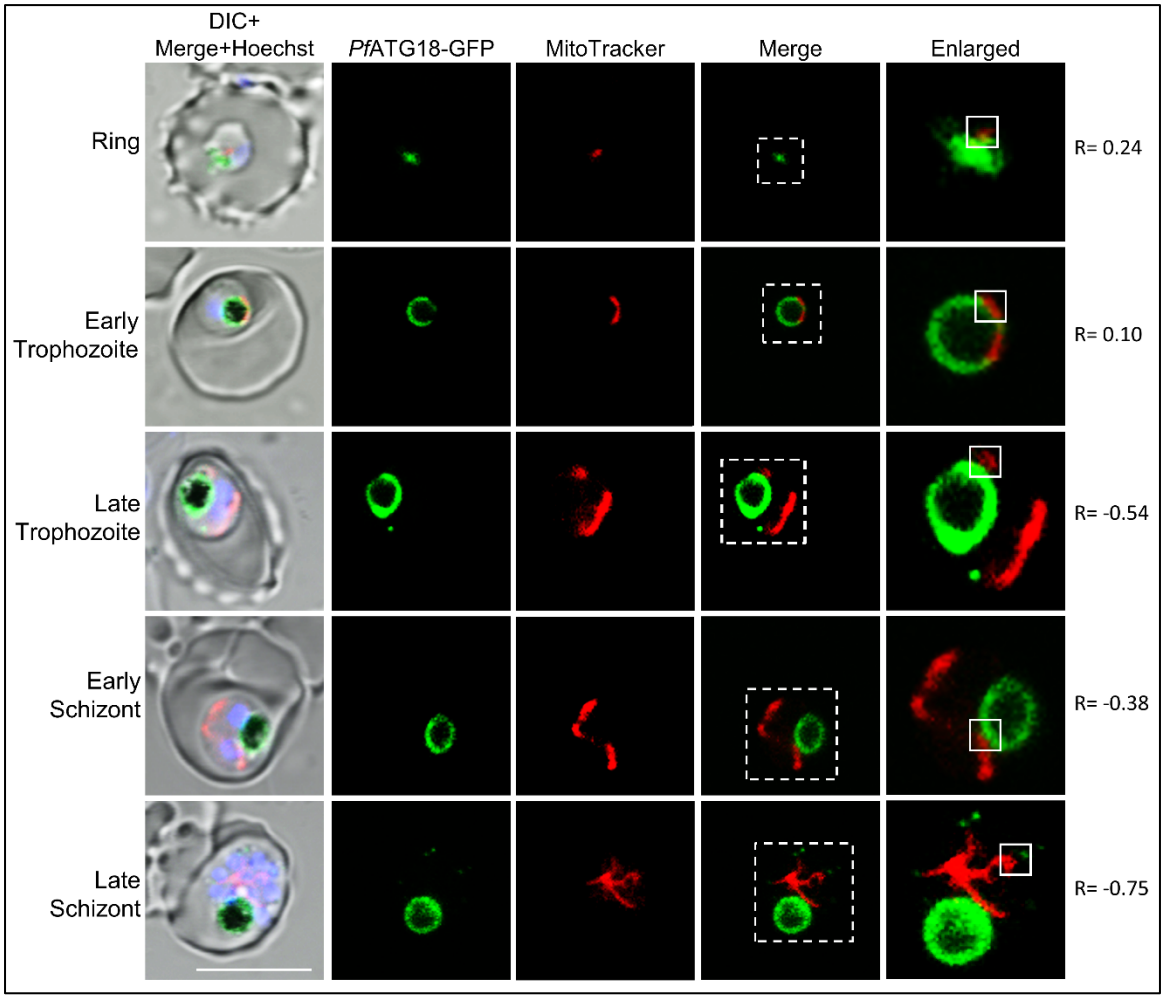

Figure 3.21: *Pf*ATG18-GFP does not localize on mitochondrion in IE stages of *P. falciparum*

Transgenic parasites expressing *Pf*ATG18-GFP were synchronized and labelled with MitoTracker Red CMXRos. Images of rings, early trophozoites, late trophozoites, early schizonts and late schizonts were acquired by live cell confocal microscopy. Enlarged panel: magnified view of the dotted region shown in the merged image. The Pearson's coefficient (R) represents the degree of colocalization between *Pf*ATG18-GFP with MitoTracker Red in the square region shown in the enlarged image. *Pf*ATG18-GFP did not localize with the mitochondrion. Nucleus was stained by Hoechst; N=25 parasites, n=3 experiments, Scale bar=5 µm.

In *P. falciparum*, mitochondrion and apicoplast have close association during IE cycle (Hopkins *et al.*, 1999). We, therefore, investigated the localization of *Pf*ATG18-GFP on the mitochondrion by live cell confocal microscopy in IE stages of transgenic parasites. Parasites were incubated with MitoTracker Red CMXRos, which specifically stains

mitochondria (Jogdand *et al.*, 2012). In agreement with the earlier report (van Dooren *et al.*, 2005), mitochondrion was observed as a single, small organelle in the early stages of the parasite development and highly branched structure in late stages of the parasite (Figure 3.21). No colocalization of *Pf*ATG18-GFP and mitochondrion was observed in asexual stages of the parasite (Figure 3.21), suggesting that *Pf*ATG18-GFP does not localize at the parasite mitochondrion during asexual blood stages.

3.3.5 Overexpression of *Pf*ATG18-GFP in *S. cerevisiae*

To understand the role of *Pf*ATG18 in autophagy and vacuolar homeostasis, we analysed the ability of *Pf*ATG18 to complement these functions in *S. cerevisiae*. Therefore, *S. cerevisiae atg18*Δ strain transiently expressing *Pf*ATG18-GFP was generated. GFP was tagged at the C-terminus of the codon-optimized *Pf*ATG18 (sequence in Appendix 2), cloned into the yeast expression vector p415-ADH (Figure 3.22A) and transformed in yeast *atg18*Δ cells. The expression of *Pf*ATG18-GFP was confirmed by western blot analysis using anti-GFP antibodies. A band of the expected size (~70 kDa) corresponding to *Pf*ATG18-GFP fusion protein was observed in yeast lysate (Figure 3.22B).

The expression of *Pf*ATG18-GFP in yeast was also confirmed by live cell confocal microscopy. The signal was observed on the yeast vacuolar membrane, which was labelled with the lipophilic dye FM4-64 (Figure 3.22C). The localization pattern of *Pf*ATG18-GFP was consistent with that of its yeast counterpart, which also localized on the vacuolar membrane in nutrient-rich conditions (Figure 3.22C) (Efe *et al.*, 2007; Tamura *et al.*, 2013). Such localization of *Pf*ATG18 is unlikely to be due to the GFP tag, as the localization of GFP alone was completely cytosolic (Figure 3.22C). These localization studies thus indicate that *Pf*ATG18, like *Sc*Atg18, localizes on the vacuolar membrane under nutrient-rich conditions.

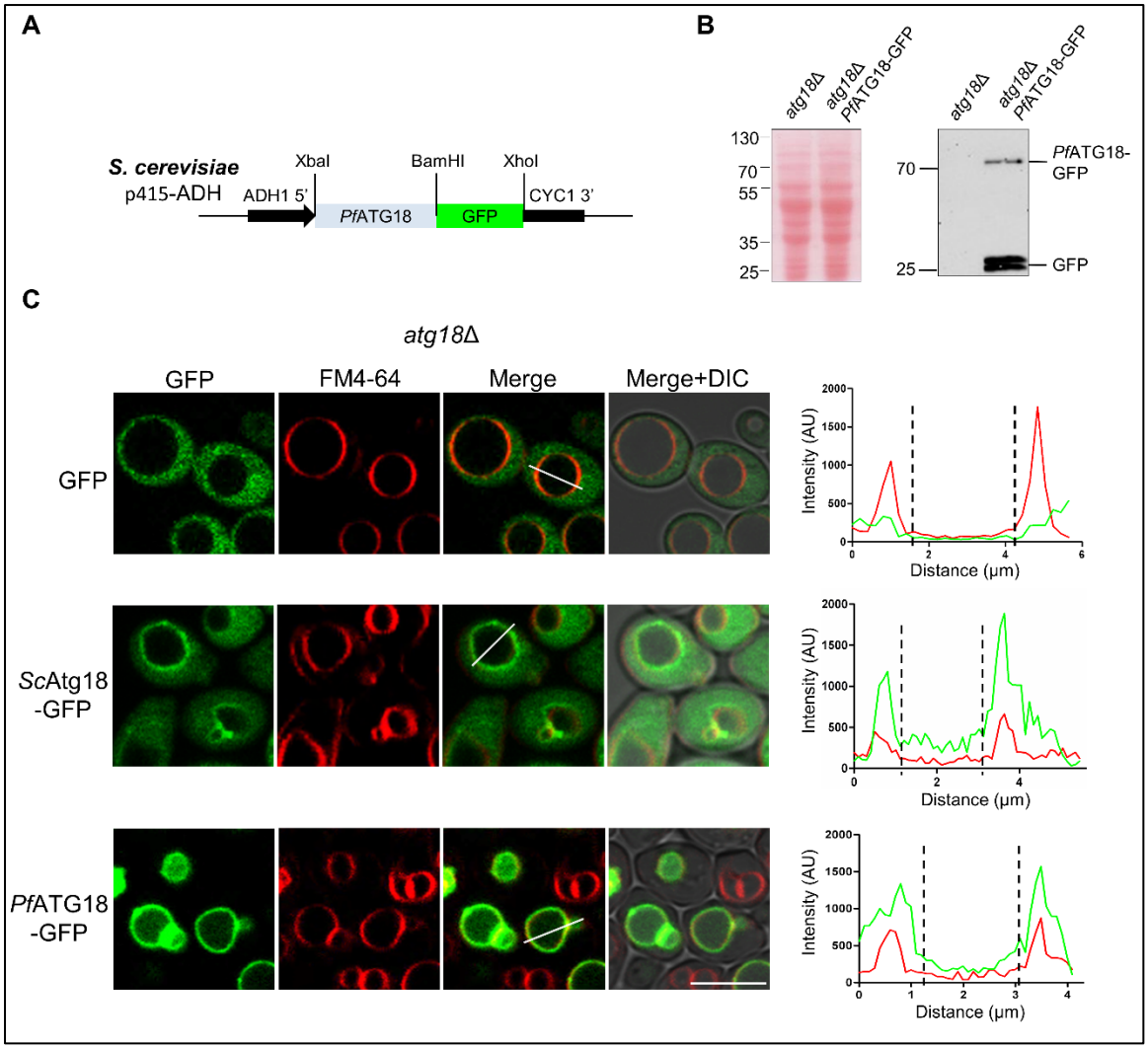

Figure 3.22: Overexpression of *Pf*ATG18-GFP in *S. cerevisiae*

(A) Schematic representation of recombinant vector constructs for episomal expression of *Pf*ATG18-GFP in *S. cerevisiae* using expression vector p415-ADH. The codon-optimized complete coding sequence of *Pf*ATG18 without stop codon was cloned in frame with GFP (green) using unique restriction sites as indicated. **(B)** Western blot for yeast lysate overexpressing *Pf*ATG18-GFP using anti-GFP antibodies detected *Pf*ATG18-GFP and GFP bands. Ponceau-stained transferred blot shows that the same amount of proteins from each fraction was resolved by SDS-PAGE; n=3 experiments. **(C)** The localization of GFP, *Sc*Atg18-GFP and *Pf*ATG18-GFP in *atg18*Δ yeast strain was observed by live cell confocal microscopy. Vacuoles in yeast were labelled with lipophilic dye FM4-64; N=100 cells, n=3 experiments, Scale bar=5 μm. Line scan analysis of fluorescence intensities along the white line (shown in the merge panel). Red: FM4-64. Green: GFP or *Sc*Atg18-GFP or *Pf*ATG18-GFP. The region within the dotted line in the line graph shows the lumen of the vacuole.

3.3.6 PI3P mediates subcellular localization of *Pf*ATG18

ATG18 in yeast binds with phospholipids PI(3,5)P_2 and PI3P via a conserved FRRG motif present within its β-propeller (Dove *et al.*, 2004; Krick *et al.*, 2006). This interaction

facilitates the localization of ATG18 on vacuolar and autophagosomal membranes, which in turn aids in its molecular functions such as vacuole fission and autophagy, respectively (Dove *et al.*, 2004; Obara *et al.*, 2008; Zieger and Mayer, 2012).

In *P. falciparum* genome, a homolog of Fab1, a kinase responsible for the generation of $PI(3,5)P_2$, is not found and thereby the parasite lacks this phospholipid (Tawk *et al.*, 2010). However, a homolog of phosphatidylinositol-3-kinase (*Pf*PI3K) is present in the parasite, and its product PI3P is found to be located on the FV, apicoplast membranes and single membrane vesicles (Tawk *et al.*, 2010). To verify the binding of *Pf*ATG18 with PI3P in the parasite, the production of PI3P was inhibited by known *Pf*PI3K inhibitors such as wortmannin (WRT) (Vaid *et al.*, 2010) and artemisinin (ART) (Mbengue *et al.*, 2015). The localization of *Pf*ATG18 and phospholipid PI3P in treated parasites were assessed by IFA using anti-*Pf*ATG18 and anti-PI3P antibodies. In control parasites, *Pf*ATG18 was observed as punctate structures near FV and colocalized with phospholipid PI3P (Figure 3.23A). Whereas in the parasites treated with WRT or ART, PI3P signal was mostly cytosolic; likewise, *Pf*ATG18 was no longer membrane-bound and was present in the parasite cytosol (Figure 3.23A). We also looked at the protein levels of *Pf*ATG18 in the parasites treated with WRT and ART by western blot analysis. The inhibition of PI3P generation by WRT and ART resulted in an increase in *Pf*ATG18 protein levels to 2.6 and 1.6 folds, respectively (Figure 3.23B). The increase in *Pf*ATG18 levels could be because of its reduced degradation as the protein is no longer delivered to the lytic organelle, FV. The binding of *Pf*ATG18 with membrane was further validated by studying the localization of *Pf*ATG18-GFP in transgenic parasites upon treatment with *Pf*PI3K inhibitors, WRT and ART. Live cell confocal microscopy showed that upon these treatments, *Pf*ATG18-GFP was mainly in the parasite cytosol (Figure 3.23C). Percentage of parasites with *Pf*ATG18-GFP signal on FV was quantified (Figure 3.23D) which showed that the association of *Pf*ATG18-GFP with the FV membrane in the treated parasites reduced by about 80%. Overall, these results indicate that the FV localization of *Pf*ATG18 is dependent upon its interaction with PI3P in the parasite, which is in line with previous reports (Bansal *et al.*, 2017; Breglio *et al.*, 2018).

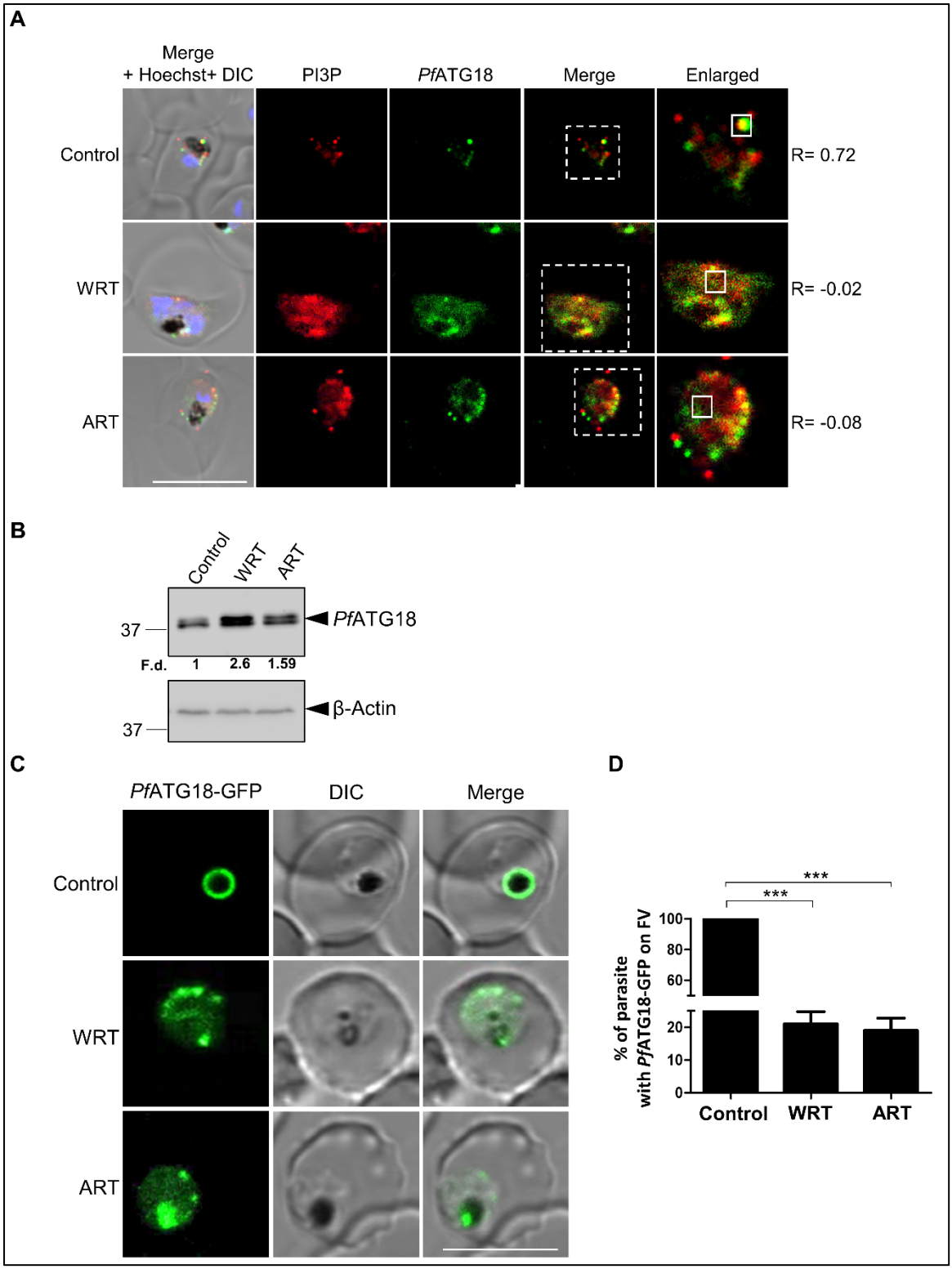

Figure 3.23: *Pf*ATG18 localizes on the FV membrane in PI3P-dependent manner in *P. falciparum*

(A) Immunofluorescence staining of *Pf*ATG18 and phospholipid PI3P using anti-*Pf*ATG18 and anti-PI3P antibodies upon treatment of parasites with *Pf*PI3K inhibitors: 5 µM wortmannin (WRT) and 75 nM artemisinin (ART) for 4 h. *Pf*ATG18 signal was mostly cytosolic upon treatment with these inhibitors. Enlarged panel: magnified view of the dotted region shown in the merged image. The Pearson's coefficient (R) represents the degree of colocalization between *Pf*ATG18 and PI3P evaluated from the signal within the square region shown in the enlarged image. Nucleus was stained by Hoechst; N=25 parasites, n=3

experiments, Scale bar=5 µm. **(B)** Western blot analysis using anti- *Pf*ATG18 antibodies showing the protein levels of *Pf*ATG18 in parasites treated with WRT and ART. β-Actin was used as a loading control. Fold difference (F.d.) as compared to normalized control is indicated below the immunoblot, n=3 experiments. **(C)** Live cell confocal microscopy of *Pf*ATG18-GFP expressing transgenic parasites treated with WRT and ART showing diffused *Pf*ATG18-GFP localization upon treatment; N=25 parasites, n=3 experiments, Scale bar=5 µm. **(D)** Graph represents the percentage of parasites showing *Pf*ATG18-GFP signal at the FV membrane. Values are mean ±SEM, *** indicates P<0.0005, analyzed by unpaired Student's *t* test.

We further wanted to understand if *Pf*ATG18 has the ability to interact with PI(3,5)P_2. In *S. cerevisiae,* PI(3,5)P_2 is synthesized from PI3P by Fab1 kinase (Cooke, 1998). In the absence of PI(3,5)P_2, *Sc*Atg18 is cytosolic (Dove *et al.*, 2004). Therefore, *Pf*ATG18-GFP was expressed in a yeast strain lacking PI(3,5)P_2 (*fab1*Δ). The fusion protein could localize to the vacuolar membrane even in the absence of PI(3,5)P_2 in *fab1*Δ cells (Figure 3.24). *Sc*Atg18 also requires PI3P for its membrane localization (Krick *et al.*, 2008). When *Pf*ATG18-GFP was expressed in the yeast strain lacking PI3P (*vps34*Δ), its signal was completely cytosolic in the yeast strain lacking PI3P (*vps34*Δ) (Figure 3.24), indicating that *Pf*ATG18-GFP interacts with PI3P but not PI(3,5)P_2 for membrane localization.

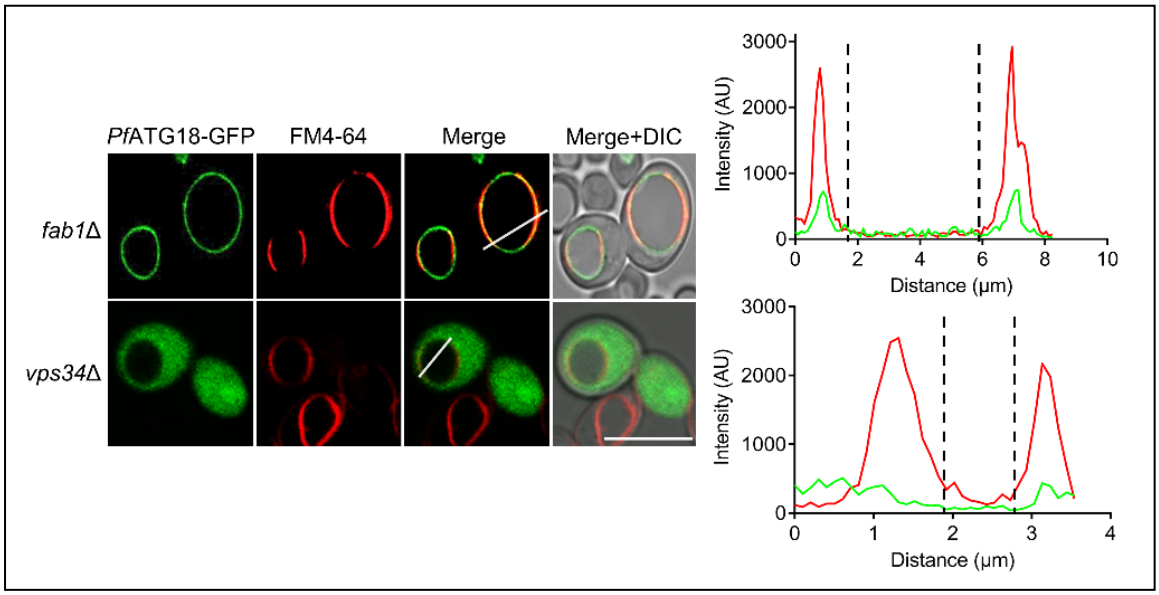

Figure 3.24: *Pf*ATG18-GFP binds with PI3P but not with PI(3,5)P_2 in *S. cerevisiae*

Confocal microscopy of *Pf*ATG18-GFP expressed in yeast *fab1*Δ (top) and *vps34*Δ (bottom) cells. Vacuoles were labelled with FM4-64. Line scan analysis of fluorescence intensities along the white line shown in the merge panel. Red: FM4-64. Green: *Pf*ATG18-GFP. The region within the dotted lines in the line graph indicates lumen of the vacuole; N=25 cells, n=3 experiments, Scale bar=5 µm.

Furthermore, the interaction between ATG18 and the phospholipid PI3P is governed by the conserved FRRG motif (Dove *et al.*, 2004). To determine if the ^{237}FRRG^{240} motif in *Pf*ATG18 is critical for its subcellular localization, the ^{237}FRRG^{240} motif was mutated to ^{237}FTTG^{240} and expressed in *atg18*Δ yeast cells and *P. falciparum* 3D7. The localization of mutant protein *Pf*ATG18^{FTTG}-GFP was studied in *atg18*Δ yeast strain and parasites by live cell confocal microscopy. *Pf*ATG18^{FTTG}-GFP signal was cytosolic in both the systems (Figure 3.25), while *Pf*ATG18-GFP was vacuolar membrane bound (Figure 3.25). This result confirms that the FRRG motif in *Pf*ATG18 is indispensable for its subcellular localization, consistent with the previous report (Bansal *et al.*, 2017).

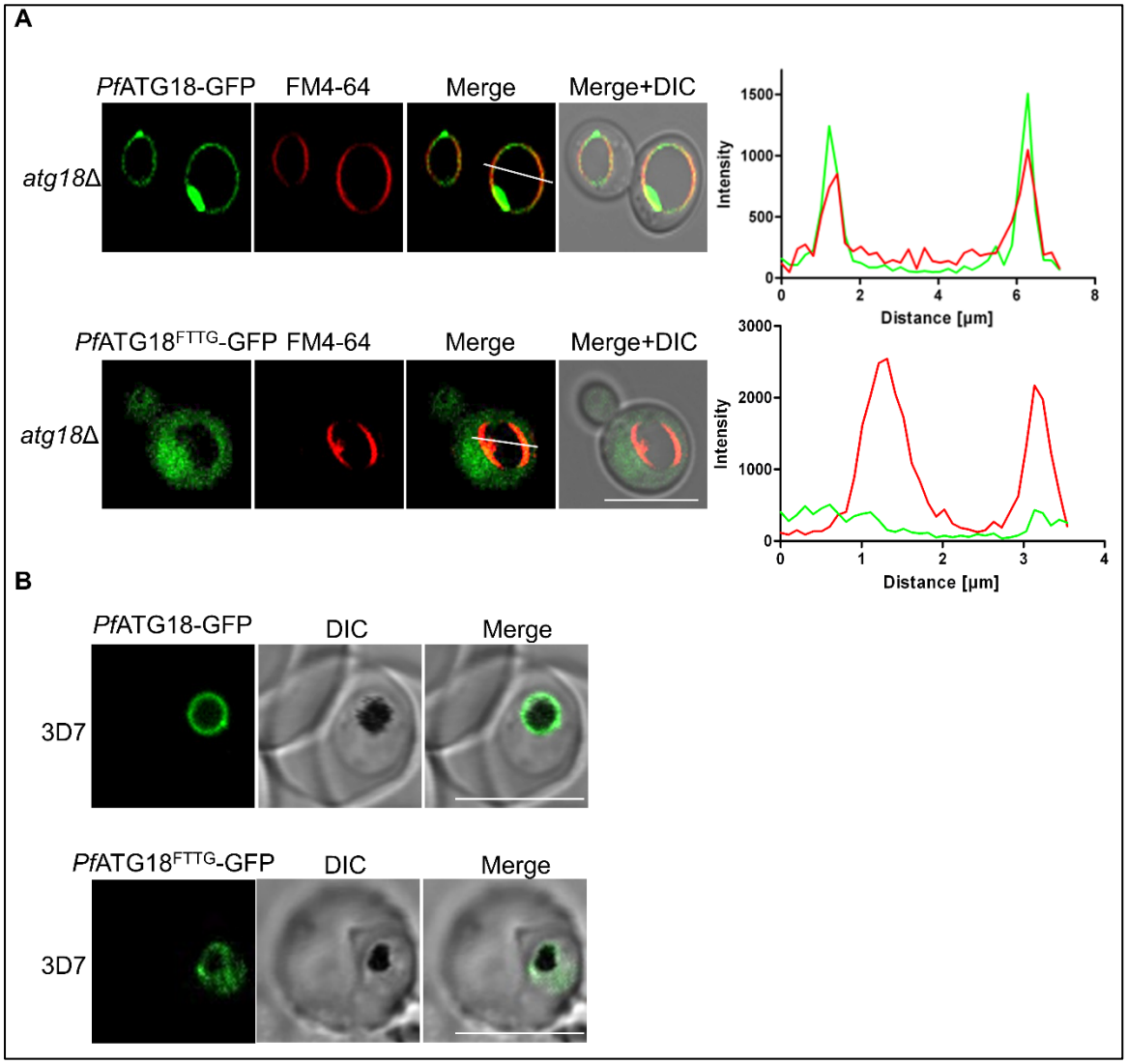

Figure 3.25: *Pf*ATG18-GFP associates with the vacuolar membrane via FRRG motif

(A) Localization of *Pf*ATG18-GFP (top) and *Pf*ATG18^{FTTG}-GFP (bottom) expressed in yeast *atg18*Δ cells was monitored by live cell confocal microscopy. Vacuoles in yeast were labelled with FM4-64. Line scan analysis of fluorescence intensities along the white line shown in the merge panel. Red: FM4-64. Green: *Pf*ATG18-GFP or *Pf*ATG18^{FTTG}-GFP; N=100 cells, n=3 experiments, Scale bar=5 µm. **(B)** Localization of

*Pf*ATG18-GFP (top) and *Pf*ATG18^{FTTG}-GFP (bottom) expressed in *P. falciparum* was monitored by live cell confocal microscopy; N=100 cells, n=3 experiments, Scale bar=5 μm.

3.3.7 *Pf*ATG18-GFP rescues the vacuolar fission defect in *atg18*Δ yeast cells

ATG18 plays a crucial role in maintaining vacuolar morphology in yeast (Efe *et al.*, 2007; Tamura *et al.*, 2013). Compared to wild-type (WT) yeast cells that have 1-5 small vacuoles, *atg18*Δ yeast cells possess a single large vacuole (Dove *et al.*, 2004). ATG18 maintains the morphology of the vacuole by mediating its fission (Efe *et al.*, 2007; Zieger and Mayer, 2012). To determine whether *Pf*ATG18 has a conserved role in vacuole fission, *Pf*ATG18 was tagged with GFP and expressed in *atg18*Δ yeast cells. We examined the morphology of vacuoles in *atg18*Δ yeast cells expressing *Pf*ATG18-GFP by live cell confocal microscopy. Vacuoles of yeast were labelled with lipophilic dye FM4-64. In accordance with the literature (Dove *et al.*, 2004; Efe *et al.*, 2007), multilobed vacuoles were detected in WT cells and *atg18*Δ yeast cells expressing *Sc*Atg18-GFP, while *atg18*Δ yeast cells possessed a single large vacuole (Figure 3.26A). Interestingly, *atg18*Δ yeast cells expressing *Pf*ATG18-GFP displayed multilobed vacuole phenotype (Figure 3.26A). The number of cells with multilobed vacuoles was quantified in each strain, which showed that the percentage of cells exhibiting multilobed vacuoles increased significantly in *atg18*Δ yeast cells expressing *Pf*ATG18-GFP as compared to *atg18*Δ cells (Figure 3.26B). This result thus indicates that *Pf*ATG18-GFP can rescue the vacuolar morphology defect in ATG18 deficient yeast cells.

Additionally, *atg18*Δ yeast cells expressing *Pf*ATG18^{FTTG}-GFP, a phosphoinositide binding mutant of *Pf*ATG18, displayed enlarged vacuole phenotype similar to *atg18*Δ yeast cells (Figure 3.26). As *Pf*ATG18^{FTTG}-GFP could not rescue vacuolar morphology defects in *atg18*Δ yeast cells, it indicates that binding of *Pf*ATG18-GFP with PI3P is essential for restoring vacuolar defects. This result also suggests that the complementation of vacuolar morphology by *Pf*ATG18-GFP is specific and is unlikely to be due to the overexpression of the protein.

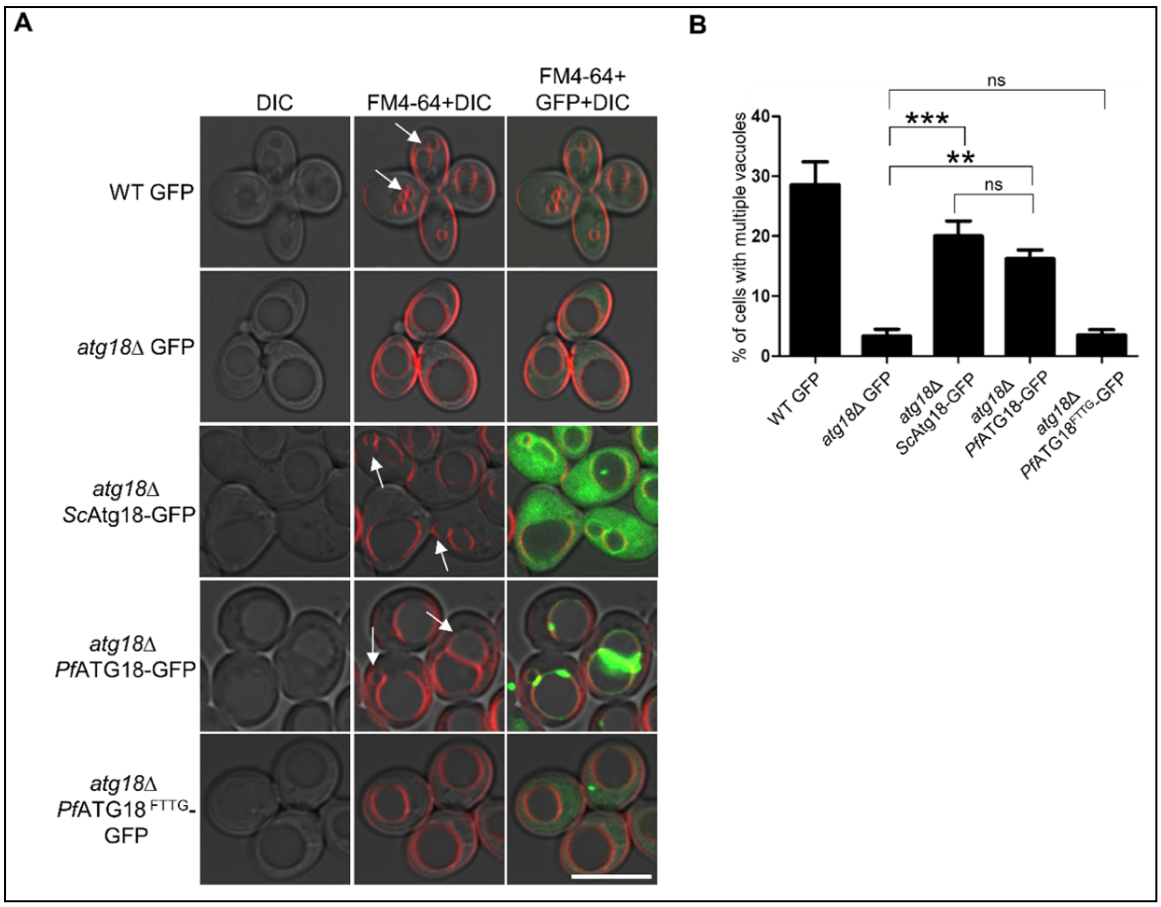

Figure 3.26: *Pf*ATG18-GFP rescues vacuolar morphology defects in *atg18*Δ yeast strain

(A) Live cell microscopy of WT GFP and *atg18*Δ yeast cells expressing GFP, *Sc*Atg18-GFP, *Pf*ATG18-GFP, or *Pf*ATG18^{FTTG}-GFP. Vacuoles are labelled by FM4-64. Arrows represent fragmented vacuoles; N=100 cells, n=3 experiments, Scale bar=5 µm. **(B)** Graph represents the percentage of yeast cells with multilobed vacuoles in the indicated strains; N=100 cells, n=3 experiments. All data are expressed as mean ± SEM. *** indicates P<0.0005, ** indicates P<0.005, values greater than P>0.05 were non-significant (ns), analyzed by unpaired Student's *t* test.

To know whether multilobed vacuoles in *atg18*Δ yeast cells expressing *Pf*ATG18-GFP were generated due to vacuole fission and to ascertain the involvement of *Pf*ATG18-GFP in this process, vacuolar dynamics and the localization of *Pf*ATG18-GFP was followed in *atg18*Δ yeast strain in the rich medium by time-resolved fluorescence microscopy. As expected, the vacuole of *atg18*Δ cells did not undergo fission during the recorded 30 min period, and only a single large vacuole was observed (Figure 3.27A). Whereas, the expression of *Sc*Atg18-GFP in *atg18*Δ yeast cells restored vacuole fission. The dynamics of a cell with single-lobed vacuole was followed at the start point of the experiment. Vacuoles were fragmented to form multilobed vacuole at a later time point (Figure 3.27B). *Sc*Atg18-GFP signal was enriched at the contact sites of multilobed vacuoles (Figure

3.27B). Later, the fragmented vacuoles fused together (Figure 3.27B). The vacuolar dynamics observed in *atg18*Δ yeast cells expressing *Sc*Atg18-GFP was in line with earlier reports (Efe *et al.*, 2007; Gopaldass *et al.*, 2017). Interestingly, vacuole fission was observed in the *atg18*Δ yeast cells expressing *Pf*ATG18-GFP as well, resulting in the formation of multilobed vacuoles (Figure 3.27C). Single-lobed vacuole containing cells were monitored by time-lapse confocal microscopy. The vacuole fission was seen as time progressed, indicating that multilobed vacuoles are formed due to fission upon expression of *Pf*ATG18. Furthermore, during the time-lapse microscopy, *Pf*ATG18-GFP signal enriched at the contact site of multiple vacuoles (Figure 3.27C), similar to *Sc*Atg18-GFP. This result suggests that *Pf*ATG18-GFP complements vacuole fission in *S. cerevisiae*.

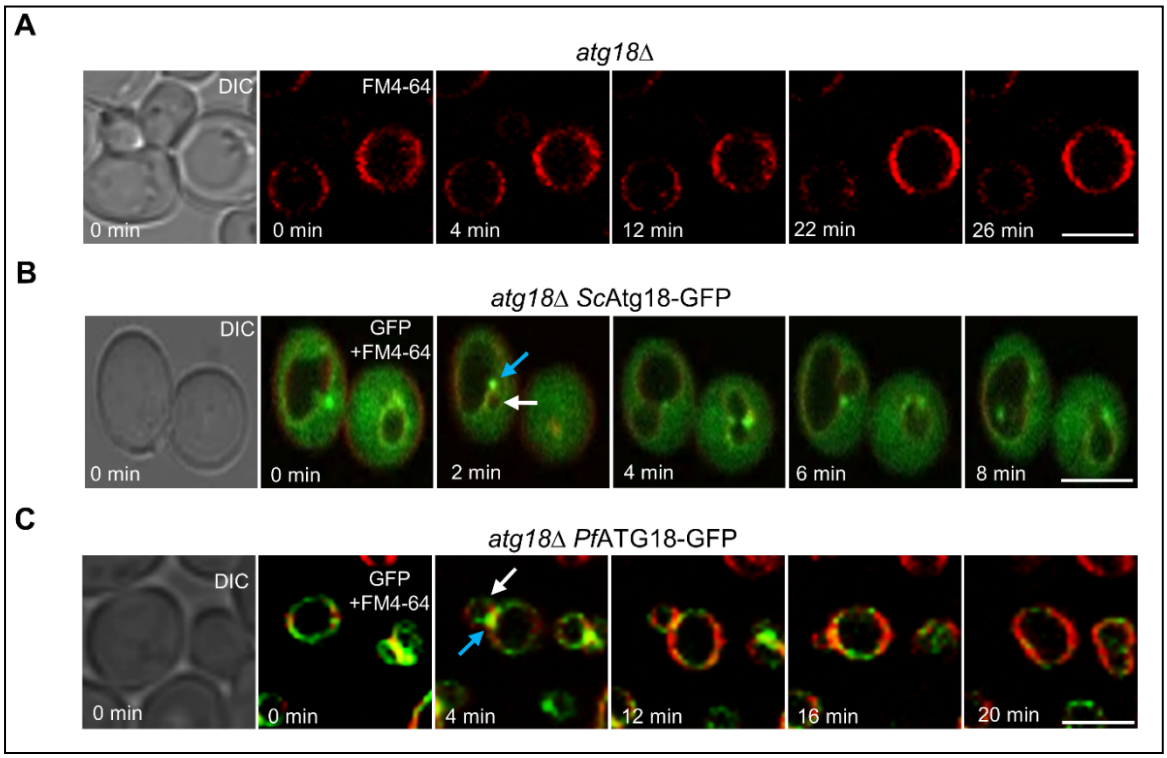

Figure 3.27: *Pf*ATG18-GFP mediates vacuole fission in *S. cerevisiae*

Time-lapse confocal microscopy of **(A)** *atg18*Δ yeast cells, **(B)** *atg18*Δ yeast cells expressing *Sc*Atg18-GFP, and **(C)** *atg18*Δ yeast cells expressing *Pf*ATG18-GFP. Vacuoles were labelled with FM4-64. Images were acquired every 2 min. Representative images at indicated time points are shown. Vacuole fission was observed in *atg18*Δ yeast cells expressing *Sc*Atg18-GFP or *Pf*ATG18-GFP. White arrows indicate fragmented vacuoles. Blue arrows indicate enrichment of *Sc*Atg18-GFP and *Pf*ATG18-GFP on the interface of multilobed vacuoles; N=10 cells, n=3 experiments, Scale bar=5 µm.

3.3.8 *Pf*ATG18 mediates the food vacuole fission in *P. falciparum*

The food vacuole (FV) of *P. falciparum* is similar to the vacuole of *S. cerevisiae*. It is an acidic organelle where cytoplasmic contents are degraded. FV is also the main site for the degradation of hemoglobin. Vacuoles are present in multiple copies in yeast and are dynamic in nature, undergo cycles of fusion and fission (Dove *et al.*, 2004). Adjusting the surface-to-volume ratio of vacuole by fusion and fission is a rapid response adapted by the cell during changes in the external conditions such as nutrient and osmotic changes and during cell division. The dynamics of FV in *P. falciparum* is not known. To understand if FV in *P. falciparum* undergoes fission, we investigated the presence of multilobed FV structures in the parasite. Parasites were immunolabelled with FV lumen protein falcipain-2 (FP-2). FV-labelled with FP-2 appeared multilobed in ~15% parasites (Figure 3.28A), indicating that FV in parasites might as well be a dynamic structure that undergoes fusion and fission. To understand further the involvement of *Pf*ATG18 in the fission process, the localization of *Pf*ATG18 was observed in the parasite containing multilobed FV. Interestingly, *Pf*ATG18 signal was enriched at the contact site of the FP-2 labelled multilobed FV (Figure 3.28B). This result was also confirmed by the localization of *Pf*ATG18-GFP in the recombinant parasites. FV of the transiently transfected parasites were labelled with FP-2 and LysoTracker Red DND99 (Figure 3.28C). Accumulation of *Pf*ATG18-GFP signal was detected at the interface of multilobed FV (Figure 3.28C), corroborating our earlier observation. This result indicates that the localization of *Pf*ATG18 in the parasite is similar to that seen in yeast during vacuole fission.

To comprehend if these multilobed FVs were generated as a result of the fission of FV and whether *Pf*ATG18 participates in the process, FV morphology was examined by time-lapse confocal microscopy in parasites expressing *Pf*ATG18-GFP. In the beginning, a single-lobed FV was observed in the parasite, which fragmented into multilobed vacuole at later time points, indicating that FV in *P. falciparum* undergoes fission. The fragmentation of the FV occurred at the site where *Pf*ATG18-GFP signal was intensified (Figure 3.28D), similar to the localization of *Pf*ATG18-GFP in yeast during vacuole fragmentation. Finally, these multilobed vacuoles coalesced and attained the single-lobed vacuole morphology again (Figure 3.28D), indicating that food vacuole undergoes cycles of fission and fusion.

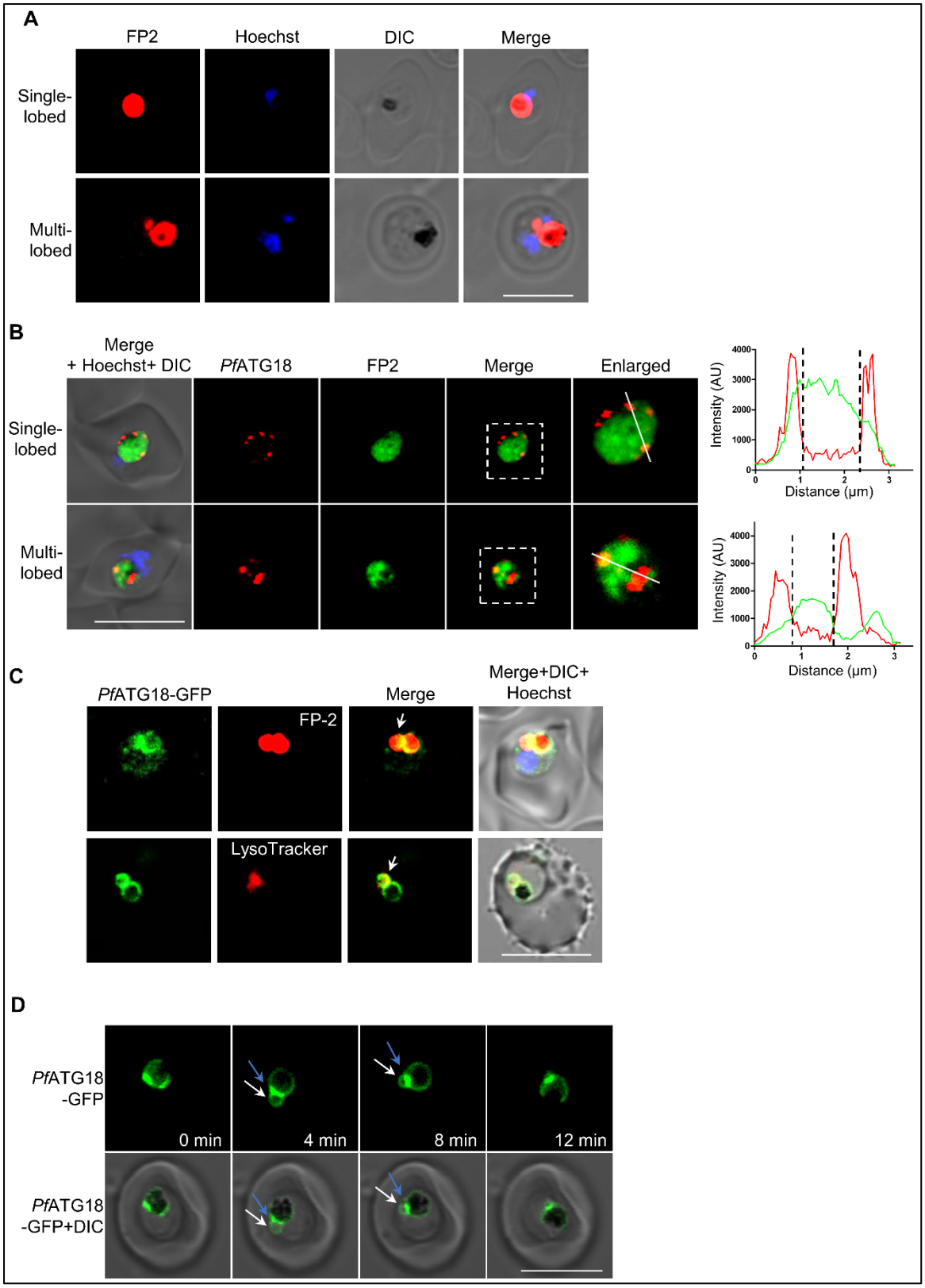

Figure 3.28: *Pf*ATG18 mediates vacuole fission in *P. falciparum*

(A) Immunofluorescence assay was carried out to visualize multilobed FV, labelled with falcipain-2 (FP-2) using anti-falcipain-2 antibodies in WT parasites growing in nutrient-rich conditions. Nucleus was stained by Hoechst; N=10 parasites, n=3 experiments, Scale bar=5 µm. **(B)** Immunofluorescence staining using anti-*Pf*ATG18 (1:400) and anti-falcipain-2 (1:200) antibodies was carried out using Zenon antibody labelling kit

to detect the localization of *Pf*ATG18 at single-lobed (top) and multilobed (bottom) FV in *P. falciparum*. Enlarged panel: magnified view of the dotted region shown in the merged image. Line scan analysis of fluorescence intensities along the white line shown in the merge panel. Red: *Pf*ATG18 Green: Falcipain-2. The region within the dotted lines in the line graph indicates the lumen of FV. Nucleus was stained by Hoechst; N=10 parasites, n=3 experiments, Scale bar=5 μm. **(C)** The localization of *Pf*ATG18-GFP at multilobed FV, labelled with FP-2 (top) using anti-falcipain-2 antibodies and LysoTracker Red DND99 (bottom) in transgenic *P. falciparum* 3D7 observed by confocal microscopy. Arrows indicate the multilobular FV; N=10 parasites, n=3 experiments, Scale bar=5 μm. **(D)** Time-lapse confocal microscopy images of *Pf*ATG18-labelled FV in transgenic *P. falciparum* 3D7. White arrow indicates fragmented vacuole and blue arrow indicates enrichment of *Pf*ATG18-GFP at the interface of the FV; N=10 parasites, n=3 experiments, Scale bar=5 μm.

3.3.9 Inhibition of cysteine proteases induce vacuole fission in *P. falciparum*

The food vacuole (FV) in *P. falciparum* is the main site for hemoglobin degradation. Proteases such as plasmepsins and falcipains are involved in the degradation of hemoglobin inside the FV (Francis *et al.*, 1997). In parasites treated with cysteine proteases inhibitors, the FV swells due to the accumulation of undegraded hemoglobin (Sijwali and Rosenthal, 2004). As *Pf*ATG18-GFP labelled the FV, we examined the morphology of the FV in parasites expressing *Pf*ATG18-GFP treated with cysteine protease inhibitors.

Parasites were treated with cysteine protease inhibitors, namely, E64d (Sijwali and Rosenthal, 2004), ALLN (Moura *et al.*, 2009) and MG132, a proteasome inhibitor which also inhibits cysteine protease falcipain in *P. falciparum* (Prasad *et al.*, 2013) and FV morphology was evaluated by live cell confocal microscopy. Upon treatment with these inhibitors for 4 h, *Pf*ATG18-GFP labelled FV was found to be enlarged (Figure 3.29 A, B and C), consistent with the earlier reports (Sijwali and Rosenthal, 2004; Moura *et al.*, 2009), but surprisingly, many small lobe vacuoles appeared near the large vacuole and *Pf*ATG18-GFP was enriched at the contact site of these lobes (Figure 3.29 A, B and C). Further, the percentage of parasites demonstrating multilobed FV phenotype increased up to 3-folds upon treatment with cysteine protease inhibitors as compared to the untreated ones (Figure 3.29D).

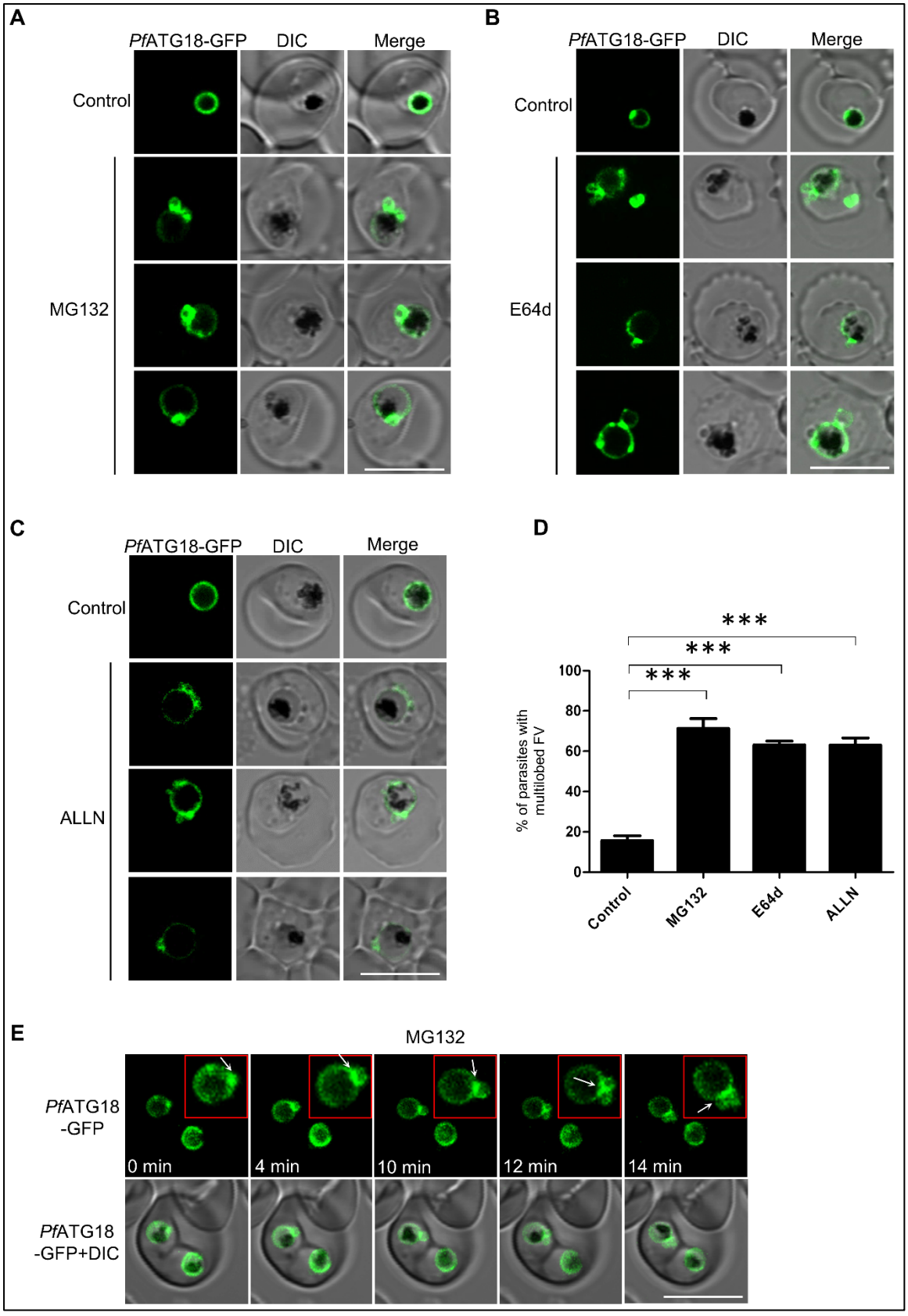

Figure 3.29: Inhibition of cysteine proteases induce vacuole fission in *P. falciparum*

*Pf*ATG18-GFP was observed by confocal microscopy upon treatment with **(A)** 400 nM MG132, **(B)** 10 µM E64d and **(C)** 10 µM ALLN for 4 h in the trophozoites; N=100 parasites, n=3 experiments, Scale bar=5 µm. **(D)** Graph shows the percentage of parasites with multilobed FV upon treatment with MG132, E64d and

ALLN; N=100 parasites, n=3 experiments. All data are expressed as mean ± SEM. *** indicates P<0.0005, analyzed by unpaired Student's *t* test. **(E)** Time-lapse confocal microscopy images of *Pf*ATG18-labelled FV in MG132 treated transgenic *P. falciparum* 3D7 cells showing FV fission. Insets represent an enlarged view of the FV. Arrows indicate enrichment of *Pf*ATG18-GFP at the contact site of multiple vacuoles. Images were acquired after every 2 min; N=10 parasites, n=3 experiments, Scale bar=5 µm.

To validate that these multilobed FVs in the treated parasites are formed due to fission, the FV morphology was assessed by time-lapse confocal microscopy upon 30 min treatment of the transgenic parasites with MG132. The MG132-treated cell in which FV appeared as a single spherical structure was chosen for investigation (Figure 3.29E). At later time point, FV fragmented to form multilobed vacuole (Figure 3.29E), further supporting our notion of the vacuolar fission in *P. falciparum* and that the process of FV fission can be induced by the inhibition of cysteine protease.

3.3.10 *Pf*ATG18 is trafficked to food vacuole via hemoglobin-containing vesicles traffic in the parasite

*Pf*ATG18 was found to localize on the FV membrane, though it lacks the signal peptide necessary for targeting proteins to the FV (Lamarque *et al.*, 2008). In the absence of the signal peptide, *Pf*ATG18 might get transported to the FV via the endocytic pathway (Lamarque *et al.*, 2008). Actin, myosin, and dynamin are involved in the formation, migration, and maturation of hemoglobin-containing vesicles (HcVs), which transport hemoglobin to the FV via endocytic pathway (Elliott *et al.*, 2008; Smythe *et al.*, 2008; Milani *et al.*, 2015). To decipher whether *Pf*ATG18 is transported to the FV via the endocytic pathway, this pathway was pharmacologically inhibited by small inhibitory molecules namely, jasplakinolide, 2,3-butanedione monoxime (BDM) and Dynasore and *Pf*ATG18 localization to the FV was monitored. Parasites were also immunolabelled with falcipain-2 (FP2). It is reported that FP2 is transported to the cytostomes and then it is trafficked to the FV via hemoglobin containing vesicles (HcVs) utilizing hemoglobin trafficking pathway (Dasaradhi *et al.*, 2007).

In control parasites, *Pf*ATG18 was present on the FV (Figure 3.30). Upon treating parasites with jasplakinolide, which stabilizes actin filaments and promotes its polymerization (Holzinger, 2009), *Pf*ATG18-labelled vesicles were observed at the parasite boundary which colocalized with FP2 (Figure 3.30). As FP2 is transported to the FV by HcVs

(Dasaradhi *et al.*, 2007), the colocalization of *Pf*ATG18 and FP2 near parasite boundary indicates that *Pf*ATG18 too localizes on HcVs. When parasites were treated with BDM, a myosin inhibitor (Ostap, 2002), *Pf*ATG18-labelled vesicles colocalized with FP2 at the parasite boundary (Figure 3.30). Parasites were also treated with Dynasore, a dynamin inhibitor. Dynamin is essential for the generation of HcVs from the distal end of the cytostome in the hemoglobin uptake pathway of *P. falciparum* (Zhou *et al.*, 2009; Milani *et al.*, 2015). Due to the lack of dynamin GTPase activity upon Dynasore treatment, *Pf*ATG18 labelled tubular structures were observed which colocalized with FP2 (Figure 3.30). Together, the inhibition of *Pf*ATG18 trafficking to the FV upon treatment of the parasites with hemoglobin trafficking pathway inhibitors indicates that *Pf*ATG18 is transported to FV via the endocytic pathway.

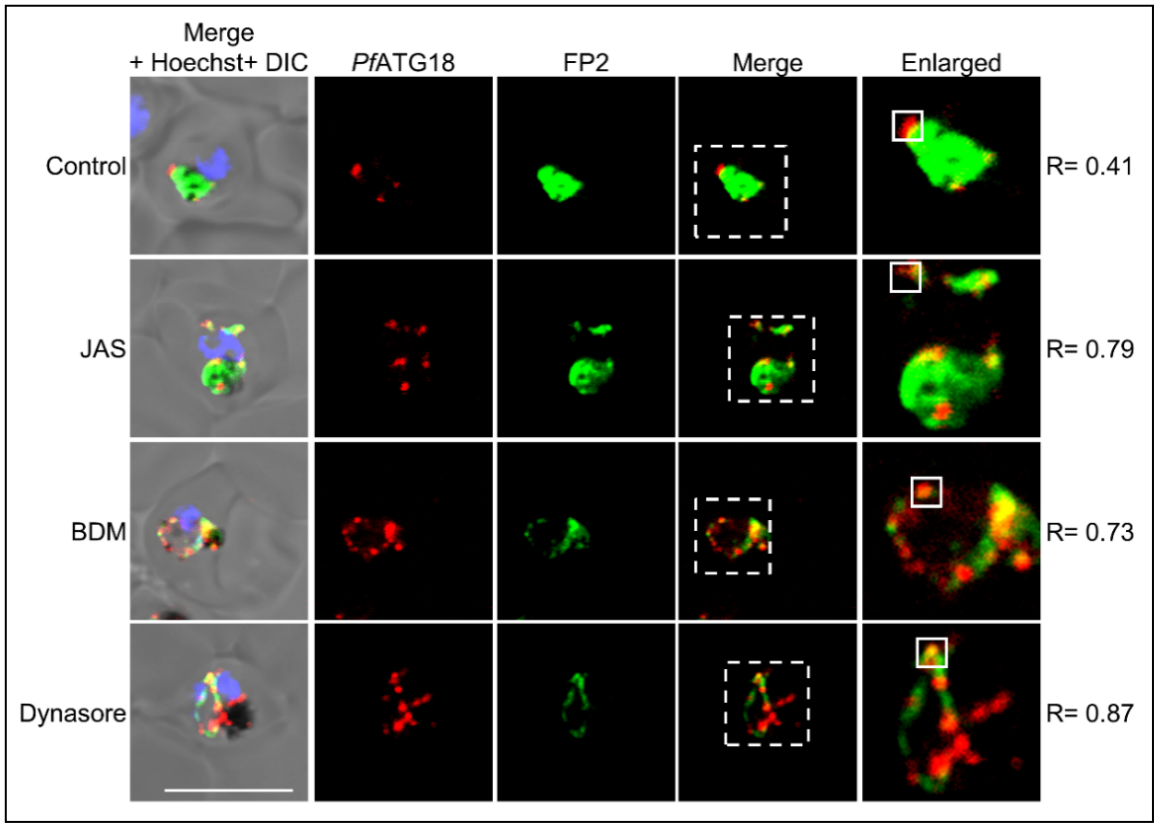

Figure 3.30: *Pf*ATG18 is transported to the FV by hemoglobin trafficking pathway in *P. falciparum*

Localization of *Pf*ATG18 upon treating parasites with endocytic trafficking inhibitors 7 µM jasplakinolide (JAS), 25 mM 2,3-Butanedione monoxime (BDM) and 200 µM Dynasore. Immunofluorescence assay (IFA) was performed on parasites immunolabelled with antibodies against *Pf*ATG18 and falcipain-2 (FP2) using Zenon antibody labelling kit. Upon treatment with endocytic trafficking inhibitors, *Pf*ATG18 colocalized significantly with FP2 at the parasite boundary and on tubular structures. Enlarged panel: magnified view of the dotted region shown in the merged image. The Pearson's coefficient (R) represents the degree of

colocalization between *Pf*ATG18 and FP2 evaluated from the signal within the square region shown in the enlarged image. Nucleus was stained by Hoechst; N=10 parasites, n=3 experiments, Scale bar=5 µm.

The trafficking of *Pf*ATG18 to the FV via HcV is also validated in *Pf*ATG18-GFP transfected cell line. In the parasites treated with JAS, the percentage of parasites with *Pf*ATG18-GFP labelled vesicles at the parasite boundary increased in the jasplakinolide-treated parasites (Figure 3.31), also, cytostome-like structures labelled with *Pf*ATG18-GFP were occasionally observed in few parasites upon this treatment (Figure 3.31), indicating a defect in the trafficking of *Pf*ATG18-GFP to the FV.

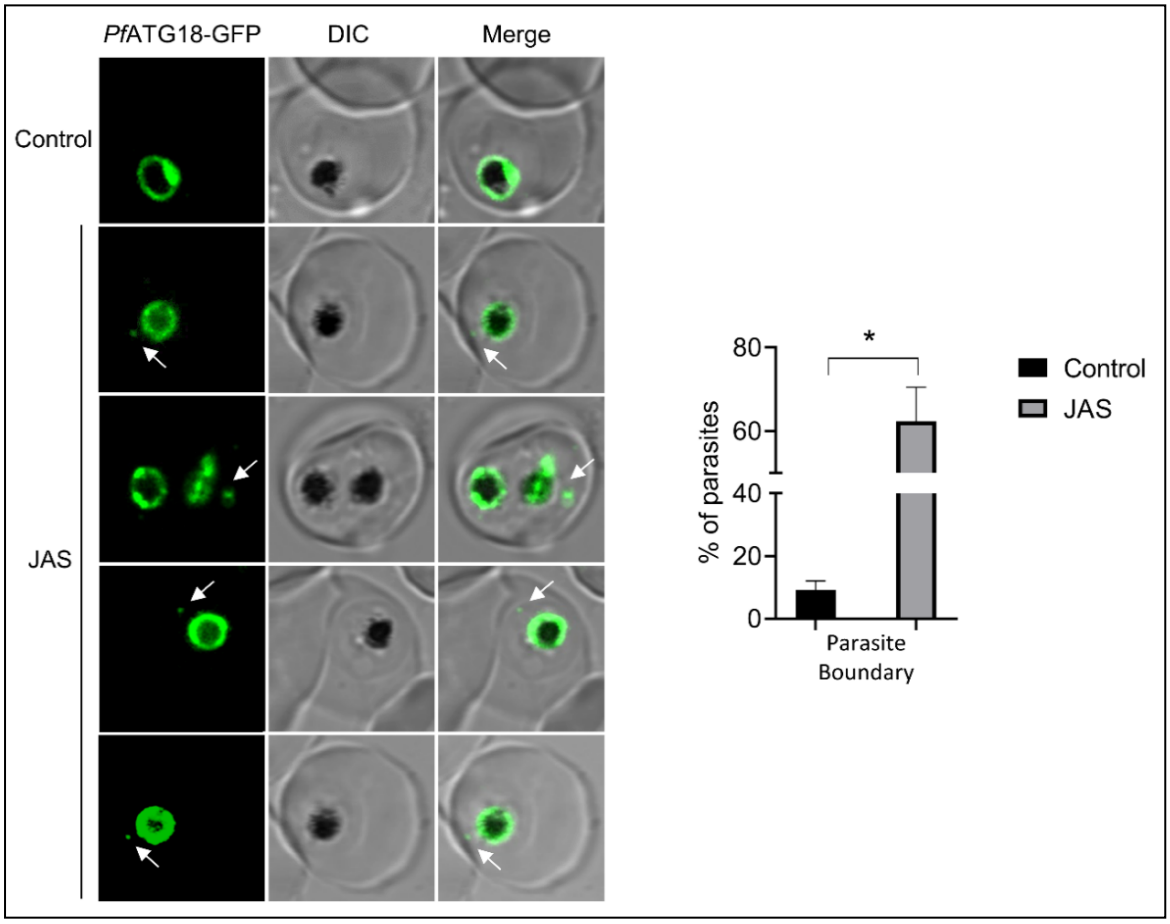

Figure 3.31: Effect of jasplakinolide on the trafficking of *Pf*ATG18-GFP in *P. falciparum*

*Pf*ATG18-GFP transgenic parasites were treated with 7 µM jasplakinolide (JAS) for 4 h in trophozoite stage. Live cell confocal microscopy comparison is shown for untreated control and JAS-treated parasites. *Pf*ATG18-GFP tagged vesicles are stalled at parasite boundary. Arrow indicates *Pf*ATG18-GFP at the parasite boundary; N=70 parasites, n=3 experiments, Scale bar=5 µm. Graph represents the percentage of parasites showing GFP signal at the parasite boundary, values are mean ± SEM. * indicates $P<0.05$, analyzed by unpaired Student's *t* test.

In the transiently transfected parasites treated with BDM, the percentage of parasites with *Pf*ATG18-GFP-labelled vesicles at the parasite boundary and tubular structures increased (Figure 3.32). *Pf*ATG18-GFP was found on vesicles containing hemozoin, which was identified by the black pigment inside the vesicles near the parasite boundary (Figure 3.32). As hemoglobin degradation and hemozoin formation are initiated inside the HcVs (Elliott *et al.*, 2008), the presence of *Pf*ATG18-GFP on hemozoin-containing vesicles thus indicate that *Pf*ATG18 traffics via hemoglobin transport pathway.

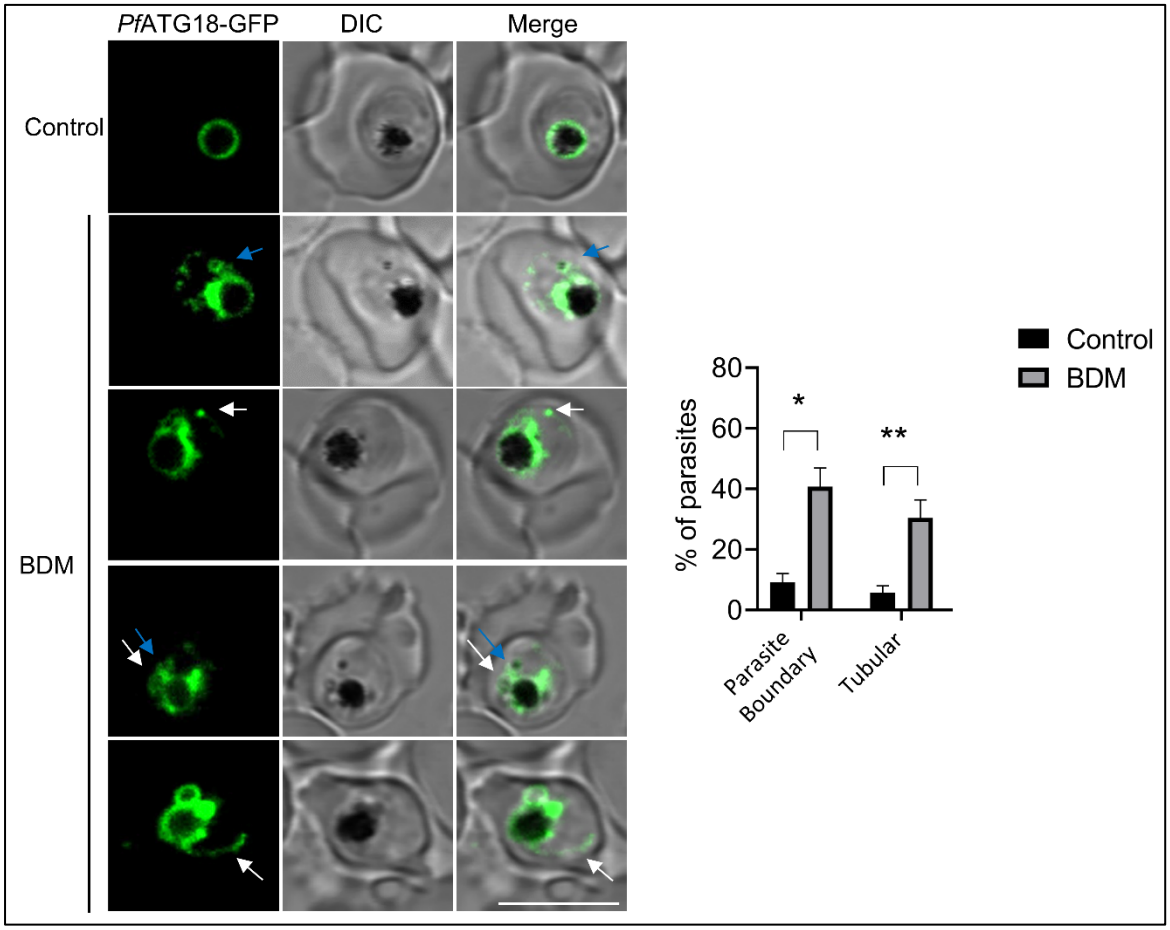

Figure 3.32: Effect of BDM on the trafficking of *Pf*ATG18-GFP in *P. falciparum*

*Pf*ATG18-GFP transgenic parasites were treated with 25 mM BDM for 1 h in trophozoite stage. Live cell confocal microscopy comparison is shown for untreated and BDM-treated parasites. White arrows indicate *Pf*ATG18-GFP tagged vesicles at the parasite boundary and tubules in BDM-treated parasites. Blue arrows indicate *Pf*ATG18-GFP labelled vesicles containing hemozoin; N=70 parasites, n=3 experiments, Scale bar=5 µm. Graph represents the percentage of parasites showing *Pf*ATG18-GFP signals observed at the parasite boundary and tubules, values are mean ± SEM. * indicates P<0.05, ** indicates P<0.005, analyzed by unpaired Student's *t* test.

In the transiently transfected parasites treated with Dynasore, the percentage of parasites displaying *Pf*ATG18-GFP-labelled tubular structures increased (Figure 3.33), also, the localization of *Pf*ATG18-GFP on the FV membrane reduced upon Dynasore treatment (Figure 3.33).

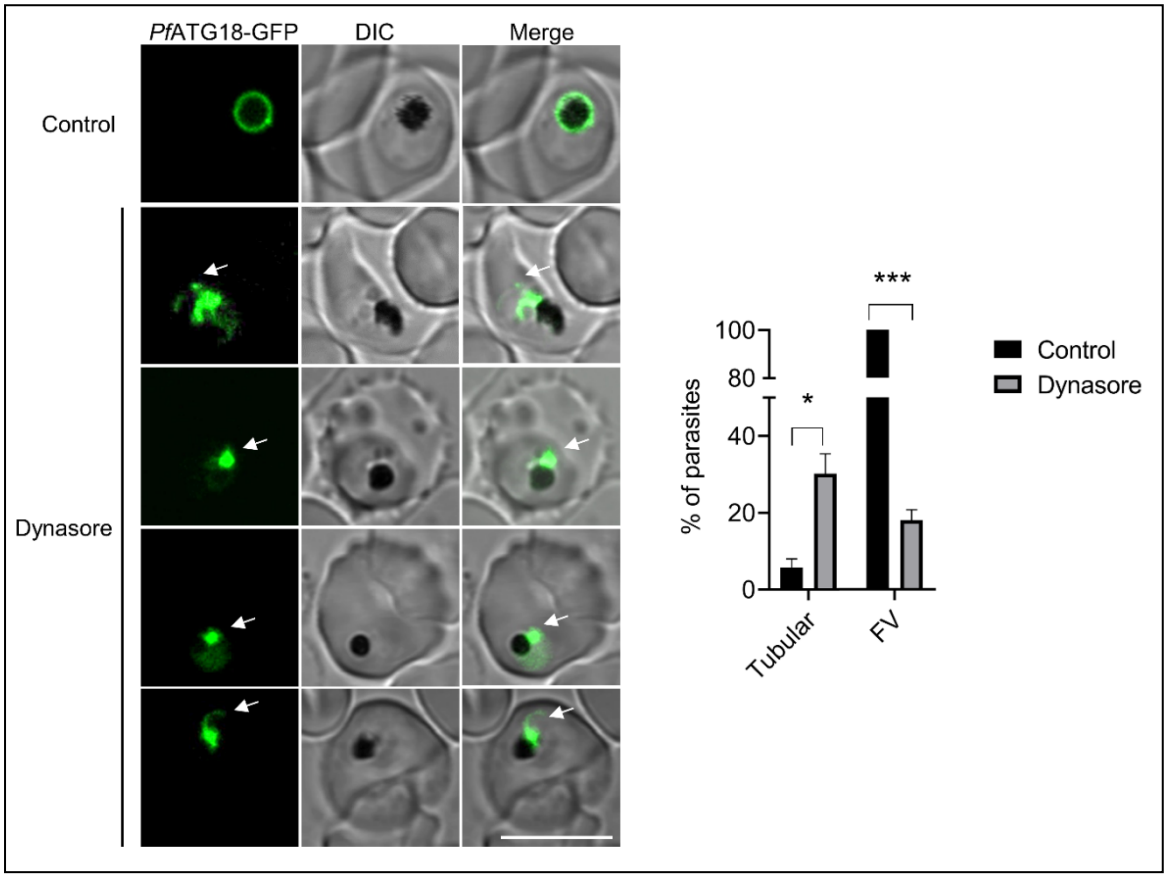

Figure 3.33: Effect of Dynasore on the trafficking of *Pf*ATG18-GFP in *P. falciparum*

*Pf*ATG18-GFP transgenic parasites were treated with 200 µM Dynasore for 4 h in trophozoite stage. Live cell confocal microscopy comparison is shown for untreated control and Dynasore-treated parasites. Parasites display *Pf*ATG18-GFP-labelled tubular structures and GFP enrichment near FV due to Dynasore treatment, indicated by arrows; N=70 parasites, n=3 experiments, Scale bar=5 µm. Graph represents the percentage of parasites showing *Pf*ATG18-GFP signals at tubules and FV, values are mean ± SEM. * indicates P<0.05, *** indicates P<0.0005, analyzed by unpaired Student's *t* test.

Furthermore, the localization of *Pf*ATG18-GFP with FP-2 and plasmepsin-II (PM-II), FV proteins that reaches FV via hemoglobin trafficking pathway (Klemba *et al.*, 2004a; Dasaradhi *et al.*, 2007), was examined upon treatment with endocytic inhibitors. Upon treatments, *Pf*ATG18-GFP colocalized with FP2 (Figure 3.34A) and PM-II (Figure 3.34B) in the parasite cytosol, indicating that trafficking of *Pf*ATG18 to the FV is mediated by hemoglobin trafficking pathway.

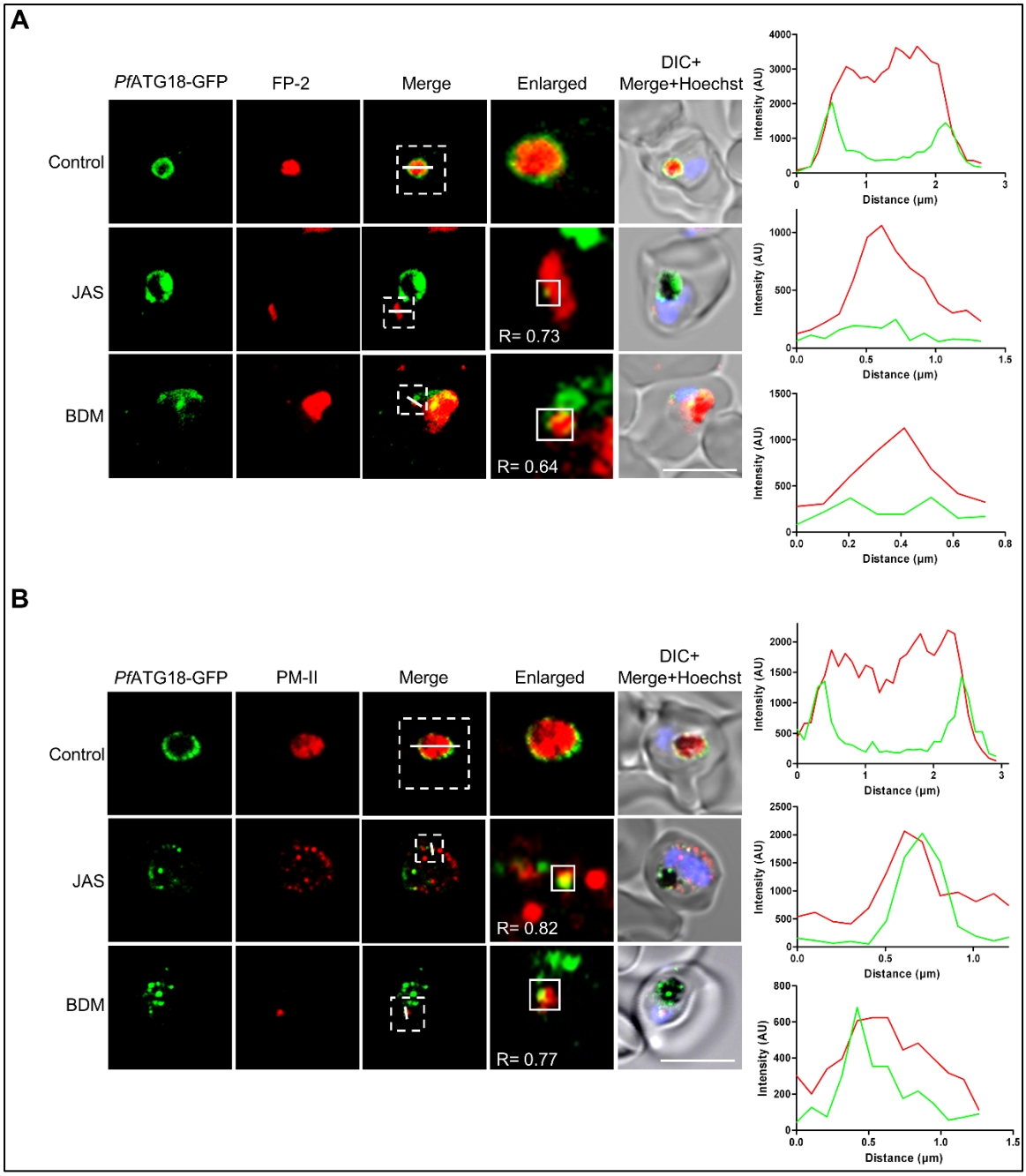

Figure 3.34: Hemoglobin trafficking pathway transports *Pf*ATG18-GFP to the FV in *P. falciparum*

Colocalization of *Pf*ATG18-GFP and FV proteases upon treatment with endocytic inhibitors jasplakinolide (JAS) and 2,3-Butanedione monoxime (BDM). Immunofluorescence assay (IFA) was performed on transgenic parasites expressing *Pf*ATG18-GFP using antibodies against **(A)** GFP and falcipain 2 (FP-2), and **(B)** GFP and Plasmepsin II (PM-II). Upon treatment with endocytic trafficking inhibitors, *Pf*ATG18-GFP partially localizes with FP-2 and PM-II. The nucleus is labelled with Hoechst (blue). Enlarged panel: magnified view of the dotted area. Arrows show the colocalization of *Pf*ATG18-GFP with FP-2 and PM-II. Line scan analysis of fluorescence intensities along the white lines shown in the merged panel. Red: Falcipain-2 A., Plasmepsin-II B., Green: *Pf*ATG18-GFP. The Pearson's coefficient (R) represents the degree of colocalization between *Pf*ATG18 and falcipain-2 (A) and plasmepsin-II (B) evaluated from the signal within the square region shown in the enlarged image.; N=30 parasites, n=3 experiments, Scale bar=5 µm.

3.3.11 *Pf*ATG18 participates in the autophagy-like pathway upon brief starvation in *P. falciparum*

ATG18 is involved in autophagosome formation in selective as well as non-selective autophagy in yeast. It forms a complex with ATG2 (ATG18-ATG2) and directs the complex to PAS by binding to PI3P. The ATG18-ATG2 complex contributes to autophagy functions such as tethering PAS to ER (Kotani *et al.*, 2018), ATG9 recycling (Reggiori *et al.*, 2004) and protecting the premature cleavage of ATG8-PE from ATG4 protease (Nair *et al.*, 2010). The mRNA levels of one of the mammalian homolog of ATG18, WIPI1 is reported to reliably indicate the levels of autophagosome formation (Tsuyuki *et al.*, 2014). To decipher the role of *Pf*ATG18 in autophagy, we analysed the transcriptional levels of *PfATG18* when parasites were cultured under amino acid deprivation, an autophagy inducing condition. Synchronized parasites at trophozoite stage were starved for 0, 2, 4 and 6 hours, harvested and qRT-PCR of *PfATG18, PfATG8, PfGAPDH* and β-Actin genes was performed using gene-specific primers. The relative gene expression of *PfATG18* was found to be upregulated by 1.5-2.2-folds in the parasites cultured under starvation conditions for 2, 4 and 6 hours, as compared to those grown under nutrient fed conditions (Figure 3.35A and B), similar to the increase in mRNA abundance of WIPI1 under nutrient deprivation. The mRNA levels of positive control *PfATG8* (Joy *et al.*, 2018) was also upregulated upon starvation (Figure 3.35A and B). While the relative gene expression of the housekeeping gene *PfGAPDH* was not altered during nutritional stress (Figure 3.35A and B). In line with the *PfATG18* gene expression, protein levels of *Pf*ATG18 also induced up to 1.7-folds upon brief starvation (Figure 3.35C). The protein levels of autophagy marker protein *Pf*ATG8 was earlier reported to increase upon starvation (Figure 3.35C), indicating that autophagy-like pathway indeed gets induced in the parasite upon starvation. Thus, the upregulation of *Pf*ATG18 gene and protein expression under starvation indicates that it has a role in autophagy-like pathway in the malaria parasite.

In yeast, ATG18 is recruited on PAS during autophagic conditions after nucleation of autophagosome formation and colocalizes with ATG8 (Suzuki *et al.*, 2007). To determine the presence of *Pf*ATG18 on autophagosome-like structures, we examined the colocalization of *Pf*ATG18 with autophagosome marker protein *Pf*ATG8 (Tomlins *et al.*, 2013; Joy *et al.*, 2018). In nutrient-rich condition, *Pf*ATG18 colocalized with *Pf*ATG8 near FV (Figure 3.35D), whereas upon brief starvation, apart from colocalization of *Pf*ATG18

and *Pf*ATG8 on FV, these proteins also colocalized on punctate structures in the parasite cytosol resembling autophagosome-like structures (Figure 3.35D), further indicating that *Pf*ATG18 participates in autophagy-like pathway in this parasite.

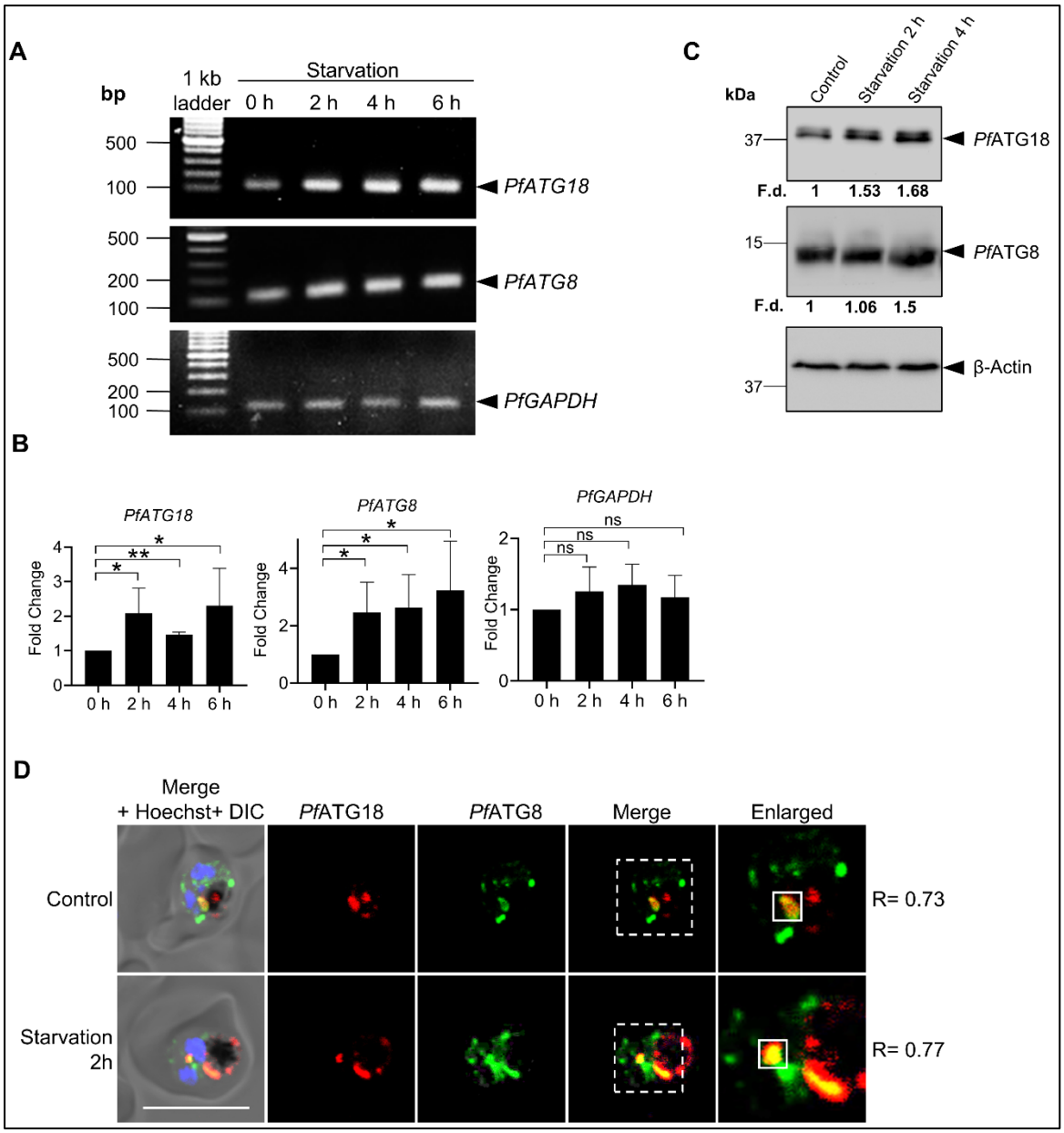

Figure 3.35: *Pf*ATG18 expression increases upon brief starvation in *P. falciparum*

(A) *P. falciparum* subjected to amino acid starvation for 2, 4 and 6 hours. The expression levels of *PfATG18*, *PfATG8* (positive control for starvation), and *PfGAPDH* (housekeeping gene) were determined in control and starved parasites by quantitative RT-PCR. *β*-Actin was used as the reference gene. Agarose gel electrophoresis images showing amplicons obtained from RT-PCR; n=3 experiments. **(B)** Graph represents fold change of relative gene expression of *PfATG18*, *PfATG8* and *PfGAPDH*. $2^{-\Delta\Delta Ct}$ method was used to determine relative gene expression; n=3 experiments. * indicates P<0.05, ** indicates P<0.005, ns indicates non-significant values higher than P>0.05, analyzed by Student's *t* test. **(C)** Effect of starvation on *Pf*ATG18 protein expression. Lysates were prepared from parasites cultured in the medium without amino acids and

serum for indicated time periods. Immunoblot was probed with anti-*Pf*ATG18 and anti-*Pf*ATG8 antibodies. β-Actin was used as a loading control. Fold difference (F.d.) as compared to normalized control is indicated below the bands, n=3 experiments. **(D)** Colocalization of *Pf*ATG18 and *Pf*ATG8 upon 2 h starvation. Immunostaining of untreated control and starved parasites with anti-*Pf*ATG18 (1:400) and anti-*Pf*ATG8 (1:600) antibodies using Zenon antibody labelling kit. Enlarged panel: magnified view of the dotted region shown in the merged image. The Pearson's coefficient (R) represents the degree of colocalization between *Pf*ATG18 and *Pf*ATG8 evaluated from the signal within the square region shown in the enlarged panel. Nucleus was stained by Hoechst. *Pf*ATG18 colocalizes with *Pf*ATG8 in control as well as starved parasites. N=10 parasites, n=3 experiments, Scale bar=5 μm.

We aimed to understand the specificity of *Pf*ATG18 function in vacuole fission and autophagy besides its reported involvement in apicoplast biogenesis (Bansal *et al.*, 2017). To achieve this, the localization of *Pf*ATG18 was determined in the apicoplast-minus parasites. Apicoplast-minus parasites were generated by treating *P. falciparum* 3D7 strain with doxycycline for 48 h (Dahl *et al.*, 2006). Parasite growth was rescued by supplementing the medium with isopentenyl pyrophosphate (IPP) for 24 h. The localization of *Pf*ATG18 and apicoplast marker *Pf*ACP was evaluated in the subsequent cycle in both control as well as apicoplast-minus parasites. In the next generation, the apicoplast was elongated and branched in control trophozoite stage parasite (Figure 3.36A), as reported previously (van Dooren *et al.*, 2005) and *Pf*ATG18 was present near FV (Figure 3.36A). Whereas, in the progeny of doxycycline-treated parasites, *Pf*ACP signal was diffused (Figure 3.36A), indicating the loss of apicoplast, as reported previously (Dahl *et al.*, 2006). However, upon loss of apicoplast, the localization of *Pf*ATG18 on FV was unaltered (Figure 3.36A). We also assessed the localization of *Pf*ATG18-GFP in recombinant parasites upon removal of the apicoplast. Similar to the localization of *Pf*ATG18 in wild-type parasites, *Pf*ATG18-GFP too, was found on FV apicoplast-minus transfected parasites (Figure 3.36B).

To understand if the removal of apicoplast affects the autophagy function of *Pf*ATG18, we determined the colocalization of *Pf*ATG18 and *Pf*ATG8 in doxycycline-treated and IPP rescued parasites upon starvation. In control as well as starved parasites, *Pf*ATG18 colocalized with *Pf*ATG8 (Figure 3.36C). As the localization of *Pf*ATG18 is not affected by the elimination of apicoplast, it indicates that *Pf*ATG18 is involved in autophagy and vacuole fission besides apicoplast biogenesis.

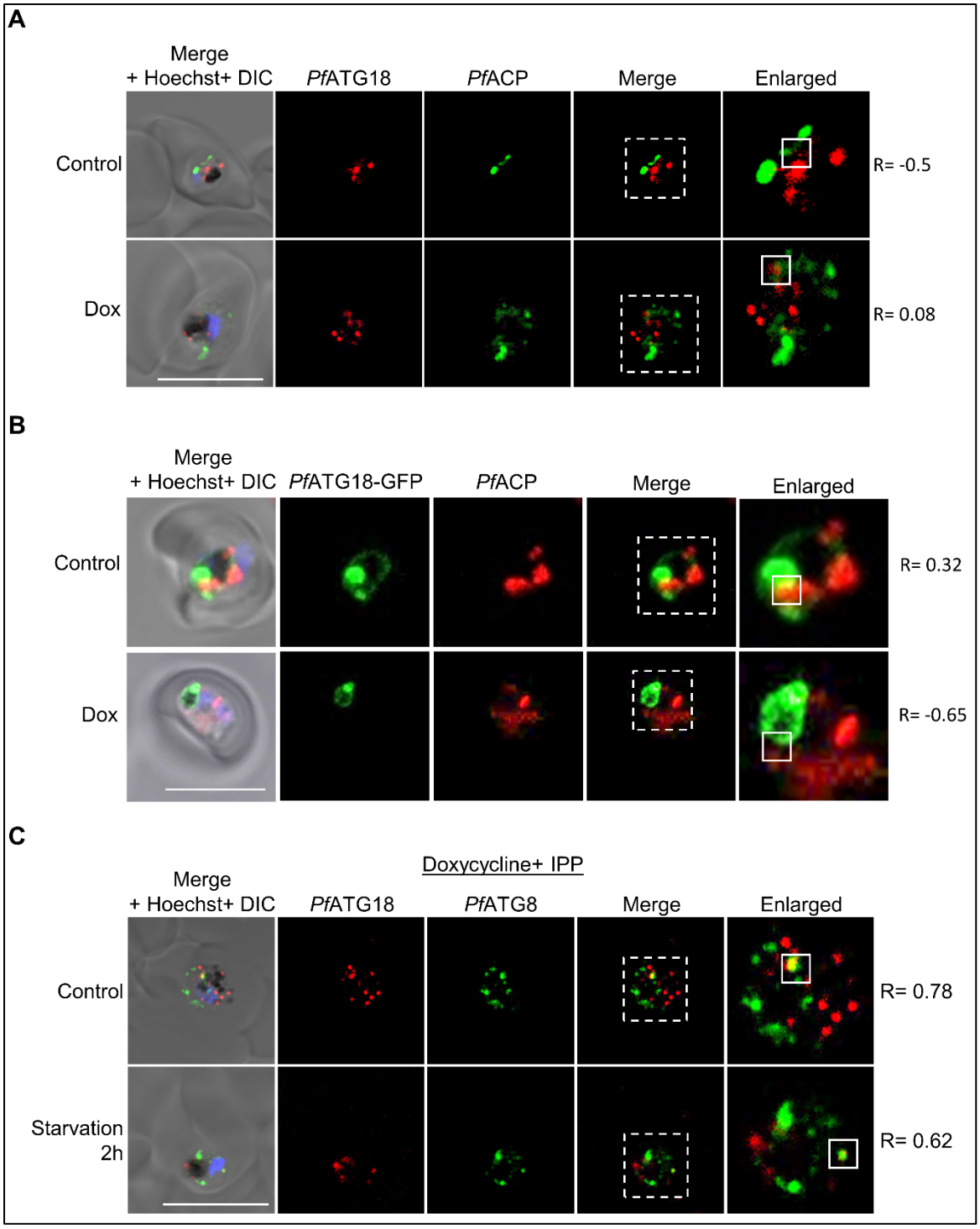

Figure 3.36: *Pf*ATG18 localization is unaltered in apicoplast-minus parasites

(A) Parasite culture was treated with 1 µM doxycycline for 48 h and supplemented with complete medium containing isopentenyl pyrophosphate (IPP) without antibiotic for an additional 24 h. These parasites were immunolabelled with anti-*Pf*ATG18 (1:400) and antibody against apicoplast marker protein *Pf*ACP (1:200) using Zenon antibody labelling kit. The localization of *Pf*ATG18 was identical in control and doxycycline-treated parasites; N=10 parasites, n=3 experiments, Scale bar=5 µm. **(B)** Immunostaining of apicoplast-minus transgenic parasites using anti-GFP (1:200) and anti-*Pf*ACP (1:200) antibodies; N=10 parasites, n=3 experiments, Scale bar=5 µm. **(C)** Colocalization of *Pf*ATG18 and *Pf*ATG8. Apicoplast-minus parasite culture was further incubated in medium without amino acids and serum for 2 h. Immunostaining of untreated

control and starved parasites using anti-*Pf*ATG18 (1:400) and anti-*Pf*ATG8 (1:600) antibodies immunolabelled with Zenon antibody labelling kit. Enlarged panel: magnified view of the dotted region shown in the merged image. The Pearson's coefficient (R) represents the degree of colocalization between *Pf*ATG18 and *Pf*ACP (A), *Pf*ATG18-GFP and *Pf*ACP (B), *Pf*ATG18 and *Pf*ATG8 (C), evaluated from the signal within the square region shown in the enlarged panel. Nucleus was stained by Hoechst; N=10 parasites, n=3 experiments, Scale bar=5 µm.

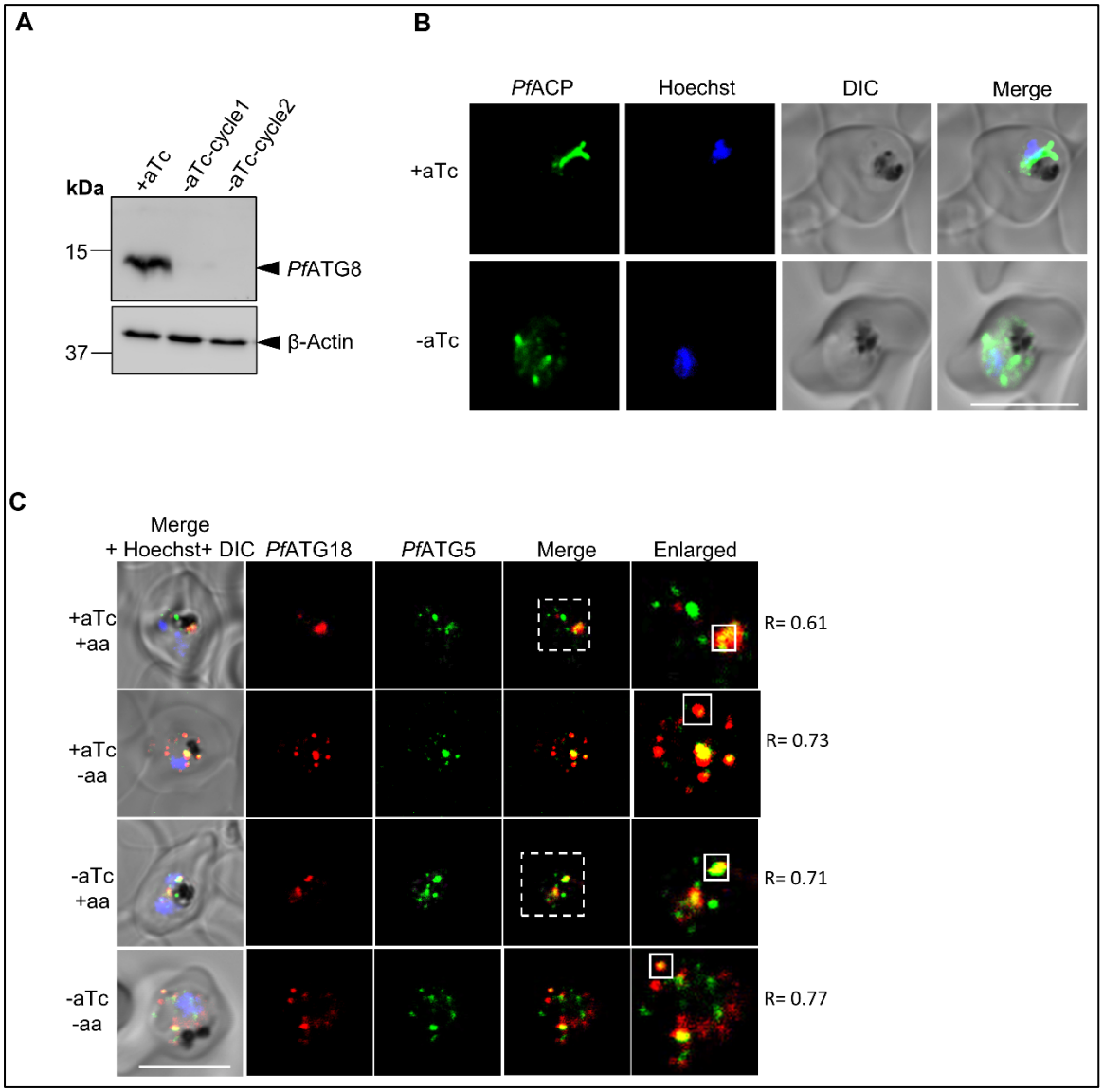

Figure 3.37: *Pf*ATG18 localization is unaltered in *Pf*ATG8 knockdown parasites

(A) Immunoblot analysis showing the knockdown of *Pf*ATG8 upon removal of anhydrotetracycline (aTC) from culture medium supplemented with isopentenyl pyrophosphate (IPP) for two intraerythrocytic cycles. β-Actin was used as a loading control; n=3 experiments. **(B)** Immunofluorescence image showing *Pf*ACP in *Pf*ATG8 knockdown parasites; N=10 parasites, n=3 experiments, Scale bar=5 µm. **(C)** Colocalization of *Pf*ATG18 and *Pf*ATG5 in *Pf*ATG8 knockdown parasites. *Pf*ATG8 expression was depleted in conditional knockdown parasite strain by removing aTC from culture medium for 36 h. The parasite growth was rescued by supplementing culture medium with isopentenyl pyrophosphate (IPP). *Pf*ATG8 knockdown parasites were

further incubated in medium without amino acids and serum for 2 h. Immunofluorescence images showing colocalization of *Pf*ATG18 and *Pf*ATG5 labelled anti-*Pf*ATG18 (1:400) and anti-*Pf*ATG5 (1:400) antibodies using Zenon antibody labelling kit in *Pf*ATG8 depleted and IPP rescued parasites. Enlarged panel: magnified view of the dotted region shown in the merged image. The Pearson's coefficient (R) represents the degree of colocalization between *Pf*ATG18 and *Pf*ATG5 evaluated from the signal within the square region shown in the enlarged panel. Nucleus was stained by Hoechst. *Pf*ATG18 colocalizes with *Pf*ATG5 in *Pf*ATG8 knockdown parasites; N=10 parasites, n=3 experiments, Scale bar=5 μm.

The involvement of *Pf*ATG18 in autophagy was also validated in *Pf*ATG8 conditional knockdown parasites (a kind gift from Dr. Yeh, Stanford Medical School, San Francisco). The apicoplast is lost in the *Pf*ATG8 depleted parasites, whose growth is rescued by IPP (Walczak *et al.*, 2018). We investigated the presence of autophagosome-like structures in *Pf*ATG8 depleted parasites upon elimination of apicoplast. In *Pf*ATG8 conditional knockdown parasites, *Pf*ATG8 expression is regulated by 3′ untranslated region (UTR) TetR-DOZI-binding aptamer sequence. In the presence of anhydrotetracycline (aTc), *Pf*ATG8 was expressed (Figure 3.37A) (Walczak *et al.*, 2018). We then monitored the expression of *Pf*ATG8 upon removal of aTc in the presence of IPP for two cycles. *Pf*ATG8 was efficiently knockdown in the same cycle of removal of aTc (Figure 3.37A), consistent with the previous report (Walczak *et al.*, 2018). *Pf*ATG8 knockdown also resulted in the elimination of the apicoplast, seen by the mislocalisation *Pf*ACP (Figure 3.37B), consistent with the report (Walczak *et al.*, 2018). To identify autophagosomes in this strain, parasites were labelled with *Pf*ATG18 and *Pf*ATG5 (Joy *et al.*, 2018). In *Pf*ATG8^{+} cells under nutrient-rich and starved conditions, *Pf*ATG18 colocalised with *Pf*ATG5 (Figure 3.37C). *Pf*ATG18 puncta continued to colocalise with *Pf*ATG5 in *Pf*ATG8^{-} cells in nutrient-rich as well as starved conditions (Figure 3.37C). This result thus indicates that *Pf*ATG18-labelled autophagosome-like structures are generated in the parasites upon *Pf*ATG8 knockdown, further corroborating our finding that *Pf*ATG18 is involved in autophagy-like pathway in *Plasmodium* besides apicoplast biogenesis.

3.3.12 *Pf*ATG18-GFP is unable to complement autophagy or cytoplasm-to-vacuole functions in *S. cerevisiae*

To further validate the role of *Pf*ATG18 in autophagy, functional complementation in *S. cerevisiae* was carried out. Yeast strain lacking ATG18 has limited viability under starvation conditions (Tsukada and Ohsumi, 1993), therefore, the growth of *atg18*Δ yeast

cells expressing *Pf*ATG18-GFP upon nitrogen starvation was assessed. While *Sc*Atg18 could restore the viability of the *atg18*Δ yeast cells under nitrogen starvation, *Pf*ATG18 could not (Figure 3.38A). This result indicates that *Pf*ATG18 is unable to restore growth in *atg18*Δ yeast cells upon starvation.

Accumulation of autophagic bodies in the vacuole upon nitrogen starvation, induced by treating yeast cells with the protease inhibitor phenylmethylsulphonyl fluoride (PMSF), is an indication of functional autophagy pathway (Tsukada and Ohsumi, 1993). In the presence of PMSF, autophagic bodies were observed within the vacuole in *atg18*Δ yeast cells expressing *Sc*Atg18-GFP (Figure 3.38B) as expected. These autophagic bodies were not detected within the vacuole of *atg18*Δ yeast cells or *atg18*Δ yeast cells expressing *Pf*ATG18-GFP (Figure 3.38B), indicating that *Pf*ATG18-GFP could not restore autophagy in autophagy-defective *atg18*Δ yeast cells.

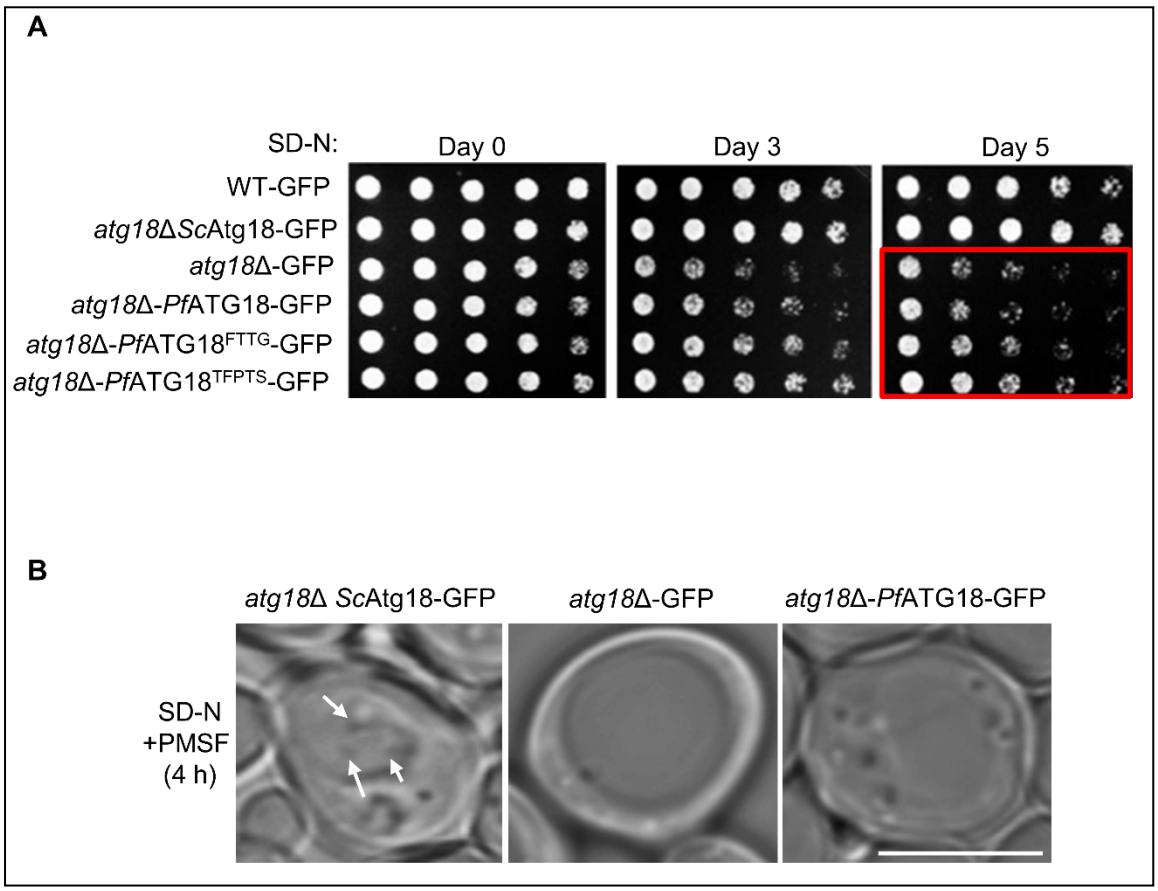

Figure 3.38: *Pf*ATG18 does not rescue growth defect or mediate autophagic bodies formation in *atg18*Δ yeast strain during nitrogen starvation

(A) Ten-fold spot dilution assay of yeast strains grown under nitrogen-deficient conditions for the indicated days. The cells were plated on leucine and uracil dropout SD plates and allowed to grow for two days at 30°C, and then images were acquired. The red box in the Day 5 panel highlights the growth defect of *atg18*Δ yeast strain expressing GFP, *Pf*ATG18-GFP and *Pf*ATG18^{FTTG}-GFP and *Pf*ATG18^{TFPTS}-GFP; n=3 experiments **(B)**

*Pf*ATG18-GFP could not participate in the formation of autophagic bodies in *atg18*Δ yeast cells. *atg18*Δ yeast cells expressing *Sc*Atg18-GFP, GFP, and *Pf*ATG18-GFP were incubated in SD(-N) medium containing 1mM PMSF at 30°C. After incubation for 4 h, cells were observed under light microscopy (DIC images). Arrows indicate autophagic bodies in the vacuole; N=50 cells, n=3 experiments, Scale bar=5 µm.

Additionally, autophagic flux was monitored by the mCherry-*Sc*Atg8 processing assay (Torggler *et al.*, 2017). The recruitment of ATG8 to the perivacuolar region or the PAS, in yeast, is not affected by the deletion of *ATG18* gene, but autophagosomes formation stalls in this mutant (Suzuki *et al.*, 2007; Obara *et al.*, 2008; Rieter *et al.*, 2013). To investigate the autophagosome biogenesis in *atg18*Δ cells expressing *Pf*ATG18-GFP, we scrutinized the autophagy flux by mCherry-Atg8 processing assay (Torggler *et al.*, 2017) using fluorescence microscopy. As reported earlier (Rieter *et al.*, 2013), in WT and *atg18*Δ cells expressing *Sc*Atg18-GFP, the autophagy pathway was found to be functional, and the mCherry signal was observed in the vacuole upon nitrogen starvation (Figure 3.39A).

However, in *atg18*Δ yeast cells expressing only GFP or *Pf*ATG18-GFP, the mCherry signal accumulated at the perivacuolar region (Figure 3.39A), indicating that *Pf*ATG18-GFP could not restore the formation of autophagosome in *atg18*Δ yeast cells, corroborating our previous results. Upon quantification of the number of cells displaying mCherry-*Sc*Atg8-positive punctate structure at perivacuolar region (Figure 3.39B), no significant differences were observed between the different strains growing in rich medium. In contrast, under autophagy conditions, expression of *Pf*ATG18-GFP in *atg18*Δ cells led to a definite increase in the number of cells showing mCherry-*Sc*Atg8-positive punctate structure at the perivacuolar region as compared to *Sc*Atg18 or WT cells (Figure 3.39B). A similar result was also obtained in the *atg18*Δ yeast cells (Figure 3.39B). These results thus indicate that *Pf*ATG18-GFP could not complement the autophagosome biogenesis in the *atg18*Δ yeast strain.

The activity of Cytoplasm-to-vacuole (Cvt) pathway is monitored by Ape1 maturation assay (Lynch-Day and Klionsky, 2010; Torggler *et al.*, 2017). In WT cells, precursor Ape1 (prApe1) is transported to the vacuole via the Cvt pathway, proteolytically cleaved and finally gets converted to the mature form (mApe1) (Torggler *et al.*, 2017). As expected, in WT and *atg18*Δ cells expressing *Sc*Atg18-GFP, the mApe1 band was observed (Figure 3.39C), indicating functional Cvt pathway (Torggler *et al.*, 2017). However, the mApe1 band was absent in the *atg18*Δ cells expressing *Pf*ATG18-GFP (Figure 3.39C) and only the

prApe1 band was noticed, demonstrating that *Pf*ATG18-GFP was unable to complement the Cvt function in yeast.

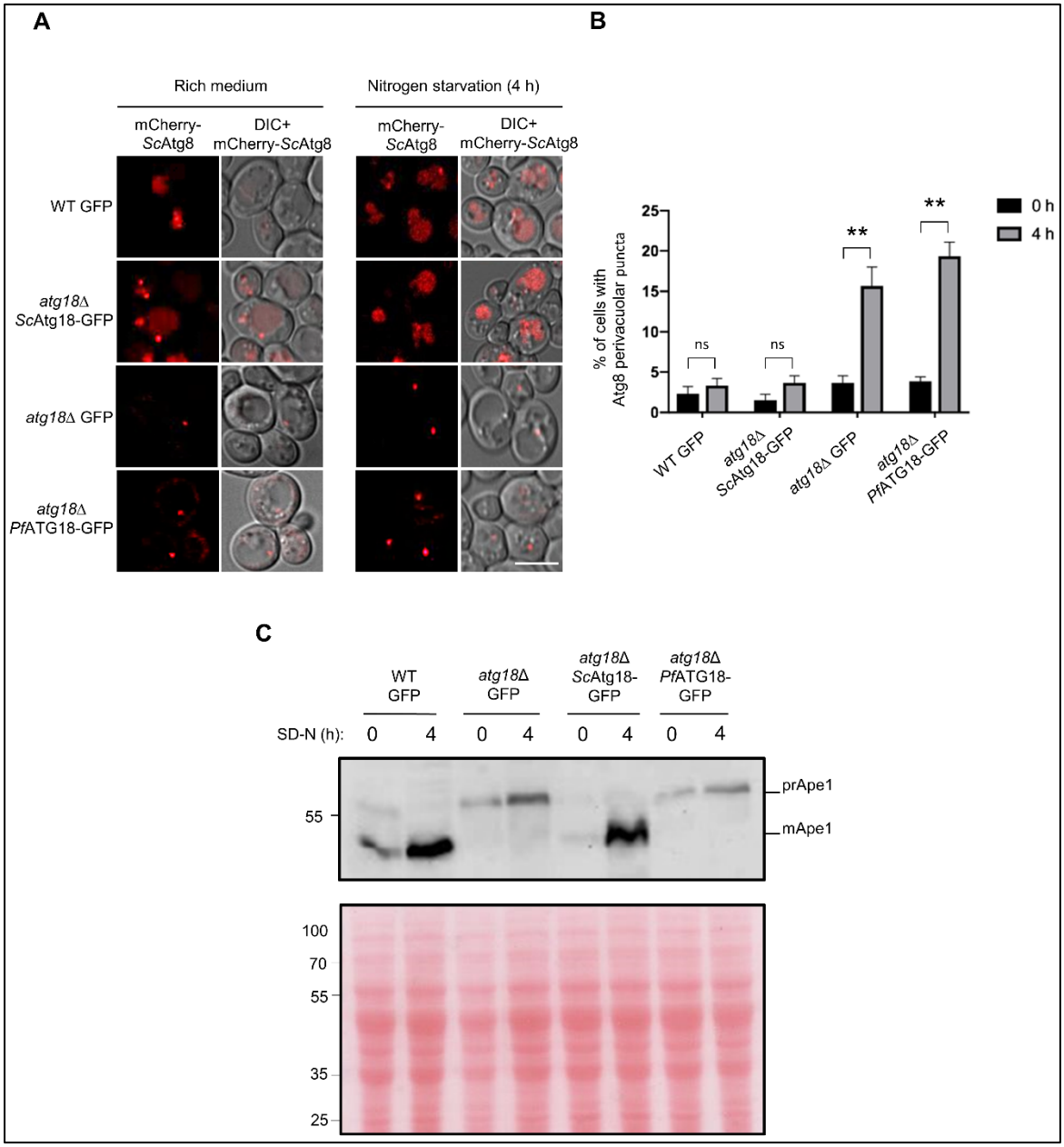

Figure 3.39: *Pf*ATG18-GFP does not complement autophagy functions in *atg18*Δ yeast strain

(A) ATG8 tagged with mCherry (mCherry-*Sc*Atg8) was transformed in yeast strains. Yeast strains were cultured in a nitrogen-deprived medium for 4 h. mCherry-*Sc*Atg8 signal was captured by fluorescence microscopy; N=100 cells, n=3 experiments, Scale bar=5 µm. **(B)** Graph represents the percentage of cells with mCherry-*Sc*Atg8 puncta at the perivacuolar region upon 4 h of nitrogen starvation in indicated yeast strains; N=100 cells, n=3 experiments. Error bar represents ± SEM; ** indicates P<0.005; ns indicates non-significant values higher than P>0.05, analyzed by unpaired Student's *t* test. **(C)** Proteolytic maturation of ApeI was analyzed by western blot using anti-ApeI antibodies (1:5000). Ponceau-stained transferred blot shows that the same amount of proteins from each fraction was resolved by SDS-PAGE. Samples were collected before and after nitrogen starvation of 4 h; n=3 experiments.

3.3.13 *Pf*ATG18-GFP does not localize on the pre-autophagosomal structure in *S. cerevisiae*

ATG18 recruitment at PAS is essential for its autophagic function (Obara *et al.*, 2008). As our results show that *Pf*ATG18-GFP could not restore autophagy in *atg18*Δ cells, we investigated whether *Pf*ATG18-GFP, labelled with mCherry-*Sc*Atg8, could localize at PAS. *Pf*ATG18-GFP was found on the vacuolar membrane and did not exhibit colocalization with mCherry-*Sc*Atg8 in nutrient-rich or starved conditions (Figure 3.40B). *Sc*Atg18-GFP, on the other hand, was present on the vacuolar membrane and as a punctum at a perivacuolar region, which colocalized with mCherry-*Sc*Atg8 in nutrient-rich as well as under starved conditions (Figure 3.40A). This is consistent with previous results (Obara *et al.*, 2008; Rieter *et al.*, 2013). These results demonstrate that *Pf*ATG18-GFP is unable to associate with the PAS.

It has been shown that ATG18-ATG2 complex formation is essential for the recruitment of ATG18 to the PAS (Obara *et al.*, 2008). Loop2 of ATG18 is essential for its interaction with ATG2 in yeast (Rieter *et al.*, 2013). When loop2 amino acids (^{93}TFPTS^{97}) of ATG18 are mutated, the association of ATG18 and ATG2 is completely abolished (Rieter *et al.*, 2013). The sequence alignment of *Sc*Atg18 and *Pf*ATG18 indicates that loop2 is partially conserved in *Pf*ATG18 (Figure 3.41A). To facilitate the interaction of *Pf*ATG18 with yeast ATG2, the residues of *Pf*ATG18 loop2 were swapped with that of *Sc*Atg18 loop2 (^{98}TFSSN^{102} is mutated to ^{98}TFPTS^{102}) by site-directed mutagenesis. Expression of this mutant was confirmed by western blotting, which detected a band at the expected molecular size (Figure 3.41B). Localization of *Pf*ATG18^{TFPTS}-GFP was monitored in nutrient-rich conditions by live cell microscopy and was observed at the vacuolar membrane (Figure 3.41C), indicating that this mutation does not affect vacuolar membrane localization of *Pf*ATG18.

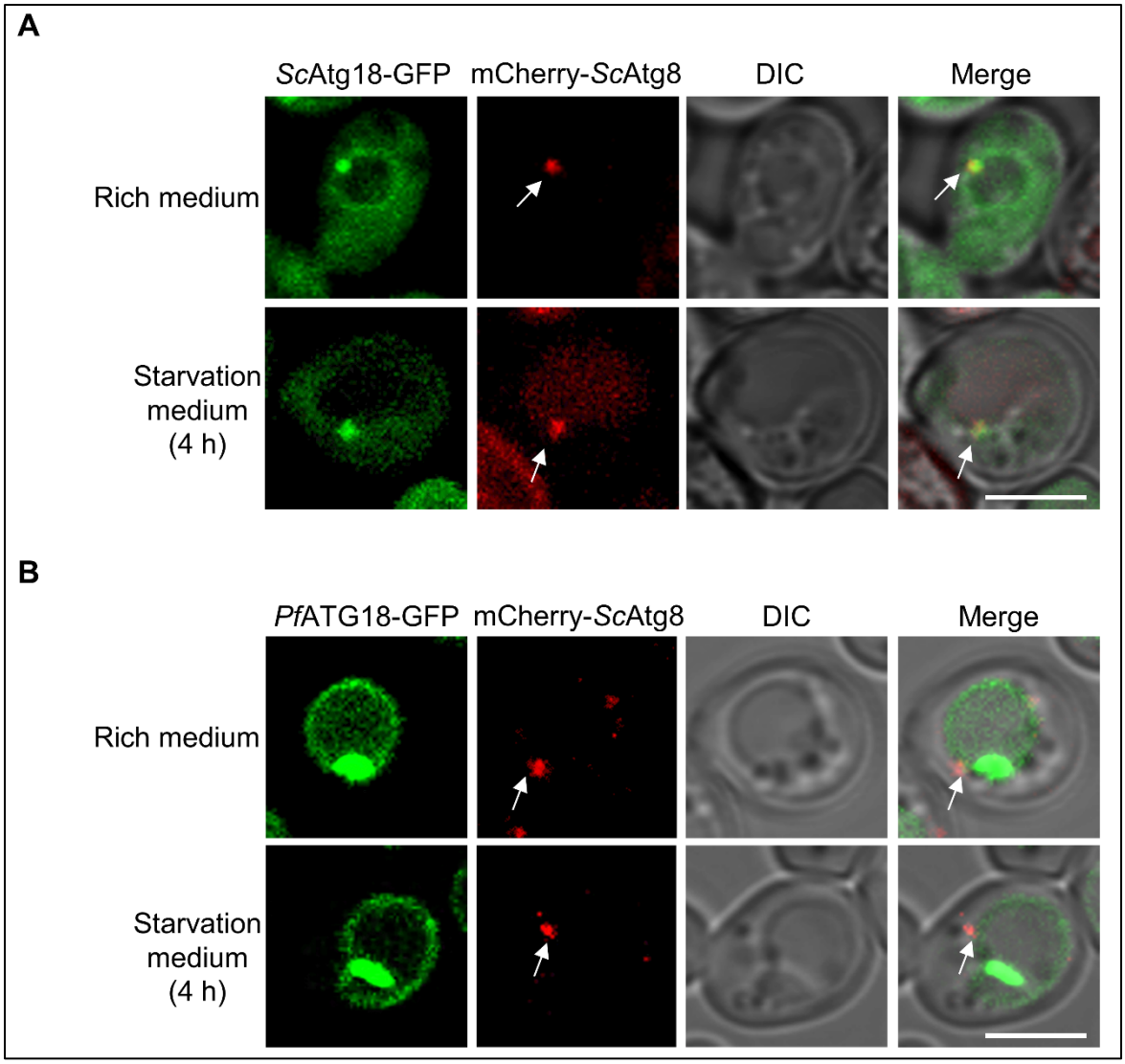

Figure 3.40: *Pf*ATG18-GFP does not localize on the PAS in *atg18*Δ yeast strain

(A) *atg18*Δ strain expressing *Sc*Atg18-GFP and mCherry-*Sc*Atg8 was cultured in a nitrogen-deprived medium for 4 h, and the fluorescence signal was detected by live cell confocal microscopy. Arrows indicate mCherry-*Sc*Atg8 signal at PAS; N=50 cells, n=3 experiments, Scale bar=2 µm. **(B)** *atg18*Δ strain carrying *Pf*ATG18-GFP and mCherry-*Sc*Atg8 was cultured in a nitrogen-deprived medium for 4 h, and the fluorescence signal was detected by live cell confocal microscopy. Arrows indicate mCherry-*Sc*Atg8 signal at PAS; N=50 cells, n=3 experiments, Scale bar=2 µm.

To investigate whether *Pf*ATG18^{TFPTS}-GFP localizes on PAS and could restore autophagy, it was transformed into *atg18*Δ cells, and autophagy assays were carried out. The *atg18*Δ yeast cells expressing *Pf*ATG18^{TFPTS}-GFP were not viable upon long-term starvation as compared to *Sc*Atg18-GFP, as observed by spot assay (Figure 3.38A). Also, mCherry-*Sc*Atg8 signal was observed at PAS in *atg18*Δ yeast cells expressing *Pf*ATG18^{TFPTS}-GFPupon nitrogen starvation (Figure 3.42A). The percentage of cells exhibiting mCherry-

*Sc*Atg8 at PAS was comparable to that of *atg18*Δ yeast cells (Figure 3.42B), suggesting that autophagy was not rescued by this mutant either. Furthermore, *Pf*ATG18^{TFPTS}-GFP did not localize to the PAS (Figure 3.42C), suggesting that the loop2 sequence alone might be insufficient for enabling the recruitment of *Pf*ATG18 to PAS.

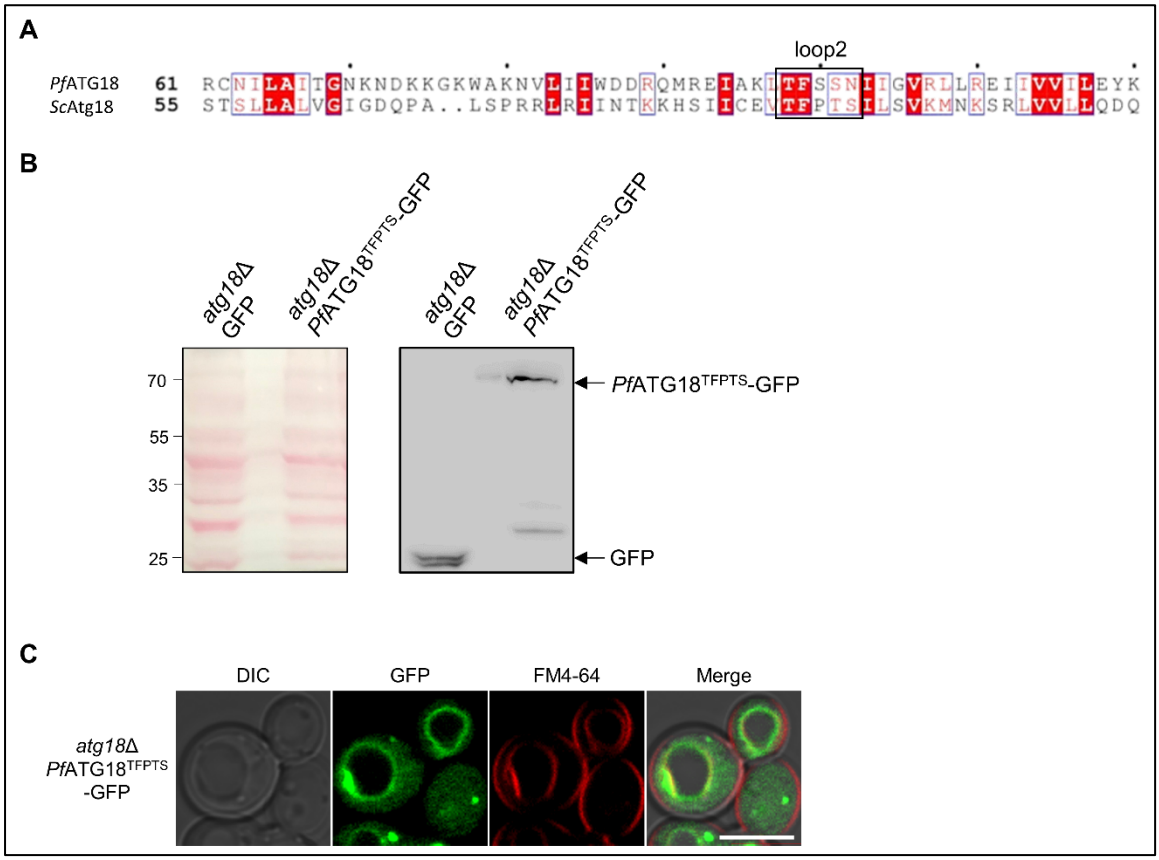

Figure 3.41: *Pf*ATG18^{TFPTS}-GFP localizes on the vacuolar membrane in *atg18*Δ yeast cells

(A) Alignment of the amino acid sequence around loop2 of the β-propeller of ATG18 from *S. cerevisiae* and *P. falciparum*. Amino acid sequences of ScAtg18 and *Pf*ATG18 were aligned using Clustal Omega software and represented using ESPRIPT 3. The conserved residues are in the red box. loop2 is bordered by a box. **(B)** Western blot analysis detected *Pf*ATG18^{TFPTS}-GFP and GFP bands in the lysates of *atg18*Δ yeast strain expressing them. Ponceau-stained transferred blot shows that the same amount of proteins from each fraction was resolved by SDS-PAGE; n=3 experiments. **(C)**The localization of *Pf*ATG18^{TFPTS}-GFP in *atg18*Δ yeast strain was observed by confocal microscopy. Vacuoles in yeast were labelled with lipophilic dye FM4-64; N=100 cells, n=3 experiments, Scale bar=5 µm.

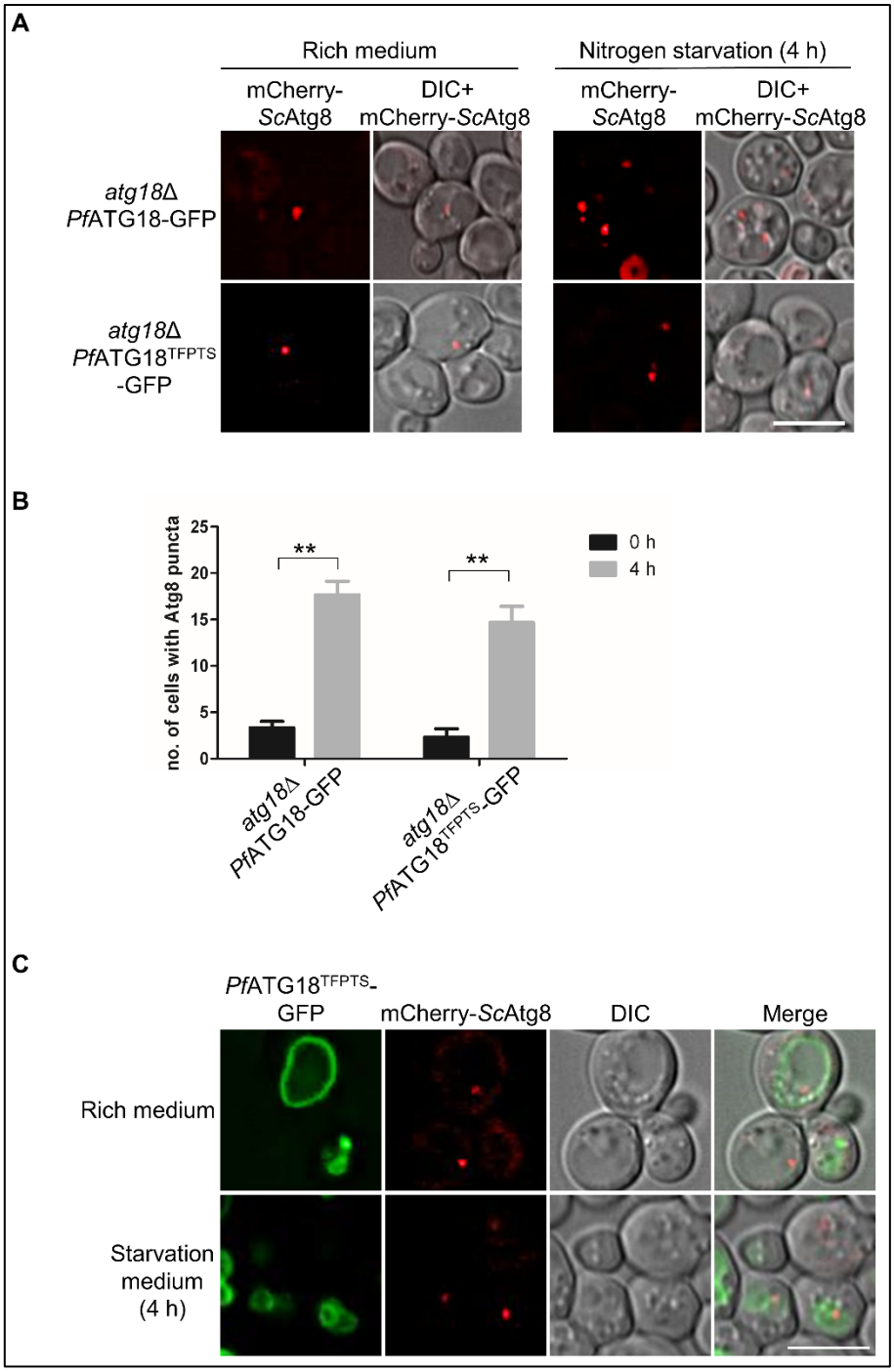

Figure 3.42: *Pf*ATG18^{TFPTS}-GFP does not complement autophagy functions in *atg18*Δ yeast strain

(A) ATG8 tagged with mCherry (mCherry-*Sc*Atg8) was transformed in *atg18*Δ yeast strain expressing *Pf*ATG18-GFP or *Pf*ATG18^{TFPTS}-GFP. Indicated yeast strains were cultured in the nitrogen-deprived medium for 4 h. mCherry-*Sc*Atg8 signal was captured by fluorescence microscopy; N=100 cells, n=3 experiments, Scale bar=5 µm. **(B)** Graph represents the percentage of cells with mCherry-*Sc*Atg8 puncta at a perivacuolar region upon 4 h of nitrogen starvation in indicated yeast strains; N=100 cells, n=3 experiments. Error bar represents ± SEM. ** indicates P<0.005, analyzed by unpaired Student's *t* test. **(C)** *atg18*Δ strain carrying *Pf*ATG18^{TFPTS}-GFP and mCherry-*Sc*Atg8 was cultured in the nitrogen-deprived medium for 4 h and the fluorescence signal was detected by live cell confocal microscopy; N=100 cells, n=3 experiments, Scale bar=5 µm.

Chapter Four

Discussion

Table of Contents

4.1 *ATG* genes expression is upregulated under autophagy-inducing conditions in *P. falciparum*

In the current study, we find that a brief period of nutrient deprivation in *P. falciparum* increases the expression of *ATG* genes. The rationale for brief starvation is that the morphology of the starved parasites remains unchanged and is comparable to that of fed parasites for first 4 h, beyond which they appear shrunken. However, the viability of parasites is not compromised for at least 24 h of starvation.

The *P. falciparum* genome encodes for a limited set of *ATG* genes (Hain and Bosch, 2013; Navale *et al.*, 2014; Cervantes *et al.*, 2014) and the participation of these genes in an autophagy-like pathway is debated. In mammals, nutrient deprivation induces autophagy (Klionsky *et al.*, 2012) and the expression of *ATG* genes (Zhao *et al.*, 2007; Tsuyuki *et al.*, 2014). Consistent with this, our data show that the expression levels of *P. falciparum ATG* genes increase during autophagy-inducing conditions, thereby providing a basis for the participation of these genes in the autophagy-like pathway. We have earlier shown that the protein expression of autophagy marker *Pf*ATG8 and its puncta number increases during brief amino acid starvation in blood stages of *P. falciparum* (Joy *et al.*, 2018). The increase in *PfATG8* gene expression in the present study corroborates with our previous finding (Joy *et al.*, 2018). Besides *PfATG8* gene, we find an increase in relative gene expression of *PfATG1*, *PfVPS34, PfATG18* and *PfATG5* upon starvation.

ATG1 is involved in the initiation of autophagy and receives a signal from the TOR pathway in eukaryotes (Yin *et al.*, 2016). The upregulation of putative *PfATG1* gene indicates that despite the lack of a functional TOR homolog in *P. falciparum* (Navale *et al.*, 2014), initiation of autophagy might occur in the parasite. ATG5 participates in the autophagosome expansion in yeast and mammals (Yin *et al.*, 2016). The increase in relative gene expression of putative *PfATG5* upon amino acid starvation indicates that it may also be involved in autophagy in the parasite. VPS34 produces phospholipid PI3P, which is essential for autophagosome formation in yeast and mammals (Yin *et al.*, 2016). In *P. falciparum*, *Pf*VPS34 synthesizes PI3P (Vaid *et al.*, 2010) and the increase in its mRNA levels upon nutrient deprivation indicates that *Pf*VPS34 might play a similar role in *P. falciparum*. A previous study has shown that *Pf*VPS34 is involved in endocytosis of hemoglobin from the host and its trafficking to the parasite (Vaid *et al.*, 2010). Therefore,

amino acid deprivation may also lead to an increase in endocytosis of hemoglobin from host cytoplasm. In mammals, WIPI1 mRNA levels highly increase during autophagic conditions and is an indicator of autophagosome formation (Tsuyuki *et al.*, 2014). Therefore, the increase in *PfATG18* gene expression in the present study indicates that *Pf*ATG18, a homolog of WIPI1/ATG18, might also be involved in the autophagy-like pathway under nutrient deprivation condition.

Starvation does not increase the expression of putative *PfATG2* (PF3D7_1320000). ATG2 is a binding partner of ATG18 in yeast. Recently, it has been shown that this putative *Pf*ATG2 localizes on the Golgi apparatus and its interaction with *Pf*ATG18 has not been found (Hallée and Richard, 2015; Hallée *et al.*, 2018) which suggests that PF3D7_1320000 might not be a homolog of ATG2. Another study using HMM search identified PF3D7_1346400 as putative *Pf*ATG2, which was also an interacting partner of *Pf*ATG8 (Cervantes *et al.*, 2014). In the future, it would be worth evaluating the mRNA levels of PF3D7_1346400 upon amino acid starvation.

SNAREs such as YKT6 and VAMP8 are involved in late endosome fusion with the lysosome (Pryor *et al.*, 2004; Tai *et al.*, 2004). These proteins are also involved in the fusion of autophagosomes with the lysosome (Wang *et al.*, 2016a). In the current study, these SNAREs, which are not specific to the autophagy-like pathway, are not transcriptionally regulated upon nutrient deprivation in *P. falciparum*. This result is in line with the previous reports that show that the expression levels of YKT6 and VAMP8 do not increase during starvation-induced autophagy conditions in *Drosophila* and mammals. However, the association of these SNAREs with lysosome is rather post-translationally regulated upon autophagy induction (Takáts *et al.*, 2018; Huang *et al.*, 2018).

Our results show that brief amino acid starvation, a widely used autophagy inducer, leads to increase in expression of few *ATG* genes in *P. falciparum*, indicating that these genes are likely to participate in an autophagy-like pathway in the parasite.

4.2 Putative *Pf*ATG5 participates in the autophagy-like pathway in *P. falciparum*

Our characterization of putative *Pf*ATG5 reveals several unique observations. *Pf*ATG5 appears as punctate structures throughout the parasite cytosol and partially colocalize with the autophagy marker *Pf*ATG8 and organelles such as ER and mitochondria, which are known to provide membranes for autophagosome biogenesis (Shibutani and Yoshimori, 2014). IEM study indicates that *Pf*ATG5 is present on double-membrane structures resembling autophagosomes. Additionally, brief starvation results in a transient increase in expression levels as well as puncta-formation of *Pf*ATG5, while inhibition of PI3P production by 3-MA, a known inhibitor of autophagosome formation, results in the reduction of *Pf*ATG5-labelled puncta. Thus, putative *Pf*ATG5 shows similar localization and modulation of puncta number as mammalian ATG5 (Mizushima *et al.*, 2001), supporting our hypothesis of this *ATG* gene participating in the autophagy-like pathway in *P. falciparum*.

In yeast and mammals, ATG5 is conjugated to ATG12 by a covalent bond, which is required for autophagosome elongation and ATG8 lipidation (Hanada *et al.*, 2007). However, in the case of *P. falciparum*, there are few differences compared with the classical ATG5-ATG12 complex found in other organisms. *Pf*ATG5 is about three times longer than its yeast and mammalian counterparts. Although it contains a conserved lysine residue, which has been shown to covalently conjugate with the C-terminal glycine of ATG12, the putative *Pf*ATG12 does not appear to contain the conserved terminal glycine (Navale *et al.*, 2014). A recent report shows that ATG5 and ATG12 do not conjugate covalently in apicomplexans such as *Plasmodium* and *Toxoplasma*; instead, the interaction is non-covalent (Pang *et al.*, 2019).

In the current study, *Pf*ATG5 is found to be associated with vesicular structures in the parasite cytoplasm during all asexual blood stages of the parasite, which is in contrast to other systems, wherein ATG5 associates with membrane only during autophagy (Mizushima *et al.*, 2001). One possible explanation for this constitutive expression could be that *Pf*ATG5 might be required for *Pf*ATG8 lipidation, which is the canonical function of ATG12-ATG5 conjugate in other systems (Hanada *et al.*, 2007). As *Pf*ATG8 always exists in the lipidated form, ATG8-PE, throughout IE stages of the parasite (Kitamura *et al.*, 2012; Mizushima and Sahani, 2014), and non-covalently formed ATG12-ATG5

complex can facilitate ATG8-PE conjugation in *Toxoplasma* and *K. phaffii* (Pang *et al.*, 2019) it seems likely that the recruitment of *Pf*ATG5 might be to augment ATG8 lipidation and contribute in basal autophagy (Joy *et al.*, 2018).

The ATG12-ATG5 conjugate is known to interact with ATG16 to form a functional complex. The latter protein is essential for recruitment of the ATG12-ATG5 complex to the isolation membrane (Mizushima *et al.*, 2003). As ATG16 homolog is not identified by bioinformatics analysis in *P. falciparum* (Navale *et al.*, 2014), the mechanism of membrane association of *Pf*ATG5 is unclear. However, it was shown in yeast, that ATG5 alone could bind to the membrane (Romanov *et al.*, 2012), which could provide a possible explanation for the association of *Pf*ATG5 with the autophagosomal membrane.

At the ultrastructure level, the IEM analysis reveals that *Pf*ATG5 localizes on double-membrane vesicles that are reminiscent of autophagosomes, though, in *P. falciparum*, hemoglobin-containing vesicles are also double-membrane-bound vesicles (Milani *et al.*, 2015). Since *Pf*ATG5 is found to colocalize with autophagy marker protein *Pf*ATG8, which has been previously shown to localize on double-membrane structures (Tomlins *et al.*, 2013), it is suggestive that *Pf*ATG5 is also present on autophagosome-like structures in this parasite. Additionally, *Pf*ATG5 appears to localize on autophagosome-like structures during its fusion with FV in the parasite by IEM. In mammalian cells, ATG5 is reported to be required for fusion of the mature autophagosome with the lysosome by interacting with TECRP1, a tethering protein found on the lysosomal membrane (Chen *et al.*, 2012; Tekirdag *et al.*, 2013). Based on our current observations, we speculate that *Pf*ATG5 might also be involved in autophagosome fusion with FV in *P. falciparum*.

Our results demonstrate that in addition to autophagosome-like structures, *Pf*ATG5 is also observed on other organelles such as ER, apicoplast and mitochondrion. In mammals, ER and mitochondria contribute membrane for autophagosome biogenesis (Mizushima *et al.*, 2001; Suzuki *et al.*, 2007; Shibutani and Yoshimori, 2014). Moreover, autophagosome biogenesis occurs at the contact site of ER and mitochondria, where ATG5 has been reported to localize (Hamasaki *et al.*, 2013). Based on these findings and our current observation, we postulate that ER, apicoplast, and mitochondrion may contribute membrane for autophagosome expansion in *P. falciparum*.

In eukaryotes, the number of autophagosomes and autophagic flux increase during nutrient deprivation, while they decrease during inhibition of autophagosome biogenesis by inhibitors such as 3-MA (Mizushima *et al.*, 2010). The modulation of *Pf*ATG5 puncta number under autophagy-inducing and -inhibiting conditions is in accordance with the change observed in mammalian ATG5 (Mizushima *et al.*, 2001), further indicating that *Pf*ATG5 participates in the autophagy-like pathway in *P. falciparum*.

In conclusion, our observations suggest that *Pf*ATG5 is a component of autophagy machinery and can be used as a biomarker for autophagosome formation in *P. falciparum*.

4.3 *Pf*ATG18 participates in food vacuole fission and the autophagy-like pathway in *P. falciparum*

Our studies uncover the role of *Pf*ATG18 in food vacuole dynamics, not reported earlier. We show that *Pf*ATG18-GFP expression in yeast lacking *Sc*Atg18 restores the wild-type vacuolar morphology by complementing *Sc*Atg18 vacuolar fission function. Notably, *Pf*ATG18-GFP demonstrates similar aspects of food vacuole dynamics in *P. falciparum*. Additionally, this study provides experimental evidence for the participation of *Pf*ATG18 in the autophagy-like pathway and can be modulated by brief starvation. *Pf*ATG18 colocalizes with autophagy marker proteins *Pf*ATG8 and *Pf*ATG5 in nutrient rich as well as starved conditions. Further, the role of *Pf*ATG18 in the autophagy-like pathway is independent of its function in apicoplast biogenesis, as its localization on autophagosome-like structures is not affected by the absence of apicoplast. *Pf*ATG18 might function upstream of *Pf*ATG8 since *Pf*ATG8 knockdown does not affect *Pf*ATG18 localization. Furthermore, we characterized the trafficking of *Pf*ATG18 to food vacuole and found that *Pf*ATG18 employs the hemoglobin uptake pathway.

*Pf*ATG18 is being detected at multiple sites in the parasite, such as on the food vacuole membrane, hemoglobin-containing vesicles (HcVs), apicoplast and also as puncta on autophagosome-like structures. It is known that yeast ATG18 localizes at multiple subcellular locations, such as PAS, vacuole, and endosomes (Guan *et al.*, 2001; Dove *et al.*, 2004; Krick *et al.*, 2008) and performs discrete functions at these sites. The vacuolar localization of *Sc*Atg18 requires its interaction with phosphoinositides PI3P and PI(3,5)P_2 (Dove *et al.*, 2004; Krick *et al.*, 2006). Our data from yeast show that the localization of *Pf*ATG18-GFP on the vacuolar membrane is dependent only on PI3P and not on PI(3,5)P_2

interaction, as opposed to *Sc*Atg18, which requires both phospholipids. In addition to this, we demonstrate that the subcellular localization of *Pf*ATG18 in *P. falciparum* is mediated by its interaction with PI3P. *Pf*ATG18 is enriched on organelles or vesicles, which contain PI3P; for instance, food vacuole and apicoplast (Tawk *et al.*, 2010). Similarly, autophagosomes in other organisms like yeast and mammals are also PI3P-rich vesicles (Yin *et al.*, 2016). Taken together, it is evident that PI3P is essential for the subcellular localization of *Pf*ATG18.

In yeast, ATG18 localization to the phosphoinositides-enriched subcellular compartments is governed by organelle-specific factors and post-translational modifications. For instance, ATG18 localization on PAS depends upon PI3P as well as on ATG2 (Obara *et al.*, 2008). Similarly, the recruitment of ATG18 at the vacuolar membrane is controlled by phosphoregulation. The dephosphorylated ATG18 associates with the vacuolar membrane and disassociates upon phosphorylation (Tamura *et al.*, 2013). Since few *Pf*ATG18 puncta do not colocalize with PI3P within the parasite, we speculate that the recruitment of *Pf*ATG18 might be not only dependent on PI3P but also require organelle-specific proteins or post-translational modifications to provide spatial and temporal regulation for organelle localization as shown in yeast.

Our comprehensive studies show that *Pf*ATG18-GFP expression in yeast lacking *Sc*Atg18 not only restores the vacuolar morphology but also participates in the vacuolar fission. Our findings are consistent with previous reports, which show that ATG18 is directly associated with the vacuolar morphology and fission (Efe *et al.*, 2007; Krick *et al.*, 2008; Zieger and Mayer, 2012; Michaillat and Mayer, 2013; Tamura *et al.*, 2013; Gopaldass *et al.*, 2017). Additionally, ATG18 is a scission-specific Fab1 effector protein that mediates vacuole fission in yeast (Efe *et al.*, 2007; Gopaldass *et al.*, 2017). Since *Pf*ATG18-GFP could mediate vacuole fission in yeast, thus indicates that this protein has a conserved membrane scission property.

Importantly, these observations with *Pf*ATG18 could be recapitulated in wild-type *P. falciparum,* indicating that *Pf*ATG18 is involved in the FV fission. Notably, we show that the FV in *P. falciparum* undergoes cycles of fission and fusion – a previously uncharacterized food vacuole dynamics. In general, vacuole fission and fusion are required for rapid readjustment of vacuole surface-to-volume ratio during cell cycle progression and in response to osmotic stress (Zieger and Mayer, 2012; Desfougères *et al.*, 2016). As the

size of FV varies in different developmental stages (Dluzewski *et al.*, 2008), FV fission and fusion might be required for restoring its surface-to-volume ratio to prevent the collapse of FV membrane and maintain vacuolar homeostasis. Given the importance of FV in the biology of the parasite for hemoglobin degradation and hemozoin polymerization (Wunderlich *et al.*, 2012), the maintenance of its homeostasis is critical for parasite survival and thus may serve as a crucial drug target.

Multilobed FV observed in this study has also been previously reported and has been referred to as secondary- or extra-FV (Bakar *et al.*, 2010; Ehlgen *et al.*, 2012). However, it was unclear whether these vesicles are formed because of failure in fusion with the existing FV or by the pinching-off from the FV (Bakar *et al.*, 2010; Ehlgen *et al.*, 2012). With time-lapse microscopy using LysoTracker Red DND99 and *Pf*ATG18-GFP as FV markers, we demonstrate that multilobed FVs are generated by fission. $PI(3,5)P_2$ is a central player in the vacuole fission in yeast and mammalian cells (Efe *et al.*, 2007; Choy *et al.*, 2018), but as $PI(3,5)P_2$ is not generated in *P. falciparum* (Tawk *et al.*, 2010), the parasite FV fission seems to be independent of $PI(3,5)P_2$.

We also show that the parasite FV fission is induced upon treatment with cysteine protease inhibitors MG132, E64d, and ALLN. Based on this observation, we hypothesize that the accumulation of undegraded hemoglobin in FV, due to the inhibition of proteases, leads to macromolecular crowding, which eventually results in enhanced FV fission. This perhaps facilitates the maintenance of optimum macromolecular concentration needed for organelle function. The precedence for such a possibility arises from studies that have suggested that macromolecular crowding influences activities of many proteins in the organelle lumen (Zhou *et al.*, 2008), and equilibrium of macromolecular concentration can be restored by vacuole fission (Desfougères *et al.*, 2016). Additionally, it has been reported that MG132-treated parasites induce stress response proteins, including *Pf*ATG18, as revealed by quantitative global proteomic analysis (Rathore *et al.*, 2015). As in the present study, we show that MG132 treatment results in an increase in FV fragmentation with enrichment of *Pf*ATG18-GFP at the interface of multilobular vacuoles, we suggest that increase in *Pf*ATG18 expression upon MG132 treatment (Rathore *et al.*, 2015) corresponds to increased vacuole fission. Additionally, since we could observe food vacuole fission and fusion using *Pf*ATG18-GFP, we propose that it can be used as a biomarker for analyzing FV dynamics.

Our data indicate that *Pf*ATG18 is trafficked to FV via HcVs. It is known that WIPI1 localizes on endosomes in mammalian cells and facilitates in the biogenesis lysosome-like organelles melanosomes (Jeffries *et al.*, 2004; Ho *et al.*, 2011). Also, in yeast, a pool of ATG18 is found on the endosomes (Krick *et al.*, 2008; Obara *et al.*, 2008), although, its function on endosomes is unclear. In parasites, we show that *Pf*ATG18 is present on HcVs, this result corroborates with the endosomal localisation of ATG18 in yeast and mammals. As *Pf*PI3K is essential for the trafficking of hemoglobin to the FV (Vaid *et al.*, 2010), it is possible that *Pf*ATG18 being an effector of PI3P might also have a role in hemoglobin trafficking. Although, at this point, we do not know whether *Pf*ATG18 is merely trafficked by these vesicles or it has a role in the hemoglobin trafficking or FV biogenesis.

Our studies also demonstrate the involvement of *Pf*ATG18 in the autophagy-like pathway. In addition to being localized on *Pf*ATG8-positive autophagosome-like structures, the levels of *Pf*ATG18 mRNA and protein increase upon autophagy-inducing conditions. In general, autophagosomes are ATG18/WIPI and ATG8 positive structures (Polson *et al.*, 2010; Rieter *et al.*, 2013) and increase in WIPI1 expression represents induction of autophagosome-formation (Polson *et al.*, 2010; Tsuyuki *et al.*, 2014; Proikas-Cezanne *et al.*, 2015). Our results reflect a similar trend in case of *Pf*ATG18, indicating that it is involved in the autophagy-like pathway in *P. falciparum*. This finding is also in accordance with our studies published recently, which show that autophagy marker proteins *Pf*ATG8 and *Pf*ATG5 are present on autophagosome-like structures and their expression levels can be modulated by autophagy inducer and inhibitor such as starvation and 3-MA (Joy *et al.*, 2018).

*Pf*ATG8 partially localises on apicoplast and is essential for apicoplast biogenesis (Kitamura *et al.*, 2012; Tomlins *et al.*, 2013; Cervantes *et al.*, 2014; Walczak *et al.*, 2018). In the apicoplast-minus parasites, *Pf*ATG8 is present on foci containing apicoplast-targeted proteins (Cervantes *et al.*, 2014). Apart from *Pf*ATG8, *Pf*ATG18 is also shown to be involved in apicoplast biogenesis (Bansal *et al.*, 2017), but unlike *Pf*ATG8, mislocalisation of *Pf*ATG18 in apicoplast-minus parasites was not observed. Instead, *Pf*ATG18 maintained its localisation on FV and autophagosome-like structures in these parasites. Thus, we suggest that the participation of *Pf*ATG18 in FV fission and the autophagy-like pathway is independent of its role in apicoplast biogenesis (Bansal *et al.*, 2017). This result was also corroborated in the *Pf*ATG8 deficient cells where autophagosome-like structures labelled

with *Pf*ATG18 and *Pf*ATG5 were observed upon removal of the apicoplast. The autophagosome formation in *Pf*ATG8 knockdown parasites is consistent with the previous report showing that autophagosomes are formed in LC3/GABARAPs, mammalian orthologs of Atg8, knockout cells (Nguyen *et al.*, 2016). Also, our result suggests that *Pf*ATG18 might function upstream of *Pf*ATG8, which is also the case in yeast and mammalian system where knockout of ATG18/WIPI results in decreased autophagosomal localisation of ATG8/LC3 (Polson *et al.*, 2010; Nair *et al.*, 2010; Nagy *et al.*, 2014). In *T. gondii*, two homologs of ATG18 are present which performs two independent functions: one is essential for parasite development for the apicoplast biogenesis (Bansal *et al.*, 2017; Nguyen *et al.*, 2018) and the other seems to be crucial during cell stress and has a role in canonical autophagy (Nguyen *et al.*, 2018). As *Plasmodium* has only one ATG18 homolog, this protein might participate in both autophagy-like as well as autophagy-independent pathways. In general, ATG18 is required for targeting ATG2 to the PAS (Obara *et al.*, 2008); together they are involved in ATG9 trafficking (Reggiori *et al.*, 2004) and providing lipid for autophagosome biogenesis (Kotani *et al.*, 2018; Valverde *et al.*, 2019). The autophagosome biogenesis in *P. falciparum* might also require these players. We have shown the involvement of *Pf*ATG18 in autophagy-like pathway in the parasite, however, its association with the putative *Pf*ATG2 (PF3D7_1346400) remains to be elucidated.

Although *Pf*ATG18-GFP was able to rescue vacuole fission and morphology in yeast, it did not participate in autophagy when expressed in *atg18*Δ yeast cells. This observation can be explained by the differential requirements for ATG18 functions in vacuole fission and autophagy. ATG18 must interact with ATG2 to form an ATG18-ATG2 complex, which is targeted to the PAS by binding to PI3P (Obara *et al.*, 2008). The ATG2-ATG18 interaction is necessary for autophagy, however ATG2-AtG18 binding is dispensable for vacuole fission (Gopaldass *et al.*, 2017). Since *Pf*ATG18-GFP could not localize on the PAS in *atg18*Δ cells, we speculate that *Plasmodium* ATG18 is unable to interact with yeast ATG2 and therefore might not be able to complement autophagy in *atg18*Δ yeast.

*Pf*ATG8 partially localises on apicoplast and is essential for apicoplast biogenesis (Kitamura *et al.*, 2012; Tomlins *et al.*, 2013; Cervantes *et al.*, 2014; Walczak *et al.*, 2018). Its localisation is disrupted in the apicoplast-minus parasites and is present on vesicles containing apicoplast-targeted proteins (Cervantes *et al.*, 2014). Apart from *Pf*ATG8, autophagy-related protein *Pf*ATG18 is also shown to be involved in apicoplast biogenesis

(Bansal *et al.*, 2017). Unlike *Pf*ATG8, disruption of *Pf*ATG18 localisation in apicoplast-minus parasites was not observed. Instead, *Pf*ATG18 maintained its localisation on FV and autophagosome-like structures in these parasites. Thus, we suggest that the participation of *Pf*ATG18 in FV fission and autophagy-like pathway is independent of its role in apicoplast biogenesis (Bansal *et al.*, 2017).

Through this study, we show the role of *Pf*ATG18 in two distinct pathways, namely autophagy and maintenance of vacuolar homeostasis. It is crucial now to identify how a point mutation in *Pf*ATG18 confers resistance to artemisinin, an antimalarial, in *P. falciparum* (Wang *et al.*, 2016b). The known mechanism of artemisinin resistance is an increase in PI3P lipid levels (Mbengue *et al.*, 2015), which results in unfolded protein response and promotes proteostasis to alleviate artemisinin-induced cell death (Suresh and Haldar, 2018). However, the PI3P binding proteins involved in this resistance mechanism are still not elucidated. *Pf*ATG18 is known effector of PI3P and its localization is affected by artemisinin treatment. While it has been reported that *Pf*ATG18 puncta-formation increases in artemisinin-resistant strain upon DHA treatment (Breglio *et al.*, 2018), it would be vital to understand whether *Pf*ATG18 provides resistance to the parasite against artemisinin via its role in autophagy or vacuole homeostasis, in order to develop antimalarial that can synergistically inhibit artemisinin-resistant parasite growth. A straightforward approach would be to introduce *PfATG18* point mutation in wild-type parasite and determine the involvement of autophagy pathway in conferring resistance by assessing *Pf*ATG8 puncta number upon artemisinin treatment in the presence and absence of autophagy inhibitor 3-MA. In parallel, the binding of mutant *Pf*ATG18 to the membrane and vacuolar dynamics in the mutant strain needs to be analysed.

In-depth studies are needed to dissect the molecular details of functions of *Pf*ATG18 in this important apicomplexan to explore the possibility of developing therapeutics.

4.4 Conclusions

This work has attempted to study the involvement of the putative *P. falciparum* ATG proteins in the autophagy-like pathway in the malaria parasite. We have functionally characterized the putative *Pf*ATG5 and *Pf*ATG18 in *P. falciparum*. Our study establishes the participation of *Pf*ATG5 and *Pf*ATG18 in the autophagy-like pathway. Further, we

show here that FV in the parasite undergoes fission and fusion and *Pf*ATG18 as one of the players of FV fission in this parasite.

We find that upon autophagy-inducing conditions, the expression of several *P. falciparum ATG* genes including *PfATG5* and *PfATG18* increases in the malaria parasite. *Pf*ATG5 is constitutively expressed throughout the IE cycle of the parasite and is present on autophagosome-like structures, even during nutrient-rich conditions. Partial colocalization of *Pf*ATG5 with ER, mitochondria and apicoplast indicate that these organelles might contribute membrane for autophagosome biogenesis. Further, we demonstrate that *Pf*ATG5 is a component of the autophagy machinery in the parasite, as its expression is modulated by canonical autophagy inducer and inhibitor (Figure 4.1).

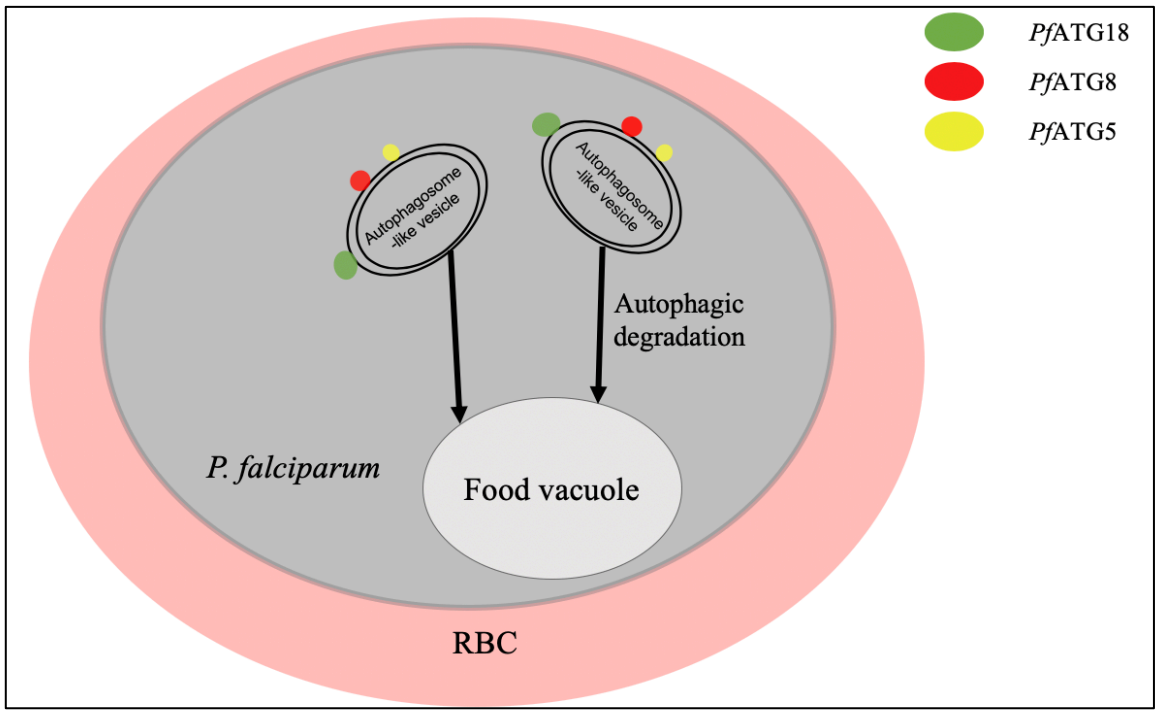

Figure 4.1: *Pf*ATG5 and *Pf*ATG18-GFP participates in the autophagy-like pathway in IE stages of *P. falciparum*

A schematic model summarizing the participation of *Pf*ATG5 (yellow) and *Pf*ATG18 (green) in the autophagy-like pathway in IE of *P. falciparum*. *Pf*ATG5 and *Pf*ATG18 colocalize with *Pf*ATG8 (red) on autophagosome-like structures. *Pf*ATG18 associates with the vesicular structures by binding with phospholipid PI3P via FRRG motif. The expression of *Pf*ATG5 and *Pf*ATG18 increases upon autophagy-inducing conditions correlating with the induced autophagosome formation.

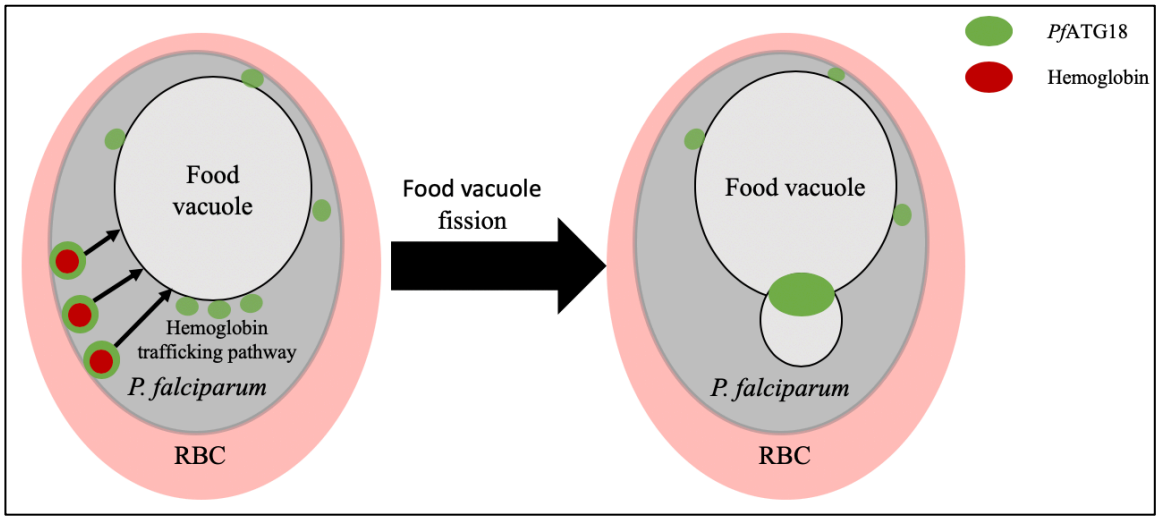

Figure 4.2: *Pf*ATG18 traffics to the food vacuole by hemoglobin trafficking pathway and participates in food vacuole fission in IE stages of *P. falciparum*

A schematic model summarizing the trafficking pathway of *Pf*ATG18 (green) to the FV and its participation in FV fission in IE stages of *P. falciparum*. *Pf*ATG18 localizes on hemoglobin-containing vesicles (red) and traffics to the FV via hemoglobin trafficking pathway. *Pf*ATG18 associates with the FV by binding with phospholipid PI3P via FRRG motif and participate in FV fission.

*Pf*ATG18 appears to perform multiple functions in the malaria parasite. Our studies suggest that it performs its conserved roles in both autophagy-like pathway and FV dynamics as in yeast and mammals, besides apicoplast biogenesis. *Pf*ATG18 is present on vesicular structures resembling autophagosome along with *Pf*ATG5 and *Pf*ATG18 (Figure 4.1). *Pf*ATG18 appears to be a part of *P. falciparum* autophagy machinery as its expression is increased during starvation. Unprecedentedly, we demonstrate that the FV in *P. falciparum* undergoes rounds of fission and fusion. We provide evidence for the involvement of *Pf*ATG18 in the FV fission in parasites (Figure 4.2). *Pf*ATG18 appears to utilize hemoglobin transport pathway to traffic to the FV membrane and associates with the membrane by binding to PI3P via FRRG motif (Figure 4.2).

Appendices

Appendix 1: Multiple sequence alignment between *Pf*ATG5, *Hs*ATG5 and *Sc*Atg5

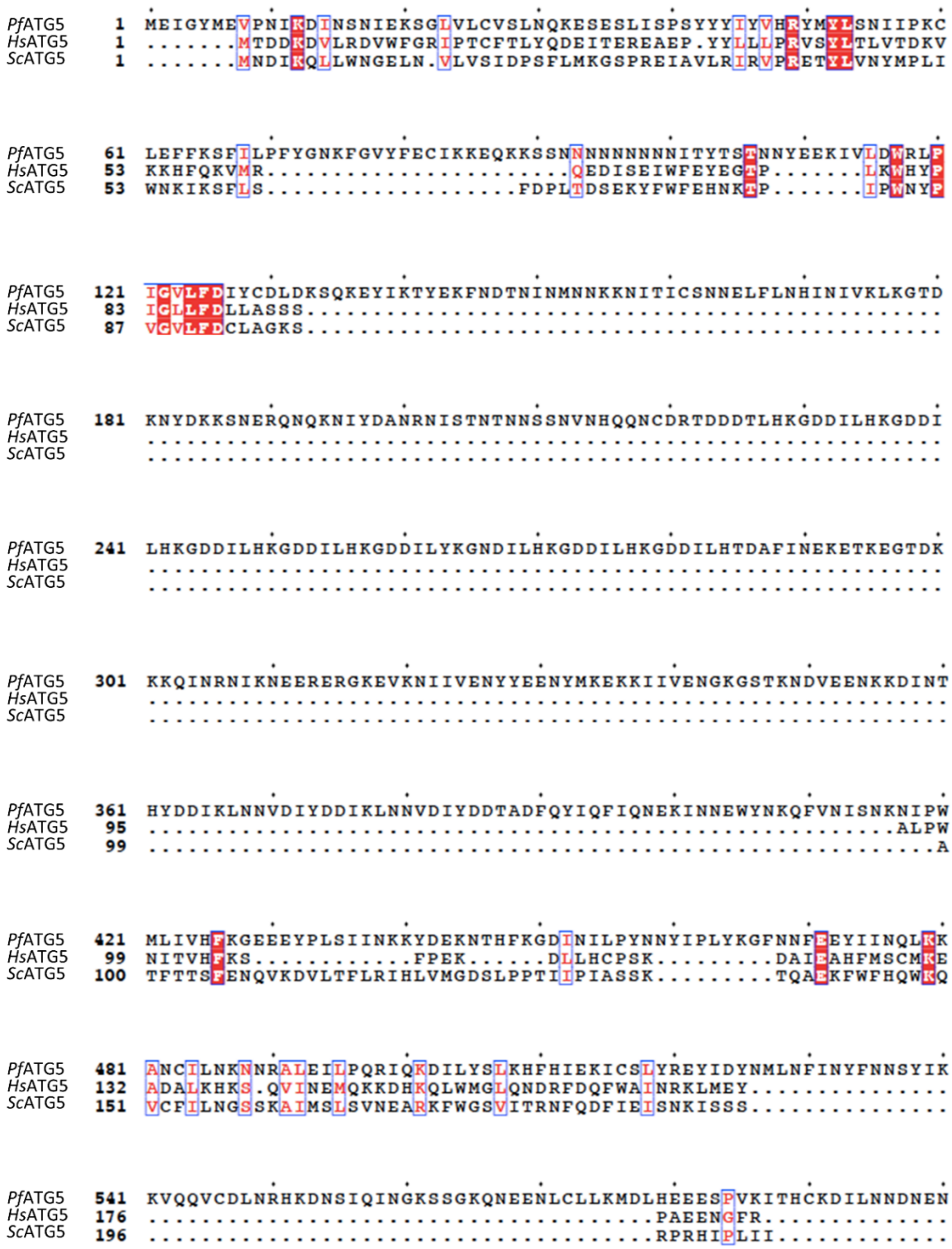


PfATG5 601 YDNENNNNENNNEHNCHRNSYDVHLNENFINDQSQKNHISNIRTSYNNDHVSDSLQTDIQ
HsATG5
ScATG5
PfATG5 661 NDFSSIILENTKEQGDHINFKNNLHNNEKYPNVYDILKDEKVLKDCPIILHIYGPPYNQI
HsATG5 184 YIPFR IY QT
ScATG5 205 QT
PfATG5 721 LTKYPFLKLIHSNNNNNNNNNDNKDNNNNSNKYDGCKKYIQNVHLNTLGDFLHEQLPSFV
HsATG5 193 TTERPFIQKLFRPVAADG QLHTLGDLLKEVCP...
ScATG5 207 SRTSGTFRISQPTISMTG VNPTLKDIEG...
PfATG5 781 RKIINKDEKNETSHILNKYDKDKYLNSETIYYFIEDDYLIFSPYMFIIVNGIQIPLNTPL
HsATG5 225 .SAIDPEDGEKKNQ VMIHGIEPMLETPL
ScATG5 235 .DILDVKEGINGND VMVICQGIEIPWHMLL
PfATG5 841 YWLAANFSQFDHFLHITIRIPPY
HsATG5 252 QWLSEHLSYPDNFLHISIIPQPTD
ScATG5 264 YDLYSKLRSFDGFLYITLVPIKGGDKASSEL

Appendix 2: Codon optimized sequence of *Pf*ATG18 gene

AAGCTTGGTACCTCTAGAATGGACTACAAAGACGATGACGACAAGATGGTTT
CTTTGAGATTAGATAACAACAGATACATTTCTTTTAATCAAGATTACGGTTGT
TTGTGTATGGCTAACGAAAAGGGTTTTAAAATATATAACACAAACCCTTTTAC
TCAAACATATTCAAGAGATTTGACTGATAGAAATAAGAACGGTTTGTATTTGG
CTGAAATGTTGTACAGATGTAACATCTTGGCAATCACAGGTAATAAGAACGA
TAAGAAAGGTAAATGGGCTAAAAATGTTTTGATTATTTGGGATGATAGACAA
ATGAGAGAAATCGCAAAATTGACTTTTTCTTCAAATATTATTGGTGTTAGATT
GTTAAGAGAAATCATCGTTGTTATTTTGGAATACAAATTGTGTATCTATAGAT
TGAAAGATATTATTTTGTTAGAAACTTTAAATACTTCTAAAAATGTTTCTGGTT
TGTGTTGTTTGTCTAACATCGATAAGAACATCATCATTGCTTATTTGTCACCAA
TTAAAGGTAGAGTTAACATCCATATCTTCGAAATTAATTCTTCAGAAAATATT
CATGAAGAATTGCCATACATCAACTTCAAGACAAATTTGTCAATCTATGCACA
TGATAACTCTATCGGTTGTATCAATTTGTCAAACGATGGTAAATTGTTAGTTA
CTTCTTCAACAAAAGGTACTATCATCAGATTGTTTAATACATTCGATGGTACT
TTGTTGAACGAGTTTAGAAGAGGTACTAAAAATGCTAAAATTTTGTCATTAAA
CATTTCTGAAGATAATAATTGGTTGTGTTTGACATCTTCAAGAAACACTGTTC
ATGTTTTCTCTATCTATAAAAAGAAAAGACCATTGAGAAAGGTTGATATTATT
TGTAAGGGTAAAAATGTTTCTCCACCAGCATTGTTGAACTACGAAAAGGAAT
CTAAAAATAAGAAATCTTCTTTGAAGTGTTTGTTACCATGTCATCCATACTTA
AATTCTGAATGGTCATTTGCTTCTTACAAATTGCCAGGTAAAAAGATTTCTTC
TATTTGTGCATTTGTTAACGATCAAAACTGTATCATCGTTATTTGTTCTAATGG
TATTATCTATAAATTGAGATTCAATGAACATATCGGTGGTGACATGTTCAAAA
TTTCTTCACATTCATTTGATGGATCCCCTAGGCTCGA

References

Alaganan, A., Singh, P., and Chitnis, C.E. (2017) Molecular mechanisms that mediate invasion and egress of malaria parasites from red blood cells. *Current Opinion in Hematology* **24**(3), 208–214.

Alvarez, V.E., Kosec, G., Sant'Anna, C., Turk, V., Cazzulo, J.J., and Turk, B. (2008) Autophagy is involved in nutritional stress response and differentiation in *Trypanosoma cruzi*. *Journal of Biological Chemistry* **283**(6), 3454–3464.

Ansorge, I., Benting, J., Bhakdi, S., and Lingelbach, K. (1996) Protein sorting in Plasmodium falciparum-infected red blood cells permeabilized with the pore-forming protein streptolysin O. *Biochemical Journal* **315**(1), 307–314.

Atkinson, C.T., Aikawa, M., Aley, S.B., and Hollingdale, M.R. (1989) Expression of Plasmodium berghei circumsporozoite antigen on the surface of exoerythrocytic schizonts and merozoites. *American Journal of Tropical Medicine and Hygiene* **41**(1), 9–17.

Autino, B., Noris, A., Russo, R., and Castelli, F. (2012) Epidemiology of malaria in endemic areas. *Mediterranean Journal of Hematology and Infectious Diseases* **4**(1), e2012060.

Babbitt, S.E., Altenhofen, L., Cobbold, S.A., Istvan, E.S., Fennell, C., Doerig, C., *et al.* (2012) Plasmodium falciparum responds to amino acid starvation by entering into a hibernatory state. *Proceedings of the National Academy of Sciences of the United States of America* **109**(47), E3278–E3287.

Bakar, N.A., Klonis, N., Hanssen, E., Chan, C., and Tilley, L. (2010) Digestive-vacuole genesis and endocytic processes in the early intraerythrocytic stages of Plasmodium falciparum. *Journal of Cell Science* **123**(Pt 3), 441–450.

Balla, T. (2013) Phosphoinositides: Tiny Lipids With Giant Impact on Cell Regulation. *Physiological Reviews* **93**(3), 1019–1137.

Banerjee, R., Liu, J., Beatty, W., Pelosof, L., Klemba, M., and Goldberg, D.E. (2002) Four plasmepsins are active in the Plasmodium falciparum food vacuole, including a protease with an active-site histidine. *Proceedings of the National Academy of Sciences of the United States of America* **99**(2), 990–995.

Bannister, L., and Mitchell, G. (2003) The ins, outs and roundabouts of malaria. *Trends in Parasitology* **19**(5), 209–213.

Bannister, L.H., Hopkins, J.M., Fowler, R.E., Krishna, S., and Mitchell, G.H. (2000) A brief illustrated guide to the ultrastructure of Plasmodium falciparum asexual blood stages. *Parasitology Today* **16**(10), 427–433.

Bansal, P., Tripathi, A., Thakur, V., Mohmmed, A., and Sharma, P. (2017) Autophagy-related protein ATG18 regulates apicoplast biogenesis in apicomplexan parasites. *MBio* **8**(5), e01468-17.

Bars, R. Le, Marion, J., Borgne, R. Le, Satiat-Jeunemaitre, B., and Bianchi, M.W. (2014) ATG5 defines a phagophore domain connected to the endoplasmic reticulum during autophagosome formation in plants. *Nature Communications* **5**(1), 4121.

Barth, H., Meiling-Wesse, K., Epple, U.D., and Thumm, M. (2001) Autophagy and the cytoplasm to vacuole targeting pathway both require Aut10p. *FEBS Letters* **508**(1), 23–28.

Baskaran, S., Ragusa, M.J., Boura, E., and Hurley, J.H. (2012) Two-site recognition of phosphatidylinositol 3-phosphate by PROPPINs in autophagy. *Molecular Cell* **47**(3), 339–348.

Bates, P.A., and Rogers, M.E. (2004) New insights into the developmental biology and transmission mechanisms of Leishmania. *Current Molecular Medicine* **4**(6), 601–9.

Beri, D., Balan, B., and Tatu, U. (2018) Commit, hide and escape: the story of *Plasmodium* gametocytes. *Parasitology* **145**(13), 1772–1782.

Besteiro, S. (2012) Which roles for autophagy in Toxoplasma gondii and related apicomplexan parasites? *Molecular and Biochemical Parasitology* **184**(1), 1–8.

Besteiro, S., Brooks, C.F., Striepen, B., and Dubremetz, J.-F. (2011) Autophagy protein Atg3 is essential for maintaining mitochondrial integrity and for normal intracellular development of Toxoplasma gondii tachyzoites. *PLoS Pathogens* **7**(12), e1002416.

Besteiro, S., Williams, R.A.M., Morrison, L.S., Coombs, G.H., and Mottram, J.C. (2006) Endosome sorting and autophagy are essential for differentiation and virulence of Leishmania major. *Journal of Biological Chemistry* **281**(16), 11384–11396.

Bhattacharjee, S., Stahelin, R. V, Speicher, K.D., Speicher, D.W., and Haldar, K. (2012) Endoplasmic reticulum PI(3)P lipid binding targets malaria proteins to the host cell.

Cell **148**(1–2), 201–212.

Biagini, G.A., Bray, P.G., Spiller, D.G., White, M.R.H., and Ward, S.A. (2003) The digestive food vacuole of the malaria parasite is a dynamic intracellular Ca2+ store. *Journal of Biological Chemistry* **278**(30), 27910–27915.

Breglio, K.F., Amato, R., Eastman, R., Lim, P., Sa, J.M., Guha, R., *et al.* (2018) A single nucleotide polymorphism in the Plasmodium falciparum atg18 gene associates with artemisinin resistance and confers enhanced parasite survival under nutrient deprivation. *Malaria Journal* **17**(1), 391.

Brennand, A., Gualdrón-López, M., Coppens, I., Rigden, D.J., Ginger, M.L., and Michels, P.A.M.M. (2011) Autophagy in parasitic protists: Unique features and drug targets. *Molecular and Biochemical Parasitology* **177**(2), 83–99.

Busse, R.A., Scacioc, A., Krick, R., Pérez-Lara, Á., Thumm, M., and Kühnel, K. (2015) Characterization of PROPPIN-phosphoinositide binding and role of loop 6CD in PROPPIN-membrane binding. *Biophysical Journal* **108**(9), 2223–2234.

CDC (2018) Malaria information and prophylaxis, by Country. https://www.cdc.gov/malaria/travelers/country_table.

Cervantes, S., Bunnik, E.M., Saraf, A., Conner, C.M., Escalante, A., Sardiu, M.E., *et al.* (2014) The multifunctional autophagy pathway in the human malaria parasite, Plasmodium falciparum. *Autophagy* **10**(1), 80–92.

Chen, D., Fan, W., Lu, Y., Ding, X., Chen, S., and Zhong, Q. (2012) A mammalian autophagosome maturation mechanism mediated by TECPR1 and the Atg12-Atg5 conjugate. *Molecular Cell* **45**(5), 629–641.

Chen, D., and Zhong, Q. (2012) A tethering coherent protein in autophagosome maturation. *Autophagy* **8**(6), 985–986.

Cheng, Q., Kyle, D.E., and Gatton, M.L. (2012) Artemisinin resistance in Plasmodium falciparum: A process linked to dormancy? *International Journal for Parasitology: Drugs and Drug Resistance* **2**, 249–255.

Choy, C.H., Saffi, G., Gray, M.A., Wallace, C., Dayam, R.M., Ou, Z.-Y.A., *et al.* (2018) Lysosome enlargement during inhibition of the lipid kinase PIKfyve proceeds through lysosome coalescence. *Journal of Cell Science* **131**(10), jcs213587.

Codogno, P., and Meijer, A.J. (2006) Atg5: More than an autophagy factor. *Nature Cell*

Biology **8**(10), 1045–1047.

Cooke, B. (1998) Participation, 'process' and management: Lessons for development in the history of organization development. *Journal of International Development* **10**(1), 35–54.

Coppens, I. (2011) Metamorphoses of malaria: The role of autophagy in parasite differentiation. *Essays in Biochemistry* **51**, 127–136.

Coronado, L.M., Nadovich, C.T., and Spadafora, C. (2014) Malarial hemozoin: From target to tool. *Biochimica et Biophysica Acta (BBA) - General Subjects* **1840**(6), 2032–2041.

Cowman, A.F., Berry, D., and Baum, J. (2012) The cellular and molecular basis for malaria parasite invasion of the human red blood cell. *Journal of Cell Biology* **198**(6), 961–971.

Cowman, A.F., and Crabb, B.S. (2006) Invasion of red blood cells by malaria parasites. *Cell* **124**(4), 755–766.

Cox-Singh, J., Davis, T.M.E., Lee, K.-S., Shamsul, S.S.G., Matusop, A., Ratnam, S., *et al.* (2008) Plasmodium knowlesi malaria in humans is widely distributed and potentially life threatening. *Clinical Infectious Diseases* **46**(2), 165–171.

Cox, F.E.G. (2010) History of the discovery of the malaria parasites and their vectors. *Parasites & Vectors* **3**(1), 5.

Crabb, B.S., Rug, M., Gilberger, T.-W., Thompson, J.K., Triglia, T., Maier, A.G., and Cowman, A.F. (2004) Transfection of the human malaria parasite Plasmodium falciparum. In *Parasite Genomics Protocols*. pp. 263–276.

Dahl, E.L., Shock, J.L., Shenai, B.R., Gut, J., DeRisi, J.L., and Rosenthal, P.J. (2006) Tetracyclines specifically target the apicoplast of the malaria parasite Plasmodium falciparum. *Antimicrobial Agents and Chemotherapy* **50**(9), 3124–3131.

Dalal, S., and Klemba, M. (2015) Amino acid efflux by asexual blood-stage Plasmodium falciparum and its utility in interrogating the kinetics of hemoglobin endocytosis and catabolism in vivo. *Molecular and Biochemical Parasitology* **201**(2), 116–122.

Das, G., Shravage, B. V, and Baehrecke, E.H. (2012) Regulation and function of autophagy during cell survival and cell death. *Cold Spring Harbor Perspectives in Biology* **4**(6), a008813.

Dasaradhi, P.V.N., Korde, R., Thompson, J.K., Tanwar, C., Nag, T.C., Chauhan, V.S., *et*

al. (2007) Food vacuole targeting and trafficking of falcipain-2, an important cysteine protease of human malaria parasite Plasmodium falciparum. *Molecular and Biochemical Parasitology* **156**(1), 12–23.

Datta, G., Hossain, M.E., Asad, M., Rathore, S., and Mohmmed, A. (2017) Plasmodium falciparum OTU-like cysteine protease (PfOTU) is essential for apicoplast homeostasis and associates with noncanonical role of Atg8. *Cellular Microbiology* **19**(9), e12748.

Deretic, V. (2005) Autophagy in innate and adaptive immunity. *Trends in Immunology* **26**(10), 523–528.

Desfougères, Y., Neumann, H., and Mayer, A. (2016) Organelle size control – increasing vacuole content activates SNAREs to augment organelle volume through homotypic fusion. *Journal of Cell Science* **156**(1), 2817–2828.

Dhingra, N., Jha, P., Sharma, V.P., Cohen, A.A., Jotkar, R.M., Rodriguez, P.S., *et al.* (2010) Adult and child malaria mortality in India: A nationally representative mortality survey. *The Lancet* **376**(9754), 1768–1774.

Dluzewski, A.R., Ling, I.T., Hopkins, J.M., Grainger, M., Margos, G., Mitchell, G.H., *et al.* (2008) Formation of the food vacuole in Plasmodium falciparum: a potential role for the 19 kDa fragment of merozoite surface protein 1 (MSP119). *PLoS One* **3**(8), e3085.

Dondorp, A.M., Nosten, F., Yi, P., Das, D., Phyo, A.P., Tarning, J., *et al.* (2009) Artemisinin Resistance in Plasmodium falciparum Malaria. *New England Journal of Medicine* **361**(5), 455–467.

Dooley, H.C., Razi, M., Polson, H.E.J., Girardin, S.E., Wilson, M.I., and Tooze, S.A. (2014) WIPI2 Links LC3 Conjugation with PI3P, Autophagosome Formation, and Pathogen Clearance by Recruiting Atg12-5-16L1. *Molecular Cell* **55**(2), 238–252.

Dooren, G.G. van, Marti, M., Tonkin, C.J., Stimmler, L.M., Cowman, A.F., and McFadden, G.I. (2005) Development of the endoplasmic reticulum, mitochondrion and apicoplast during the asexual life cycle of Plasmodium falciparum. *Molecular Microbiology* **57**(2), 405–419.

Dove, S.K., Piper, R.C., McEwen, R.K., Yu, J.W., King, N.C., Hughes, D.C., *et al.* (2004) Svp1p defines a family of phosphatidylinositol 3,5-bisphosphate effectors. *EMBO*

Journal **23**(9), 1922–1933.

Duszenko, M., Ginger, M.L., Brennand, A., Gualdrón-López, M., Colombo, M.I., Coombs, G.H., *et al.* (2011) Autophagy in protists. *Autophagy* **7**(2), 127–158.

Efe, J.A., Botelho, R.J., and Emr, S.D. (2007) Atg18 regulates organelle morphology and Fab1 kinase activity independent of its membrane recruitment by phosphatidylinositol 3,5-bisphosphate. *Molecular Biology of the Cell* **18**(11), 4232–4244.

Ehlgen, F., Pham, J.S., Koning-Ward, T. de, Cowman, A.F., and Ralph, S.A. (2012) Investigation of the Plasmodium falciparum food vacuole through inducible expression of the chloroquine resistance transporter (PfCRT). *PLoS One* **7**(6), e38781.

Eickel, N., Kaiser, G., Prado, M., Burda, P.-C., Roelli, M., Stanway, R.R., and Heussler, V.T. (2013) Features of autophagic cell death in Plasmodium liver-stage parasites. *Autophagy* **9**(4), 568–580.

Elliott, D.A., McIntosh, M.T., Hosgood, H.D., Chen, S., Zhang, G., Baevova, P., and Joiner, K.A. (2008) Four distinct pathways of hemoglobin uptake in the malaria parasite Plasmodium falciparum. *Proceedings of the National Academy of Sciences of the United States of America* **105**(7), 2463–2468.

Engelbrecht, D., and Coetzer, T.L. (2013) Turning up the heat: Heat stress induces markers of programmed cell death in Plasmodium falciparum in vitro. *Cell Death and Disease* **4**(12), e971.

Erbil, S., Oral, O., Mitou, G., Kig, C., Durmaz-Timucin, E., Guven-Maiorov, E., *et al.* (2016) RACK1 is an interaction partner of ATG5 and a novel regulator of autophagy. *Journal of Biological Chemistry* **291**(32), 16753–16765.

Eskelinen, E.-L. (2008) New insights into the mechanisms of macroautophagy in mammalian cells. *International Review of Cell and Molecular Biology* **266**, 207–247.

Fairhurst, R.M., and Dondorp, A.M. (2016) Artemisinin-Resistant Plasmodium falciparum Malaria. In *Emerging Infections 10*. American Society of Microbiology, pp. 409–429.

Feng, Y., He, D., Yao, Z., and Klionsky, D.J. (2014) The machinery of macroautophagy. *Cell Research* **24**, 24–41.

Fidock, D.A., and Wellems, T.E. (1997) Transformation with human dihydrofolate reductase renders malaria parasites insensitive to WR99210 but does not affect the intrinsic activity of proguanil. *Proceedings of the National Academy of Sciences of the*

United States of America **94**(20), 10931–10936.

Fiorentino, L., Cavalera, M., Menini, S., Marchetti, V., Mavilio, M., Fabrizi, M., *et al.* (2013) Loss of TIMP3 underlies diabetic nephropathy via FoxO1/STAT1 interplay. *EMBO Molecular Medicine* **5**(3), 441–455.

Francis, S.E., Sullivan, D.J., and Goldberg, and D.E. (1997) Hemoglobin metabolism in the malaria parasite Plasmodium falciparum. *Annual Review of Microbiology* **51**(1), 97–123.

Fujita, N., Itoh, T., Omori, H., Fukuda, M., Noda, T., and Yoshimori, T. (2008) The Atg16L complex specifies the site of LC3 lipidation for membrane biogenesis in autophagy. *Molecular Biology of the Cell* **19**(5), 2092–2100.

Garcia, C.R.S., Markus, R.P., and Madeira, L. (2001) Tertian and quartan fevers: Temporal regulation in malarial infection. *Journal of Biological Rhythms* **16**(5), 436–443.

Gaviria, D., Paguio, M.F., Turnbull, L.B., Tan, A., Siriwardana, A., Ghosh, D., *et al.* (2013) A Process similar to autophagy is associated with cytocidal chloroquine resistance in Plasmodium falciparum. *PLoS One* **8**(11), e79059.

Geng, J., and Klionsky, D.J. (2008) The Atg8 and Atg12 ubiquitin-like conjugation systems in macroautophagy. 'Protein modifications: Beyond the usual suspects'' review series.' *EMBO Reports* **9**(9), 859–864.

George, M.D., Baba, M., Scott, S. V, Mizushima, N., Garrison, B.S., Ohsumi, Y., and Klionsky, D.J. (2000) Apg5p functions in the sequestration step in the cytoplasm-to-vacuole targeting and macroautophagy pathways. *Molecular Biology of the Cell* **11**(3), 969–982.

Ghosh, D., Walton, J.L., Roepe, P.D., and Sinai, A.P. (2012) Autophagy is a cell death mechanism in Toxoplasma gondii. *Cellular Microbiology* **14**(4), 589–607.

Ghosh, S., and Rahi, M. (2019) Malaria elimination in India - The way forward. *Journal of Vector Borne Diseases* **56**(1), 32–40.

Gietz, R.D., and Schiestl, R.H. (2007) High-efficiency yeast transformation using the LiAc / SS carrier DNA / PEG method. *Nature Protocols* **2**(1), 31–34.

Goldberg, D.E. (2013) Complex nature of malaria parasite hemoglobin degradation. *Proceedings of the National Academy of Sciences of the United States of America* **110**(14), 5283–5284.

Goldberg, D.E., Slater, A.F., Cerami, A., and Henderson, G.B. (1990) Hemoglobin degradation in the malaria parasite Plasmodium falciparum: An ordered process in a unique organelle. *Proceedings of the National Academy of Sciences of the United States of America* **87**(8), 2931–2935.

Golstein, P., and Kroemer, G. (2007) Cell death by necrosis: Towards a molecular definition. *Trends in Biochemical Sciences* **32**(1), 37–43.

Gopaldass, N., Fauvet, B., Lashuel, H., Roux, A., and Mayer, A. (2017) Membrane scission driven by the PROPPIN Atg18. *EMBO Journal* **36**(22), 3274–3291.

Grand, R.J.A., Milner, A.E., Mustoe, T., Johnson, G.D., Owen, D., Grant, M.L., and Gregory, C.D. (1995) A novel protein expressed in mammalian cells undergoing apoptosis. *Experimental Cell Research* **218**(2), 439–451.

Grüring, C., Heiber, A., Kruse, F., Flemming, S., Franci, G., Colombo, S.F., *et al.* (2012) Uncovering common principles in protein export of malaria parasites. *Cell Host & Microbe* **12**(5), 717–729.

Guan, J., Stromhaug, P.E., George, M.D., Habibzadegah-Tari, P., Bevan, A., Dunn, W.A., and Klionsky, D.J. (2001) Cvt18/Gsa12 is required for cytoplasm-to-vacuole transport, pexophagy, and autophagy in Saccharomyces cerevisiae and Pichia pastoris. *Molecular Biology of the Cell* **12**(12), 3821–3838.

Hain, A.U.P., Bartee, D., Sanders, N.G., Miller, A.S., Sullivan, D.J., Levitskaya, J., *et al.* (2014) Identification of an Atg8-Atg3 protein–protein interaction inhibitor from the medicines for malaria venture malaria box active in blood and liver stage Plasmodium falciparum parasites. *Journal of Medicinal Chemistry* **57**(11), 4521–4531.

Hain, A.U.P., and Bosch, J. (2013) Autophagy in Plasmodium, a multifunctional pathway? *Computational and Structural Biotechnology Journal* **8**(11), e201308002.

Hain, A.U.P., Miller, A.S., Levitskaya, J., and Bosch, J. (2016) Virtual screening and experimental validation identify novel inhibitors of the Plasmodium falciparum Atg8-Atg3 Protein-Protein Interaction. *ChemMedChem* **11**(8), 900–910.

Hain, A.U.P., Weltzer, R.R., Hammond, H., Jayabalasingham, B., Dinglasan, R.R., Graham, D.R.M., *et al.* (2012) Structural characterization and inhibition of the Plasmodium Atg8–Atg3 interaction. *Journal of Structural Biology* **180**(3), 551–562.

Hallée, S., and Richard, D. (2015) Evidence that the malaria parasite Plasmodium

falciparum putative Rhoptry Protein 2 localizes to the Golgi apparatus throughout the erythrocytic cycle. *PLoS One* **10**(9), e0138626.

Hallée, S., Thériault, C., Gagnon, D., Kehrer, J., Frischknecht, F., Mair, G.R., and Richard, D. (2018) Identification of a Golgi apparatus protein complex important for the asexual erythrocytic cycle of the malaria parasite Plasmodium falciparum. *Cellular Microbiology* **20**(8), e12843.

Hamasaki, M., Furuta, N., Matsuda, A., Nezu, A., Yamamoto, A., Fujita, N., *et al.* (2013) Autophagosomes form at ER–mitochondria contact sites. *Nature* **495**(7441), 389–393.

Hammond, E.M., Brunet, C.L., Johnson, G.D., Parkhill, J., Milner, A.E., Brady, G., *et al.* (1998) Homology between a human apoptosis specific protein and the product of APG5, a gene involved in autophagy in yeast. *FEBS Letters* **425**(3), 391–395.

Hanada, T., Noda, N.N., Satomi, Y., Ichimura, Y., Fujioka, Y., Takao, T., *et al.* (2007) The Atg12-Atg5 conjugate has a novel E3-like activity for protein lipidation in autophagy. *Journal of Biological Chemistry* **282**(52), 37298–37302.

Hanssen, E., Goldie, K.N., and Tilley, L. (2010) Ultrastructure of the asexual blood stages of Plasmodium falciparum. In *Methods in Cell Biology*. pp. 93–116.

Heiber, A., and Spielmann, T. (2014) Preparation of parasite protein extracts and Western blot analysis. *Bio-Protocol* **4**(11), e1136.

Ho, H., Kapadia, R., Al-Tahan, S., Ahmad, S., and Ganesan, A.K. (2011) WIPI1 coordinates melanogenic gene transcription and melanosome formation via TORC1 inhibition. *The Journal of Biological Chemistry* **286**(14), 12509–12523.

Holzinger, A. (2009) Jasplakinolide: an actin-specific reagent that promotes actin polymerization. In *Cytoskeleton Methods and Protocols*. Humana Press, pp. 71–87.

Hopkins, J., Fowler, R., Krishna, S., Wilson, I., Mitchell, G., and Bannister, L. (1999) The plastid in Plasmodium falciparum asexual blood stages: A three-dimensional ultrastructural analysis. *Protist* **150**(3), 283–295.

Hott, A., Casandra, D., Sparks, K.N., Morton, L.C., Castanares, G.-G., Rutter, A., and Kyle, D.E. (2015) Artemisinin-resistant Plasmodium falciparum parasites exhibit altered patterns of development in infected erythrocytes. *Antimicrobial Agents and Chemotherapy* **59**(6), 3156–3167.

Howe, R., Kelly, M., Jimah, J., Hodge, D., and Odom, A.R. (2013) Isoprenoid biosynthesis

inhibition disrupts Rab5 localization and food vacuolar integrity in Plasmodium falciparum. *Eukaryotic Cell* **12**(2), 215–223.

Huang, L., Yuan, P., Yu, P., Kong, Q., Xu, Z., Yan, X., *et al.* (2018) O-GlcNAc-modified SNAP29 inhibits autophagy-mediated degradation via the disturbed SNAP29-STX17-VAMP8 complex and exacerbates myocardial injury in type I diabetic rats. *International Journal of Molecular Medicine* **42**(6), 3278–3290.

Iyer, J., Grüner, A.C., Rénia, L., Snounou, G., and Preiser, P.R. (2007) Invasion of host cells by malaria parasites: a tale of two protein families. *Molecular Microbiology* **65**(2), 231–249.

Jayabalasingham, B., Bano, N., and Coppens, I. (2010) Metamorphosis of the malaria parasite in the liver is associated with organelle clearance. *Cell Research* **20**(9), 1043–1059.

Jayabalasingham, B., Voss, C., Ehrenman, K., Romano, J.D., Smith, M.E., Fidock, D.A., *et al.* (2014) Characterization of the ATG8-conjugation system in 2 *Plasmodium* species with special focus on the liver stage. *Autophagy* **10**(2), 269–284.

Jeffries, T.R., Dove, S.K., Michell, R.H., and Parker, P.J. (2004) PtdIns-specific MPR pathway association of a novel WD40 repeat protein, WIPI49. *Molecular Biology of the Cell* **15**(6), 2652–2663.

Jin, N., Lang, M.J., and Weisman, L.S. (2016) Phosphatidylinositol 3,5-bisphosphate: regulation of cellular events in space and time. *Biochemical Society Transactions* **44**(1), 177–184.

Jogdand, P.S., Singh, S.K.S., Christiansen, M., Dziegiel, M.H., Singh, S.K.S., and Theisen, M. (2012) Flow cytometric readout based on Mitotracker Red CMXRos staining of live asexual blood stage malarial parasites reliably assesses antibody dependent cellular inhibition. *Malaria Journal* **11**(1), 235–245.

Joy, S., Thirunavukkarasu, L., Agrawal, P., Singh, A., Sagar, B.K.C., Manjithaya, R., and Surolia, N. (2018) Basal and starvation-induced autophagy mediates parasite survival during intraerythrocytic stages of Plasmodium falciparum. *Cell Death Discovery* **5**(1), 43–55.

Kakkilaya, B.S. (2018) Life cycle of the malaria parasite. https://www.malariasite.com/life-cycle/.

Kakkilaya, B.S. (2019) Malaria in India. https://www.malariasite.com/malaria-india/.

Kiel, J.A.K.W. (2010) Autophagy in unicellular eukaryotes. *Philosophical Transactions of the Royal Society B: Biological Sciences* **365**(1541), 819–830.

Kim, J., Kamada, Y., Stromhaug, P.E., Guan, J., Hefner-Gravink, A., Baba, M., *et al.* (2001) Cvt9/Gsa9 functions in sequestering selective cytosolic cargo destined for the vacuole. *Journal of Cell Biology* **153**(2), 381–396.

Kitamura, K., Kishi-Itakura, C., Tsuboi, T., Sato, S., Kita, K., Ohta, N., and Mizushima, N. (2012) Autophagy-related Atg8 localizes to the apicoplast of the human malaria parasite Plasmodium falciparum. *PLoS One* **7**(8), e42977.

Klemba, M., Beatty, W., Gluzman, I., and Goldberg, D.E. (2004a) Trafficking of Plasmepsin II to the food vacuole of the malaria parasite Plasmodium falciparum. *Journal of Cell Biology* **164**(1), 47–56.

Klemba, M., Gluzman, I., and Goldberg, D.E. (2004b) A Plasmodium falciparum dipeptidyl aminopeptidase I participates in vacuolar hemoglobin degradation. *Journal of Biological Chemistry* **279**(41), 43000–43007.

Klionsky, D.J., Abdalla, F.C., Abeliovich, H., Abraham, R.T., Acevedo-Arozena, A., Adeli, K., *et al.* (2012) Guidelines for the use and interpretation of assays for monitoring autophagy. *Autophagy* **8**(4), 445–544.

Klionsky, D.J., Abdelmohsen, K., Abe, A., Abedin, M.J., Abeliovich, H., Acevedo Arozena, A., *et al.* (2016) Guidelines for the use and interpretation of assays for monitoring autophagy (3rd edition). *Autophagy* **12**(1), 1–222.

Klionsky, D.J., and Codogno, P. (2013) The mechanism and physiological function of macroautophagy. *Journal of Innate Immunity* **5**(5), 427–433.

Kobayashi, T., Suzuki, K., and Ohsumi, Y. (2012) Autophagosome formation can be achieved in the absence of Atg18 by expressing engineered PAS-targeted Atg2. *FEBS Letters* **586**(16), 2473–2478.

Koenderink, J.B., Kavishe, R.A., Rijpma, S.R., and Russel, F.G.M. (2010) The ABCs of multidrug resistance in malaria. *Trends in Parasitology* **26**(9), 440–446.

Kotani, T., Kirisako, H., Koizumi, M., Ohsumi, Y., and Nakatogawa, H. (2018) The Atg2-Atg18 complex tethers pre-autophagosomal membranes to the endoplasmic reticulum for autophagosome formation. *Proceedings of the National Academy of Sciences of*

the United States of America **115**(41), 10363–10368.

Koyama-Honda, I., Itakura, E., Fujiwara, T.K., and Mizushima, N. (2013) Temporal analysis of recruitment of mammalian ATG proteins to the autophagosome formation site. *Autophagy* **9**(10), 1491–1499.

Krick, R., Busse, R.A., Scacioc, A., Stephan, M., Janshoff, A., Thumm, M., and Kühnel, K. (2012) Structural and functional characterization of the two phosphoinositide binding sites of PROPPINs, a β-propeller protein family. *Proceedings of the National Academy of Sciences of the United States of America* **109**(30), E2042–E2049.

Krick, R., Henke, S., Tolstrup, J., and Thumm, M. (2008) Dissecting the localization and function of Atg18, Atg21 and Ygr223c. *Autophagy* **4**(7), 896–910.

Krick, R., Tolstrup, J., Appelles, A., Henke, S., and Thumm, M. (2006) The relevance of the phosphatidylinositolphosphat-binding motif FRRGT of Atg18 and Atg21 for the Cvt pathway and autophagy. *FEBS Letters* **580**(19), 4632–4638.

Kruger, N.J. (2009) The Bradford method for protein quantitation. In *The Protein Protocols Handbook*. Springer, pp. 17–24.

Kuma, A., Mizushima, N., Ishihara, N., and Ohsumi, Y. (2002) Formation of the ~350-kDa Apg12-Apg5·Apg16 multimeric complex, mediated by Apg16 oligomerization, is essential for autophagy in yeast. *Journal of Biological Chemistry* **277**(21), 18619–18625.

Lamarque, M., Tastet, C., Poncet, J., Demettre, E., Jouin, P., Vial, H., and Dubremetz, J.F. (2008) Food vacuole proteome of the malarial parasite Plasmodium falciparum. *Proteomics - Clinical Applications* **2**(9), 1361–1374.

Lambros, C., and Vanderberg, J.P. (1979) Synchronization of Plasmodium falciparum erythrocytic stages in culture. *The Journal of Parasitology* **65**(3), 418–420.

Langreth, S.G., Reese, R.T., Motyl, M.R., and Trager, W. (1979) Plasmodium falciparum: Loss of knobs on the infected erythrocyte surface after long-term cultivation. *Experimental Parasitology* **48**(2), 213–219.

Lazarus, M.D., Schneider, T.G., and Taraschi, T.F. (2008) A new model for hemoglobin ingestion and transport by the human malaria parasite Plasmodium falciparum. *Journal of Cell Science* **121**(11), 1937–1949.

Lévêque, M.F., Berry, L., Cipriano, M.J., Nguyen, H.-M., Striepen, B., and Besteiro, S.

(2015) Autophagy-related protein ATG8 has a noncanonical function for apicoplast inheritance in Toxoplasma gondii. *MBio* **6**(6), e01446-15.

Li, F., Shen, Q., Wang, C., Sun, Y., Yuan, A.Y., and He, C.Y. (2012) A role of autophagy in Trypanosoma brucei cell death. *Cellular Microbiology* **14**(8), 1242–1256.

Li, S.C., and Kane, P.M. (2009) The yeast lysosome-like vacuole: Endpoint and crossroads. *Biochimica et Biophysica Acta (BBA)* **1793**(4), 650–663.

Liu, J., Istvan, E.S., Gluzman, I.Y., Gross, J., and Goldberg, D.E. (2006) Plasmodium falciparum ensures its amino acid supply with multiple acquisition pathways and redundant proteolytic enzyme systems. *Proceedings of the National Academy of Sciences of the United States of America* **103**(23), 8840–8845.

Livak, K.J., and Schmittgen, T.D. (2001) Analysis of relative gene expression data using real-time quantitative PCR and the 2-ΔΔCT method. *Methods* **25**(4), 402–408.

Lynch-Day, M.A., and Klionsky, D.J. (2010) The Cvt pathway as a model for selective autophagy. *FEBS Letters* **584**(7), 1359–1366.

Martin, R.E., and Kirk, K. (2007) Transport of the essential nutrient isoleucine in human erythrocytes infected with the malaria parasite Plasmodium falciparum. *Blood* **109**(5), 2217–2224.

Maskey, D., Yousefi, S., Schmid, I., Zlobec, I., Perren, A., Friis, R., and Simon, H.-U. (2013) ATG5 is induced by DNA-damaging agents and promotes mitotic catastrophe independent of autophagy. *Nature Communications* **4**(1), 2130.

Massey, A., Kiffin, R., and Cuervo, A.M. (2004) Pathophysiology of chaperone-mediated autophagy. *The International Journal of Biochemistry & Cell Biology* **36**(12), 2420–2434.

Matsushita, M., Suzuki, N.N., Obara, K., Fujioka, Y., Ohsumi, Y., and Inagaki, F. (2007) Structure of Atg5·Atg16, a complex essential for autophagy. *Journal of Biological Chemistry* **282**(9), 6763–6772.

Mbengue, A., Bhattacharjee, S., Pandharkar, T., Liu, H., Estiu, G., Stahelin, R. V, *et al.* (2015) A molecular mechanism of artemisinin resistance in Plasmodium falciparum malaria. *Nature* **520**(7549), 683–687.

McIntosh, M.T., Drozdowicz, Y.M., Laroiya, K., Rea, P.A., and Vaidya, A.B. (2001) Two classes of plant-like vacuolar-type H(+)-pyrophosphatases in malaria parasites.

Molecular and Biochemical Parasitology **114**(2), 183–195.

McIntosh, M.T., Vaid, A., Hosgood, H.D., Vijay, J., Bhattacharya, A., Sahani, M.H., *et al.* (2007) Traffic to the malaria parasite food vacuole: a novel pathway involving a phosphatidylinositol 3-phosphate-binding protein. *Journal of Biological Chemistry* **282**(15), 11499–11508.

Melo, R.C.N., Morgan, E., Monahan-Earley, R., Dvorak, A.M., and Weller, P.F. (2014) Pre-embedding immunogold labeling to optimize protein localization at subcellular compartments and membrane microdomains of leukocytes. *Nature Protocols* **9**(10), 2382–2394.

Michaillat, L., and Mayer, A. (2013) Identification of genes affecting vacuole membrane fragmentation in Saccharomyces cerevisiae. *PLoS One* **8**(2), e54160.

Mijaljica, D., Prescott, M., and Devenish, R.J. (2011) Microautophagy in mammalian cells: Revisiting a 40-year-old conundrum. *Autophagy* **7**(7), 673–682.

Mijaljica, D., Prescott, M., Klionsky, D.J., and Devenish, R.J. (2007) Autophagy and vacuole homeostasis: A case for self-degradation? *Autophagy* **3**(5), 417–421.

Milani, K.J., Schneider, T.G., and Taraschi, T.F. (2015) Defining the morphology and mechanism of the hemoglobin transport pathway in Plasmodium falciparum-infected erythrocytes. *Eukaryotic Cell* **14**(4), 415–426.

Miller, L.H., Ackerman, H.C., Su, X., and Wellems, T.E. (2013) Malaria biology and disease pathogenesis: Insights for new treatments. *Nature Medicine* **19**(2), 156–167.

Miotto, O., Amato, R., Ashley, E.A., Macinnis, B., Almagro-Garcia, J., Amaratunga, C., *et al.* (2015) Genetic architecture of artemisinin-resistant Plasmodium falciparum. *Nature Genetics* **47**(3), 226–234.

Mishra, P., Dauphinee, A.N., Ward, C., Sarkar, S., Gunawardena, A.H.L.A.N., and Manjithaya, R. (2017) Discovery of pan autophagy inhibitors through a high-throughput screen highlights macroautophagy as an evolutionarily conserved process across 3 eukaryotic kingdoms. *Autophagy* **13**(9), 1556–1572.

Mitchell, J.S., Li, N., Weinhold, N., Försti, A., Ali, M., Duin, M. van, *et al.* (2016) Genome-wide association study identifies multiple susceptibility loci for multiple myeloma. *Nature Communications* **7**(1), 12050.

Mizushima, N. (2007) Autophagy: Process and function. *Genes and Development* **21**(22),

2861–2873.

Mizushima, N. (2018) A brief history of autophagy from cell biology to physiology and disease. *Nature Cell Biology* **20**(5), 521–527.

Mizushima, N., Kuma, A., Kobayashi, Y., Yamamoto, A., Matsubae, M., Takao, T., *et al.* (2003) Mouse Apg16L, a novel WD-repeat protein, targets to the autophagic isolation membrane with the Apg12-Apg5 conjugate. *Journal of Cell Science* **116**(9), 1679–1688.

Mizushima, N., Noda, T., and Ohsumi, Y. (1999) Apg16p is required for the function of the Apg12p–Apg5p conjugate in the yeast autophagy pathway. *EMBO Journal* **18**(14), 3888–3896.

Mizushima, N., Noda, T., Yoshimori, T., Tanaka, Y., Ishii, T., George, M.D., *et al.* (1998a) A protein conjugation system essential for autophagy. *Nature* **395**(6700), 395–398.

Mizushima, N., and Sahani, M.H. (2014) ATG8 localization in apicomplexan parasites: Apicoplast and more? *Autophagy* **10**(9), 1487–1494.

Mizushima, N., Sugita, H., Yoshimori, T., and Ohsumi, Y. (1998b) A new protein conjugation system in human. *Journal of Biological Chemistry* **273**(51), 33889–33892.

Mizushima, N., Yamamoto, A., Hatano, M., Kobayashi, Y., Kabeya, Y., Suzuki, K., *et al.* (2001) Dissection of autophagosome formation using Apg5-deficient mouse embryonic stem cells. *Journal of Cell Biology* **152**(4), 657–668.

Mizushima, N., Yoshimori, T., and Levine, B. (2010) Methods in mammalian autophagy research. *Cell* **140**(3), 313–326.

Mizushima, N., Yoshimori, T., and Ohsumi, Y. (2011) The role of Atg proteins in autophagosome formation. *Annual Review of Cell and Developmental Biology* **27**(1), 107–132.

Moll, K., Kaneko, A., Scherf, A., and Wahlgren, M. (2013) DNA isolation from Plasmodium falciparum. In *Methods in Malaria Research*. pp. 259–260.

Moura, P.A., Dame, J.B., and Fidock, D.A. (2009) Role of Plasmodium falciparum digestive vacuole plasmepsins in the specificity and antimalarial mode of action of cysteine and aspartic protease inhibitors. *Antimicrobial Agents and Chemotherapy* **53**(12), 4968–4978.

Nagy, P., Hegedűs, K., Pircs, K., Varga, Á., and Juhász, G. (2014) Different effects of Atg2 and Atg18 mutations on Atg8a and Atg9 trafficking during starvation in Drosophila. *FEBS Letters* **588**(3), 408–413.

Nair, U., Cao, Y., Xie, Z., and Klionsky, D.J. (2010) Roles of the lipid-binding motifs of Atg18 and Atg21 in the cytoplasm to vacuole targeting pathway and autophagy. *Journal of Biological Chemistry* **285**(15), 11476–11488.

Navale, R., Allanki, A.D., Sijwali, P.S., and others (2014) Characterization of the autophagy marker protein Atg8 reveals atypical features of autophagy in Plasmodium falciparum. *PLoS One* **9**(11), e113220.

Ngotho, P., Soares, A.B., Hentzschel, F., Achcar, F., Bertuccini, L., and Marti, M. (2019) Revisiting gametocyte biology in malaria parasites. *FEMS Microbiology Reviews* **43**(4), 401–414.

Nguyen, H.M., Hajj, H. El, Hajj, R. El, Tawil, N., Berry, L., Lebrun, M., *et al.* (2017) *Toxoplasma gondii* autophagy-related protein ATG9 is crucial for the survival of parasites in their host. *Cellular Microbiology* **19**(6), e12712.

Nguyen, H.M., Liu, S., Daher, W., Tan, F., and Besteiro, S. (2018) Characterisation of two Toxoplasma PROPPINs homologous to Atg18/WIPI suggests they have evolved distinct specialised functions. *PLoS One* **13**(4), e0195921.

Nguyen, T.N., Padman, B.S., Usher, J., Oorschot, V., Ramm, G., and Lazarou, M. (2016) Atg8 family LC3/GABARAP proteins are crucial for autophagosome-lysosome fusion but not autophagosome formation during PINK1/Parkin mitophagy and starvation. *The Journal of Cell Biology* **215**(6), 857–874.

Noda, N.N., Fujioka, Y., Hanada, T., Ohsumi, Y., and Inagaki, F. (2012) Structure of the Atg12–Atg5 conjugate reveals a platform for stimulating Atg8–PE conjugation. *EMBO Reports* **14**(2), 206–211.

Noedl, H., Se, Y., Schaecher, K., Smith, B.L., Socheat, D., Fukuda, M.M., and Artemisinin Resistance in Cambodia 1 (ARC1) Study Consortium (2008) Evidence of artemisinin-resistant malaria in western Cambodia. *New England Journal of Medicine* **359**(24), 2619–2620.

Nye, E.R. (2002) Alphonse Laveran (1845–1922): Discoverer of the malarial Parasite and Nobel Laureate, 1907. *Journal of Medical Biography* **10**(2), 81–87.

Obara, K., Sekito, T., Niimi, K., and Ohsumi, Y. (2008) The Atg18-Atg2 complex is recruited to autophagic membranes via phosphatidylinositol 3-phosphate and exerts an essential function. *Journal of Biological Chemistry* **283**(35), 23972–23980.

Ohsumi, Y. (2014) Historical landmarks of autophagy research. *Cell Research* **24**(1), 9–23.

Omara-Opyene, A.L., Moura, P.A., Sulsona, C.R., Bonilla, J.A., Yowell, C.A., Fujioka, H., *et al.* (2004) Genetic disruption of the Plasmodium falciparum digestive vacuole Plasmepsins demonstrates their functional redundancy. *Journal of Biological Chemistry* **279**(52), 54088–54096.

Ostap, E.M. (2002) 2,3-Butanedione monoxime (BDM) as a myosin inhibitor. *Journal of Muscle Research and Cell Motility* **23**(4), 305–308.

Pang, Y., Yamamoto, H., Sakamoto, H., Oku, M., Mutungi, J.K., Sahani, M.H., *et al.* (2019) Evolution from covalent conjugation to non-covalent interaction in the ubiquitin-like ATG12 system. *Nature Structural & Molecular Biology* **26**(4), 289–296.

Parzych, K.R., and Klionsky, D.J. (2014) An overview of autophagy: Morphology, mechanism, and regulation. *Antioxidants & Redox Signaling* **20**(3), 460–473.

Pattaradilokrat, S., Mu, J., Awadalla, P., and Su, X.Z. (2013) *Malaria parasites: Comparative genomics, evolution and molecular biology*. Caister Academic Press, .

Payne, S.H., and Loomis, W.F. (2006) Retention and loss of amino acid biosynthetic pathways based on analysis of whole-genome sequences. *Eukaryotic Cell* **5**(2), 272–276.

Percário, S., Moreira, D.R., Gomes, B.A.Q., Ferreira, M.E.S., Gonçalves, A.C.M., Laurindo, P.S.O.C., *et al.* (2012) Oxidative stress in malaria. *International Journal of Molecular Sciences* **13**(12), 16346–16372.

Phillips, M.A., Burrows, J.N., Manyando, C., Huijsduijnen, R.H. van, Voorhis, W.C. Van, and Wells, T.N.C. (2017) Malaria. *Nature Reviews Disease Primers* **3**, 17050.

Pierdominici, M., Vomero, M., Barbati, C., Colasanti, T., Maselli, A., Vacirca, D., *et al.* (2012) Role of autophagy in immunity and autoimmunity, with a special focus on systemic lupus erythematosus. *The FASEB Journal* **26**(4), 1400–1412.

Polson, H.E.J., Lartigue, J. De, Rigden, D.J., Reedijk, M., Urbé, S., Clague, M.J., and

Tooze, S.A. (2010) Mammalian Atg18 (WIPI2) localizes to omegasome-anchored phagophores and positively regulates LC3 lipidation. *Autophagy* **6**(4), 506–522.

Prasad, R., Atul, Kolla, V.K., Legac, J., Singhal, N., Navale, R., *et al.* (2013) Blocking Plasmodium falciparum development via dual inhibition of hemoglobin degradation and the ubiquitin proteasome system by MG132. *PloS One* **8**(9), e73530.

Proikas-Cezanne, T., Ruckerbauer, S., Stierhof, Y.-D., Berg, C., and Nordheim, A. (2007) Human WIPI-1 puncta-formation: a novel assay to assess mammalian autophagy. *FEBS Letters* **581**(18), 3396–3404.

Proikas-Cezanne, T., Takacs, Z., Donnes, P., and Kohlbacher, O. (2015) WIPI proteins: Essential PtdIns3P effectors at the nascent autophagosome. *Journal of Cell Science* **128**(2), 207–217.

Proikas-Cezanne, T., Waddell, S., Gaugel, A., Frickey, T., Lupas, A., and Nordheim, A. (2004) WIPI-1α (WIPI49), a member of the novel 7-bladed WIPI protein family, is aberrantly expressed in human cancer and is linked to starvation-induced autophagy. *Oncogene* **23**(58), 9314–9325.

Proto, W.R., Jones, N.G., Coombs, G.H., and Mottram, J.C. (2014) Tracking autophagy during proliferation and differentiation of Trypanosoma brucei. *Microbial Cell* **1**(1), 9–20.

Pryor, P.R., Mullock, B.M., Bright, N.A., Lindsay, M.R., Gray, S.R., Richardson, S.C.W., *et al.* (2004) Combinatorial SNARE complexes with VAMP7 or VAMP8 define different late endocytic fusion events. *EMBO Reports* **5**(6), 590–5.

Pyo, J.-O., Jang, M.-H., Kwon, Y.-K., Lee, H.-J., Jun, J.-I., Woo, H.-N., *et al.* (2005) Essential roles of Atg5 and FADD in autophagic cell death. *Journal of Biological Chemistry* **280**(21), 20722–20729.

Quevillon, E., Spielmann, T., Brahimi, K., Chattopadhyay, D., Yeramian, E., and Langsley, G. (2003) The Plasmodium falciparum family of Rab GTPases. *Gene* **306**, 13–25.

Rathore, S., Datta, G., Kaur, I., Malhotra, P., and Mohmmed, A. (2015) Disruption of cellular homeostasis induces organelle stress and triggers apoptosis like cell-death pathways in malaria parasite. *Cell Death and Disease* **6**(7), e1803.

Reggiori, F., Tucker, K.A., Stromhaug, P.E., and Klionsky, D.J. (2004) The Atg1-Atg13 complex regulates Atg9 and Atg23 retrieval transport from the pre-autophagosomal

structure. *Developmental Cell* **6**(1), 79–90.

Richards, A., Veses, V., and Gow, N.A.R. (2010) Vacuole dynamics in fungi. *Fungal Biology Reviews* **24**(3–4), 93–105.

Rieter, E., Vinke, F., Bakula, D., Cebollero, E., Ungermann, C., Proikas-Cezanne, T., and Reggiori, F. (2013) Atg18 function in autophagy is regulated by specific sites within its -propeller. *Journal of Cell Science* **126**(2), 593–604.

Rigden, D.J., Michels, P., and Ginger, M.L. (2009) Autophagy in protists: Examples of secondary loss, lineage-specific innovations, and the conundrum of remodeling a single mitochondrion. *Autophagy* **5**(6), 784–794.

Romanov, J., Walczak, M., Ibiricu, I., Schüchner, S., Ogris, E., Kraft, C., and Martens, S. (2012) Mechanism and functions of membrane binding by the Atg5-Atg12/Atg16 complex during autophagosome formation. *The EMBO Journal* **31**(22), 4304–4317.

Rosano, G.L., and Ceccarelli, E.A. (2014) Recombinant protein expression in Escherichia coli: Advances and challenges. *Frontiers in Microbiology* **5**, 172.

Rosenthal, P.J. (2018) Artemisinin Resistance Outside of Southeast Asia. *The American Journal of Tropical Medicine and Hygiene* **99**(6), 1357–1359.

Rubinsztein, D.C., Mariño, G., and Kroemer, G. (2011) Autophagy and aging. *Cell* **146**(5), 682–695.

Rusten, T.E., and Stenmark, H. (2006) Analyzing phosphoinositides and their interacting proteins. *Nature Methods* **3**(4), 251–258.

Salmon, B.L., Oksman, A., and Goldberg, D.E. (2001) Malaria parasite exit from the host erythrocyte: A two-step process requiring extraerythrocytic proteolysis. *Proceedings of the National Academy of Sciences of the United States of America* **98**(1), 271–276.

Scacioc, A., Schmidt, C., Hofmann, T., Urlaub, H., Kühnel, K., and Pérez-Lara, Á. (2017) Structure based biophysical characterization of the PROPPIN Atg18 shows Atg18 oligomerization upon membrane binding. *Scientific Reports* **7**(1), 14008.

Settembre, C., Malta, C. Di, Polito, V.A., Arencibia, M.G., Vetrini, F., Erdin, S., *et al.* (2011) TFEB links autophagy to lysosomal biogenesis. *Science* **332**(6036), 1429–1433.

Shibutani, S.T., and Yoshimori, T. (2014) A current perspective of autophagosome biogenesis. *Cell Research* **24**(1), 58–68.

Sijwali, P.S., and Rosenthal, P.J. (2004) Gene disruption confirms a critical role for the cysteine protease falcipain-2 in hemoglobin hydrolysis by Plasmodium falciparum. *Proceedings of the National Academy of Sciences of the United States of America* **101**(13), 4384–4389.

Smythe, W.A., Joiner, K.A., and Hoppe, H.C. (2008) Actin is required for endocytic trafficking in the malaria parasite Plasmodium falciparum. *Cellular Microbiology* **10**(2), 452–464.

Spielmann, T., and Gilberger, T.-W. (2015) Critical steps in protein export of Plasmodium falciparum blood stages. *Trends in Parasitology* **31**(10), 514–525.

Strømhaug, P.E., Reggiori, F., Guan, J., Wang, C.-W., and Klionsky, D.J. (2004) Atg21 is a phosphoinositide binding protein required for efficient lipidation and localization of Atg8 during uptake of Aminopeptidase I by selective autophagy. *Molecular Biology of the Cell* **15**(8), 3553–3566.

Suresh, N., and Haldar, K. (2018) Mechanisms of artemisinin resistance in Plasmodium falciparum malaria. *Current Opinion in Pharmacology* **42**, 46–54.

Surolia, N., and Surolia, A. (2001) Triclosan offers protection against blood stages of malaria by inhibiting enoyl-ACP reductase of Plasmodium falciparum. *Nature Medicine* **7**(2), 167–173.

Suzuki, H., Osawa, T., Fujioka, Y., and Noda, N.N. (2017) Structural biology of the core autophagy machinery. *Current Opinion in Structural Biology* **43**, 10–17.

Suzuki, K., Kubota, Y., Sekito, T., and Ohsumi, Y. (2007) Hierarchy of Atg proteins in pre-autophagosomal structure organization. *Genes to Cells* **12**(2), 209–218.

Tai, G., Lu, L., Wang, T.L., Tang, B.L., Goud, B., Johannes, L., and Hong, W. (2004) Participation of the syntaxin 5/Ykt6/GS28/GS15 SNARE complex in transport from the early/recycling endosome to the trans-Golgi network. *Molecular Biology of the Cell* **15**(9), 4011–22.

Takáts, S., Glatz, G., Szenci, G., Boda, A., Horváth, G. V., Hegedűs, K., *et al.* (2018) Non-canonical role of the SNARE protein Ykt6 in autophagosome-lysosome fusion. *PLoS Genetics* **14**(4), e1007359.

Tamura, N., Oku, M., Ito, M., Noda, N.N., Inagaki, F., and Sakai, Y. (2013) Atg18 phosphoregulation controls organellar dynamics by modulating its

phosphoinositidebinding activity. *The Journal of Cell Biology* **202**(4), 685–698.

Tawk, L., Chicanne, G., Dubremetz, J.-F., Richard, V., Payrastre, B., Vial, H.J., *et al.* (2010) Phosphatidylinositol 3-Phosphate, an essential lipid in Plasmodium, localizes to the food vacuole membrane and the apicoplast. *Eukaryotic Cell* **9**(10), 1519–1530.

Tekirdag, K.A., Korkmaz, G., Ozturk, D.G., Agami, R., and Gozuacik, D. (2013) MIR181A regulates starvation- and rapamycin-induced autophagy through targeting of ATG5 . *Autophagy* **9**(3), 374–385.

Tomlins, A.M., Ben-Rached, F., Williams, R.A., Proto, W.R., Coppens, I., Ruch, U., *et al.* (2013) Plasmodium falciparum ATG8 implicated in both autophagy and apicoplast formation. *Autophagy* **9**(10), 1540–1552.

Tong, Z. (2011) Yeast vacuole staining with FM4-64. *Bio-Protocol* **1**(1), e18.

Tong, Z. (2012) Spot assay for yeast. *Bio-Protocol* **2**(1), e16.

Tonkin, C.J., Dooren, G.G. Van, Spurck, T.P., Struck, N.S., Good, R.T., Handman, E., *et al.* (2004) Localization of organellar proteins in Plasmodium falciparum using a novel set of transfection vectors and a new immunofluorescence fixation method. *Molecular and Biochemical Parasitology* **137**(1), 13–21.

Tonkin, C.J., Pearce, J.A., McFadden, G.I., and Cowman, A.F. (2006) Protein targeting to destinations of the secretory pathway in the malaria parasite Plasmodium falciparum. *Current Opinion in Microbiology* **9**(4), 381–387.

Torggler, R., Papinski, D., and Kraft, C. (2017) Assays to monitor autophagy in Saccharomyces cerevisiae. *Cells* **6**(3), 23.

Trager, W., and Jensen, J.B. (1976) Human malaria parasites in continuous culture. *Science* **193**(4254), 673–675.

Tsukada, M., and Ohsumi, Y. (1993) Isolation and characterization of autophagy-defective mutants of Saccharomyces cerevisiae. *FEBS Letters* **333**(1–2), 169–174.

Tsuyuki, S., Takabayashi, M., Kawazu, M., Kudo, K., Watanabe, A., Nagata, Y., *et al.* (2014) Detection of WIPI1 mRNA as an indicator of autophagosome formation. *Autophagy* **10**(3), 497–513.

Vaid, A., Ranjan, R., Smythe, W.A., Hoppe, H.C., and Sharma, P. (2010) PfPI3K, a phosphatidylinositol-3 kinase from Plasmodium falciparum, is exported to the host erythrocyte and is involved in hemoglobin trafficking. *Blood* **115**(12), 2500–2507.

Valverde, D.P., Yu, S., Boggavarapu, V., Kumar, N., Lees, J.A., Walz, T., *et al.* (2019) ATG2 transports lipids to promote autophagosome biogenesis. *The Journal of Cell Biology* **218**(6), 1787–1798.

Vanrell, M.C., Losinno, A.D., Cueto, J.A., Balcazar, D., Fraccaroli, L.V., Carrillo, C., and Romano, P.S. (2017) The regulation of autophagy differentially affects Trypanosoma cruzi metacyclogenesis. *PLoS Neglected Tropical Diseases* **11**(11), e0006049.

Vaughan, A.M., and Kappe, S.H.I. (2017) Malaria parasite liver infection and exoerythrocytic biology. *Cold Spring Harbor Perspectives in Medicine* **7**(6), a025486.

Vernick, K.D., Oduol, F., Lazzaro, B.P., Glazebrook, J., Xu, J., Riehle, M., and Li, J. (2005) Molecular genetics of mosquito resistance to malaria parasites. In *Malaria: Drugs, Disease and Post-Genomic Biology*. Springer, pp. 383–415.

Voss, C., Ehrenman, K., Mlambo, G., Mishra, S., Kumar, K.A., Sacci, J.B., *et al.* (2016) Overexpression of Plasmodium berghei ATG8 by liver forms leads to cumulative defects in organelle dynamics and to generation of noninfectious merozoites. *MBio* **7**(3), e00682-16.

Walczak, M., Ganesan, S.M., Niles, J.C., and Yeh, E. (2018) ATG8 is essential specifically for an autophagy-independent function in apicoplast biogenesis in blood-stage malaria parasites. *MBio* **9**(1), e02021-17.

Walker, D.M., Mahfooz, N., Kemme, K.A., Patel, V.C., Spangler, M., and Drew, M.E. (2013) Plasmodium falciparum erythrocytic stage parasites require the putative autophagy protein PfAtg7 for normal growth. *PLoS One* **8**(6), e67047.

Wang, J., Zhang, C.J., Chia, W.N., Loh, C.C.Y., Li, Z., Lee, Y.M., *et al.* (2015) Haem-activated promiscuous targeting of artemisinin in Plasmodium falciparum. *Nature Communications* (6), 10111.

Wang, Y., Li, L., Hou, C., Lai, Y., Long, J., Liu, J., *et al.* (2016a) SNARE-mediated membrane fusion in autophagy. *Seminars in Cell & Developmental Biology* **60**, 97–104.

Wang, Z., Cabrera, M., Yang, J., Yuan, L., Gupta, B., Liang, X., *et al.* (2016b) Genome-wide association analysis identifies genetic loci associated with resistance to multiple antimalarials in Plasmodium falciparum from China-Myanmar border. *Scientific Reports* **6**, 33891.

Watanabe, Y., Kobayashi, T., Yamamoto, H., Hoshida, H., Akada, R., Inagaki, F., *et al.* (2012) Structure-based analyses reveal distinct binding sites for Atg2 and phosphoinositides in Atg18. *The Journal of Biological Chemistry* **287**(38), 31681–31690.

Williams, R.A.M., Smith, T.K., Cull, B., Mottram, J.C., and Coombs, G.H. (2012) ATG5 is essential for ATG8-dependent autophagy and mitochondrial homeostasis in Leishmania major. *PLoS Pathogens* **8**(5), e1002695.

Williams, R.A.M., Woods, K.L., Juliano, L., Mottram, J.C., and Coombs, G.H. (2009) Characterization of unusual families of ATG8-like proteins and ATG12 in the protozoan parasite *Leishmania major*. *Autophagy* **5**(2), 159–172.

Wilson, R.J.M.I. (2005) Parasite plastids: Approaching the endgame. *Biological Reviews of the Cambridge Philosophical Society* **80**(1), 129–153.

World Health Organisation (2018) World Malaria Report. http://www.who.int/iris/handle/10665/275867.

Wunderlich, J., Rohrbach, P., and Dalton, J.P. (2012) The malaria digestive vacuole. *Frontiers in Bioscience* **4**, 1424–1448.

Xia, H.-G., Zhang, L., Chen, G., Zhang, T., Liu, J., Jin, M., *et al.* (2010) Control of basal autophagy by calpain1 mediated cleavage of ATG5. *Autophagy* **6**(1), 61–6.

Xu, Y., and Eissa, N.T. (2010) Autophagy in Innate and Adaptive Immunity. *Proceedings of the American Thoracic Society* **7**(1), 22–28.

Yang, Y.P., Hu, L.F., Zheng, H.F., Mao, C.J., Hu, W.D., Xiong, K.P., *et al.* (2013) Application and interpretation of current autophagy inhibitors and activators. *Acta Pharmacologica Sinica* **34**(5), 625–635.

Yang, Z., and Klionsky, D.J. (2010) Eaten alive: A history of macroautophagy. *Nature Cell Biology* **12**(9), 814–822.

Yin, Z., Pascual, C., and Klionsky, D.J. (2016) Autophagy: Machinery and regulation. *Microbial Cell* **3**(12), 588–596.

Yorimitsu, T., and Klionsky, D.J. (2005) Autophagy: molecular machinery for self-eating. *Cell Death and Differentiation* **12 Suppl 2**(S2), 1542–52.

Yousefi, S., Perozzo, R., Schmid, I., Ziemiecki, A., Schaffner, T., Scapozza, L., *et al.* (2006) Calpain-mediated cleavage of Atg5 switches autophagy to apoptosis. *Nature*

Cell Biology **8**(10), 1124–1132.

Zhao, J., Brault, J.J., Schild, A., Cao, P., Sandri, M., Schiaffino, S., *et al.* (2007) FoxO3 Coordinately Activates Protein Degradation by the Autophagic/Lysosomal and Proteasomal Pathways in Atrophying Muscle Cells. *Cell Metabolism* **6**(6), 472–483.

Zhou, H.-X., Rivas, G., and Minton, A.P. (2008) Macromolecular Crowding and Confinement: Biochemical, Biophysical, and Potential Physiological Consequences. *Annual Review of Biophysics* **37**, 375–397.

Zhou, H.C., Gao, Y.H., Zhong, X., and Wang, H. (2009) Dynamin like protein 1 participated in the hemoglobin uptake pathway of Plasmodium falciparum. *Chinese Medical Journal* **122**(14), 1686–1691.

Zieger, M., and Mayer, A. (2012) Yeast vacuoles fragment in an asymmetrical two-phase process with distinct protein requirements. *Molecular Biology of the Cell* **23**(17), 3438–3449.

Publications

Joy, S., Thirunavukkarasu, L., Agrawal, P., Singh, A., Sagar, B.K.C., Manjithaya, R., and Surolia, N. (2018) Basal and starvation-induced autophagy mediates parasite survival during intraerythrocytic stages of *Plasmodium falciparum*. *Cell Death Discovery* **5**(1), 43–55.

Agrawal, P., Manjithaya, R., & Surolia, N. *Plasmodium falciparum* autophagy-related protein *Pf*ATG18 participates in food vacuole fission dynamics and autophagy-like pathway. (Manuscript under revision).